https://doi.org/10.15388/vu.thesis.33

VILNIUS UNIVERSITY

Audrius
LAURYNĖNAS

Investigation and modeling of complex biocatalytic and bioelectrocatalytic processes

DOCTORAL DISSERTATION

Natural Sciences,
Biochemistry, N 004

VILNIUS 2020

This dissertation was written between 2011 and 2015 during doctoral studies in Vilnius University

The dissertation is defended on an external basis

Academic consultant:
Acad. Prof. Habil. Dr. Juozas Kulys
(Vilnius University, natural sciences, biochemistry, N 004).

This doctoral dissertation will be defended in a public meeting of the Dissertation Defence Panel:
Chairman – Prof. Habil. Dr. Arūnas Ramanavičius (Vilnius University, natural sciences, biochemistry, N 004).
Members: (members listed in alphabetical order of surnames)
Dr. Visvaldas Kairys (Vilnius University, natural sciences, biochemistry, N 004),
Prof. Dr. Dalius Navakauskas (Vilnius Gediminas Technical University, technology sciences, informatics engineering, T 007),
Prof. Dr. Rasa Pauliukaitė (Center for Physical Sciences and Technology, natural sciences, chemistry, N 003),
Prof. Dr. Tautgirdas Ruzgas (Malmö University, natural sciences, biochemistry, N 004).

The dissertation shall be defended at a public/closed meeting of the Dissertation Defence Panel at 13:00 on June 29, 2020 in room R-401 of the Vilnius University Life Sciences Center.
Address: Saulėtekio al. 7, R-401,Vilnius, Lithuania
Tel. +370 69 269 623 ; e-mail: audrius.laurynenas@bchi.vu.lt
The text of this dissertation can be accessed at the library of Vilnius University, as well as on the website of Vilnius University: www.vu.lt/lt/naujienos/ivykiu-kalendorius

https://doi.org/10.15388/vu.thesis.33

VILNIAUS UNIVERSITETAS

Audrius
LAURYNĖNAS

Sudėtingų biokatalizinių bei bioelektrokatalizinių procesų tyrimas ir modeliavimas

DAKTARO DISERTACIJA

Gamtos mokslai,
Biochemija, N 004

VILNIUS 2020

Disertacija rengta 2011– 2015 metais studijuojant doktorantūrą Vilniaus universitete

Disertacija ginama eksternu

Mokslinis konsultantas:
akad. prof. habil. dr. Juozas Kulys
(Vilniaus universitetas, gamtos mokslai, biochemija, N 004)

Gynimo taryba:
Pirmininkas – **prof. habil. dr. Arūnas Ramanavičius** (Vilniaus universitetas, gamtos mokslai, biochemija, N 004).
Nariai:
dr. Visvaldas Kairys (Vilniaus universitetas, gamtos mokslai, biochemija, N 004),
prof. dr. Dalius Navakauskas (Vilniaus Gedimino technikos universitetas, technologijos mokslai, informatikos inžinerija, T 007),
prof. dr. Rasa Pauliukaitė (Fizinių ir technologijos mokslų centras, gamtos mokslai, chemija, N 003),
prof. dr. Tautgirdas Ruzgas (Malmö University, gamtos mokslai, biochemija, N 004).

Disertacija ginama viešame Gynimo tarybos posėdyje 2020 m. birželio mėn. 29 d. 13:00 val. Vilniaus universiteto Gyvybės mokslų centro R-401 auditorijoje. Adresas: Saulėtekio al. 7, R-401,Vilnius, Lietuva, tel. +370 69 269 623 ; el. paštas audrius.laurynenas@bchi.vu.lt .

Disertaciją galima peržiūrėti Vilniaus universiteto bibliotekoje ir VU interneto svetainėje adresu: https://www.vu.lt/naujienos/ivykiu-kalendorius

CONTENTS

1 INTRODUCTION

The majority of biochemical processes found in living organisms are oxidation-reduction reactions. These reactions are catalyzed by a diverse class of enzymes called oxidoreductases. They catalyze the transfer of electrons from one substrate to another and utilize a variety of cofactors. The diversity of oxidoreductases represents the diversity of life itself. For example, nitrogenases facilitate the electron transfer from reduced ferredoxin to nitrogen and enable bacteria to capture nitrogen and use it in a biosynthesis. Its cofactor is a cluster made of iron, molybdenum and sulfur. Another example is a glucose oxidase – a FAD-containing enzyme produced by specific fungi. The function of this enzyme is to catalyze the oxidation of glucose to gluconolactone while reducing oxygen to hydrogen peroxide. Hydrogen peroxide is used as an antimicrobial agent to kill bacteria or inhibit their growth. Other exemplary enzymes are laccases, which catalyze degradation of lignin to organic monomers in fungi, and an oxidative coupling of monolignols in plants. Four copper ions perform the cofactor role in laccases, oxygen being the final electron acceptor.

Oxidoreductases are important research objects from various perspectives. From scientific point of view, oxidoreductases posses the diversity of catalysis mechanisms that stimulate theoretical developments of electron transfer theories in enzymes, as well as attempts to modify the catalytic properties of enzymes or use them for synthesis and detection of various substances. A selection of industrial applications for oxidoreductases is as diverse as the enzymatic class itself, starting from various biosensors, biofuel cells, enzymatic synthesis systems, biodegradation of pollutants or waste, applications in paper and textile industries and ending with a production of lacquerware.

Modeling and experimental data fitting are indispensable for a better understanding of the processes. However, models tend to be complex because biocatalytic and bioelectrocatalytic processes themselves can be, and actually are, complex phenomena. Still, to have equations that model a process and to use them are quite different tasks.

Attempts to model complex bio(electro)catalytic processes are frequently plagued by various mathematical problems, such as failures of optimization of parameters to converge to meaningful results, or numer-

ical instabilities. These problems are always associated with underlying mathematical assumptions in the algorithm, which is used for numerical computations. The diversity of optimization and integration algorithms shows not only the mathematical interest, but the diversity of problems to solve as well. Quantitative results, despite these obstacles, acquired from experimental data, are valuable themselves in direct comparison of an experiment and a theory or as a quantitative start for designing industrial applications.

Problems, which require mathematical modeling to understand and interpret experimental results, cover a range of biochemical interests, from the homogeneous and heterogeneous catalysis to the transfer of electron and proton in biological molecules. An effective and powerful biochemical kinetics modeling and data fitting algorithm allows modeling the alternative hypotheses and distinguishing between them, as well as acquiring valuable rate parameters, which are needed for any discussion about the efficiency of a reaction mechanism of enzymatic catalysis.

The first part of this thesis is dedicated to the creation of an algorithm for the calculation of rate parameters from experiments for complex biochemical reactions. In the second part of this thesis, the algorithm is used to interpret biochemical kinetics of laccases in homogeneous medium and reconcile its properties with ones observed on the electrode. In the third part of this thesis, the algorithm is used to acquire rate parameters for peroxidase-catalyzed oxidations and deduce the mechanism of peroxidase compound II in terms of proton and electron transfer.

1.1 Goals and tasks of the thesis

The goal of the thesis is to develop a method for the calculation of reaction rate parameters of complex homogeneous biochemical reactions and to apply it for the investigation of oxidation/reduction processes catalyzed by enzymes in homogeneous media and on surfaces.

The originating tasks to achieve this goal are following:

1. To develop biochemical kinetics modeling and experimental data fitting methods, suitable for the investigation of chemical and biochemical kinetics.

2. To apply the developed methods for the investigation of complex

multi-step biocatalytic reactions in homogeneous and heterogeneous media.

3. To apply the developed methods for the investigation of electron and proton transfer in reactions catalyzed by oxidoreductases.

1.2 Statements of the doctoral thesis

1. The method for the search and analysis of multiple reaction rate constants minima is applicable for the analysis of problems in chemical and biochemical kinetics.

2. The developed method allows to calculate relevant rate parameters from experimental data with greater accuracy and to model complex homogeneous and heterogeneous biocatalytic processes.

3. Immobilized on the electrode laccase from *Didymocrea* sp. J6 is reduced by direct electron transfer from the electrode to the T2/T3 active center in laccase.

4. The reduction rate of peroxidase compound II from *Coprinus cinereus* is determined by both electron and proton transfer rates.

5. The transfer of electron and proton in reactions catalyzed by peroxidases is explained by Marcus theory of electron transfer and nonadiabatic internal proton transfer model.

1.3 Scientific novelty of the thesis

1. An algorithm and software were developed for a general chemical and biochemical kinetics data fitting and modeling, which allows the investigation of catalytic systems of interest efficiently and with less experimental effort.

2. It was shown that laccase from *Didymocrea* sp. J6 on the electrode is reduced by the direct electron transfer from the electrode to the T2/T3 center. This electron transfer route is weakly inhibited by fluoride ions and allows to achieve a higher oxygen electroreduction potential of the laccase electrode.

3. The reduction of *Coprinus cinereus* peroxidase compound II is composed of two resolvable elementary steps – electron and intramolecular proton transfers

4. The rate of *Coprinus cinereus* peroxidase compound II reduction is limited by both electron and proton transfer steps. The rates of these steps are described by Marcus electron transfer and intramolecular proton transfer theories.

1.4 Contributions of the author

All homogeneous kinetics experiments, viscosity measurements and electrochemical measurements of reduction potentials of substrates were carried out by the author. Laccase biocathode design, fabrication and measurements were carried out by dr. Dalius Ratautas and dr. Marius Dagys. Spectroelectrochemical titrations of the laccase were performed by dr. Marius Dagys and prof. dr. Sergey Shleev. Modeling of systems, data analysis, quantum calculations, derivation of equations and the development of a method for calculations of reaction rate parameters were carried out by the author with the supervision and expertise provided by the thesis consultant prof. habil. dr. Juozas Kulys. The developed method was implemented into the software package "rModeler" by Justinas V. Daugmaudis and Audrius Laurynėnas. All publications were prepared in close cooperation between all the co-authors.

2 MATERIALS AND METHODS

2.1 Chemicals

Laccase from *Didymocrea sp*. J6 (LAC) and quinoprotein D-glucose dehydrogenase from *Acinetobacter calcoaceticus* LMD (LMD) were kindly provided by R. Meškys (Vilnius university Institute of Biochemistry, Lithuania, concentrations of enzymes were determinated by using Lowry method(Lowry et al., 1951)). Recombinant *Coprinus cinereus* peroxidase (CiP) is a product of Novo Nordisk A/S, Denmark. Chicken intestinal phosphatase was acquired from REANAL, Hungary. Enzymes in experiments were used without any additional purification.

Promazine hydrochloride (PZ, 98% purity), chlorpromazine hydrochloride (CPZ, 98% purity), 4-nitrophenyl phosphate di-sodium salt hexahydrate (PNP, 99% purity), hydrochloric acid (37%), sulfuric acid (97%), N,N,N′,N′-tetramethyl-p-phenylenediamine dihydrochloride (TMPD, 97% purity), d-glucose (99.5%) were purchased from Sigma-Aldrich; acetonitrile for chromatography, 2,6-dichlorophenolindophenol sodium salt (DCPIP, 98% purity) were purchased from Merc; 2,2'-azino-bis-(3-ethylbenzthiazoline-6-sulfonic acid) disodium salt (ABTS, 98% purity) and syringaldazine (SYR, 97% purity) were purchased from Fluka; sodium dihydrogenphosphate and di-sodium hydrogen phosphate, potassium dihydrogenphosphate and di-potassium hydrogen phosphate, hydrogen peroxide 30% solution, citric acid, sodium sulfate, potassium ferrocyanide and potassium hydroxide were purchased from Roth; sodium fluoride from Penta, Czech Republic; TRIS free base was acquired from BIO-RAD; variamine blue (VB), thionine (TH) and methylene blue (MB) (Reachim) were purified with activated charcoal (Sigma) and recrystallized before use (Armarego and Chai, 2013). 1-(N,N-dimethylamine)-4-(4-morpholinyl)benzene (AMB) and 1,4-di(4-morpholinyl) benzene (DMB) were synthesized at the University of Copenhagen (Buch-Rasmussen et al., 1992). 10-(2-hydroxyethyl) phenoxazine (HEPX) and 3-(4a,10a-dihydro- phenoxazin-10-yl)-propane-1-sulfonic acid (PPSA) were synthesized in Novo Nordisk A/S, Denmark. Structures of complex organic molecules used in measurements are depicted in figure 2.1.

Buffer solution for peroxidase experiments was made by mixing 50 mM K_2HPO_4 and 50 mM KH_2PO_4 solutions; TRIS buffer for alka-

line phosphatase was made by titration of TRIS 50 mM solution with hydrochloric acid. Buffer solution for laccase was made from 50 mM Na_2HPO_4 and 0.2 M Na_2SO_4 and adjusted to required pH with citric acid. InoLab pH-meter and SenTix glass pH electrode was used to adjust the required pH of buffer solutions used. Experiments of 4-nitrophenyl phosphate hydrolysis were carried out in pH 8.5 50 mM TRIS buffer solutions. Substrates for enzymatic reactions were dissolved in methanol (SYR, AMB, DMB, HEPX, VB) or deionized water (DCPIP, ABTS, PPSA, TMPD, CPZ, PZ, TH, MB, PNP). H_2O_2 solutions were prepared from a stock solution (30 %) and were verified spectrophotometrically at $240\ \mathrm{nm}$ by using the molar absorbance $43.6\ \mathrm{M^{-1}cm^{-1}}$(Hildebrandt and Roots, 1975). The Concentration of CiP was determinated spectrophotometrically at 405 nm using the molar absorbance $1.08\ \mathrm{M^{-1}cm^{-1}}$(Farhangrazi et al., 1994a; Dunford, 1991). Deionized water ($18.2\ \mathrm{M\Omega\ cm^{-2}}$) was used for preparation of all the solutions used in research.

Molar absorbances for oxidized substrates SYR, AMB, DMB, HEPX, DCPIP, ABTS, PPSA, TMPD, CPZ, PZ, PNP were referred from literature. VB, TH, MB had their molar absorbances after purification determinated by spectrophotometrical titration.

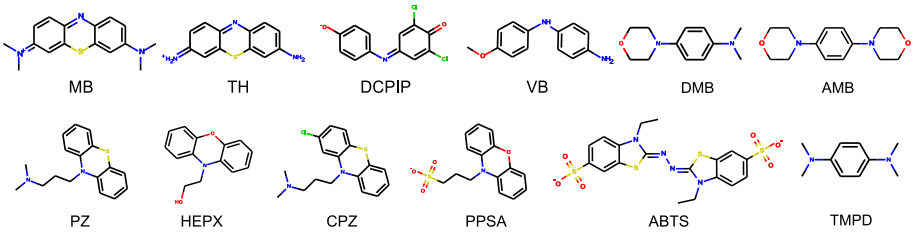

Figure 2.1: Structures of complex organic compounds

2.2 Physicochemical methods of reaction rate and standard reduction potential determination

2.2.1 Spectrophotometric methods

Spectrophotometric measurements of reaction kinetics and absorbances were carried out in thermostated spectrophotometer (Nicolet Evolution 300, USA) or by using a stopped-flow spectrophotometer (Otsuka 401-RA, Japan; Lauda 3M thermostat, Germany). In all the measurements quartz cuvette (optical path length $1.00\ \mathrm{cm}$) was used.

Phosphatase concentration in 4-nitrophenyl phosphate hydrolysis experiments was $5\ mg/ml$. The concentration of 4-nitrophenyl phosphate (PNP) was varied from $5\ \mu\mathrm{M}$ to $150\ \mu\mathrm{M}$. Experiments were carried out in pH 8.5 50 mM TRIS buffer solutions. The hydrolysis of PNP was monitored spectrophotometrically at $\lambda = 405\ \mathrm{nm}$ at $25 \pm 0.1\ ^{\circ}\mathrm{C}$.

Laccase kinetics measurements were carried out in pH 4.0, 5.5 and 7.4 50 mM $\mathrm{Na_2HPO_4}$ and 0.2 M $\mathrm{Na_2SO_4}$ phosphate-citrate buffer solutions in a thermostated spectrophotometric cell at $25 \pm 0.1^{\circ}\mathrm{C}$. The concentration of oxygen in buffer solutions was assumed to be as $253\ \mu\mathrm{M}$ (Weiss, 1970). Laccase concentrations in experiments were $8\ \mathrm{nM}$ at pH $4.0 \div 5.5$ and $55\ \mathrm{nM}$ at pH 7.4. Potassium ferrocyanide and sodium fluoride concentrations were varied from $22\ \mu\mathrm{M}$ to $197\ \mu\mathrm{M}$ and from $116\ \mu\mathrm{M}$ to $0.1\ \mathrm{M}$, respectively. ABTS concentrations were varied form $3.75\ \mu\mathrm{M}$ to $30\ \mu\mathrm{M}$. $\mathrm{K_4[Fe(CN)_6]}$ oxidation was monitored by formation of potassium ferricyanide at $\lambda = 420\ \mathrm{nm}$ and $\epsilon = 1\ \mathrm{mM^{-1}cm^{-1}}$. ABTS oxidation was monitored by the formation of radical cation at $\lambda = 420\ \mathrm{nm}$ and $\epsilon = 36\ \mathrm{mM^{-1}cm^{-1}}$.

Peroxidase concentration in experiments were varied over a range from nanomolar to micromolar concentrations, hydrogen peroxide concentrations in experiments with other substrates were around $\sim 110\ \mu\mathrm{M}$ and in all cases were determinated spectrophotometrically after the solutions were made. The only exception, when $\mathrm{H_2O_2}$ concentration was larger than $110\ \mu\mathrm{M}$, was the oxidation of CiP resting state to CiP Cpd I. Measurements were carried out at $\lambda = 405\ \mathrm{nm}$ and experiments repeated for at least 10 times. Mean absorbance change over time was fitted directly into the reaction scheme eq. 1.40, using extinction coefficients 109 $\mathrm{mM^{-1}cm^{-1}}$, 109 $\mathrm{mM^{-1}cm^{-1}}$ and 66 $\mathrm{mM^{-1}cm^{-1}}$ for reduced, intermediate and oxidized enzyme forms, respectively. Initial concentrations of the enzyme were calculated from the first curve point (~0.850 $\mu\mathrm{M}$), hydrogen peroxide concentration was 4.09 $\mu\mathrm{M}$.

AMB, DMB, HEPX, DCPIP, ABTS, PPSA, TMPD, CPZ, PZ, VB, TH, MB oxidations with CiP experiments were carried out in pH $7.00\ 50\ \mathrm{mM}$ phosphate buffer solutions in a range of temperatures from $10^{\circ}\mathrm{C}$ to $30^{\circ}\mathrm{C}$. Data from these experiments were used to estimate a reaction rate constant dependence on the temperature and to calculate free energy of activation. In order to eliminate various possible side reactions, concentrations of CiP and substrates were selected to complete the reaction in

less than $30\ \mathrm{s}$. Stopped-flow spectrophotometric measurements were repeated for up to 20 times, the outliers arising in initial cuvette filling with solutions or other random glitches were discarded and the average kinetic curve was analyzed. In the cases of AMB, DMB, HEPX, ABTS, PPSA, TMPD, CPZ, PZ, VB, substrate and H_2O_2 solutions were contained in one syringe and the solution of CiP in the other. Experiments with DCPIP, TH and MB were more complicated due to the oxidized state of these compounds. These compounds were investigated under anaerobic conditions in solutions deaerated with argon. Reduced forms of DCPIP, TH and MB were produced by the reduction of compounds with glucose catalyzed by LMD. The LMD concentration was selected such that the presence of the enzyme in a reaction mixture does not influence CiP reaction rates over short time intervals. Typical the reduction half-time was $3 - 4\ \mathrm{min}$. An oxidation of substrates catalyzed by CiP kinetic curves were measured at wavelengths summarized in table 2.1. Listed molar absorption coefficients were used for data fitting.

2.2.2 Electrochemical methods

Electrochemical experiments were performed with Series G™ 750 Potentiostat/Galvanostat/ZRA from Gamry Instruments, Inc. (Warminster, PA, USA) in a thermostated ($25 \pm 0.1\ ^\circ\mathrm{C}$) three electrode cell ($5\ \mathrm{ml}$) under anaerobic conditions in a Faraday cage. Before each measurement all solutions were purged with argon. The reference electrode was Ag | AgCl | 3 M KCl and a platinum wire served as the auxiliary electrode (all from BASi West Lafayette, IN, USA). 50 mM phosphate buffer solutions, pH 7.00, were used as working buffer solutions. Glassy carbon (GC, $d = 3\ \mathrm{mm}$) and gold (Au, $d = 1.6\ \mathrm{mm}$) disk electrodes from BASi West Lafayette, IN, USA were used as working electrodes.

Gold electrodes were polished using alumina paste (0.3 µm diameter from Buehler (Lake Bluff, IL, USA)), ultra-sonicated in deionized water for 10 min, rinsed with water, and cleaned by 30 electrochemical oxidation-reduction cycles in $50\ \mathrm{mM}$ KOH solution between 0 and -2.0 V vs. NHE at a scan rate of $0.3\ \mathrm{Vs}^{-1}$ and in 0.5 M sulfuric acid between 0 and 1.9 V vs. NHE at a scan rate of $0.3\ \mathrm{Vs}^{-1}$(Fischer et al., 2009). Glassy carbon electrodes were polished using alumina paste (0.3 µm diameter from Buehler (Lake Bluff, IL, USA)), ultra-sonicated in acetonitrile for 10 min, then ultra-sonicated in deionized water for 10 min, rinsed with

Table 2.1: Molar absorption coefficients and absorbance maxima for investigated compounds.

Compound	Absorbance maximum	Molar absorbance	Remarks
ABTS	420 nm	$3.6 \times 10^4 \mathrm{M}^{-1}\mathrm{cm}^{-1}$ (Childs and Bardsley, 1975)	radical cation
AMB	604 nm	$9.8 \times 10^3 \mathrm{M}^{-1}\mathrm{cm}^{-1}$ (Kulys et al., 1994)	radical cation
MB	665 nm	$6.41 \times 10^4 \mathrm{M}^{-1}\mathrm{cm}^{-1}$*	fully oxidized
CPZ	514 nm	$8.9 \times 10^3 \mathrm{M}^{-1}\mathrm{cm}^{-1}$ (Kulys et al., 2000)	radical cation
DCPIP	600 nm	$1.83 \times 10^4 \mathrm{M}^{-1}\mathrm{cm}^{-1}$ (Armstrong, 1964)	fully oxidized
DMB	618 nm	$9.8 \times 10^3 \mathrm{M}^{-1}\mathrm{cm}^{-1}$ (Kulys et al., 1994)	radical cation
HEPX	524 nm	$16.0 \times 10^3 \mathrm{M}^{-1}\mathrm{cm}^{-1}$(Kulys et al., 2000)	radical cation
PNP	405 nm	$18.3\ \mathrm{mM}^{-1}\mathrm{cm}^{-1}$(Bowers et al., 1980)	hydrolysis product
PPSA	524 nm	$16.0 \times 10^3 \mathrm{M}^{-1}\mathrm{cm}^{-1}$(Kulys et al., 2000)	radical cation
PZ	514 nm	$8.9 \times 10^3 \mathrm{M}^{-1}\mathrm{cm}^{-1}$(Kulys et al., 2000)	radical cation
SYR	530 nm	$6.5 \times 10^5 \mathrm{M}^{-1}\mathrm{cm}^{-1}$(Bauer and Rupe, 1971)	fully oxidized
TMPD	611 nm	$1.2 \times 10^4 \mathrm{M}^{-1}\mathrm{cm}^{-1}$(Nickel et al., 1979)	radical cation
TH	600 nm	$6.07 \times 10^4 \mathrm{M}^{-1}\mathrm{cm}^{-1}$*	fully oxidized
VB	455 nm	$5.8{\times}10^3 \mathrm{M}^{-1}\mathrm{cm}^{-1}$*	fully oxidized

* Determinated in this work.

water. Electrodes were cleaned before each measurement by procedure described above. Before each experiment a baseline were recorded.

All experiments were performed in a cyclic voltammetry mode with varying scan rates and bounds. Concentrations of compounds varied from tens micromolar (for compounds with poor solubility) to milimolar range (for compounds with good solubility). ABTS, PZ, CPZ, HEPX, VB, TH, MB and DCPIP cyclic voltammgrams were recorded on glassy carbon electrode. SYR, AMB, TMPD, DMB, PPSA cyclic voltammgrams were recorded on gold electrode. Cyclic voltammgrams were used to

estimate standard reduction potentials vs. Ag | AgCl | 3 M KCl (0.21 V vs. NHE). When experiment resulted in a quasi-reversible process with the oxidation and reduction current peaks well-formed, the reduction potential was estimated as:

$$E^0 = \frac{E_c + E_a}{2} \tag{2.1}$$

Where E_c is the potential of cathodic peak and E_a is the potential of anodic peak.

Experiments with **enzymes adsorbed on the rotating disk electrodes** were performed by dr. Dalius Ratautas and spectroelectrochemical titrations of laccase were performed by dr. Marius Dagys and prof. dr. Sergey Shleev, therefore only data and mathematical modeling is presented in the thesis.

2.3 Description of chemical and biochemical reactions with differential equations

2.3.1 Rate equations for homogeneous chemical and biochemical reactions

Every reaction mechanism could be represented or approximated by a reaction scheme as in Michaelis-Menten example (a recent translation of this seminal paper (Johnson and Goody, 2011)):

$$\begin{array}{ccc} E + S & \underset{k_{-1}}{\overset{k_1}{\rightleftharpoons}} & ES \\ ES & \overset{k_{cat}}{\rightarrow} & E + P \end{array}, \tag{2.2}$$

Where E is an enzyme, S – substrate, ES – enzyme-substrate complex and P –product.

The general representation of any reaction scheme is described by a system of coupled chemical reactions, where bidirectional reactions are split into unidirectional reactions:

$$\sum_{n=1}^{N} \xi_i \gamma_{n,i} A_n \overset{k_i}{\rightarrow} \sum_{n=1}^{N} \xi_i \gamma'_{n,i} A_n, \; i = 1 \dots I, \tag{2.3}$$

Where A_n are reagents participating in a reaction scheme, $\gamma_{n,i} \geq 0$ and $\gamma'_{n,i} \geq 0$ are stoichiometric coefficients for an i_{th} reaction and $\xi_i \in \{-1, +1\}$ $i = 1 \dots I$ are progress variables, which represent a reaction

direction after splitting bidirectional reactions. From the reaction scheme 2.3 the stoichiometric matrix $\mathbf{\Omega}$ is constructed as follows:

$$\mathbf{\Omega} = \begin{bmatrix} \xi_1 \left(\gamma'_{1,1} - \gamma_{1,1}\right) & \dots & \xi_1 \left(\gamma'_{N,1} - \gamma_{N,1}\right) \\ \vdots & \ddots & \vdots \\ \xi_I \left(\gamma'_{1,I} - \gamma_{1,I}\right) & \dots & \xi_I \left(\gamma'_{N,I} - \gamma_{N,I}\right) \end{bmatrix}, \tag{2.4}$$

The rate equations vector $\mathbf{V}$, which represents the rate of each reaction in terms of the participating reagents and the rate constant, is constructed accordingly:

$$\mathbf{V} = \begin{bmatrix} k_1 \prod_{\substack{n=1 \\ \gamma_{n,i}>0}}^{N} A_n^{\gamma_{n,1}} \\ \vdots \\ k_I \prod_{\substack{n=1 \\ \gamma_{n,i}>0}}^{N} A_n^{\gamma_{n,I}} \end{bmatrix}. \tag{2.5}$$

Then the system of differential equations, representing the reaction scheme 2.3, is defined as:

$$\frac{d\mathbf{A}}{dt} = \mathbf{\Omega}\mathbf{V}. \tag{2.6}$$

This system of differential equations is the starting point for further manipulations such as *a priori* application of a quasi steady state assumptions or a direct integration (numerical or analytical, depending on the solvability of a system).

In most of biochemical experiments concentrations of enzymes are much smaller than concentrations of substrates. These conditions frequently validates the use of the quasi-steady assumption. Quasi-steady conditions results in a dimensional reduction of reaction rate constants and in a simplification of differential equations in a system of interest. It is generally treated with these assumptions:

1. All forms of enzyme ($\{Enz_1,\ Enz_2 ... Enz_i\}$) should be accounted for in the reaction scheme 2.3.

2. At least one catalytic cycle between forms of enzyme should exist.

3. At least one common substrate in multiple catalytic cycles of an enzyme should exist. Terms of non-ezymatic side reactions are

omitted, the simplest equation rate equation of a substrate consumption or a product production is selected.

4. In any reaction in the reaction scheme eq. 2.3 the enzyme term should appear only once on both sides.

Under these preconditions, from eq. 2.6 a subset of differential equations ($\{dEnz_1/dt,\ dEnz_2/dt...dEnz_i/dt\}$), governing a time course of enzyme forms is extracted. Setting each equation to zero:

$$\{dEnz_1/dt,\ dEnz_2/dt...dEnz_i/dt\} = 0 \tag{2.7}$$

Leads to a system of algebraic equations linear with respect to enzyme forms $\{Enz_1,\ Enz_2...Enz_i\}$, which, with the auxiliary equation:

$$\sum_{i=1}^{J} Enz_i = Enz_0 \tag{2.8}$$

Where Enz_0 is an initial concentration of an enzyme, leads to analytical equations for each form of an enzyme with respect to rate constants and concentrations of substrates, participating in catalytic cycle. These equations are substituted in the rate equation for a substrate. From this equation general reaction rate parameters are extracted as combinations of rate constants defined in the reaction scheme 2.3.

2.3.2 Mathematical model of the electrode reactions

Electrochemical reactions occurring on electrode are surface-liquid interface reactions and should be modeled by a different mathematical apparatus than homogeneous reactions described above (partial differential equations vs. ordinary differential equations). These reactions could be accompanied by a homogeneous component as well. The general system of differential equations 2.6 should be rewritten in a way to account for a diffusion component too (one dimensional case applicable for disk electrodes):

$$\frac{\partial \mathbf{A}(x,t)}{\partial t} = \mathbf{\Omega V} + \mathbf{D}\frac{\partial^2 \mathbf{A}(x,t)}{\partial x^2} \tag{2.9}$$

Where $\mathbf{D}$ is a vector of corresponding diffusion constants. However, this equation describes only homogeneous processes that include diffusion. It is extended to electrode reactions domain by adding a subset

of reactions, which occur on electrode and generally are described as a system of the electrode reactions:

$$\frac{\partial \mathbf{B}(x,t)}{\partial x}|_{x=0} = \mathbf{\Omega}'\mathbf{V}' \tag{2.10}$$

Where $\mathbf{B}$ could be a subset of $\mathbf{A}$ or only constitute species interacting with $\mathbf{A}$. In the equation 2.10 some subset of reactions are electron transfer reactions between reagents and an electrode. For them current is described as:

$$i(t) = FA \sum_{m=1}^{M} n(k_{f,m}C_{O,m}(0,t) - k_{r,m}C_{R,m}(0,t)), \tag{2.11}$$

Here F is Faraday constant, A – electrode surface area, M – number of electrode reactions of general electrode reaction in form:

$$O + n\overline{e} \underset{k_b}{\overset{k_f}{\rightleftharpoons}} R \tag{2.12}$$

Where O represents oxidized species and R represents reduced species, k_f is a reduction and k_b is an oxidation rate constants on a surface. Rate constants k_f and k_b, mostly (relatively fresh extension in a framework of Marcus electron transfer theory are Marcus-Hush-Chidsey equations (CHIDSEY, 1991)), are described by Butler-Volmer model(Bard and Faulkner, 2000; Butler, 1924):

$$\begin{cases} k_f = & k_0 e^{-\alpha(E-E^0)\frac{nF}{RT}} \\ k_b = & k_0 e^{(1-\alpha)(E-E^0)\frac{nF}{RT}} \end{cases} \tag{2.13}$$

Where E^0 is a standard reduction potential, E – potential applied to a working electrode, R – gas constant, T – temperature, n – number of electrons participating in a reaction 2.12, F – Faraday constant, α – charge transfer coefficient and k_0 – rate constant of a surface reaction at $E^0 = E$. With initial concentrations and distributions of reagents over coordinate x, this is the general framework for the analysis of electrochemical data.

2.4 Numerical integration and optimization methods

2.4.1 The method of least squares

All the data fitting is done in the framework of least squares method. Let's assume we have a set of measured data points, which are ordered in vectors $\{x_0,\ x_1,\ x_2,\ ...,x_n\ ,y_i\}$, where $\mathbf{x}_i = \{x_0,\ x_1,\ x_2,\ ...,x_n\}$ are independent variables, set in an experiment as parameters or initial conditions which is known, and y_i is an outcome of the experiment. Suppose a model, represented by function $f(\mathbf{x}_i)$ with unknown parameters, exists. Then the distance of experiment data points from a model is described as:

$$S = \sum_{i=1}^{N} (y_i - f(\mathbf{x}_i))^2 \tag{2.14}$$

This equation is adequate to fit one curve to some model of interest. The coefficient $1/n$ in the formula below transforms the least squares sum to the statistical data set property variance as defined in(Papoulis and Pillai, 2002) and accounts for multiple data sets and different sizes of data sets:

$$\sigma^2 = \frac{1}{N}\sum_{i=1}^{N}(y_i - f(\mathbf{x}_i))^2 \ and\ S` = \sum_{i=1}^{k}\sigma_i^2 \tag{2.15}$$

Minimization of $S`$ function, where k is the number of independent experiments, with respect to unknown parameters results a fitted model with know parameters. However, the success of fitting procedure depends on choice of an optimization method and an initial guess of parameters to be optimized.

2.4.2 The numerical integration algorithm

LSODA numerical integration algorithm was used for all numerical integrations in homogeneous kinetics and electrode reactions. Systems of differential equations were directly passed to LSODA in homogeneous kinetics cases. Partial differential equations, used to model electrode processes, were discretized by method of lines(Schiesser, 2012) due to stability of method in contrast to Crank-Nicolson scheme(Crank and Nicolson, 1947). LSODA was selected over more traditional Runge-

Kutta 4th order integration algorithm due to its stability, robustness, efficiency and ability to cope with stiff differential equations (which is an Achilles heel of Runge-Kutta integration algorithm). Main idea behind LSODA numerical integration algorithm is the ability to detect stiffness of differential equations on the fly and select numerical algorithms for stiff and non-stiff systems of differential equations. For stiff systems BDF (Backward differentiation formulas) up to 5th order is used. For non-stiff systems Adams integration method up to 12th order is used. This makes LSODA an universal algorithm for numerical integration purposes(Petzold, 1983).

2.4.3 The numerical optimization algorithms

All the data fitting problems heavily depend on optimization algorithms. Diversity of problems and tasks naturally forced the creation of a variety of optimization methods. Ones described further are particularly handy in data fitting due to their specific properties.

Powell optimization algorithm is a relatively slow quadratically-convergent algorithm, whose exceptional feature is indifference to derivatives. The algorithm is based on simple idea of line search in some directions. The algorithm starts with some initial guess of parameters to be fitted $\mathbf{p}_0$ and some initial search direction vector $\mathbf{u}_i$, which is initialized as unit vector. Search is performed as a linear movement of point along separate vector components until function of interest stops decreasing on some point $\mathbf{p}_1$. At this point new search directions are calculated as $\mathbf{u}_n = \mathbf{p}_{n-1} - \mathbf{p}_{n-2}$ until a desired convergence is achieved(Powell, 1964).

Nelder-Mead or downhill simplex method is another optimization method capable optimizing nonlinear functions with unknown derivatives in a multidimensional parameter space. This algorithm starts with some initial guess of points $\mathbf{p}_0$, which are ordered by increase of $f(\mathbf{p}_0)$. Then a centroid $\mathbf{p}_c$ of set of points $\mathbf{p}_0$ minus worst point is calculated. At this stage the algorithm decides whether it should replace the worst point with new one calculated from centroid, or should it increase/decrease the search radius (Nelder and Mead, 1965).

BFGS or Broyden–Fletcher–Goldfarb–Shanno algorithm is an approximate Newton method, which uses a gradient of function with respect to parameters, but does not need a hessian matrix. It is an approximated from gradients at different points instead and is updated in the course

of optimization. This method is a valuable tool for search of stationary points of function, where hessian matrix computation is too costly to perform (Avriel, 2003).

2.5 Quantum and molecular mechanics calculations

2.5.1 Docking of substrates into the active site of enzymes

Docking of substrates in the active site of enzyme are performed with Autodock Vina software. Autodock Vina is a relatively new software tool for enzyme-substrate complex structure prediction. It performs much better in terms of binding energy accuracy and geometry of enzyme-substrate complex, in comparison to the older Autodock version. It is based on an approximate and parameterized force field taken from molecular mechanics and weights for separate forces such as Van der Waals or Coulomb. Software is simple to use and input requirements are reduced to a structure of an enzyme and substrate, and a plausible location of an active center. However, binding energies or structures calculated by Autodock Vina should not be taken for granted - the software serves merely as a starting point for further refinement and calculations(Trott and Olson, 2010).

2.5.2 Molecular structure calculations using quantum mechanics methods

Molecular structures of modeled compounds were build from SMILEs, modified manually to reflect various possible protonation states of neutral and radical species. Initial refinements were performed with the GAFF(Wang et al., 2004) force field which is a part of Avogadro molecular structure visualization package. Structures optimized with GAFF were further optimized with the semi-empirical AM1 method, then reoptimized with the Hartree-Fock (HF) method and MINI basis set, further refined with HF 6-31+G(d,p) basis set.The RHF wave function was used for singlet and the ROHF wavefunction was used for doublet species. This level of theory widely accepted as "The Pauling point", where errors of HF approximation an relatively small basis set compensate each other. At this level of theory zero point energies were calculated for structures (in all cases hessian indicated stationary state of molecule). The calculations of energies were performed with density functional theory (DFT) hybrid B3LYP functional and 6-31+G(d,p) basis

set, RHF wave function for singlet species and ROHF wavefunction for doublets. Calculations were performed both in vacuum and using PCM(Li and Jensen, 2004) solvation model. These calculations were performed with Gamess-US software package (Schmidt et al., 1993).

2.5.3 Standard reduction potential calculations

Standard reduction potential calculations for radicals were performed using the B3LYP/6-31+G(d,p) energy of at B3LYP/6-31+G(d,p) level optimized structures in PCM solvation model and the zero point energy calculated at HF/6-31+G(d,p) level. Calculations were performed using the thermodynamic cycle for radicals(Fu et al., 2005):

$$\begin{array}{ccccc} A_g^{ox} & + & e_g & \overset{\Delta G_g}{\rightarrow} & A_g^{red} \\ \uparrow{\scriptstyle \Delta G^{ox}_{desolv}} & & \uparrow{\scriptstyle \Delta G^{e}_{desolv}} & & \downarrow{\scriptstyle \Delta G^{red}_{solv}} \\ A_{aq}^{ox} & + & e_{aq} & \overset{\Delta G_{aq}}{\rightarrow} & A_{aq}^{red} \end{array} \tag{2.16}$$

Where $\Delta G^{e}_{desolv} = 35.5\,\mathrm{kcal/mol}$ (Chang-Guo Zhan* et al., 2003). From the thermodynamic cycle 2.16 follows:

$$\Delta G_{aq} = \Delta G^{ox}_{desolv} + \Delta G_g + \Delta G^{red}_{solv} + \Delta G^{e}_{desolv} \tag{2.17}$$

However, these calculations are referred to $1\ atm$ standard state and transition to $1\ \mathrm{M}$ standard state is guided by:

$$\Delta G(1M) = \Delta G(1\ atm) + RT \ln 24.46 \tag{2.18}$$

The absolute standard reduction potential is calculated as:

$$E^0 = -\frac{\Delta G}{F} \tag{2.19}$$

Which could be converted to the standard reduction potential vs. NHE by using the adjustment value of $4.43\ \mathrm{V}$ (Reiss and Heller, 1985):

$$E^0(vs.\ NHE) = E^0 - 4.43 \tag{2.20}$$

For cases of two electron reduction, the standard reduction potential is calculated as a mean of standard potentials of two separate one electron reduction steps.

Calculation of reorganization energies in solvent. Reorganization

energies of substrates were calculated using the quantum mechanical reorganization energy estimation method with solvation model(Bader et al., 1997):

$$\lambda = (\lambda_1 + \lambda_2)/2,$$
$$where: \ \lambda_1 = E(A \ at \ A^+) - E(A \ at \ A) \ and$$
$$\lambda_2 = E(A^+ \ at \ A) - E(A^+ \ at \ A^+) \quad (2.21)$$

Where, λ_1 represents solvent and inner reorganization energy of oxidation process and is calculated as the energy of a reduced molecule at geometry of an oxidized molecule; λ_2 represents the reorganization energy of the opposite process.

2.5.4 The rate constant of proton transfer

The multistate nonadiabatic rate constant of proton transfer is described as (Borgis and Hynes, 1996):

$$k_p = \sum_n \sum_m P_n \frac{V_{nm}^2}{\hbar} \sqrt{\frac{\pi}{\lambda_p k_B T}} \exp\left(-\frac{\Delta G_{nm}^{\ddagger}}{k_B T}\right) \quad (2.22)$$

$$\Delta G_{nm}^{\ddagger} = \frac{(\Delta G_p + E_m - E_n + \lambda_p)}{4\lambda_p} \quad (2.23)$$

Here P_n is a probability (from Boltzmann distribution) of transition from n-th reactant state, V_{nm} a vibrational coupling between reactant and product wavefunctions, λ_p a reorganization energy of proton transfer; E_n and E_m energies of reactants and products in states n and m, respectively. The energies and overlap integrals can be calculated using harmonic oscillator potential approximation with resulting wave functions(Piela, 2013):

$$\psi_n(x) = \frac{e^{-\frac{1}{2}x^2\sqrt{\frac{k\,m_p}{\hbar^2}}} \sqrt{\frac{2^{-n}\sqrt[4]{\frac{k\,m_p}{\hbar^2}}}{n!}} H_n\left(x\sqrt[4]{\frac{k\,m_p}{\hbar^2}}\right)}{\sqrt[4]{\pi}} \quad (2.24)$$

where k is a force constant associated with reorganization energy ($k = 2\lambda/\delta x^2$) and m_p is a mass of proton. The vibronic coupling integrals is calculated as described in (Farazdel et al., 1990):

$$V_{nm} = \frac{H_{nm} - \frac{S_{nm}(H_{nn}+H_{mm})}{2}}{(1 - S_{nm})^2} \tag{2.25}$$

where S_{nm} is overlap integral between wave functions $\psi_n(x)$ and $\psi_m(-x + \delta x)$ ($S_{nm} = \langle \psi_n(x) | \psi_m(-x + \delta x) \rangle$). The matrix elements are calculated as:

$$H_{nm} = \left\langle \psi_n(x) | \widehat{H} | \psi_m(-x + \delta x) \right\rangle$$

3 CALCULATION OF REACTION RATE PARAMETERS FOR COMPLEX BIOCHEMICAL REACTIONS

This part of the thesis is dedicated to the (bio)chemical kinetics modeling and experimental data fitting. The biochemical kinetics modeling and experimental data fitting are the cornerstones in any quantitative approach to the enzymatic catalysis, because they provide the necessary rate parameters. These parameters can be further used for a design of industrial processes or for an interpretation and understanding of a mechanisms of a catalysis. In this part, we review the historical perspective and development in these fields, describe, according to our perspective, the pitfalls of current state of art, and suggest the means to ameliorate them. The suggested approach is published in the article "An exhaustive search approach for chemical kinetics experimental data fitting, rate constants optimization and confidence interval estimation", Nonlinear Analysis: Modeling and Control, Vol. 20 No. 1 (2015), and the development resulted in the (bio)chemical kinetics modeling and data fitting software Rmodeler (available at www.ubicalc.com). The algorithm described in this part is further used in the other parts of the thesis to acquire rate parameters from experiments.

3.1 Experimental data analysis challenges in the biochemical kinetics

The biochemical kinetics is a wide field dedicated to mechanisms of enzymatic catalysis. The main goal of the discipline is to describe catalytic properties of an enzyme quantitatively in terms of rate constants, a reaction schema or a reaction mechanism. The need of such description is not self-evident if one is concerned only about the fact that the enzyme converts some R (reagent) to P (product). Yet, the biochemical kinetics is necessary if one wants to rationally re-engineer an enzyme, to modify its properties for technological needs, to control the catalysis process or to understand the biological importance of an enzyme. To illustrate the problematics of biochemical kinetics, consider a simple reaction schema of enzymatic reaction:

$$S + E \underset{k_{-1}}{\overset{k_1}{\rightleftharpoons}} ES \overset{k_2}{\rightarrow} E + P \tag{3.1}$$

Here S is a substrate, E is an enzyme, ES – enzyme-substrate complex and P is a product of reaction. In the ideal case the quest of the biochemical kinetics is to deduce whether a scheme adequately describes the properties of an enzyme and to calculate all the important rate constants (as, for example in scheme above, –k_1, k_{-1} andk_2). These constants can be used to devise a technological process or to relate rate parameters further with the structure of substrates and enzymes.

The biochemical kinetics was born, possibly, as a quantitative sibling of the enzymology, which itself appeared only in first half on 19th century. And from the very beginning, the central role in the biochemical kinetics is played by the modeling and data analysis. There are few constraints for biochemical kinetics experiments in general and the most important ones are economical or physical. Economical constraints manifest themselves via availability and price of reagents. Physical difficulties arise from methods used to observe experiments, limitations of equipment, physicochemical properties of reactants. These problems are greatly ameliorated by a good design of the experiment and clever approach for data analysis.

The first steps towards the discipline, as it is seen today, were taken in seminal paper written in 1913 by Leonor Michaelis and Maud Menten(Menten and Michaelis, 1913). Despite the fact that now-famous equation of the initial rate of an enzymatic reaction is named after them, the first one who derived it was Victor Henri. However, he failed to provide correct experimental data to illustrate it(Johnson, 2013). Years later, Briggs and Haldane derived the same equation in a much more general and transparent way, which is now known as the quasi-steady state approximation. It is based on a very simple and sleek idea – the concentration of some reactants changes very little in the course of a reaction. Therefore, one can equate relevant rates to zero and greatly simplify equations. For example, in case of the reaction scheme above, relevant differential equations, which describe the reaction kinetics, are:

$$\begin{cases} \frac{d[E]}{dt} = & -k_1[E][S] + k_2[ES] + k_{-1}[ES] \\ \frac{d[ES]}{dt} = & k_1[E][S] - k_2[ES] - k_{-1}[ES] \\ \frac{d[S]}{dt} = & k_1[E][S] - k_{-1}[ES] \\ \frac{d[P]}{dt} = & k_2[ES] \end{cases} \tag{3.2}$$

Reactants, for which rates are equated to zero are ES and E. By using the quasi-steady state approximation it is possible to derive an initial rate equation for virtually any enzymatic mechanism, as long as the quasi-steady state assumption is valid(Briggs and Haldane, 1925; Menten and Michaelis, 1913). To facilitate derivations for even a simple "pen and paper" approach, a method using diagrams was devised, which now is called King-Altman method(King and Altman, 1956). Derived equations can be used further to predict outcomes of experiments and analyze data with fairly common data fitting algorithms or outdated transformations such as Lineweaver–Burk or Eadie–Hofstee plot, to name a few. From some point of view it may appear that here the story of biochemical kinetics should end. Yet, the quasi-steady state approximation has a cost. Firstly, it requires a large set of initial concentrations to be screened. It can be and sometimes is prohibitively costly. Secondly, it requires an experiment to be designed in a such way that the quasi-steady state approximation is valid. Sometimes it is impossible, for example, when only an intermediate or a short-lived reactant can be observed, or when the kinetics is complicated by a various pre-steady state kinetics or lag phases. Good examples of such cases could be the enzyme activation, when an enzyme, due to some reason, transits from an inactive to an active form, as some laccases do. By the definition, the initial rate of such reaction is zero, and the measurements of initial rates are pointless.

The alternative analysis methods, which should be more general and able to incorporate various kinetic effects, are based on the integration of differential equations governing a reaction. This approach has some limitations in the case when only analytic solution is desired, because just a handful of nonlinear differential equations has a solution. Yet, if governing equations can in some ingenious way be simplified and the explicit formula would be obtainable for an integral curve, it can be used to fit all data of the experiment to produce rate parameters. This approach is better than initial rate measurements, because it uses all the experimental information about rate parameters, not only just the initial rate. Moreover, it simplifies experiments and reduces time and resources costs, because from one experiment it is possible to reliably calculate more (or, at least the same number) parameters than from the initial rate. For example, Michaelis-Menten rate equation in principle is solvable using the special function called Lambert W function, which is

the solution of the differential equation:

$$\frac{d[S]}{dt} = -\frac{v_{max}[S]}{K_M + [S]} \tag{3.3}$$

It can be used directly to fit K_M and v_{max} parameters from an experiment curve, and it is occasionally done in a such way(Goudar et al., 2004; Goličnik, 2012). Yet, this example is not an analytic one, because Lambert W calculation is a numeric routine, which simply hides a numerical method behind a name of a special function. Actually, this can be said about every transcendental function used (sinus, exponential, logarithm to name few of them). Therefore, in this perspective, the desire for explicit formulas should be relinquished and general methods of numeric integration of differential equations should be used to numerically model and analyze kinetics of reactions.

To the best of our knowledge, the first example of rate equation numerical solver was published in 1983, and it was named KINSIM. It used Gear method for the integration of differential equations and the user was able to get simulated reaction progress curves in a matter of seconds (*sic!*). However, in the first version of the program the user was not able to carry out the optimization of the rate constants and to obtain fit of data. One was forced to simply guess rate parameters and visually inspect an outcome, until the agreement between a simulation and an experiment was obtained(Barshop et al., 1983). Of course, for some unlucky guessers, such as the author of this thesis, such data fitting experience should be a nightmare. Later the extension of KINSIM, a program called FITSIM appeared, which was able to fit rate constants for an arbitrary mechanism, and the rate parameters were optimized using Levenberg–Marquardt algorithm(Svir et al., 2002), which is a local optimum search algorithm. FITSIM greatly extended data analysis capabilities, but it was based on the user-provided guess of initial rate parameters, same as KINSIM. Therefore, the optimization problem was somewhat automated, but still dependent on the user's ability to guess rate parameters close enough to be useful for the optimization. The next improvement came by changing the integration method from Gear to LSODA, which is much more robust and it is suitable for stiff differential equations. The new iteration of data fitting programs was called DYNAFIT (Kuzmič, 2009). These programs, despite their existence and

availability, were not used very much by the scientific community, and reasons of such reluctance was never discussed in public. We believe that reasons of reluctance are the following. Firstly, a program requires to provide a working reaction schema to fit data. To obtain a plausible reaction schema, many experiments are needed, and they are typically initial rate measurements. From this perspective, it is much more easier to fit data to the apparent Michaelis-Menten equation or some variation of the theme. However, if the reaction scheme is known, it is much more practical to use the integral curve data fitting approach. Secondly, the complex reaction schema, if it is large enough, can fit virtually any experimental data. Generally, this problem can be greatly ameliorated by building up the reaction scheme from some minimal plausible case and carefully increase the complexity with strong supporting evidences for the complications of interest (use Occam's razor, speaking in a laconic way). Thirdly, one still needs to guess initial rate parameters for the optimization algorithm. The correct guess of three parameters is simple, but to guess five or six is a lottery with little chance to hit the jackpot. For these reasons, DYNAFIT ultimately received a global optimization algorithm which is a brute force enumeration and screening of all rate constants within prescribed bounds. This algorithm has limited ability to find an initial guess of rate constants, which optimization with other techniques may lead to global minimum. The price - the complexity of reaction schema exponentially increases the search space and running time.

Drawbacks of kinetics fitting programs described above are, if not published before, very familiar for practitioners in the field. However, there is an overlook of the important hypothesis on which all programs are based. It is the assumption that for every set of data and every reaction schema exists the unique global minimum of optimal reaction rate constants exists. We found that this hypothesis is not true and devised an algorithm of the kinetics analysis which uses this lack of fit uniqueness to properly analyze the data.

3.2 Results and discussion

3.2.1 Analysis of the fitting scoreof the first order reaction

The tradition of data analysis in biochemistry is based on three major methods – the initial rate analysis, the quasi-steady state approximation and the integral equation fitting. All of them depend on some optimization algorithm, which in an ideal case should result in a good data fit (if a model is correct one). However, in a practice even a simple case can be a challenge. These challenges arise from various reasons, but the main one is the necessity of an initial guess to initialize the optimization algorithm. Most of data analysis packages provide means of control of the user's initial guess. Still, the guess provided by user rarely leads to a good fit when the model is a complicated multi parametric function (as it is in most cases in biochemical kinetics). This problem can be demonstrated on a trivial case from the chemical kinetics. Suppose we have a first or pseudo-first order reaction:

$$A \xrightarrow{k} B \tag{3.4}$$

$$\frac{dA}{dt} = -kA, \quad \frac{dB}{dt} = kB \tag{3.5}$$

which can be easily converted to differential equations using the mathematical apparatus described in the section 2.3.1 and solved with initial conditions $A(0) = A_0$ and $B(0) = 0$. The kinetic curve (or integral curve) is a simple function $A(t) = A_0 e^{-kt}$. Data to this equation can be fitted by a linear regression (the equation can be linearized by logarithmation), or by a numeric optimization. The latter case is a much more general. Both approaches require the method of least squares (or some other metric) to formulate a problem of the optimal fit. We assume$A_0 = 1$, as it is a simple scaling factor. k is the actual rate constant and r is the rate constant to fit. In the context of the least squares method, the problem is recasted in to the optimization of function S (goodness of fit) with respect to r:

$$S = \int_0^T (e^{-kt} - e^{-rt})^2 dt \tag{3.6}$$

Let's replace the summation over data points by a continuous inte-

gration using:

$$\int_a^b y(x)dx \stackrel{def}{\equiv} \lim_{\delta x \to 0} \sum_{x=a}^{x=b} y(x)\delta x \tag{3.7}$$

This equation 3.6 has an analytic solution:

$$\frac{1}{2}\left(\frac{4(e^{T(-k-r)}-1)}{k+r} + \frac{1-e^{-2kT}}{k} + \frac{1-e^{-2rT}}{r}\right) \tag{3.8}$$

It depends on two variables: T – the length of experiment and r – the rate constant to fit. The behavior of a function S and its gradient with respect to r is plotted in fig. 3.1 with a selected value $k = 1$. When the experiment duration is limited to some finite value, the data fitting with an initial rate constant guess outside two orders of magnitude of an actual rate constant will result in a flat score function, and most likely the the optimal solution will not be found. However, when the measurement time is infinite, the fit could always be found if the initial guess is below the actual rate constant. Of course, in this particular case it is trivial to make a good guess, but this triviality disappears if the reaction schema consists of more rate constants. Using the insights from the case above, a better algorithm for the data fitting can be:

- The evaluation of the fitting score on a logarithmic rate constants grid, using some arbitrary selected step size (an exhaustive search approach – well known general method for solving various problems).
- The selection of some set of grid points with the best fitting score as an initial guesses for an optimization procedure.
- The optimization of selected multiple initial guesses.
- The analysis of fitted rate constants values.

3.2.2 Analysis of the complex reaction fitting score surface

To verify the behavior of the algorithm outlined above, a system of an enzymatic reactions coupled with a chemical step was selected:

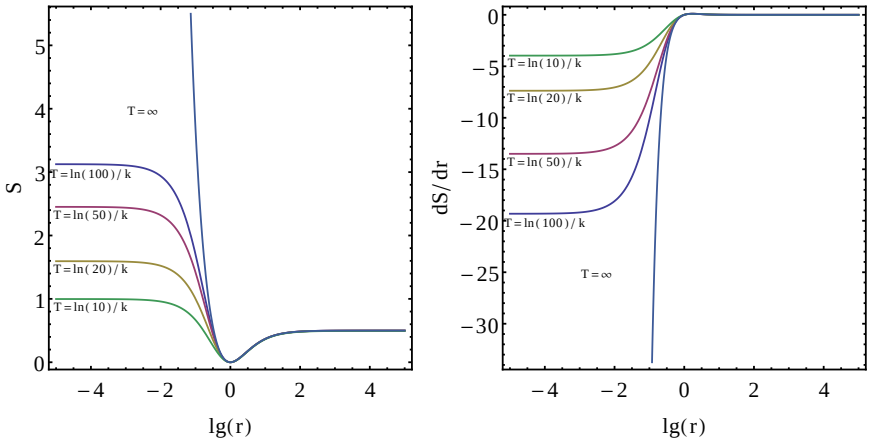

Figure 3.1: Left – S (eq. 3.8) dependence on r; right – gradient of S dependence on r with $k = 1$.

$$\begin{aligned} E_{ox} + S &\overset{k_1}{\rightarrow} E_{red} + P \\ E_{red} + M_{ox} &\overset{k_2}{\rightarrow} E_{ox} + M_{red} \\ F_{ox} + M_{red} &\underset{k_{-3}}{\overset{k_3}{\rightleftarrows}} F_{red} + M_{ox} \end{aligned} \tag{3.9}$$

In the scheme $E_{ox}$and E_{red} are oxidized and reduced forms of an enzyme, respectively,S – substrate for an enzyme regeneration and P – a reaction product. The substrate of interest and a mediator is denoted as F and M (a simplified mechanism from (Kulys et al., 2010)), respectively. Somewhat "unnatural" representation of the enzymatic catalysis as bimolecular reactions is justified by selecting initial concentrations of S and M_{ox} below than corresponding Michaelis-Menten constants. This reaction scheme is represented by a set of differential equations:

$$
\begin{aligned}
\frac{d[E_{ox}]}{dt} &= -k_1[E_{ox}][S] + k_2[E_{red}][M_{ox}] \\
\frac{d[E_{red}]}{dt} &= k_1[E_{ox}][S] - k_2[E_{red}[M_{ox}] \\
\frac{d[F_{ox}]}{dt} &= k_{-3}[F_{red}][M_{ox}] - k_3[F_{ox}][M_{red}] \\
\frac{d[F_{red}]}{dt} &= -k_{-3}[F_{red}][M_{ox}] + k_3[F_{ox}][M_{red}] \\
\frac{d[M_{ox}]}{dt} &= -k_2[E_{red}][M_{ox}] + k_3[F_{ox}][M_{red}] - k_{-3}[F_{red}][M_{ox}] \\
\frac{d[M_{red}]}{dt} &= k_2[E_{red}][M_{ox}] - k_3[F_{ox}][M_{red}] + k_{-3}[F_{red}][M_{ox}] \\
\frac{d[P]}{dt} &= k_1[E_{ox}][S] \\
\frac{d[S]}{dt} &= -k_1[E_{ox}][S]
\end{aligned}
\quad , \tag{3.10}
$$

with initial concentrations $S(0),\ P(0), E(0),\ E_{red}(0), , F(0),\ F_{red}(0),$ $M_{ox}(0)$ and $M_{red}(0)$. It is a nonlinear system of differential equations, which does not have an analytical solution. Still, it can be integrated numerically using previously the described LSODA method. The numerical integration provide means to inspect whether this system has a global minimum over various combinations of rate constants. Let's suppose that initial conditions of our test system are selected fairly realistically – $\mathrm{E_{ox}} = 10^{-9}$ M, $\mathrm{M_{ox}} = 10^{-6}$ M, $\mathrm{F_{ox}} = 10^{-4}$ M, $\mathrm{S} = 10^{-3}$ M with rate constants $\mathrm{k_1} = 10^5\ \mathrm{M^{-1}s^{-1}}$, $k_2 = 10^8\ \mathrm{M^{-1}s^{-1}}$, $k_{-3} = 10^5\ \mathrm{M^{-1}s^{-1}}$, $k_3 = 10^6\ \mathrm{M^{-1}s^{-1}}$. Other initial concentrations are set to zero. F_{ox} concentration is measured in an experiment (parameters were selected in analogy (Kulys et al., 2010; Kulys and Dapkūnas, 2007)).

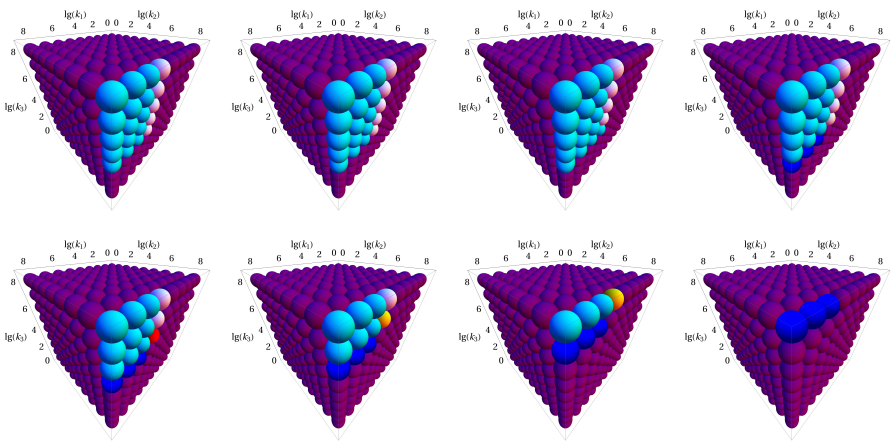

Figure 3.2: Fitting score evaluation on constants grid, from left top to right bottom $k_{-3} = \{10^0,\ 10^2,\ 10^3\ , 10^4,\ 10^5,\ 10^6,\ 10^7,\ 10^8\}$. Purple – poor, red – perfect fit.

The four-dimensional surface of the score function over a logarithmic grid is plotted in fig. 3.2. Here the grid bounds are from 1 to 10^8 and the grid itself is of9x9x9x9 size. The score function behaves in the same way as was predicted in the analysis of the simple exponential case. As in the previous case, the surface of the score function is flat when rate parameters are an order of magnitude away from actual rate constants. This behavior results in the paradox of data analysis – researcher should know values of parameters (in accuracy of order of magnitude) in order to be able to fit them. The proposed algorithm solves the problem, at least in this case, without the need of guess. The only needed input in this case is a reasonable range of rate constants to scan. However, this example is an idealistic one, because the search grid itself has a minimum point. A more complex test set was investigated with six cases and different combinations of rate constants (values listed in table 3.1). It was found that approximately 3^k points with a minimal score should be selected for the further optimization as initial values. The optimization was performed with Powell method and for all initial guesses optimization reached convergence criteria and terminated normally. Best and worst solutions are listed in the table 3.1 with corresponding score values.

Table 3.1: Fitting constants for one kinetic curve (coarse 9x9x9x9 grid). Initial concentrations: $E_{ox} = 10^{-9},\ M_{ox} = 10^{-6},\ F_{ox} = 10^{-4},\ S = 10^{-3}$.

Case	Rate constants used to generate test data $\lg(k_1)\ \lg(k_2)\ \lg(k_3)\ \lg(k_{-3})$	Worst Solution	Best solution
#1	6.3 7.3 6.3 5.3	$S = 1.63 * 10^{-10}$ 8.00 8.00 7.23 8.00	$S = 3.35 * 10^{-21}$ 6.30 7.30 8.00 7.00
#2	5.3 7.3 6.3 5.3	$S = 1.70 * 10^{-10}$ 8.00 8.00 7.18 8.00	$S = 6.81 * 10^{-17}$ 5.52 7.28 8.00 6.99
#3	5.3 6.3 6.3 5.3	$S = 2.22 * 10^{-10}$ 7.75 8.00 6.11 8.00	$S = 2.11 * 10^{-19}$ 5.32 6.30 6.77 5.77
#4	5.3 6.3 5.3 5.3	$S = 4.04 * 10^{-11}$ 8.00 6.08 8.00 0.32	$S = 5.37 * 10^{-21}$ 5.17 6.30 5.26 5.26
#5	5.3 6.3 5.3 4.3	$S = 7.72 * 10^{-13}$ 6.29 8.00 3.78 7.04	$S = 3.19 * 10^{-23}$ 6.57 6.30 5.30 4.30
#6	5.0 8.0 7.0 7.0	$S = 3.41 * 10^{-11}$ 8.00 8.00 6.45 6.81	$S = 9.24 * 10^{-21}$ 5.00 8.00 7.00 7.00

The comparison of rate constants used in the simulation and re-

covered from the fitting procedure (table 3.1) reveals that one kinetic curve does not have enough data to fit the rate constants. It is a result of fundamental properties of the system of ordinary differential equations, because the solution depends not only on rate constants, but also on initial conditions as well. The simultaneous fitting of three simulated experimental curves with different initial M_{ox} concentrations ($10^{-4},\ 10^{-5},\ 10^{-6}$) is a different story. Three kinetic curves with different initial concentrations sufficiently represent a hyper surface of rate constants/initial conditions . Results of three curves fitting summarized in 3.2. There is a practically perfect agreement between rate constants, used in simulations, and rate constants, recovered after the optimization.

Table 3.2: Fitting constants for three kinetic curves (coarse 9x9x9x9 grid). Initial concentrations: $E_{ox} = 10^{-9},\ M_{ox} = 10^{-(4\div6)},\ F_{ox} = 10^{-4},\ S = 10^{-3}$. Complete solutions listing is provided in appendix A.

Case	Rate constants used to generate test data $\lg(k_1)\ \lg(k_2)\ \lg(k_3)\ \lg(k_{-3})$	Worst Solution	Best solution
#1	6.3 7.3 6.3 5.3	$S = 2.86 * 10^{-10}$ 6.75 8.00 5.54 6.30	$S = 1.10 * 10^{-15}$ 6.30 7.30 6.43 5.43
#2	5.3 7.3 6.3 5.3	$S = 3.23 * 10^{-10}$ 5.60 8.00 7.17 8.00	$S = 1.48 * 10^{-19}$ 5.30 7.30 6.30 5.30
#3	5.3 6.3 6.3 5.3	$S = 4.19 * 10^{-10}$ 5.64 8.00 6.12 8.00	$S = 2.11 * 10^{-19}$ 5.30 6.30 6.24 5.24
#4	5.3 6.3 5.3 5.3	$S = 1.72 * 10^{-10}$ 4.69 6.09 6.86 0.00	$S = 4.14 * 10^{-20}$ 5.30 6.30 5.35 5.35
#5	5.3 6.3 5.3 4.3	$S = 2.71 * 10^{-11}$ 5.63 8.00 1.42 2.74	$S = 2.87 * 10^{-20}$ 5.30 6.30 5.24 4.24
#6	5.0 8.0 7.0 7.0	$S = 4.08 * 10^{-10}$ 4.78 8.00 8.00 2.24	$S = 5.29 * 10^{-20}$ 5.00 8.00 7.00 7.00

However, these examples are still very idealized cases from a practical perspective. Possibly, no experiment is achievable without an interference of a noise; initial concentrations or molar absorptivities is known only to some certainty as well. Therefore, all experimental uncertainties are transferred to uncertainties of reaction rate parameters. A simplest case of noisy data analysis is based on the assumption that the differences $(x_{i,exp} - x_{i,calc})$ are distributed normally with zero mean value. Then the lowest possible score value can be estimated by starting with

an expectation value definition (Papoulis and Pillai, 2002):

$$E[g(x)] \stackrel{\text{def}}{=} \int_{-\infty}^{\infty} g(x)f(x)dx \tag{3.11}$$

where $g(x)$ is an arbitrary function of x, and $f(x)$ is a probability distribution function (in our case$g(x) = x^2$ and $f(x) = \frac{e^{-\frac{x^2}{2\sigma^2}}}{\sigma\sqrt{2\pi}}$). The substitution and integration leads to:

$$\sum_{i=1}^{n}(x_{i,exp} - x_{i,calc})^2 \approx \int_{-\infty}^{\infty} \frac{e^{-\frac{x^2}{2\sigma^2}}}{\sigma\sqrt{2\pi}} x^2 dx = \sigma^2 \tag{3.12}$$

This result means that the score should only be lifted by σ^2. However, it is not true. The noise from the normal distribution ($\sigma^2 = 2 * 10^{-6}$ and $\mu = 0$ – fairly reasonable parameters in an experiment; a simulation and a fit in fig. 3.3) changes fitting results again. The fitting score is lifted by an expected value by dividing the fitting score by 3 (the number of curves). Taking fitting score of $1.06 * 10^{-11}$ from the first row of the table 3.3 and diving by 3 and taking the square root, yields $1.87 * 10^{-6}$, which is close to the theoretical value of $\sigma = 2.0 * 10^{-6}$. But, as seen from the same table, even with the grid search it is not possible to find k_3 and k_{-3} (despite the fact that k_1 and k_2 are fitted perfectly).

However, the inability to fit k_3 and k_{-3} values is not the fault of the algorithm. The closer inspection of fitted values reveals that they are related to the same equilibrium constant as do values used in the simulation. It is a result of the formed quasi-steady state in the third reaction of eq. 3.9. A simple illustration of quasi-steady state effects could be derived from an equation:

$$\frac{d[F_{ox}]}{dt} = k_{-3}[F_{red}][M_{ox}] - k_3[F_{ox}][M_{red}] \tag{3.13}$$

which under the quasi-steady state assumption becomes:

$$0 = k_{-3}[F_{red}][M_{ox}] - k_3[F_{ox}][M_{red}]$$

$$\frac{k_3}{k_{-3}} = \frac{[F_{red}][M_{ox}]}{[F_{ox}][M_{red}]} = K_{eq} \tag{3.14}$$

Eq. 3.14 represents the fact that in quasi-steady conditions some concentrations of reagents are governed not by absolute values of rate

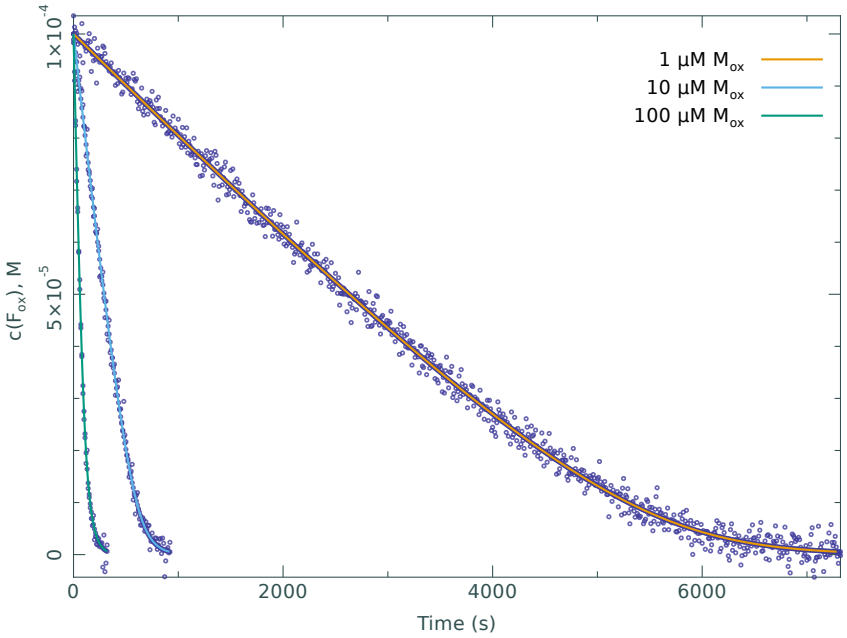

Figure 3.3: Biased and unbiased data examples for the case #1.

constants, but by the equilibrium constant. The proposed algorithm demonstrated the property of quasi-steadiness in this particular system and provided means to detect it in other systems. However, there is still a problem about how to select a subset of true solutions from a set of optimized rate constants (because the optimized set of rate constants is a set of solutions, which reached convergence criteria of optimization algorithm). Examples in the biased case fitting resulted in differences of orders of magnitude in fitted scores. These differences should be interpreted as a result of a grid sampling and is just a mere chance to find a reasonable fit. Therefore the statistical analysis should be used to interpret the results.

Table 3.3: Fitting constants for three biased kinetic curves (coarse 9x9x9x9 grid, bias from normal distribution $\sigma^2 = 2 * 10^{-6}$, and $\mu = 0$). Initial concentrations: $E_{ox} = 10^{-9},\ M_{ox} = 10^{-(4 \div 6)},\ F_{ox} = 10^{-4},\ S = 10^{-3}$.

Case	Rate constants used to generate test data $\lg(k_1)$ $\lg(k_2)$ $\lg(k_3)$ $\lg(k_{-3})$	Worst Solution	Best solution
#1	6.3 7.3 6.3 5.3	$S = 2.95 * 10^{-10}$ 6.75 8.00 5.55 6.31	$S = 1.06 * 10^{-11}$ 6.30 7.31 4.05 3.01
#2	5.3 7.3 6.3 5.3	$S = 3.35 * 10^{-10}$ 5.60 8.00 7.17 8.00	$S = 1.33 * 10^{-11}$ 5.30 7.31 4.45 3.44
#3	5.3 6.3 6.3 5.3	$S = 4.19 * 10^{-10}$ 8.00 6.20 8.00 0.11	$S = 1.15 * 10^{-11}$ 5.30 6.30 8.00 7.02
#4	5.3 6.3 5.3 5.3	$S = 2.04 * 10^{-10}$ 4.69 6.09 6.48 0.11	$S = 1.21 * 10^{-11}$ 5.30 6.30 7.56 7.56
#5	5.3 6.3 5.3 4.3	$S = 4.32 * 10^{-10}$ 5.63 8.00 6.12 8.00	$S = 1.18 * 10^{-11}$ 5.30 6.30 3.75 2.74
#6	5.0 8.0 7.0 7.0	$S = 4.17 * 10^{-10}$ 4.78 8.00 8.00 2.09	$S = 1.18 * 10^{-11}$ 5.00 8.00 7.00 7.00

3.2.3 Statistical analysis framework

The statistical analysis is composed from two procedures – an estimation of a maximum likelihood region, and an estimation of standard errors of fitting parameters. The maximum likelihood region is calculated as (Bates and Watts, 1988):

$$c = \frac{s^2}{1 - I^{-1}_{1-\alpha}(\frac{P}{2}, \frac{N-P}{2})} \tag{3.15}$$

where N – a total number of data points from all experimental curves, P – a number of parameters, α – a significance value, I^{-1} – an inverse beta regularized function, s^2 – a standard deviations. This formula estimates the maximal score, which should be expected with a significance value α. However, s^2 is a priori unknown, but it can be expected to be close to the smallest score value found in the optimization procedure. Because the fitting procedure is generalized for a multiple experiment's analysis, the correction factor, which accounts different lengths of data sets and the number of experiments, is needed. It is (Papoulis and Pillai, 2002):

$$\frac{\sum_{i=1}^{k}\left(\frac{n_i}{n_i-1}\right)}{k} \tag{3.16}$$

The correction factor arise from the transformation of biased standard deviations into unbiased ones (with reasonable assumption that standard deviations are equal in all experimental curves). The formula can be used if standard deviations in all experiments are approximately the same (as it should be true, provided the noise level does not depend on signal level).

Here n_i – a number of data points in a certain experimental curve and k – a number of experimental curves. Putting it together with the maximum likelihood estimation results a final formula:

$$c = \frac{s^2}{1 - I^{-1}_{1-\alpha}\left(\frac{P}{2}, \frac{N-P}{2}\right)} \left[\frac{\sum_{i=1}^{k}\left(\frac{n_i}{n_i-1}\right)}{k}\right] \tag{3.17}$$

The inverse beta-regularized function arise from Fisher-Snedecor distribution cumulative distribution function, which is known as $I_{\frac{xn}{xn+m}}(n, m)$, where I – beta regularized function, by solving equation $I_{\frac{xn}{xn+m}}(n, m) = 1 - \alpha$ for x (Wolfram Research, 2008). The estimation of errors is a by-product of fitting.

In all test cases first two constants are perfectly fitted with small uncertainties. For k_3 and k_{-3} – confidence intervals in logarithmic form show uncertainties of several orders of magnitude. However, analysis of fitted k_3 and k_{-3} reveals perfect a correlation between these constants (the correlation coefficient = 0.999972÷1; 1.1). As emphasized earlier, this effect comes from the chemical equilibrium formed in the third reaction, with particular initial concentration's and rate constants compensation in the fitting score optimization. The perfect correlation between constants and the chemical equilibrium implies a dimensionality reduction of k_3 and k_{-3} by simply combining them into the equilibrium constant. The resulting equilibrium constant has much smaller uncertainties as a consequence of the perfect correlation.

3.2.4 Calculation of reaction rate parameters for the alkaline phosphatase from the progress curves

In the biochemical kinetics, the data analysis of a simple enzymatic catalysis begins with Michaelis-Menten reaction scheme (a recent translation of this seminal paper (Johnson and Goody, 2011)):

$$\begin{array}{rcl} E + S & \underset{k_{-1}}{\overset{k_1}{\rightleftharpoons}} & ES, \\ ES & \overset{k_{cat}}{\rightarrow} & E + P. \end{array} \tag{3.18}$$

where S is a substrate, P – a product, E and ES are an enzyme and an enzyme/substrate complex, respectively, k_1, k_{-1} and k_{cat} - reaction's rate constants, respectively. This system under quasi-steady state conditions is described by equations:

$$\frac{d[S_0]}{dt} = -\frac{v_{max}[S_0]}{K_M + [S_0]},\ where\ K_M = \frac{k_{-1} + k_{cat}}{k_1}\ and\ v_{max} = k_{cat}[E_0]. \tag{3.19}$$

The success of these equations mostly comes from a definition of v_{max}, which essentially is a concentration of an enzyme multiplied by a catalytic constant. Today, the determination of an enzyme concentration is a diminished problem, yet it was a conundrum in early 20th century. However, the abuse of the schema becomes a problem, because almost any initial reaction rate dependence on an initial substrate concentration could be fitted into Michaelis-Menten equation (or, at least, into Hill equation (Weiss, 1997)). For example, one could overlook an enzyme inhibition by a reaction product if using only the initial rate approximation. Such case is found in the alkaline phosphatase catalyzed hydrolysis of para-nitrophenylphosphate ((Bowers and McComb, 1966)).

As the initial rate well fit into Michaelis-Menten equation with $K_m = 92 \pm 15$ μM and $v_{max} = 0.13 \pm 0.1$ $\mu\mathrm{Ms}^{-1}\mathrm{mg}^{-1}$ (fit in fig. 3.5, d), only experiments with an addition of para-nitrophenol or phosphate will show if there is any inhibition with products. On the other hand, the direct data fitting into the reaction scheme (3.18) instantly reveals that the fit is not suitable to describe the reaction kinetics (fig. 3.4, left).

The following reaction scheme accounts the inhibition with product (the third reaction in (3.20)) in the alkaline phosphatase case:

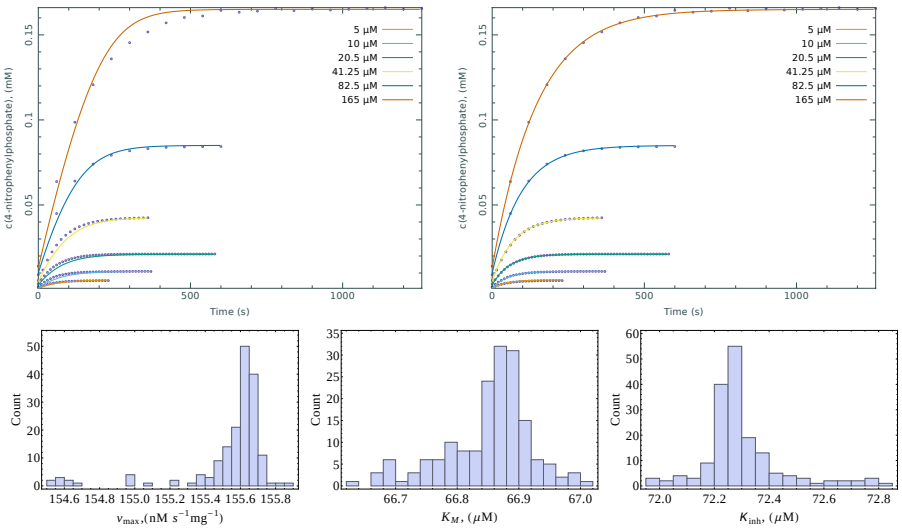

Figure 3.4: The 4-nitrophenyl phosphate hydrolysis fitted into the scheme (3.18) (left – plain Michaelis-Menten kinetics) and the scheme (3.20) (right – Michaelis-Menten kinetics with inhibition). Data (circles) from experiments with different initial 4-nitrophenyl phosphate concentrations, curves represent the best fit. Histograms bellow – distributions of fitted parameters k_{cat}, K_M and K_{inh}.

$$\begin{aligned} E + S &\underset{k_{-1}}{\overset{k_1}{\rightleftharpoons}} ES, \\ ES &\overset{k_{cat}}{\rightarrow} EP, \\ E + P &\underset{k_{-2}}{\overset{k_2}{\rightleftharpoons}} E_{inh}. \end{aligned} \tag{3.20}$$

This scheme results in ideal fits (fig. 3.4, right). However, without further experiments it can not be determinated which of products - paranitrophenol or phosphate -is the competitive inhibitor of the alkaline phosphatase. Although we definitely could find values of K_m, v_{max}(which is product of a guessed enzyme concentration and fitted k_{cat} – due to reaction scheme properties, the initial enzyme concentration only scales k_{cat}) and K_{inh} from fitting results (numerical values of fitted rate constants plotted in fig. 3.5 a, b and c).

From cross-plots in fig. 3.5 a, b and c it is seen that in this case the fitting procedure resulted in a set of multiple minima, which are the manifestation of the quasi-steady state. Other data fitting tools, which are based on the uniqueness of optimal fit (Rovati et al., 1996; Mendes, 1997; Kuzmič, 2009; Kuzmič, 1996; Svir et al., 2002), will give

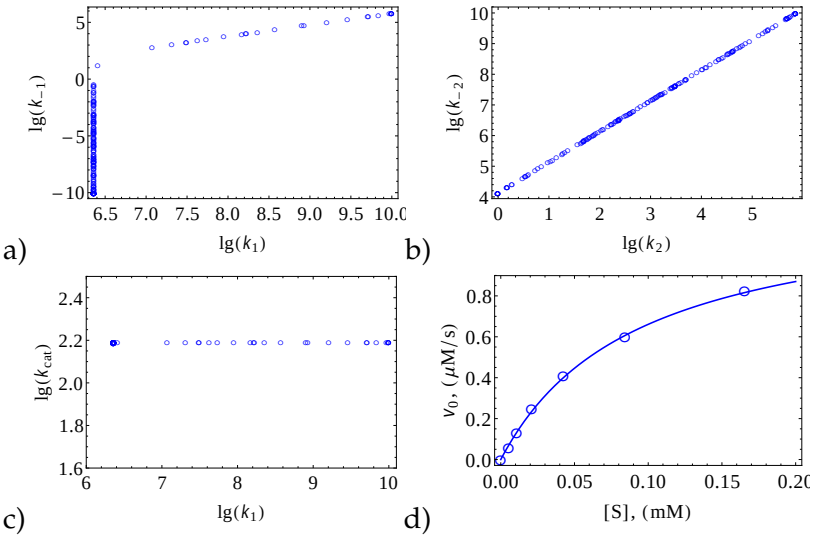

Figure 3.5: Found relations between rate constants (a, b, c) and initial rate dependence on substrate concentration (d).

one solution with values for all rate constants in the reaction scheme (3.20). The analytical derivation of the initial rate equation, based on the quasi-steady approximation, for the reaction scheme (3.20) would yield:

$$v_0 = \frac{[E_0]k_{cat}[S_0]}{K_M(1 + \frac{[P_0]}{K_{inh}}) + S}, \tag{3.21}$$

where $K_M = \frac{k_{-1}+k_{cat}}{k_1}$ and $K_{inh} = \frac{k_2}{k_{-2}}$. Using these relations K_M and K_{inh} are calculated from multiple minima. This result should be interpreted as an *impossibility* to fit real values of separate rate constants k_1, k_{-1}, k_2, k_{-2} if the experiment is carried out in the quasi-steady state. Only values of k_{cat}, K_M and K_{inh} in this case could be recovered. Indeed, the linear relation k_2 and k_{-2} in logarithmic coordinates (fig. 3.5 b) is the result of the quasi-equilibrium in the third reaction (3.20). The same applies to the logarithmic relation for constants $k_1$and k_{-1} in a more complicated manner. Here two cases exist:

- the first, when $k_{-1} \gg k_{cat}$ and $K_M = \frac{k_{-1}+k_{cat}}{k_1}$ simplifies to $K_M \approx \frac{k_{-1}}{k_1}$.
- the second, when $k_{cat} \gg k_{-1}$ and $K_M = \frac{k_{-1}+k_{cat}}{k_1}$ simplifies to $K_M \approx \frac{k_{cat}}{k_1}$.

These relations are found in this case (fig. 3.5 A). The only definitely fitted rate constant, which shows no dependence on other rate constants, is k_{cat}. Value of K_M is calculated using relations $K_M = \frac{k_{-1}+k_{cat}}{k_1} = 66.9 \pm 0.5\ \mu\mathrm{M}$, $v_{max} = [E_0]k_{cat} = 156 \pm 1\ \mathrm{nMs^{-1}mg^{-1}}$, $K_{inh} = \frac{k_2}{k_{-2}} = 72.3 \pm 0.1\ \mu\mathrm{M}$ using fitted values shown in fig. 3.5. Distributions of calculated parameters are plotted in fig. 3.4 (histograms below) and represents a valuable information from the multiple minima optimization – the uncertainty of values of parameters and the sensitivity of the reaction to variation of parameters. These values are comparable (within the order of magnitude, taking into account different measurement conditions and alkaline phosphatase producents) to ones found in the literature (Cyboron and Wuthier, 1981; Van Belle, 1976). The distribution of calculated parameters (K_M, v_{max}, K_{inh}) is plotted in fig. 3.4 and represents the uncertainty of fitted parameter's values. Uncertainties of fitted values are 10 to 20 times lower than calculated from the initial rate approximation. Asymmetric distributions of parameters values are expected as a result of data fitting to the nonlinear model.

3.2.5 Calculation of rate parameters for the oxidation of promazine with the consecutive radical cation disproportionation

There is a variety of enzymatic reactions, which involve multiple substrates in a catalytic cycle. Oxidoreductases are examples of such enzymes. The involvement of multiple substrates greatly complicates a reaction scheme and the derivation of initial rate equations, which are traditionally used to fit data. Besides that, a large amount of measured initial rate's values is needed to precisely estimate rate parameters of a reaction scheme. The following example is intended to demonstrate how could a data analysis be done in a different and more effective way. *Coprinus cinereus* peroxidase is one of enzymes, whose catalytic cycle depends on at least two substrates. Typically, peroxidases use two substrates — a terminal electron acceptor hydrogen peroxide and an electron donor, which could be one of a wast selection of possible substrates. One of such substrates is promazine — an old antipsychotic drug, which belong to the phenothiazine class of antipsychotics (Schiele, 1962).

Its oxidation scheme is relatively simple and could be approximated in a way where the one-electron oxidation is assumed:

$$
\begin{aligned}
E_{red} + H_2O_2 &\overset{k_p}{\rightarrow} Comp_I, \\
Comp_I + S &\underset{k_{-1}}{\overset{k_1}{\rightleftharpoons}} Comp_IS, \\
Comp_IS &\overset{k_{cat,1}}{\rightarrow} Comp_{II} + S^{\bullet+}, \\
Comp_{II} + S &\underset{k_{-2}}{\overset{k_2}{\rightleftharpoons}} Comp_{II}S, \\
Comp_{II}S &\overset{k_{cat,2}}{\rightarrow} E_{red} + S^{\bullet+}, \\
S^{\bullet+} + S^{\bullet+} &\underset{k_{-3}}{\overset{k_3}{\rightleftharpoons}} S + S_{ox}, \\
S_{ox} + H_2O &\overset{k_{hyd}}{\rightarrow} S_{sulfoxide} + 2H^+,
\end{aligned}
\tag{3.22}
$$

which is composed from reaction schemes given in (Berglund et al., 2002; Blankert et al., 2005; Kulys et al., 2000). Here $S^{\bullet+}$ represents the radical cation of the promazine oxidation, whose absorbance at λ_{514nm} is monitored during the reaction ($\epsilon_{514} = 8.9\,\mathrm{mM}^{-1}\mathrm{cm}^{-1}$ (Kulys et al., 2000), experiment data are represented by curves).

This reaction scheme is more or less typical for various peroxidases (for example *Coprinopsis cinerea* or *Armoracia rusticana*) and they are well-studied, allowing us to compare some rate constants found in the literature with our computed estimates. Alternatively, the reaction could be approximated by the simplified version of the reaction scheme composed form only first five reactions from (3.22). Such approximation under steady-state conditions and an assumption that limiting step is the compound II reduction with promazine will yield the equation for the rate of radical cation formation:

$$
[S^{\bullet+}]'[t] = \frac{2[E_0]k_{cat,1}k_{cat,2}k_p[H_2O_2][S]}{k_{cat,2}(k_{cat,1}[S] + k_p[H_2O_2](K_{M,1} + [S])) + k_{cat,1}k_p[H_2O_2](K_{M,2} + [S])}, \tag{3.23}
$$

where $K_{M,n} \rightarrow \frac{k_{cat,n}+k_{-n}}{k_n}$. This could be simplified, assuming that the reaction with hydrogen peroxide proceeds much faster than others:

$$
[S^{\bullet+}]'[t] = \frac{2[E_0]k_{cat,1}k_{cat,2}[S]}{k_{cat,2}(K_{M,1} + [S]) + k_{cat,1}(K_{M,2} + [S])}. \tag{3.24}
$$

This equation could be recast into general Michaelis-Menten form:

$$[S^{\bullet+}]'[t] = v = \frac{2[E_0]k_{cat}[S]}{K_M+[S]},\ where\ k_{cat} = \frac{k_{cat,1}k_{cat,2}}{k_{cat,1}+k_{cat,2}} \\ and\ K_M = \frac{k_{cat,1}K_{M,2}+K_{M,1}k_{cat,2}}{k_{cat,1}+k_{cat,2}} \tag{3.25}$$

From experiments carried out for five different initial concentrations (experimental details are provided in Appendix) of promazine and using initial rates and Michaelis-Menten approximation, apparent $k_{cat} = (1.6 \pm 0.3) \times 10^2\ \mathrm{s}^{-1}$ and $K_M = 60 \pm 20\ \mu\mathrm{M}$ were calculated. The following apparent bimolecular rate constant $k_{ox} = \frac{k_{cat}}{K_M} = (3 \pm 1) \times 10^6\ \mathrm{M}^{-1}\mathrm{s}^{-1}$ was estimated. These results are comparable to published ones (Kulys et al., 2000).

The same data could befitted into a more complicated reaction scheme (3.22) (value $k_p = 9.9 \times 10^6\ \mathrm{M}^{-1}\mathrm{s}^{-1}$ (Abelskov et al., 1997) was fixed, other rate constants were optimized). Resulting fits are plotted with data in fig. 3.6. From the optimized set of rate constants, as in the previous example, a synthetic rate constants were calculated: $k_{cat} = \frac{k_{cat,1}k_{cat,2}}{k_{cat,1}+k_{cat,2}} = 147 \pm 1\ \mathrm{s}^{-1}$, $K_M = \frac{k_{cat,1}K_{M,2}+K_{M,1}k_{cat,2}}{k_{cat,1}+k_{cat,2}} = 43.2 \pm 0.3\ \mu\mathrm{M}$, $k_{ox} = \frac{k_{cat}}{K_M} = (3.40 \pm 0.05) \times 10^6\ \mathrm{M}^{-1}\mathrm{s}^{-1}$, $k_3 = 1900 \pm 4\ \mathrm{M}^{-1}\mathrm{s}^{-1}$, $k_{-3} = (3.12 \pm 0.07) \times 10^4\ \mathrm{M}^{-1}\mathrm{s}^{-1}$, $k_{hyd} = (2.2 \pm 0.1) \times 10^{-3}\ \mathrm{M}^{-1}\mathrm{s}^{-1}$.

Rate parameters k_{cat} and K_M are well-comparable with constants, calculated from the initial rate approximation. The results differ by reduced error bounds (15 times for k_{cat}, 60 times for K_M) and additional three parameters k_3, k_4, k_{hyd}, which are inaccessible from these data in the initial rate approximation framework. Distributions of fitted parameters (k_{cat}, K_M, k_3, k_4, k_{hyd}) are plotted in fig. 3.6 (histograms below). As in the previous case, distributions represent the uncertainty of parameters and the reaction scheme sensitivity to the variation of parameters.

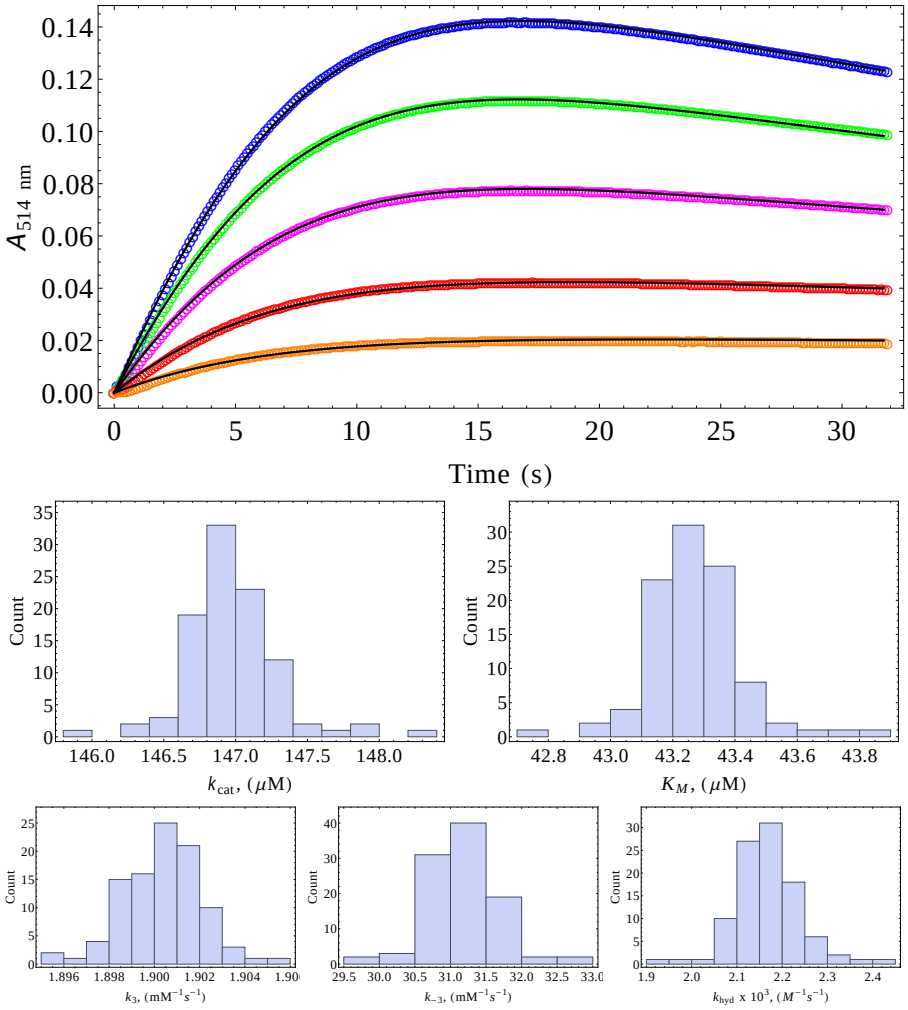

Figure 3.6: PZ oxidation with CiP data (circles) and fits (black curves). Histograms bellow – distributions of fitted rate constants in the oxidation of promazine .

3.3 Résumé

In this part of the thesis the (bio)chemical kinetics modeling and data fitting were investigated. It was found that in general case the fits of experimental data can be represented by multiple rate parameter sets. This finding indicates that the assumption about the uniqueness and existence of global minimum is incorrect in the case where experimental data are biased by a noise. Therefore, any (bio)chemical kinetics data fitting algorithm based on the uniqueness and existence of the global

minimum will result in incorrect fits of experimental data under certain conditions. The data fitting algorithm is proposed, which allows to find multiple sets of reaction rate parameters that perfectly fits to a reaction schema, and it was demonstrated that analysis of these fits allows the precise and correct calculation of reaction rate parameters for a reaction schema of the interest. The application of the algorithm was demonstrated using synthetic and experimental data. The fitting results exhibit the correct representation of a reaction schema and tighter error bounds of calculated rate parameters, requiring less experimental effort as compared to other methods.

4 INVESTIGATION AND MODELING OF THE LACCASE KINETICS AND ELECTROCATALYSIS

This part of the thesis is dedicated to the investigation and modeling of laccase kinetics and electrocatalysis. Laccases is a very interesting subclass of multicopper oxidases with a substantial industrial and scientific interest. The application of these enzymes for a fabrication of biocathodes for biofuel cells and biosensors is an actively pursued trend in the bioelectrochemistry. The problematics in application of laccases for a fabrication of biocathodes split in two main research areas – the first one is concerned with the physical fabrication of the effective and stable bioanodes, and another one - with the catalysis mechanism in homogeneous media and on an electrode. Obviously, the first one gets most of the attention. This disproportion in the research is understandable from the immediate pressure from the green energy demands, industrial requirements of implantable electronics, etc.. However, we believe that the field can benefit from the mechanistic investigation as well. In many cases of the fabrication of bioelectrodes, properties of an enzyme on an electrode are different from observable in a homogeneous medium. Generally, these differences without a deeper investigation are attributed to "a flattening of enzyme", "double layer properties", "a local change of pH" and other effects. Here we investigate the homogeneous and heterogeneous catalysis of a very peculiar laccase, purified from *Didymocrea* sp. J6, and show that the properties of the enzyme is same in both cases, despite apparent catalytic differences. In this part, the biochemical kinetics of the laccase was analyzed and modeled using methods developed in the previous part of the thesis. Results presented here are published in the article "Oxygen electroreduction catalyzed by laccase wired to gold nanoparticles *via* the trinuclear copper cluster" Energy Environ. Sci., 2017,10, 498-502.

4.1 Structural, catalytic properties and applications of laccases

Laccases Oxidoreductases are a structurally and functionally diverse class of enzymes involved in a catalysis of oxidation and reduction reactions. Multicopper oxidases is a subfamily of these enzymes. As the name implies, these enzymes has something to do with copper. Indeed,

copper ions act as cofactors of multicopper oxidases. This fact is quite surprising, because copper itself is an nonreactive metal belonging to the same group of metals as silver and gold. However, it serves very well as a cofactor and is abundant in an enzymatic catalysis. The family of multicopper oxidases involve such enzymes as ceruloplasmin (EC 1.16.3.1)(Peisach and Levine, 1963), copper-containing nitrite reductase (EC 1.7.2.1)(Li et al., 2015), laccase (EC 1.10.3.2) and closely related l-ascorbate oxidase (EC 1.10.3.3)(Messerschmidt et al., 1992). All are very interesting, but the laccase is the hero here.

Laccases are enzymes, which are used (albeit unknowingly) since 5th millennium BC(Bagley, 1999). The enzyme is named after urshiol-based lacquer, which is a product of laccase-catalyzed polymerization and is derived from the sap of *Toxicodendron vernicifluum*. The lacquer itself is a hard and shiny-finish material used for millennia in production of lacquerware – the utensils, varying in sophistication, from usual to amusing artistic objects (fig. 4.1).

Laccases (EC 1.10.3.2, also know as p-diphenol:dioxygen oxidoreductases) are divided into families according to the source organism – plant and fungi. However, such division is incomplete, because laccases are found in insects(Arakane et al., 2005) and bacteria(Desai and Nityanand, 2011) as well. These enzymes are ubiquitous in fungi and occur not only as a single enzyme, but as various isoforms as well. Plant laccases, however, are somewhat scarce in comparison with fungal. There are only a few higher plants species producing laccases (including previously mentioned *Toxicodendron vernicifluum*). Yet, this apparent underrepresentation is partially explained by difficulties in detecting laccase activity in crude extracts. Usually, fungal laccases are found in cytosol, but there are many examples of secreted enzymes as well. The activity of plant laccases are usually observed near/in lignifying cells. Most enzymes from eucaryotes are glycoproteins glycosylated to a various degree. The function attributed for plant laccases is a cell wall reconstitution and remodeling in early phases (i.e. first steps in oxidative coupling of monolignols)(Mayer and Staples, 2002). Functions of fungal laccases are better studied and include ligninolysis, synthesis of pigments, plant pathogenesis etc.(Rivera-Hoyos et al., 2013).

Both fungal and plant laccases catalyze more or less the same oxidation reaction, where an electron-donating substrate oxidises *via* one

Figure 4.1: Carved red lacquer on wood core, Ming dynasty, Wanli mark and period, 1573-1620.

electron pathway to a radical cation, and four electrons are accumulated to reduce one dioxygen molecule to two molecules of water. Laccases can accommodate a wide range of possible electron donating substrates, starting with naturally occurring polyphenols, monolygnols, and ending with various synthetic compounds such as phenylendiamines, phenoxazines, phenothiazines and diphenols. As it is mentioned previously, fungal laccases are much better studied than those from plants. There is a plethora of known structures of bacterial and fungal laccases. However, there is not a single structure of a plant laccase published (at least when this sentence was written). Therefore, a direct comparison of enzymatic structures is not possible. Yet, it is known, that laccases (from plants or fungi) and l-ascorbate oxidases (from plants) are structurally similar

despite the poor similarity in sequence(Awasthi et al., 2015) (fig. 4.2).

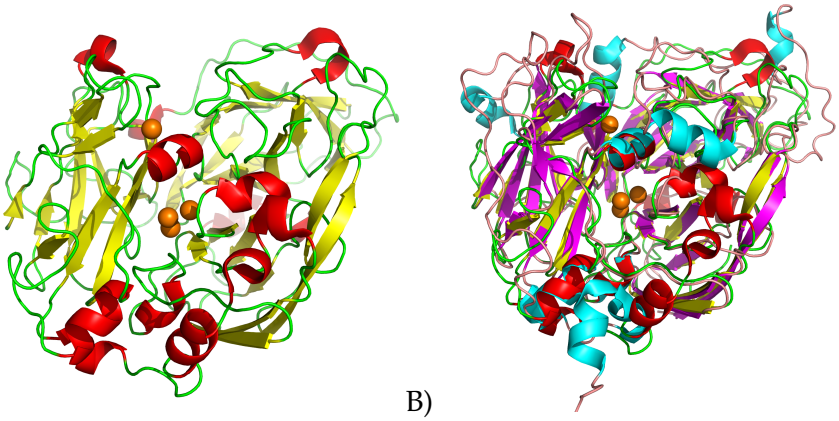

Figure 4.2: A) Structure of laccase from *Trametes versicolor* (PDBID:1GYC); copper ions are represented by orange spheres; B) Superposition of laccase from *Trametes versicolor* and l-ascorbate oxidase from *Cucurbita pepo* (PDBID:1ASO).

Structural properties and catalysis mechanism Laccases have four copper ions in their active centers (fig. 4.2A). These ions are grouped into three types – T1, T2 and T3 copper ions. This differentiation is based on spectroscopic properties of relevant ions. T1 copper ion exhibits an intense absorption band near 600 nm when oxidized (hence enzyme solutions are blue, and enzymes themselves are called "blue laccases"). The binuclear T3 ion cluster exhibits the broad absorption band near 300 nm, and the T2 copper ion is the only one detectable by the electron paramagnetic resonance spectroscopy (Solomon, 2006). These features are more or less observable for all multicopper oxidases (Jones and Solomon, 2015).

A typical active center of laccases is illustrated in fig. 4.3. As seen from fig. 4.3, T2 and T3 centers are constituted of copper ions complexed entirely with histidines. Copper ions in the T3 binuclear cluster are antiferromagnetically coupled and, therefore, silent in the electron paramagnetic resonance spectroscopy. T1 copper ion, typically, is complexed by two histidines and cysteine. The broad absorption band at 600 nm is caused by a covalent nature of Cu-S(Cys) bond (Solomon, 2006). T2 and T3 copper ions form the T2/T3 redox center and T1 forms the second one. The separating distance between these centers is ~13 Å.

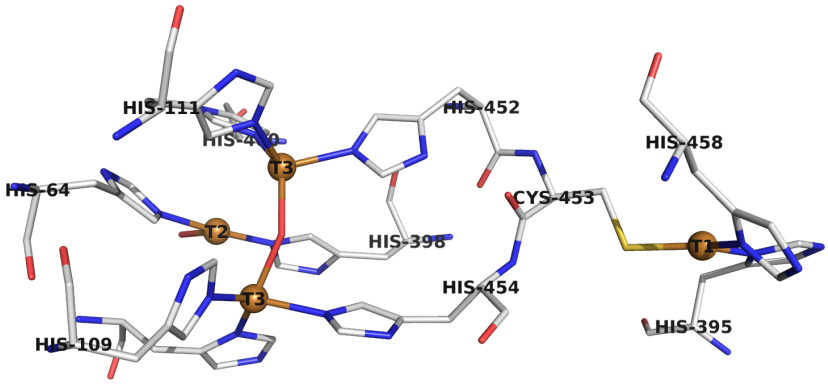

Figure 4.3: Structure of active center of *Trametes versicolor* laccase (PDBID:1GYC) with T1, T2 and T3 copper ions indicated.

T1 and T2/T3 redox centers are responsible for the catalytic activity of laccases. In the native intermediate state, all copper ions are oxidized to Cu(II) state and two hydroxide ions (one to T3 binuclear cluster and one to T2 and T3 copper ions) are bound in the T2/T3 cluster. The T1 center serves as an initial redox couple, which is reduced by a substrate *via* one-electron pathway. Upon a reduction, copper ion changes its redox state from Cu(II) to Cu(I). The next step in the catalysis is internal electron transfer between T1 and T2/T3 centers accompanied with release of one water molecule. However, it is not known which of hydroxide ions bound is released as water. After the internal electron transfer, the T1 redox center is returned to Cu(II) state and can oxidize a new molecule of a substrate. This scheme with one electron reductions of T1, the internal electron transfer between T1 and T2/T3 and release of water proceeds until all copper ions are reduced to Cu(I) state (i.e. the fully reduced enzyme state). The fully reduced enzyme finally binds dioxygen and is oxidized to the native intermediate. This oxidation cycle is accompanied by a very peculiar resting fully oxidized state, which can be reduced by one molecule of substrate to the new form, which slowly decays to the enzyme, which can return back to the catalytic cycle. The overall catalysis scheme is illustrated in fig. 4.4, as proposed in the literature (Solomon et al., 1996).

The apparent bimolecular rate constant of the enzymatic reaction

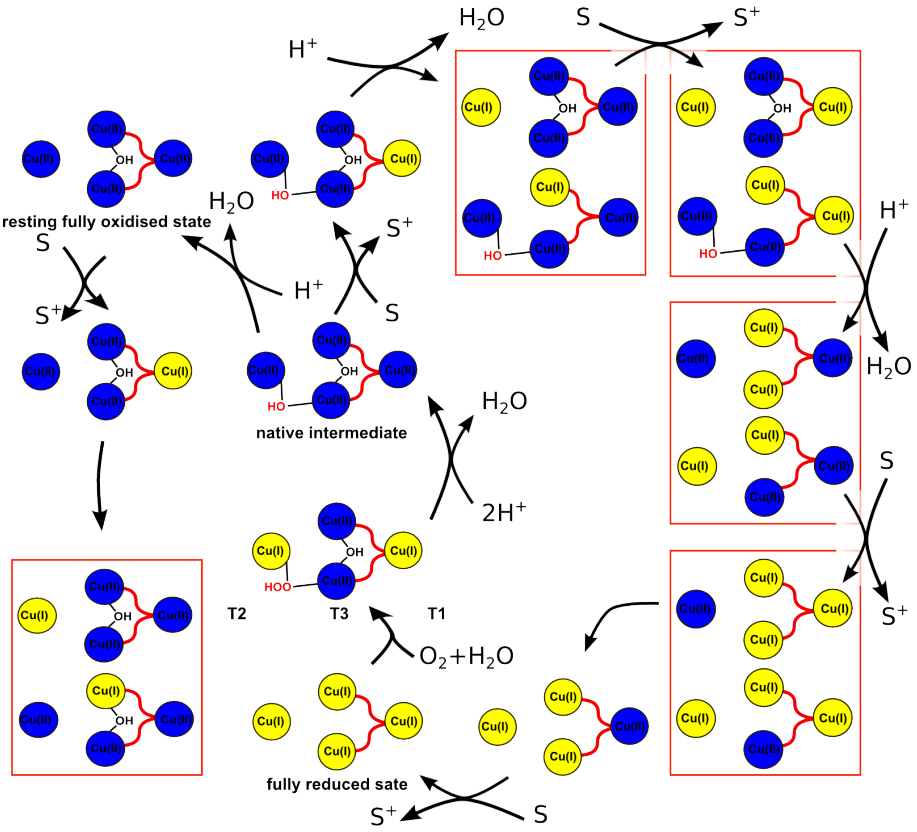

Figure 4.4: Laccase catalysis mechanism scheme proposed in literature (adapted from (Solomon et al., 1996)). Blue color indicates oxidized Cu(II) and yellow represents reduced Cu(I) ions. Structures in red rectangles are possible alternatives of relevant state.

with oxygen is somewhat around $2 \times 10^6\ M^{-1}s^{-1}$(Cole et al., 1991; Andréasson et al., 1976; Bukh et al., 2006). Nevertheless, kinetic properties of laccases vary from an enzyme to an enzyme and are affected by ionic strength of buffers solutions (Lee et al., 1984). Apparent bimolecular rate constants of a laccase-catalyzed oxidation of substrates reported in the literature ranges from virtually zero to $2 \times 10^8\ \mathrm{M^{-1}s^{-1}}$(Krikstopaitis et al., 1998; Kulys et al., 2000; Xu, 1996). An inhibition of the laccase activity is observed with various compounds, particularly with chelating agents and small ions such as azide, fluoride and cyanide (Brändén et al., 1973; Bligny and Douce, 1983). The inhibition mechanism is attributed to a small ion binding to the T2/T3 cluster and disturbing oxygen binding and/or reduction. However, theoretical studies provided another

explanation – binding of small ions changes the reduction potential and the reorganization energy of the T2/T3 cluster (Kepp, 2014).

Most of the differences in the laccase catalysis arise from reduction potentials of T1 and T2/T3 centers. The reduction potentials of T1 is determinated by spectroelectrochemical redox titration methods for a substantial number of laccases. It was found that the potential is pH-dependent and varies from around 430 mV vs NHE to 780 mV vs NHE at pH 7 (the influence of pH is around 15 mV/pH)(Shleev et al., 2005c). Reduction potentials of the T2/T3 cluster were proposed to be around 400 mV vs NHE (Shleev et al., 2005c; Christenson et al., 2006; Shleev et al., 2005b). However, at least for *T. versicolor* and *T. hirsuta* laccases, very similar to T1 reduction potentials were found for T2/T3 cluster (~ 780 mV vs NHE, pH 5.5) (Farver et al., 2011). These potentials are more consistent with the driving force needed for the internal electron transfer between T1 and T2/T3 redox centers and the potential of oxygen reduction at the relevant pH. These intricate potential differences and dependencies on pH are the main reason for laccases being much more active in acidic pH.

Rate constants of the internal electron transfer between T1 and T2/T3 centers for laccases are the important factor controlling the overall catalytic activity of enzymes. Rate constants of the internal electron transfer for laccases from *T. hisrsuta* of $25\ \mathrm{s}^{-1}$ and from *Rhus vernicifera* of $1.1\ \mathrm{s}^{-1}$ are found(Farver et al., 2011). These constants are rather small, but nevertheless, large enough to provide the catalytic efficiency for laccases. However, it is found that the rate constant is dependent on the oxidation state of a laccase, at least for the laccase from *Streptomyces coelicolor*. The rate constant equal to $8\ \mathrm{s}^{-1}$ for the fully oxidized enzyme was found (Farver et al., 2011). For intermediate steps, rate constants of $15\ \mathrm{s}^{-1}$ and $186\ \mathrm{s}^{-1}$ were found (Farver et al., 2011).

Applications of laccases All applications of laccases use an ability of these enzymes to oxidize substrates and to reduce molecular oxygen. The use of molecular oxygen is the most important feature here, because this molecule is one of the most abundant materials in our planet and it reduces to a harmless and "green" substance – water. Oxidative properties of laccases are used in various applications, starting from a bioremediation and ending with oxidative couplings in a chemical

synthesis.

The versatility of laccases is, possibly, illustrated in the best way by the application of enzyme in the textile industry. Possibly, most obvious applications of laccase is oxidative fiber bleaching (i.e. removal of pigments and whitening of material). However, enzymes are much larger molecules than typical chemical reagents used in the textile industry. Therefore, there are some problems associated with enzymes reaching their substrates in fiber agglomerates. These problems were solved by using ultrasound- or mediator-assisted methods. It was found that the ultrasonic treatment improves the laccase bleaching activity due to an enhanced diffusion of an enzyme in cotton fibers(Basto et al., 2007). Small molecules called mediators can improve the efficiency of the process via a different approach. For example, a laccase can oxidize a small molecule (for example 1-hydroxybenzotriazole), which further oxidizes a colored material in fibers. Such method was demonstrated in various publications (for example, for the paper pulp bleaching in (Camarero et al., 2004)). Yet, the fiber bleaching is not the only application of laccases in the textile industry. A "green" process for the denim dyeing was also developed. This process uses the enzyme's ability to oxidize leucoindigo (chemically it is done by using harsh oxidizers such as sodium hypochlorite) and was commercialized by Novozyme under "DeniliteI" trademark(Pezzella et al., 2015).

Another important process, which shows the potential for the use of laccase, is the waste bioremediation. Various waste waters containing phenol compounds or other oxidizable products from paper, pharma and other industries, can benefit from the enzyme-catalyzed waste removal both from economical and ecological viewpoints(Strong and Claus, 2011).

Laccases show the potential in applications in the food industry as well. For example, laccases can be used to cross-link arabinoxylans, thus improving dough machinability, increasing volume and reducing stickiness(Selinheimo et al., 2006). In the wine and beer industry, laccases can be used to control a polyphenolic content *via* an oxidative coupling and sedimentation(Minussi et al., 2002). This method is applicable for a fruit juice clarification as well.

Laccases have found application in various chemical syntheses, starting with a polymerization and ending with a precise synthesis of phar-

maceuticals. A synthesis of novel $\beta-$lactams (antibiotics) using a laccase-catalyzed oxidative amination(Mikolasch et al., 2006), anti-cancer agents such as anhydrovinblastine (Sagui et al., 2009) and plethora of others methods were demonstrated (thoroughly described in this review study(Pezzella et al., 2015)).

Application of laccases in biosensors and the bioelectrochemistry, particularly with the emphasis on biofuel cells, is not very novel, but still a very trendy and complex research area. In the fabrication of electrochemical laccase biosensors, typically, a laccase ability to oxidize various substrates and transfer electrons to an electrode is utilized. This transfer of electrons to an electrode surface gives, usually, a measurable increase in a current, which is also proportional to the concentration of a substrate in a medium. The electron transfer between electrodes and laccases can proceed *via* two modes – as mediated or as direct electron transfer. The mediated electron transfer is realized in bioelectroenzymatic systems using some small molecules that can be oxidized/reduced on an electrode and reduced/oxidized by an enzyme. The direct electron transfer, as implied in its name, is a mediatorless transfer of electrons from an active center of enzyme directly to an electrode.

There is a plethora of biosensors based on laccases. Most of them are designed for a detection of phenols and aminophenols, which are more or less natural substrates of laccases. The rationale of phenol detection is based on a prevalence of these compounds in industrial waste waters(Chen et al., 2013). Some biosensors are non-specific and are intended to measure an overall oxidizable content of an analyte (with prevalence of phenols), other are specific and respond to a particular kind of a substance such as catechol (Li et al., 2014) or bisphenol A (Portaccio et al., 2013). These biosensors, typically, are constructed from various nanocomposites with a redox polymer such as polydopamine or poorly soluble redox dyes such as thionine.

Laccases, along with similar multicoper oxidases, are used in the field of biofuel cells for a fabrication of biocathodes. The main reason for the necessity of the direct electron transfer in biocathodes is the energetic economy and efficiency of such operation mode. The direct electron transfer lowers the over potential of an electrochemical system. Therefore, a larger portion of the energy can be extracted. Yet, there are countless examples concerning usage of various mediators and redox polymers

for a fabrication of laccase-based biocathodes (Le Goff et al., 2015). The direct electron transfer for laccase based electrodes were demonstrated in late eighties on a carbon-black modified electrode (Tarasevich et al., 1979). From then on, the laccase catalysis performance was demonstrated on medium weight carbon nanotubes (Tominaga et al., 2017), carbon particles (Shleev et al., 2010), nanoporous gold (Salaj-Kosla et al., 2012), bare and thiol modified gold (Shleev et al., 2006), graphite (Shleev et al., 2004) and many on other materials. In these examples, as well as in a mediator or a redox polymer based ones, it is assumed that electrons from an electrode, due to a favorable enzyme orientation, are injected to the enzyme's T1 center first, then further to the T2/T3 center, where the oxygen reduction proceeds. There were attempts published to orient a laccase via the T2/T3 copper cluster. However, these attempts failed to demonstrate the efficient catalysis of oxygen bioelectroreduction to water(Shleev et al., 2005a). The approach is desirable, because it can overcome possible catalysis limitations in the internal electron transfer.

4.2 Results and discussion

The kinetic and electrochemical investigations of laccase systems are rarely compared to each other. The principal reason of such lack of the integration is the traditional and practical division between the enzyme kinetics and electrochemical experiments. However, the full integration of data from very different kinds of experiments can reveal new and interesting insights in the enzymatic catalysis. The following section is intended to integrate homogeneous kinetic measurements performed by myself, spectroelectrochemical titration experiments performed by dr. Marius Dagys, and the laccase biocathode fabrication and measurements carried out by dr. Dalius Ratautas. Here we analyzed data and modeled catalysis mechanism of a particular small-size laccase, extracted and purified from *Didymocrea* sp. J6 by scientific group of prof. dr. Rolandas Meškys in Vilnius University, Institute of Biochemistry. I hope that the reader of this thesis will be benevolent and will take measurements of spectroelectrochemical titrations and electrochemical investigations for granted as published in the our joint paper (Dagys et al., 2017), allowing myself to concentrate about my part of the work. Therefore, peculiarities of the electrode fabrication, performance and applicability questions are omitted, as well as any explanations about the exceptional

laccase stability in high pH, paying attention only on the laccase catalysis mechanism in homogeneous and heterogeneous media.

4.2.1 Catalytic oxidation of ferrocyanide and ABTS by the laccase

The investigation of laccase from *Didymocrea* sp. J6 (LAC) kinetics was carried out to gather data needed to compare catalysis mechanisms and properties of LAC in homogeneous media and on the electrode. The choice of possible LAC substrates for the investigation of kinetics here is arbitrary. We selected two different compounds for such measurements – ABTS and ferrocyanide. Measurements were carried out in three solutions of different pH (4.0, 5.5 and 7.4; 50 mM phosphate-citrate with 100 mM potassium sulfate) at 25°C temperature. The LAC inhibition with fluoride ions was investigated both with ABTS and ferrocyanide. The initial concentrations of ABTS and ferrocyanide in these studies were varied from 3.75 to 30 μM and from 22 to 200 μM, respectively. The Initial oxygen concentration was assumed to be 253 μM. Initial concentrations of the enzyme during experiments at pH 4.0, 5.5 and 7.4 were 8.0, 8.0, and 55 nM, respectively. The concentration of fluoride ions was varied from 0 to 0.1 M. An example set of experiments is presented in fig. 4.5, alongside with data fits.

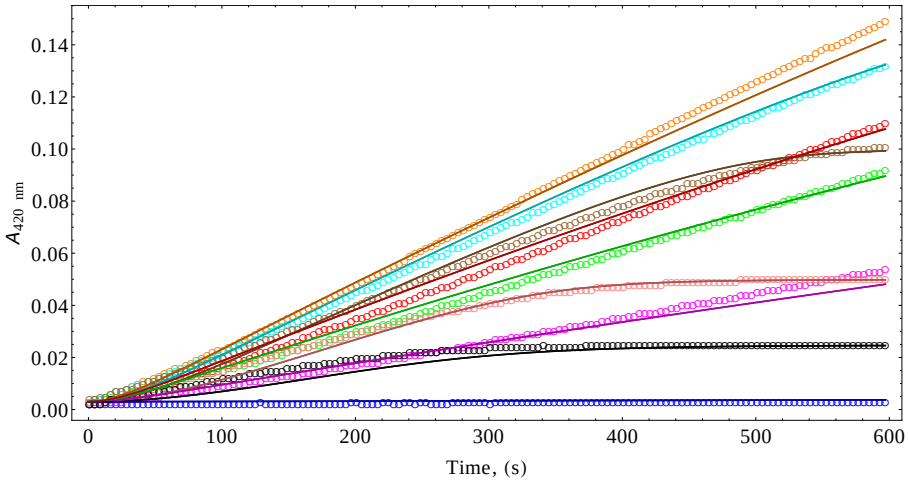

Figure 4.5: The oxidation of potassium ferrocyanide with oxygen at pH 4.0 in the phosphate-citrate buffer solution, catalyzed by the laccase, and inhibition of the catalysis with fluoride, data (circles) and fits (curves).

It was found that the laccase-catalyzed ferrocyanide oxidation with

oxygen have a well pronounced lag-phase (fig. 4.5), which was not observed in the oxidation of ABTS. Lag-phases occur, mostly, in consecutive reactions, mediated processes (for example (Martinello and da Silva, 2006)) or reactions where the inactivation/reactivation of an enzyme is involved (Tetianec et al., 2014). In the consecutive process the initial rate, by its definition, is zero. In the inactivation/reactivation case, only a reactivation of an enzyme with a substrate is observed. Therefore, it was impossible to calculate relevant rate constants of the oxidation process here by using standard quasi-steady state assumption and the initial rate approach without some extensive redesign of experiments. However, in the previous part of this thesis the algorithm was described, which is intended to solve such problems and, therefore, it was applied here for the data analysis. The assumed reaction schema is taken from Solomon et al. (illustrated previously in fig. 4.4) and is the same for both ABTS and ferrocyanide(Solomon et al., 1996):

$$\begin{aligned} Lac_{resting} + S_{red} &\overset{k_{act}}{\rightarrow} Lac_2 + S_{ox}, \\ Lac_1 + S_{red} &\overset{k_1}{\rightarrow} Lac_2 + S_{ox}, \\ Lac_2 + S_{red} &\overset{k_2}{\rightarrow} Lac_3 + S_{ox}, \\ Lac_3 + S_{red} &\overset{k_3}{\rightarrow} Lac_4 + S_{ox}, \\ Lac_4 + S_{red} &\overset{k_4}{\rightarrow} Lac_{red} + S_{ox}, \\ Lac_{red} + O_2 &\overset{k_{ox}}{\rightarrow} Lac_1 + 2H_2O, \\ Lac_1 &\overset{k_{inact}}{\rightarrow} Lac_{resting}. \end{aligned} \tag{4.1}$$

Here S_{red} and S_{ox} are reduced and oxidized forms of the substrate (ABTS or ferrocyanide); $Lac_{resting}$ – resting form of the enzyme; Lac_1 , Lac_2 , Lac_3 and Lac_4 – enzyme forms at four different stages of one-electron reductions of LAC; Lac_{red} – fully reduced enzyme form; k_{act} – apparent bimolecular enzyme activation rate constant, k_1 , k_2 , k_3 and k_4 – apparent bimolecular one - electron reduction constants; k_{inact} – LAC inactivation rate constant.

In some cases the existence of laccase in resting form is not manifested in experiments. It depends purely on a quantitative relation of k_{act} and k_1(as well as the rate of consecutive steps). If $min\{k_1,\ k_2,\ k_3,\ k_4\} \gg k_{act}$, then the lag-phase is pronounced in the experiments. One of such examples is the oxidation of ferrocyanide catalyzed by the laccase. The traditional initial rate analysis will lead to the underestimation of potas-

sium ferrocyanide oxidation rate constant due to the clearly pronounced lag-phase. But it is not the case when entire curves from experiments are fitted. Of course, the quasi-steady state kinetics does not permit differentiation between rate constants k_1, k_2, k_3 and k_4. Therefore, the rate-limiting rate constant k_{red} of LAC reduction is estimated as defined:

$$\frac{1}{k_{red}} = \frac{1}{k_1} + \frac{1}{k_2} + \frac{1}{k_3} + \frac{1}{k_4}. \tag{4.2}$$

The inhibition with fluoride was accounted by a reaction (Yaropolov et al., 1994):

$$Lac_{red} + F^- \underset{k_d}{\overset{k_a}{\rightleftharpoons}} Lac_{red}F, \tag{4.3}$$

where $Lac_{red}F$ is an inhibited form of enzyme (regardless which enzymatic form is inhibited, the fitting results same rate parameters); $k_a$and k_d – association and dissociation rate constants of fluoride interacting with the LAC active center, respectively. The inhibition constant with fluoride is defined as:

$$K_{inh} = \frac{k_d}{k_a} \tag{4.4}$$

Data were fitted simultaneously for series of experiments. All kinetic curves from ABTS and ferrocyanide experiments alongside with the fluoride inhibition experiments were used in the same fitting run at relevant pH. This approach allows calculating consistent rate constants which should be the same regardless the substrate – LAC rate constant with oxygen k_{ox}, transition to the resting state rate constantk_{inact} and LAC inhibition with fluoride ions constantK_{inh}. Fitted rate constants are listed in the table 4.1.

Table 4.1: Fitted rate constants for *Didymocrea* sp. J6 laccase-catalyzed oxidation of ABTS and ferrocyanide in buffer solution (100 mM phosphate-citrate, 50 mM potassium sulfate) at pH 4.0, 5.5 and 7.4, measured at $25°\mathrm{C}$.

pH	$k_{act\ ABTS}(\mathrm{M^{-1}s^{-1}})$	$k_{act\ Ferro}(\mathrm{M^{-1}s^{-1}})$	$k_{inact}(\mathrm{s^{-1}})$	$k_{ox}(\mathrm{M^{-1}s^{-1}})$
4.0	$> 6.3 \times 10^6$	$(2.7 \pm 0.1) \times 10^2$	0.71 ± 0.05	$(4.17 \pm 0.06) \times 10^4$
5.5	$(1.3 \pm 0.4) \times 10^4$	$> 3.2 \times 10^6$	0.037 ± 0.003	$(2.31 \pm 0.02) \times 10^4$
7.4	$(9.4 \pm 0.2) \times 10^2$	$(1.06 \pm 0.06) \times 10^3$	0.12 ± 0.03	$(7.14 \pm 0.07) \times 10^3$

pH	$k_{red\ ABTS}$	$k_{red\ Ferro}$	K_{inh}
4.0	$(1.548 \pm 0.007) \times 10^5\ \mathrm{M^{-1}s^{-1}}$	$(8.2 \pm 0.3) \times 10^5\ \mathrm{M^{-1}s^{-1}}$	$22.9 \pm 0.2\ \mu\mathrm{M}$
5.5	$(5.18 \pm 0.02) \times 10^4\ \mathrm{M^{-1}s^{-1}}$	$(4.66 \pm 0.08) \times 10^5\ \mathrm{M^{-1}s^{-1}}$	$187 \pm 3\ \mu\mathrm{M}$
7.4	$(1.2 \pm 0.1) \times 10^4\ \mathrm{M^{-1}s^{-1}}$	$(2.8 \pm 0.9) \times 10^5\ \mathrm{M^{-1}s^{-1}}$	$290 \pm 20\ \mu\mathrm{M}$

From the table 4.1 it is seen that in acidic pH rate constant k_{ox} of laccase reaction with oxygen is only $(4.17 \pm 0.06) \times 10^4\ \mathrm{M^{-1}s^{-1}}$ and decreases with increasing alkalinity of a buffer solution. It is surprising, because typical rate constants are $> 10^6\ \mathrm{M^{-1}s^{-1}}$(Cole et al., 1991; Andréasson et al., 1976; Bukh et al., 2006). The fluoride inhibition constant K_{inh} was found to be very small ($22.9 \pm 0.2\ \mu\mathrm{M}$) in $\mathrm{pH}\ 4.0$, and was increased with increasing alkalinity. The value of this inhibition constant is particularly interesting in the context of the following section, because the electrochemically-observed inhibition constant K_{inh} of laccase, immobilized on the electrode covered with gold nanoparticles, is around three orders higher (up to ~$20\ \mathrm{mM}$) in the same buffer solutions as in homogeneous kinetics measurements.

4.2.2 Electrochemistry of the laccase from *Didymocrea* sp. J6 adsorbed on gold electrode covered with gold nanoparticles

The electrochemical measurements of laccase from *Didymocrea* sp. J6 adsorbed on the gold electrode covered with gold nanoparticles , at the presence of various concentrations of fluoride ions in buffer solutions, were carried out by dr. Dalius Ratautas, Vilnius University. These measurements are different from results measured in homogeneous conditions (see above; data in fig. 4.6). Firstly, inhibition constants with fluoride are orders of magnitude larger than observed in the homogeneous kinetics for the same laccase. Secondly, these inhibition constants are unprecedented for laccases adsorbed or immobilized on electrodes (*T. hirsuta* laccase is inhibited completely at $13\ \mathrm{mM}$ of fluoride ions (Vaz-

Dominguez et al., 2008)). Thirdly, the half-wave of reduction potential shifts towards more negative potentials(fig. 4.6).

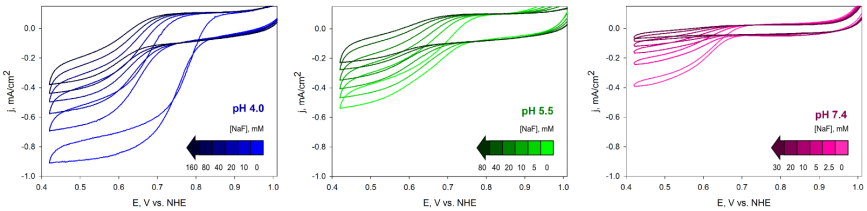

Figure 4.6: Electrochemical responses of laccase from *Didymocrea* sp. J6 adsorbed on gold rotating disk electrode (1000 rpm) covered with gold nanoparticles at presence of various concentrations of fluoride ions, measured in buffer solutions.

The quantitative mathematical modeling of electrochemical data was carried out to describe and understand these observations. However, the information about laccase T1 center reduction potential was necessary in order to properly model the bioelectrocatalytic system. This potential for the laccase was measured by dr. Marius Dagys, Vilnius University, using a spectroelectrochemical titration cell setup, developed and refined by prof. dr. Sergey Shleev, Malmö University, Sweden(fig. 4.7). Absorbance dependencies on a potential were used to calculated reduction potentials of T1 centers, they were determinated to be 683, 716, and $720\ \mathrm{mV}$ at $\mathrm{pH}\ 4.0$, $\mathrm{pH}\ 4.0$ with $20\ \mathrm{mM}$ NaF, and $\mathrm{pH}\ 7.4$ without NaF, respectively.

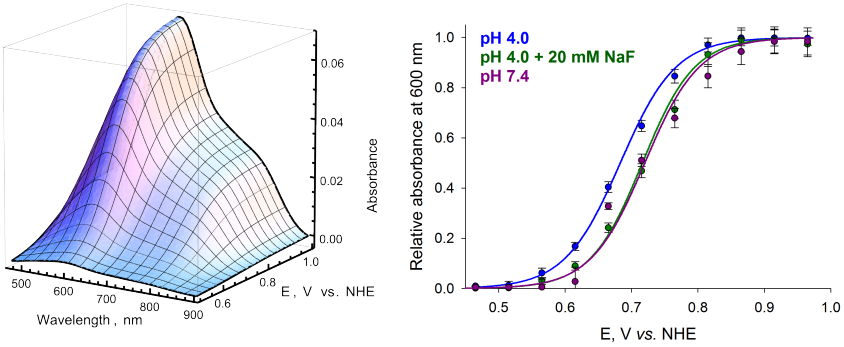

Figure 4.7: Spectroelectrochemical measurements of laccase. Left – absorbace spectrum dependence on reduction potential at $\mathrm{pH}\ 4.0$. Right – dependence of relative absorbace at $600\ \mathrm{nm}$ on reduction potential.

It is widely accepted that the oxygen reduction mechanism in homogeneous medium and on electrodes is the same. Therefore, the catalysis

cycle involves both T1 and T2/T3 redox centers. All previous strategies to construct laccase biocathodes were based on attempts to orient the T1 center of an enzyme sufficiently close to an electrode, which is then reduced. Afterwards, the electrons should be transferred to the T2/T3 center and finally to oxygen (Solomon et al., 1996; Sakurai and Kataoka, 2007). This approach should ensure proper direct electron transfer from an electrode to the T1 center (fig. 4.8A) and facilitate the fabrication of effective biocathode, which can produce larger currents and operate at higher potentials. There are some examples of an enzyme adsorbed on an electrode via T2/T3 center (fig. 4.8). However, such systems were unable to catalyze the bioelectroreduction of oxygen to water(Shleev et al., 2005a).

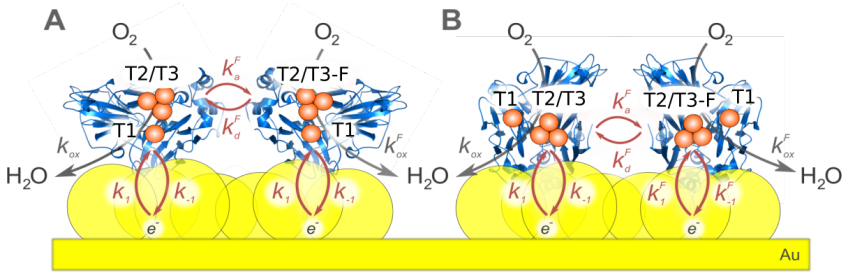

Figure 4.8: Schemes representing J6 laccase wiring via T1 redox center (A) and via T2/T3 redox center (B) electrochemistry and inhibition with fluoride.

Initially, we tried to use the widely-accepted model for laccase biocathodes of the electron transfer *via* T1 center (fig. 4.8A). To derive equations, we made few necessary assumptions. The measurements in fig. 4.6 were made using rotating disk electrode. It was observed that above 1000 rpm, the maximum current does not increase further. Therefore, it was assumed that the observed current is limited by the kinetics of catalysis and not by a mass diffusion of substrates. Additional assumptions were made as well:

1. Measurements were made under the oxygen concentration much smaller than Michaelis constant.

2. Fluoride ion binds to the T2/T3 redox center and modifies the apparent bimolecular oxygen reduction rate constant.

3. Inhibition with fluoride ion constants are the same both for reduced and oxidized forms.

4. The current density is limited by the oxygen reduction catalyzed by laccase.

5. The enzyme-fluoride association constant is infinitely large.

6. Laccase is adsorbed on the electrode *via* T1 center.

Assuming that the laccase is wired to the electrode *via* T1 center and by using the reaction scheme in fig. 4.8A, one can write a set of equations describing proceeding reactions. In this case, the reaction scheme can be approximated by these reactions (assuming existence of one-electron transfer limiting step) happening on the electrode surface:

$$\begin{gathered}
Lac_{T1O}^{T2T3O} + e \overset{k_{e1}}{\underset{k_{e2}}{\rightleftharpoons}} Lac_{T1R}^{T2T3O} \\
Lac_{T1R}^{T2T3O} \overset{k_{ie1}}{\underset{k_{ie2}}{\rightleftharpoons}} Lac_{T1O}^{T2T3R} \\
Lac_{T1O}^{T2T3R} + O_2 \overset{k_{ox}}{\rightarrow} Lac_{T1O}^{T2T3O} + H_2O \\
Lac_{T1O}^{T2T3OF} + e \overset{k_{e1f}}{\underset{k_{e2f}}{\rightleftharpoons}} Lac_{T1R}^{T2T3OF} \\
Lac_{T1R}^{T2T3OF} \overset{k_{ie1f}}{\underset{k_{ie2f}}{\rightleftharpoons}} Lac_{T1O}^{T2T3RF} \\
Lac_{T1O}^{T2T3RF} + O_2 \overset{k_{fox}}{\rightarrow} Lac_{T1O}^{T2T3OF} + H_2O \\
Lac_{T1O}^{T2T3O} + F^- \overset{k_a^f}{\underset{k_d^f}{\rightleftharpoons}} Lac_{T1O}^{T2T3OF} \\
Lac_{T1R}^{T2T3O} + F^- \overset{k_a^f}{\underset{k_d^f}{\rightleftharpoons}} Lac_{T1R}^{T2T3OF} \\
Lac_{T1O}^{T2T3R} + F^- \overset{k_a^f}{\underset{k_d^f}{\rightleftharpoons}} Lac_{T1O}^{T2T3RF}
\end{gathered} \tag{4.5}$$

where indices represent redox state and fluoride binding to the enzyme. For example, in Lac_{T1R}^{T2T3O} the upper index represents oxidized T2/T3 center (hence O in T2T3O), meanwhile the lower index indicates reduced T1 center (R for "reduced" in T1R). Reaction rate constants k_{e1}, k_{e2},k_{e1f} and k_{e2f} are the rate constants of heterogeneous oxidation and reduction reactions on the electrode. Rate constants, designated as k_{ie*} are the rate constants of internal electron transfer between T1 and T2/T3 centers. The reaction scheme above results in this set of differential equations:

$$
\begin{aligned}
\frac{d\Gamma_{T1O}^{T2T3O}}{dt} = \quad & -k_{e1}\Gamma_{T1O}^{T2T3O} + k_{e2}\Gamma_{T1R}^{T2T3O} + k_{ox}\Gamma_{T1O}^{T2T3R}[O_2] \\
& -k_a^f\Gamma_{T1O}^{T2T3O}[F^-] + k_d^f\Gamma_{T1O}^{T2T3OF} \\
\frac{d\Gamma_{T1O}^{T2T3OF}}{dt} = \quad & k_a^f\Gamma_{T1O}^{T2T3O}[F^-] - k_d^f\Gamma_{T1O}^{T2T3OF} - k_{e1f}\Gamma_{T1O}^{T2T3OF} \\
& +k_{e2f}\Gamma_{T1R}^{T2T3OF} + k_{fox}\Gamma_{T1O}^{T2T3RF}[O_2] \\
\frac{d\Gamma_{T1O}^{T2T3R}}{dt} = \quad & k_{ie1}\Gamma_{T1R}^{T2T3O} + k_{ie2}\Gamma_{T1O}^{T2T3R} - k_{ox}\Gamma_{T1O}^{T2T3R}[O_2] \\
& -k_a^f\Gamma_{T1O}^{T2T3R}[F^-] + k_d^f\Gamma_{T1O}^{T2T3RF} \\
\frac{d\Gamma_{T1O}^{T2T3RF}}{dt} = \quad & k_a^f\Gamma_{T1O}^{T2T3R}[F^-] - k_d^f\Gamma_{T1O}^{T2T3RF} + k_{ie1f}\Gamma_{T1R}^{T2T3OF} \\
& -k_{ie2f}\Gamma_{T1O}^{T2T3RF} + k_{fox}\Gamma_{T1O}^{T2T3RF}[O_2] \\
\frac{d\Gamma_{T1R}^{T2T3O}}{dt} = \quad & k_{e1}\Gamma_{T1O}^{T2T3O} - k_{e2}\Gamma_{T1R}^{T2T3O} - k_a^f\Gamma_{T1R}^{T2T3O}[F^-] \\
& +k_d^f\Gamma_{T1R}^{T2T3OF} - k_{ie1}\Gamma_{T1R}^{T2T3O} + k_{ie2}\Gamma_{T1O}^{T2T3R} \\
\frac{d\Gamma_{T1R}^{T2T3OF}}{dt} = \quad & k_{e1f}\Gamma_{T1O}^{T2T3OF} - k_{e2f}\Gamma_{T1R}^{T2T3OF} + k_a^f\Gamma_{T1R}^{T2T3O}[F^-] \\
& -k_d^f\Gamma_{T1R}^{T2T3OF} - k_{ie1f}\Gamma_{T1R}^{T2T3OF} + k_{ie2f}\Gamma_{T1O}^{T2T3RF} \\
\Gamma^{tot} = \quad & \Gamma_{T1O}^{T2T3O} + \Gamma_{T1O}^{T2T3OF} + \Gamma_{T1O}^{T2T3R} \\
& +\Gamma_{T1O}^{T2T3RF} + \Gamma_{T1R}^{T2T3O} + \Gamma_{T1R}^{T2T3OF}
\end{aligned}
\tag{4.6}
$$

where Γ represents the surface concentration ($\mathrm{mol/cm^2}$) of relevant species of enzyme on the electrode and Γ^{tot} is the total concentration of enzyme on the electrode. [O_2] and $[F^-]$ are bulk concentrations ($\mathrm{mol/cm^3}$) of oxygen and fluoride ions, respectively. The set of differential equations can be simplified by assuming the quasi-steady state and, hence, equating all the derivatives $\frac{d\Gamma}{dt}$ to zero. The resulting set of algebraic equations can be solved for each form of the enzyme and substituted into the current equation, defined as:

$$
i = -nF(k_{ox}\Gamma_{T1O}^{T2T3R}[O_2] + k_{fox}\Gamma_{T1O}^{T2T3RF}[O_2]) \tag{4.7}
$$

where n is a number of electrons needed to reduce one oxygen molecule (4) and F is a Faraday constant. The final equation, which represents the traditional laccase electrocatalysis scheme in fig. 4.8A, is:

$$
\begin{aligned}
i \;=\; & -n(\Gamma^{tot}F([F^-]k^f_{e1}+k_{e1}K_{inh})([F^-]k^f_{ie1}+ \\
& k_{ie1}K_{inh})([F^-]k^f_{ox}+K_{inh}k_{ox})[O_2])/ \\
& (([F^-]+K_{inh})([F^-]^2(k^f_{ox}k^f_{ie1}[O_2]+ \\
& k^f_{e2}(k^f_{ie2}+k^f_{ox}[O_2])+k^f_{e1}(k^f_{ie1}+ \\
& k^f_{ie2}+k^f_{ox}[O_2]))+K^2_{inh}(k_{ie1}k_{ox}[O_2]+ \\
& k_{e2}(k_{ie2}+k_{ox}[O_2])+k_{e1}(k_{ie1}+k_{ie2}+ \\
& k_{ox}[O_2]))+[F^-]K_{inh}(k^f_{e2}k_{ie2}+k_{e2}k^f_{ie2}+ \\
& k_{e2}k^f_{ox}[O_2]+k^f_{ox}k_{ie1}[O_2]+k^f_{e2}k_{ox}[O_2]+ \\
& k^f_{ie1}k_{ox}[O_2]+k_{e1}(k^f_{ie1}+k^f_{ie2}+k^f_{ox}[O_2])+ \\
& k^f_{e1}(k_{ie1}+k_{ie2}+k_{ox}[O_2])))))
\end{aligned}
\tag{4.8}
$$

Here $K_{inh} = \frac{k^f_d}{k^f_a}$. We assume that the heterogeneous rate constant k_{e1} is equal to k_{e1f} and k_{e2} is equal to k_{e2f}, because fluoride ions bind to the T2/T3 center, therefore the potential of T1 center should not be affected by a fluoride binding event. These constants are expressed by using Butler-Volmer model:

$$
k_{e1} = k_{e1f} = k_0 e^{-\alpha(E-E^0_{T1})\frac{F}{RT}} \tag{4.9}
$$

$$
k_{e2} = k_{e2f} = k_0 e^{(1-\alpha)(E-E^0_{T1})\frac{F}{RT}} \tag{4.10}
$$

Here E^0_{T1} is the reduction potential of T1 center, R – gas constant, T – temperature and α is a charge transfer coefficient, which accounts for the asymmetry of a charge transfer event. Equations above were used to fit data illustrated in fig. 4.6. The mathematical form of the equation 4.8 is very general and, therefore, fits the data very well. However, the optimal fit results in the reduction potential $E^0_{T1} = 0.227 \pm 0.003$ V and $k_{ie1} = 1.2 \times 10^{12}$ s^{-1} at pH $= 4.0$. This fit should be dismissed as nonsensical due to following reasons. Firstly, it contradicts the spectroelectrochemically measured value of $E^0_{T1} = 0.683$ V. Secondly, it requires of enormous rate constant of internal electron transfer, which is unprecedented and surpasses any rate constant of internal electron transfer known before for laccases by twelve orders of magnitude (Farver et al., 2011). Thirdly, the rate constant's value is impossible in electron transfer theory due to 13 Å distance between T1 and T2/T3 centers. These results imply that the reaction scheme describing the process of bioelectrocatalysis via T1 center wired to the electrode is not selected

appropriately. There is another possible scheme, which describes the observed bioelectrocatalysis of laccase via direct contact of the T2/T3 center with the gold electrode coated with gold nanoparticles (fig. 4.8B). We investigated this reaction scheme further, however, it should be noted, that there are no publications providing any example of the bioelectrocatalysis of a laccase with the direct electron transfer from an electrode to the T2/T3 center. In fact, there are publications claiming that a laccase was allegedly adsorbed via the T2/T3 center, but no oxygen reduction is observed(Shleev et al., 2005a). To model the bioelectrocatalysis of oxygen reduction with the laccase immobilized on the electrode *via* the T2/T3 center, the following assumptions were made:

1. Measurements were made under the oxygen concentration much smaller than Michaelis constant.

2. The impact of the T1 redox center in the electron transfer is negligible and electron transfer occurs between the T2/T3 redox center and the electrode.

3. Fluoride ion binds to the T2/T3 redox center and modifies heterogenic rate constants and the apparent bimolecular oxygen reduction rate constant.

4. Inhibition with fluoride ion constants are the same both for reduced and oxidized forms.

5. The current density is limited by the catalytic oxygen reduction by the laccase.

6. The enzyme-fluoride association constant is infinitely large.

Similarly, as in the case of laccase wiring *via* T1 center, for the scheme in fig. 4.8B, a system of differential equations is constructed:

$$\begin{aligned}
\frac{d\Gamma^O}{dt} &= k_2\Gamma^R - k_1\Gamma^O + k_{ox}\Gamma^R[O_2]) + k_d^f\Gamma^{FO} - k_a^f\Gamma^O[F^-] \\
\frac{d\Gamma^R}{dt} &= k_1\Gamma^O - k_2\Gamma^R - k_{ox}\Gamma^R[O_2] + k_d^f\Gamma^{FR} - k_a^f\Gamma^R[F^-] \\
\frac{d\Gamma^{FO}}{dt} &= k_2^f\Gamma^{FR} - k_1^f\Gamma^{FO} + k_{ox}^f\Gamma^{FR}[O_2] + k_a^f\Gamma^O[F^-] - k_d^f\Gamma^{FO} \\
\frac{d\Gamma^{FR}}{dt} &= -k_2^f\Gamma^{FR} + k_1^f\Gamma^{FO} - k_{ox}^f\Gamma^{FR}[O_2] - k_d^f\Gamma^{FR} + k_a^f\Gamma^R[F^-]
\end{aligned} \tag{4.11}$$

where $\Gamma(\mathrm{mol/cm^2})$ represents the surface coverage of various oxidation and fluoride binding states of the laccase; $[F]$ and $[O_2]$ are bulk concentrations $(\mathrm{mol/cm^3})$ of fluoride and oxygen, respectively. Assuming the steady-state and adding the mass balance equation for the enzyme surface coverage and the current density equation:

$$\Gamma^O + \Gamma^R + \Gamma^{FO} + \Gamma^{FR} = \Gamma^{Tot} \tag{4.12}$$

$$i = -nF(k_{ox}^f \Gamma^{FR}[O_2] + k_{ox}\Gamma^R[O_2]) \tag{4.13}$$

$$\frac{k_d^f}{k_a^f} = K_{inh} \tag{4.14}$$

it is possible to solve all surface coverages of enzyme forms and put solutions in to the current equation, substitute fluoride dissociation rate constants with $k_d^f \to k_a^f K_{inh}$, simplify expression and to take limit $k_a^f \to \infty$:

$$i = \frac{-nF\Gamma^{Tot}[O_2]([F]k_1^f + k_1 K_{inh})([F]k_{ox}^f + K_{inh}k_{ox})}{([F] + K_{inh})([F](k_1^f + k_2^f + k_{ox}^f[O_2]) + K_{inh}(k_1 + k_2 + k_{ox}[O_2]))} \tag{4.15}$$

where:

$$k_1 = k_0 e^{-\alpha(E - E_{T2}^0)\frac{F}{RT}} \tag{4.16}$$

$$k_2 = k_0 e^{(1-\alpha)(E - E_{T2}^0)\frac{F}{RT}} \tag{4.17}$$

$$k_1^f = k_0^f e^{-\alpha(E - E_{T2}^{F0})\frac{F}{RT}} \tag{4.18}$$

$$k_2^f = k_0^f e^{(1-\alpha)(E - E_{T2}^{F0})\frac{F}{RT}} \tag{4.19}$$

The equation 4.15 is much simpler and more elegant than equation 4.8. This simplicity is a result of elimination of the T1 center from the reaction scheme. The proposed model of the laccase wired to the electrode *via* T2/T3 center bioelectrocatalysis (eq. 4.15) was used to fit data presented in fig. 4.6. The fit with data is illustrated in fig. 4.9. As

seen from fig. 4.9, the model describes experiments very well (the total concentration of enzyme on the electrode $\Gamma^{tot} = 220$ pM were used in data fitting; concentration determination details in (Dagys et al., 2017)). Therefore, modeling studies allows us to conclude that for the first time the direct electron transfer from the electrode to the T2/T3 center and the simultaneous enzymatic oxygen reduction was observed. However, the reader may not entirely be satisfied with this conclusion and and require to demonstrate, how do equations 4.8 and 4.15 apply in the case, when it is known that the laccase is oriented on the electrode *via* T1 center. Indeed, this control experiment was performed and it was demonstrated that in such case the equation 4.8 fits the data and equation 4.15 does not describe the experiment (details in (Dagys et al., 2017)).

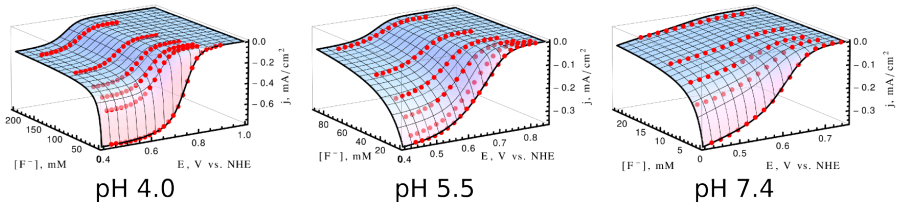

Figure 4.9: The model of the laccase wired to the electrode via T2/T3 center bioelectrocatalysis (eq. 4.15) fitted to the data from fig. 4.6.

Fitted parameters for eq. 4.15 are listed in the table 4.2. As seen from the table, the oxygen reduction rate constant k_{ox} for all pH values is nicely comparable to relevant rate constant estimated in homogeneous kinetics experiments (table 4.1). Surprisingly, the fluoride binding to the T2/T3 center does not nullify the bioelectrocatalytic reduction of oxygen with the laccase. Rate constants of the fluoride ion bound T2/T3 center are found at most of order of magnitude smaller than in the absence of fluoride ions (for example, at pH 5.5 in table 4.1). Found values of reduction potentials of the T2/T3 center reduction potentials $E^0_{T2/T3}$ are interesting, because they explain various peculiarities of laccase catalysis. At pH 4.0 $E^0_{T2/T3}$ (752 ± 1 mV) is larger than E^0_{T1} (683 mV) and smaller than the oxygen reduction potential (989 mV in pH 4.0). Therefore, the thermodynamically favorable flow of electrons is ensured. However, at larger pH values $E^0_{T2/T3}$ becomes smaller than E^0_{T1} and the electron flow is disrupted between T1 and T2/T3 centers. Therefore, apparent bimolecular rate constants k_{red} (table 4.1), which are synthetic and accounts for the internal electron transfer between T1 and T2/T3

centers as well, gradually decreases with pH values.

Table 4.2: Fitted parameters for data and the model (eq. 4.15) in fig. 4.9

Parameter	pH 4.0	pH 5.5	pH 7.4
k_0, s^{-1}	30 ± 1	3.4 ± 0.2	6.0 ± 0.4
k_{ox}, $\mathrm{M}^{-1}\mathrm{s}^{-1}$	$(3.72 \pm 0.01) \times 10^4$	$(1.71 \pm 0.01) \times 10^4$	$(2.3 \pm 0.2) \times 10^4$
$E^0_{T2/T3}$, mV	752 ± 1	674 ± 1	599 ± 3
α	0.31 ± 0.01	0.36 ± 0.01	0.13 ± 0.03
k^f_0, s^{-1}	7.0 ± 0.3	2.3 ± 1.5	0.36 ± 0.21
$E^{F0}_{T2/T3}$, mV	600 ± 1	570 ± 1	500 ± 90
k^f_{ox}, $\mathrm{M}^{-1}\mathrm{s}^{-1}$	$(1.01 \pm 0.01) \times 10^4$	$(0.17 \pm 0.03) \times 10^4$	$(2 \pm 170) \times 10^4$ ‡
α^f	0.34 ± 0.03	0.21 ± 0.07	0.16 ± 0.02
K_{inh}, mM	5.63 ± 0.06	19.6 ± 0.7	6.9 ± 1.4

‡Values are difficult to establish due to low current density and narrow CV profiles of NaF-inhibited systems working at pH 7.4.

4.2.3 Comparison of laccase's homogeneous and heterogeneous kinetics.

Observed rate constants k_{ox} of the oxygen reduction, determined from electrochemical and spectrophotometrical measurements, are well-comparable. This finding suggests that the general outline of the catalysis mechanism is well grasped in both cases. However, there is the obvious discrepancy observed concerning the inhibition with fluoride ions constant(K_{inh}). For example, from the homogeneous kinetics it is found that $K_{inh} = 22.9 \pm 0.2\ \mu\mathrm{M}$ at $\mathrm{pH} = 4.0$. Electrochemical measurements and data analysis resulted in $K_{inh} = 5.63 \pm 0.06\ \mathrm{mM}$ at $\mathrm{pH} = 4.0$. The difference of two orders of magnitude is serious enough to require an explanation, without which electrochemical and homogeneous measurements are not reconciled. The most obvious and trivial explanation would be the change of the laccase affinity for fluoride ions upon an adsorption on the electrode due to some kind of enzyme structural changes and an influence of double layer effects. Yet, this explanation completely ignores the similarities in k_{ox} values. Below we provide a model which reconciles these discrepancies.

Firstly, one should note that K_{inh} values are calculated using different reaction schemes in the homogeneous and heterogeneous kinetics. These differences are rooted in necessity to use as little as possible variables to describe the system. Therefore, the homogeneous kinetics was

approximated with this scheme (the laccase inactivation and reactivation were removed for clarity):

$$\begin{aligned} Lac_1 + S_{red} &\overset{k_1}{\rightarrow} Lac_2 + S_{ox}, \\ Lac_2 + S_{red} &\overset{k_2}{\rightarrow} Lac_3 + S_{ox}, \\ Lac_3 + S_{red} &\overset{k_3}{\rightarrow} Lac_4 + S_{ox}, \\ Lac_4 + S_{red} &\overset{k_4}{\rightarrow} Lac_{red} + S_{ox}, \\ Lac_{red} + O_2 &\overset{k_{ox}}{\rightarrow} Lac_1 + 2H_2O, \\ Lac_{red} + F^- &\underset{k_d}{\overset{k_a}{\rightleftharpoons}} Lac_{red}F. \end{aligned} \tag{4.20}$$

For this scheme, the quasi-steady state equation of the oxygen consumption is:

$$\frac{d[O_2]}{dt} = -\frac{[S_{red}][O_2][E_0]k_{red}k_{ox}K_{inh}}{4[O_2]k_2K_{inh} + [S_{red}]k_{red}([F^-] + K_{inh})} \tag{4.21}$$

where k_{red} is as previously defined:

$$\frac{1}{k_{red}} = \frac{1}{k_1} + \frac{1}{k_2} + \frac{1}{k_3} + \frac{1}{k_4}. \tag{4.22}$$

This scheme poorly reflects the internal electron transfer, which occurs between T1 and T2/T3 redox centers. Under our experimental conditions, rate constants of the internal electron transfer are merged in to other constants and are not recoverable. However, one can compare the equation 4.21 with a more general scheme for the laccase kinetics, which accounts the internal charge transfer and is much more similar to the scheme used to fit data in electrochemical experiments:

$$\begin{aligned} Lac_1 + S_{red} &\overset{k_1}{\rightarrow} Lac_2 + S_{ox}, \\ Lac_2 + S_{red} &\overset{k_2}{\rightarrow} Lac_3 + S_{ox}, \\ Lac_3 + S_{red} &\overset{k_3}{\rightarrow} Lac_4 + S_{ox}, \\ Lac_4 + S_{red} &\overset{k_4}{\rightarrow} Lac^{ox}_{red} + S_{ox}, \\ Lac^{ox}_{red} &\underset{k_b}{\overset{k_f}{\rightleftharpoons}} Lac^{red}_{ox} \\ Lac^{red}_{ox} + O_2 &\overset{k_{ox}}{\rightarrow} Lac_1 + 2H_2O, \\ Lac^{ox}_{red} + F^- &\underset{k_d}{\overset{k_a}{\rightleftharpoons}} Lac^{ox}_{red}F. \end{aligned} \qquad \begin{aligned} Lac_1F + S_{red} &\overset{k_1}{\rightarrow} Lac_2F + S_{ox}, \\ Lac_2F + S_{red} &\overset{k_2}{\rightarrow} Lac_3F + S_{ox}, \\ Lac_3F + S_{red} &\overset{k_3}{\rightarrow} Lac_4F + S_{ox}, \\ Lac_4F + S_{red} &\overset{k_4}{\rightarrow} Lac^{ox}_{red}F + S_{ox}, \\ Lac^{ox}_{red}F &\underset{k_b^F}{\overset{k_f^F}{\rightleftharpoons}} Lac^{red}_{ox}F \\ Lac^{red}_{ox}F + O_2 &\overset{k^F_{ox}}{\rightarrow} Lac_1F + 2H_2O, \end{aligned} \tag{4.23}$$

From this scheme one can derive the quasi-steady state rate equation, which is:

$$\begin{gathered}\frac{d[O_2]}{dt} = -[S_{red}][O_2][E_0]k_{red}([F^-]k_{ox}^F + k_{ox}K_{inh})/ \\ (4[O_2]([F^-]k_{ox}^F + k_{ox}K_{inh}) + [S_{red}]k_{red}([F^-](1 + \beta[O_2] + (K_{eq}^F)^{-1}) \\ +K_{inh}(1 + \alpha[O_2] + (K_{eq})^{-1})))\end{gathered} \tag{4.24}$$

where, $(K_{eq})^{-1} = \frac{k_b}{k_f}$, $(K_{eq}^F)^{-1} = \frac{k_b^F}{k_f^F}$, $\alpha = \frac{k_f}{k_{ox}}$ and $\beta = \frac{k_f^F}{k_{ox}^F}$. The k_f and k_b are rate constants of the limiting step in the electron transfer from T1 to T2/T3 center (we assume that one of four electron transfer is the slowest and limits the electron transfer process), respectively. This equation appears very different from the simpler equation 4.21 discussed above. However, by rearranging terms in both equations, assuming low $[F^-]$ concentration and excluding terms which are not fluoride-dependent, one can find that the inhibition constant K_{inh}^{hom},which was measured in homogeneous medium, is related to the inhibition constant K_{inh}^{het} found from the electrode kinetics:

$$K_{inh}^{hom} = \frac{K_{inh}^{het}}{1 + \beta[O_2] + (K_{eq}^F)^{-1}} \tag{4.25}$$

which, assuming $1 + \beta[O_2] \ll (K_{eq}^F)^{-1}$, is simplified to:

$$K_{inh}^{hom} = K_{inh}^{het}K_{eq}^F \tag{4.26}$$

The equilibrium constant K_{eq}^F can be directly related to reduction potentials of T1 and fluoride bound T2/T3 centers, which were experimentally determinated earlier. K_{eq}^F can be expressed using Nernst equation *via* reduction potentials:

$$K_{eq}^F = \exp(\frac{(E_{T2/T3}^F - E_{T1})nF}{RT}) \tag{4.27}$$

Therefore, ratios $K_{inh}^{het}/K_{inh}^{hom}$ were used to calculate standard reduction potentials of the electron transfer from T1 to the fluoride-bound T2/T3 center from heterogeneous and homogeneous inhibition constants. These potentials were found to be -120 mV, -130 mV and -120 mV at pH 4.0, 5.5 and 7.4, respectively. Reduction potentials found from inhibition constants are comparable to reduction potentials measured electrochemically (-140 mV, -120 mV and -80 mV at pH 4.0, 5.5 and 7.4

respectively). Therefore, we conclude that discrepancies of inhibition constants in homogeneous and heterogeneous processes are fully explained by the proposed model. Furthermore, small inhibition constants with fluoride ions found by other authors with different laccases and bilirubin oxidases actually reflect not a pure inhibition, but rather a complex process, when a bound ligand influences redox properties of redox centers and disrupts the thermodynamics of the electron transfer.

4.3 Résumé

It was demonstrated that the catalytic properties of laccase from *Didymocrea* sp. J6 are the same both in the homogeneous medium and on the surface of electrode coated with gold nanoparticles. The modeling of the bioelectrocatalysis allowed differentiation between two proposed mechanisms of the oxygen reduction on the electrode and showed that in this specific case the oxygen reduction proceeds by the direct transfer of electrons from the electrode to the T2/T3 active center. To our best knowledge it is the first catalytically active laccase-based biocathode, which functions *via* the direct electron transfer to the T2/T3 center. These findings are further supported by the comparison of results with the homogeneous kinetics, because oxygen reduction rate constants at $\mathrm{pH}\ 4.0$, 5.5 and 7.4 are similar in both homogeneous and heterogeneous cases. It was found that the fluoride binding to the T2/T3 center shifts reduction potentials of the center and therefore impairs the electron transfer from T1 to T2/T3 center in the homogeneous case. This effect results in the large difference in fluoride inhibition constants in the homogeneous and heterogeneous catalysis, which is fully explainable and predictable from reduction potentials of the laccase T1 and T2/T3 centers with and without bound fluoride.

5 INVESTIGATION AND MODELING OF THE ELECTRON AND PROTON TRANSFER IN *COPRINOPSIS CINEREA* PEROXIDASE COMPOUND II REDUCTION

While in the first part of the thesis the method for general biochemical kinetics data analysis was developed and in the second part it was applied to the investigation of the laccase catalysis, in the third part the concern is about the much more complex catalysis of peroxidase. In particular, the investigation of electron and proton transfer in the reduction of *Coprinopsis cinerea* peroxidase compound II is described. The long-standing problematics of enzymatic catalysis, which we address here for a particular enzyme, is about how are the properties of substrates and enzymes related to the efficiency of catalysis and how can it be modeled and predicted. Here we address this problem by experimental and theoretical means and demonstrate that, despite the general opinion in the literature, the limiting step in the substrate oxidation by peroxidase is not always a transfer of the electron. It is a much complicated process where proton transfer rate influences catalytic efficiency as well.

5.1 Charge transfer theories and peroxidase structure and catalysis mechanism

The Marcus theory for a charge transfer Redox reactions are basic building blocks of a metabolism in living things, energy and matter changes in nature and industrial applications. All these reactions are orchestrated by the transfer of two particles – electron and proton. The theoretical basis of the electron transfer (which is applicable to the proton transfer as well) was laid in mid-sixties by Rudolph A. Marcus in his seminal works (Marcus, 1956b; Marcus, 1959; Marcus, 1960). The Marcus electron transfer theory was born surrounded by, as R. A. Marcus points out himself, very fortunate and fruitful circumstances. The nuclear technology boomed (in a literal and commercial meaning) after World War II and made radioactive isotopes abundant for a research, medicine and technology. The studies of the electron transfer started from simple isotopic self-exchange reactions such as:

$$ {}^{*}Fe^{3+} + Fe^{2+} \rightarrow {}^{*}Fe^{2+} + Fe^{3+} \tag{5.1} $$

Here the isotope is noted with the asterisk. These self-exchange reactions allowed removing one of a reaction rate controlling factors – a reaction driving force ($-\Delta G^0$) and focus on more immediate questions. Another invention was a stopped-flow apparatus for the investigation of reaction kinetics rates. Technological advances eventually resulted in a large field of research concerned with the electron transfer(Marcus, 1999) (depicted in fig. 5.1).

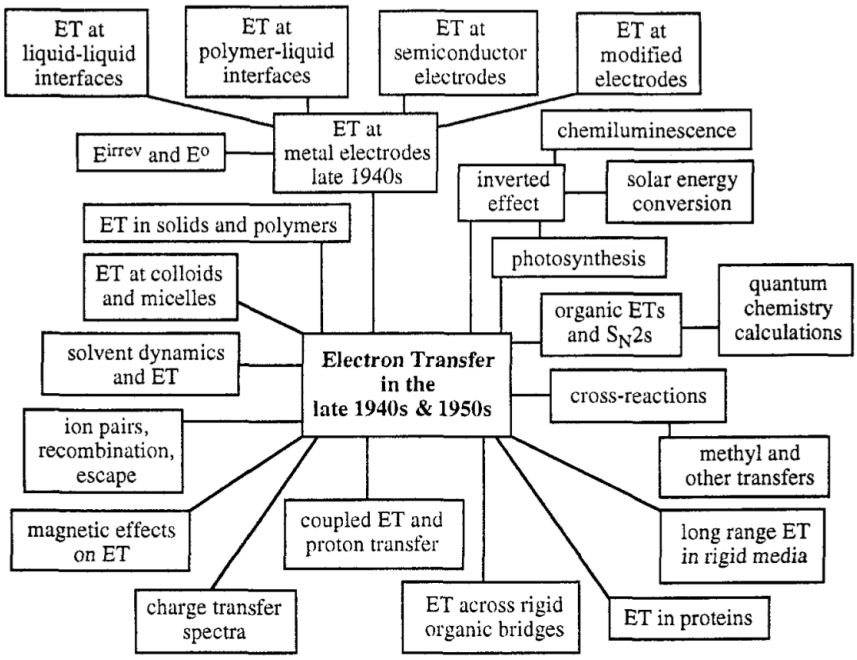

Figure 5.1: Electron transfer topics after 1940 (from R.A. Marcus "Electron transfer past and future")(Marcus, 1999).

The investigation of isotopic self-exchange reactions revealed an interesting trend – small ions reacted much slower than those of larger radiuses. This behavior was attempted to explain qualitatively by Libby(Libby, 1952) by employing a Frank-Condon principle (i. e., a probability of electronic or vibronic transition is proportional to the overlap of initial and final wave functions). It was reasoned that ions in a solvent forms solvation shells, which should reorganize on an event of the electron transfer. Therefore, small "naked" ions should undergo more drastic changes upon a redox event than large complexes. R. A. Marcus took this idea and formulated it quantitatively in a very elegant

way – by imagining not ions or atoms, but two conductive spheres submerged in a dielectric medium. This creative simplification led to the *classical* Marcus electron transfer theory, because it reformulated the electron transfer into an electrostatical problem. The process to be modeled is a charge transfer from one sphere to other.

Conducting spheres charged with some amount of electronic charge generates an electrostatic field, which induces a polarization in a dielectric. On the event of a charge transfer, a dielectric should reorganize its electric dipole moments to accommodate new a charge distribution on conducting spheres. Following Marcus ideas (Marcus, 1956b), the solvent polarization $\boldsymbol{P}(\boldsymbol{r})$, which arises from the electrostatic field $\boldsymbol{E}(\boldsymbol{r})$, is separated into "slow" $\boldsymbol{P}_u(\boldsymbol{r})$ and "fast" $\boldsymbol{P}_e(\boldsymbol{r})$ contributions:

$$\boldsymbol{P}(\boldsymbol{r}) = \boldsymbol{P}_u(\boldsymbol{r}) + \boldsymbol{P}_e(\boldsymbol{r}) \tag{5.2}$$

These polarization components represent electronic, atomic and orientational parts, which reorganize on the charge transfer. The "fast" $\boldsymbol{P}_e(\boldsymbol{r})$ part represents an electronic contribution, which reorganizes immediately after the charge transfer. The "slow" $\boldsymbol{P}_u(\boldsymbol{r})$ contribution represents what is left (a reorientation of molecules of a dielectric to accommodate a new charge distribution) and relaxes much later. Therefore, on the charge transfer, $\boldsymbol{P}_e(\boldsymbol{r})$ is readjusted instantly to a new equilibrium, and $\boldsymbol{P}_u(\boldsymbol{r})$ is not. The free energy difference between an initial equilibrium state and a state after the charge transfer is defined by Marcus as a solvent (dielectric) reorganization energy:

$$\lambda_s = F^* - F_{eq} \tag{5.3}$$

Where F^* is a non-equilibrium free energy of a state with the transferred charge and F_{eq} is an equilibrium free energy of an initial state before the charge transfer. For both states it is assumed that $\boldsymbol{P}_u(\boldsymbol{r}) = \boldsymbol{P}_u^*(\boldsymbol{r})$. Free energies F^* and F_{eq} are expressed as(Marcus, 1956a):

$$F^* = \frac{1}{2}\int\left(\frac{\mathbf{E}_c^{*2}}{4\pi} - \mathbf{P}^*\cdot\mathbf{E}_c^* + \mathbf{P}_u\cdot\left(\frac{\mathbf{P}_u}{\alpha_u} - \mathbf{E}^*\right)\right)dV + PV \tag{5.4}$$

$$F_{eq} = \frac{1}{2}\int \left(\frac{\mathbf{E}_c^2}{4\pi} - \mathbf{P}\cdot\mathbf{E}_c + \mathbf{P}_u \cdot \left(\frac{\mathbf{P}_u}{\alpha_u} - \mathbf{E} \right) \right) dV + PV \tag{5.5}$$

where α_u is the slow component of total polarizability $\alpha = \alpha_u + \alpha_e$ and $\mathbf{E}_c$ is an electric field strength in a vacuum. This component is expressed in terms of static and optical dielectric constants as:

$$4\pi\alpha_u = D_s - D_{op} \tag{5.6}$$

By assumption that a system volume does not change and that no overall change of the charge occurs in the system, one can deduce that parts of integrals involving $\mathbf{E}_c^{*2}$ and $\mathbf{E}_c^2$ are equal (assuming same sizes of spheres and symmetry of integrals). Therefore, negligible influence of the slow polarization $\boldsymbol{P}_u(\boldsymbol{r})$ results:

$$\lambda_s = F^* - F = \frac{1}{2}\int (\mathbf{P} - \mathbf{P}^*)\cdot\mathbf{E}_c dV \tag{5.7}$$

Where polarizations is substituted with $\mathbf{E}_c$ multiplied by corresponding polarizabilities:

$$\mathbf{P} = \alpha\mathbf{E} = \frac{\alpha}{1+4\pi\alpha}\mathbf{E}_c \;\; and \;\; \mathbf{P}^* = \alpha_e\mathbf{E}^* = \frac{\alpha_e}{1+4\pi\alpha_e}\mathbf{E}_c \tag{5.8}$$

With expressions for α and α_e in terms of static and optical dielectric constants:

$$\epsilon^{op} = 4\pi\alpha + 1 and \;\; \epsilon^{st} = 4\pi\alpha_e + 1$$

The result:

$$\lambda_s = \frac{1}{8\pi}\int (\frac{1}{\epsilon^{op}} - \frac{1}{\epsilon^{st}})\mathbf{E}_c^2 dV \tag{5.9}$$

which is integrated by substituting $\mathbf{E}_c^2$ by the corresponding field produced by charged spheres:

$$\lambda_s = (\frac{1}{\epsilon^{op}} - \frac{1}{\epsilon^{st}}) \left[\int_0^{-\Delta e} \frac{q_A}{r_A} dq_A + \int_0^{\Delta e} \frac{q_D}{r_D} dq_D + \int_\infty^{R_{DA}} \frac{\Delta e^2}{r^2} dr \right] \tag{5.10}$$

Where r_A and r_D are radiuses of donor and acceptor spheres, respectively, R_{DA} is a distance between spheres. Final integration yields the famous Marcus equation, which describes the reorganization energy for two conducting spheres:

$$\lambda_s = (\frac{1}{2r_D} + \frac{1}{2r_A} - \frac{1}{R_{AD}})(\frac{1}{\epsilon^{op}} - \frac{1}{\epsilon^{st}})\Delta e^2 \tag{5.11}$$

This famous equation is a major factor of another Marcus invention – Marcus parabolas (fig. 5.2). As seen from the equation 5.11, it is parabolic in the term of a transferred charge Δe. Therefore, a general form of an energy dependence on the change of a charge have a form $E_r(\Delta e) = \lambda(\Delta e)^2 + E_r$ for reagents and $E_p(\Delta e) = \lambda(\Delta e - 1)^2 + E_p$ for products (here 1 charge molar equivalent is transferred).

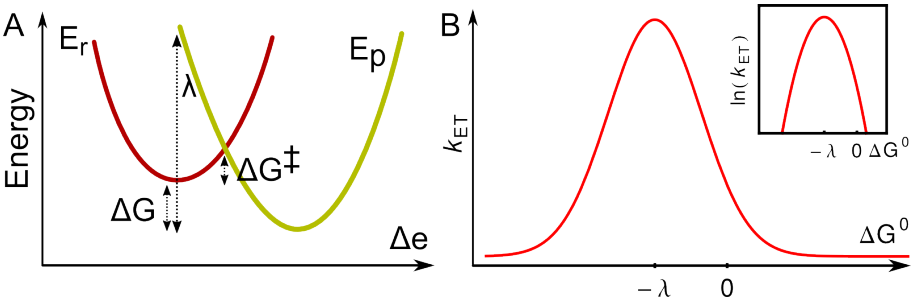

Figure 5.2: a) Graphical representation of Marcus parabolas. b) Reaction rate constant dependence on a free energy of the reaction (inset - expression in logarithmic coordinates).

Here E_r and E_p are equilibrium energies of reagents and products before and after the charge transfer. The Frank-Condon principle maintains that energies should be equal on the transfer, therefore:

$$\lambda(\Delta e)^2 + E_r = E_p(\Delta e) = \lambda(\Delta e - 1)^2 + E_p \tag{5.12}$$

By denoting $E_p - E_r = \Delta G$, the equation can be rearranged and solved for the charge transfer coordinate Δe of parabolas' intersection:

$$\Delta e = \frac{\Delta G + \lambda}{2\lambda} \tag{5.13}$$

And the energy of the intersection of parabolas is an activation free energy (fig. 5.2):

$$\Delta G^{\ddagger} = \frac{(\Delta G + \lambda)^2}{4\lambda} \tag{5.14}$$

This equation is substituted into Arrhenius equation and results the following charge transfer rate constant:

$$k = Ae^{\frac{(\Delta G+\lambda)^2}{4\lambda k_B T}} \tag{5.15}$$

This equation is a classical result of Marcus charge transfer theory. It, of course, has limitations. Firstly, the solvent was assumed to be a polarizable medium, which, in a case of specific interaction between a solvent and a solute, is not true. Secondly, it represents the non-adiabadic case of the electron transfer, where reactants and products retain their identity. Quantum effects were introduced into the theory later with the following equation:

$$k = \frac{\pi}{\hbar} V_{if}^2 \frac{e^{-\frac{(\Delta G+\lambda)^2}{4\lambda k_b T}}}{\sqrt{\lambda \pi k_b T}} \tag{5.16}$$

where k is a rate constant, V_{if} – electronic (protonic) coupling between initial and final states, $\hbar$ – reduced Planck constant, k_b – Boltzmann constant, T – temperature, λ – reorganization energy, ΔG – Gibbs free energy of a reaction (also known as the driving force). This equation represents an adiabatic case, and is result of the application of Landau-Zener theory for two state system. In an adiabatic case, the reactants and products merges in two new potential energy surfaces and V_{if} effectively lowers the activation free energy via particle tunneling trough a potential barrier mechanism.

Earlier, the proportional increase of ET rate together with the driving force ($-\Delta G$) of a reaction has been considered as the *only* trend possible. The Marcus theory predicts a different picture – the ET rate constant should increase up to some maximum value at $\Delta G^0 = -\lambda$ and then decrease back to zero (the so called "inverted region"), as illustrated in fig. 5.2B. It was a controversial and surprising prediction. The theory was applied to a wide range of chemical and biochemical reactions. It was used to rationalize reactivities of aromatic radical cations(Schlesener et al., 1986), reduction of halides (Eberson, 1982) and cycloadditions, redox reactions between transitional metal complexes(Chou et al., 1977; Marcus, 1960; Ballardini et al., 1978), protein-protein electron transfer(Armstrong

et al., 1997; Xu and Schulten, 1994; Wherland and Pecht, 1978), photoninduced electron transfer (Tanaka et al., 2007; Xu and Schulten, 1994; Paczkowski et al., 1996). However, it took almost twenty years to experimentally find Marcus the most controversial prediction – the existence of so called "inverted region"(Miller et al., 1984).

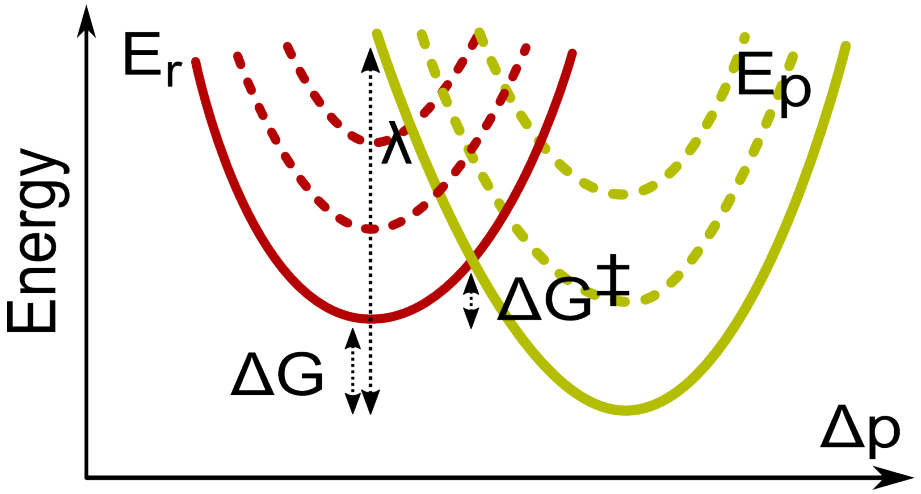

Figure 5.3: Illustration of multi-state charge transfer. Continuous curves represent potential energy of ground states. Dashed parabolas attributed to potential energies of excited states.

Another important species in charge transfer reactions is the proton transfer. The Marcus theory is applicable here as well. However, there are some major changes due to a much larger (~1800 times) proton mass in comparison with one of the electron. The mass difference implies that proton vibronic levels are much more closely spaced. Therefore, the proton transfer can proceed not only from the lowest state of potential energy surface, but from exited states as well. In such case, the rate constant of PT is calculated using a multi-state non-adiabatic proton theory by Borgis and Hynes ((Borgis and Hynes, 1996)):

$$k_{PT} = \sum_n \sum_m P_n \frac{V_{nm}^2}{\hbar} \sqrt{\frac{\pi}{\lambda_p k_B T}} \exp\left(-\frac{\Delta G_{nm}^{\ddagger}}{k_B T}\right) \tag{5.17}$$

$$\Delta G_{nm}^{\ddagger} = \frac{(\Delta G_p + E_m - E_n + \lambda_p)^2}{4\lambda_p} \tag{5.18}$$

Here P_n is a probability (from Boltzmann distribution) of transition from n-th reactant state, V_{nm} - vibrational coupling between reactant and

product wave functions, λ_p - reorganization energy of proton transfer; E_n and E_m - energies of reactants in state n and products in state m, respectively (dashed parabolas in fig. 5.3).

The applicability of Marcus theory in the kinetics of oxidoreductases is somewhat limited. Some conceptual differences between the classic thermodynamic diagram of enzymatic catalysis cycle and Marcus theory viewpoint is represented in fig 5.4. However, there were attempts to exploit various homologous series of substrates with different standard reduction potentials to probe the inverted parabola dependence of the logarithm of rate constants on a reaction driving force (inset in fig. 5.2), i.e., to rationalize the enzymatic electron and proton transfer using Marcus theoretical predictions.

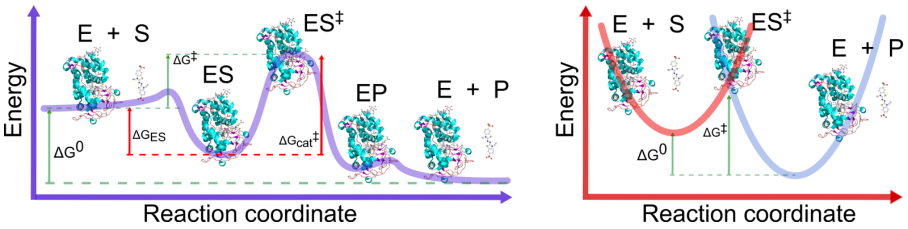

Figure 5.4: Thermodynamic scheme of enzymatic reaction and corresponding representation in Marcus theory in terms of ΔG^0 and $\Delta G^{\ddagger}$.

However, this approach allows only a very limited range of driving force variation and is based on hypothesized V_{if} and λ similarities along a series of substrates. In various examples, observed rate constants of redox reactions indicate *only* predicted trends, not *clear* quantitative relations. For example, the predicted dependence was found in the case of oxidation catalyzed by peroxidases of structurally similar quinones (Folkes and Candeias, 1997), anilines, phenols and indolacetic acids(Candeias et al., 1996; Candeias et al., 1997; Sakurada et al., 1990), to some lesser extent in the oxidation of phenylendiamines and phenoxazines/phenothiazines(Kulys et al., 2000; Krikstopaitis et al., 1998), and no dependence was found when substrates were structurally dissimilar. The same lack of the quantitative relation was found in an intramolecular electron transfer in engineered azurins (Farver et al., 2014) and in various attempts to relate proton transfer rates in proteins to the reaction driving force using Marcus theory(Silverman, 2000; Silverman et al., 1993). Despite these obstacles, the Marcus theory provides a major way

to interpret result in the chemical, eletrochemical and enzymatic electron transfer. In the results and discussion section we will provide a more general way to experimentally probe and analyze the enzymatic electron transfer within the framework of Marcus theory.

Peroxidases Peroxidases are one of the oldest known classes of enzymes, which were discovered in the late 19th century in horseradish. These enzymes catalyze an oxidation of various substrates and use hydrogen peroxide as an electron acceptor. Such properties were found useful in various organic synthesis, biotransformations, chemiliuninescent and imunoanalysis(Veitch, 2004). However, peroxidases are not exclusively produced by plants, they are found in fungi as well.

The most extensive kinetic, thermodynamic and modeling investigations are done on one particular class of enzymes – heme-containing peroxidases (EC 1.11.1.7; also known as class III peroxidases in plants and class II in fungi). However, these peroxidases are only one subclass of a broader family of enzymes. The family (EC 1.11.x) consist of non-heme peroxidases and heme containing peroxidases. Good example of a non-heme peroxidase is rubrerythrin, which contains two iron atoms in the active site, which are coordinated only with histidines and glutamates(Jin et al., 2002). Heme-containing peroxidases, as the name suggests, contain heme – a cofactor consisting of iron ion and porphyrin. These enzymes are further split into various families such as intracellular (class I), secreted by fungi (class II), secreted by plants (class III), catalases, di-heme peroxidases, haloperoxidases etc. (Hofrichter et al., 2010).

Plant peroxidases are responsible for many functions, such as regulation of hydrogen peroxide levels and an oxidative coupling of phenols in a lignin biosynthesis(Kawaoka et al., 1994). However, plant peroxidases have many more functions than attributed earlier. They participate in germination by producing $^{\bullet}OH$ radicals to cope with pathogens; are active in cellular growth and cell wall remodeling processes; are produced under chemical, biological and physical stress. All these functions are summarized in a wonderful review by Passardi et al. 2005 (Passardi et al., 2005). Fungi peroxidases participate mainly in reverse process – lignolysis(Hammel and Cullen, 2008). Peroxidases are well covered in the literature over past century of scientific research, yet, new insights into

the catalytic mechanism of the peroxidases are found constantly. Some even contradict to each other, for example, experimental and modeling debates whereas peroxidase compound II is protonated or not are still not finalized(Casadei et al., 2014; Karlin, 2010; Derat and Shaik, 2006; Berglund et al., 2002; Kwon et al., 2016). In the following text aside-by-side review of properties of two classical peroxidases – horseradish (*Armoracia rusticana*) peroxidase C (HRP) and peroxidase from ink cap fungus (*Coprinopsis cinerea*; CiP) – is presented.

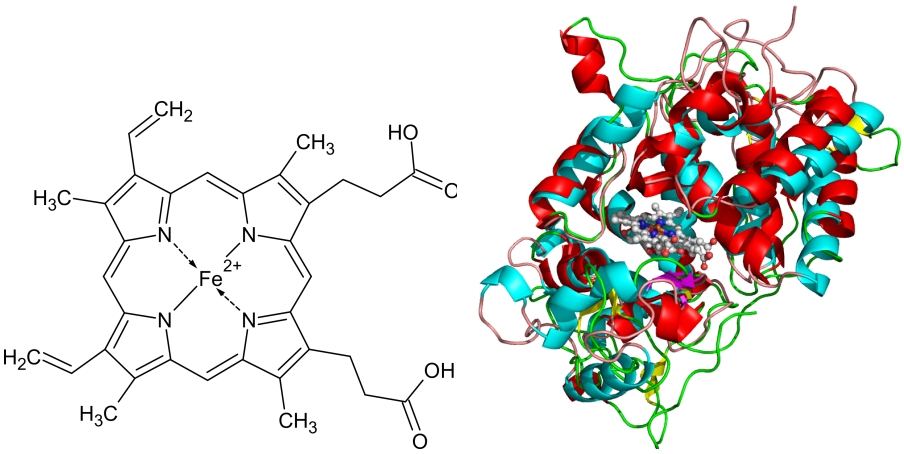

Figure 5.5: Structure of ferrous heme B and structural overlap of HRP (cyan alpha helices) and CiP (red alpha helices).

The molecular structure and the catalysis mechanism of peroxidases Both peroxidases (HRP and CiP) contains the cofactor – heme B (fig. 5.5), which is essential for the HRP and CiP catalytic activity. It is a protoporphyrin IX prosthetic group with iron (III) ion, which undergoes redox changes upon an oxidation or reduction. Despite very poor sequence similarity (~20%) and different sources of peroxidases (plant and fungus), structures of enzymes are strikingly similar (fig. 5.5). However, one can note that the HRP active center, where heme resides, is more restricted. Yet, the overall geometry of active centers in both peroxidases is almost identical (fig. 5.6).

Despite overall similarities of active centers of HRP and CiP, kinetic properties of both enzymes are different. A general peroxidase catalysis is described by a scheme, which is composed of three steps:

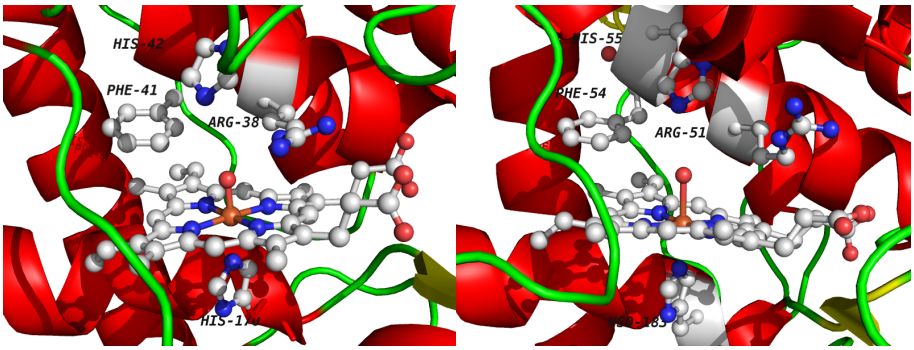

Figure 5.6: Structures of HRP (left; PDBID:1HCH) and CiP (right; PDBID:1H3J) active centers.

$$
\begin{aligned}
(I) \qquad & E_{red} + H_2O_2 \overset{k_p}{\rightarrow} CpdI \\
(II) \qquad & CpdI + S \underset{k_{-1}}{\overset{k_1}{\rightleftharpoons}} CpdI\,S \\
& CpdI\,S \overset{k_{1,cat}}{\rightarrow} CpdII + S^{\bullet +} \\
(III) \qquad & CpdII + S \underset{k_{-2}}{\overset{k_2}{\rightleftharpoons}} CpdII\,S \\
& CpdIIS \overset{k_{2,cat}}{\rightarrow} E_{red} + S^{\bullet +}
\end{aligned}
\tag{5.19}
$$

where E_{red} represents a reduced enzyme state (Fe(III), ground state), which, upon oxidation with H_2O_2, forms an oxidized form known as a compound I (CpdI). The reaction rate constant k_p for HRP is $(1.6 \pm 0.1) \times 10^7 \mathrm{M^{-1}s^{-1}}$(Shiro et al., 1986) and is around twice smaller ($(9.9 \pm 0.9) \times 10^6 \mathrm{M^{-1}s^{-1}}$) for CiP (Abelskov et al., 1997). For HRP it is known that His170 and His42 mutants show only the residual activity ($k_p \sim 10\ \mathrm{M^{-1}s^{-1}}$). Phe41 blocks substrate access to ferryl oxygen in CpdI and ARG38 stabilizes CpdI (k_p of mutants $1.1 \times 10^4\ \mathrm{M^{-1}s^{-1}}$) (Veitch and Smith, 2000). CpdI is further reduced by substrates (S) in one-electron transfer steps via compound II (CpdII) back to E_{red}. CpdI and CpdII, both in HRP and CiP, can oxidize a wide range of compounds such as anilines, quinones, various heterocycles, etc., with rate constants up to $10^8\ \mathrm{M^{-1}s^{-1}}$. Therefore, peroxidases are strikingly efficient enzymes. This is associated with the relatively open active center and high reduction potentials of CpdI (0.93 V vs NHE for HRP (Hayashi and Yamazaki, 1979) and 0.915 V vs NHE for CiP (Farhangrazi et al., 1994a)) and CpdII (0.91 V vs NHE for HRP (Hayashi and Yamazaki, 1979) and 0.982 V vs NHE for CiP (Farhangrazi et al., 1994b)) at pH 7. However, it

is known that CiP oxidizes substrates with rate constants of order of magnitude larger than HRP, despite the similar reduction potentials and active centers. The reaction scheme 5.19 appears simple and neat, but, as it is usual in such cases, incomplete. To satisfy the curiosity, a complete peroxidase catalysis scheme, which is complicated with an oxidase catalytic cycle, is depicted in fig. 5.7 (Berglund et al., 2002).

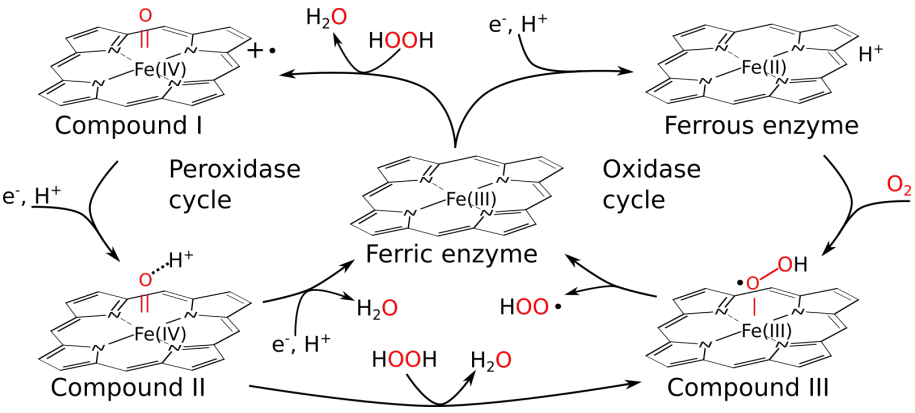

Figure 5.7: Full catalytic cycle of HRP (adopted from (Berglund et al., 2002)).

Catalytic properties of peroxidases are associated with the electronic structure of heme. They are particularly interesting due to a change of electronic spin during the course of the catalysis. In the reduced state (i.e. ferric enzyme; main catalytic peroxidase cycle, fig. 5.7), the heme spin multiplicity (sextet) is fully associated with iron (III) ion. Hemes in both peroxidases are coordinated by histidine side chains (His170 in HRP and His183 in CiP; fig. 5.6) and water molecules (Loew and Dupuis, 1997). In the fully oxidized state (i.e. after reaction with H_2O_2),CpdI, contains an iron-bound oxygen atom ($Fe^{IV} = O$). The nature of CpdI is much more complicated. The overall spin of heme is the quartet, which is composed from the overall triplet of $Fe^{IV} = O$ moiety and the porphyrin radical cation (Schulz et al., 1984) (fig. 5.7). The radical cation nature of porphyrin was attributed to be the main cause of the CpdI reduction being of order of magnitude faster than reduction of CpdII with same substrates (Folkes and Candeias, 1997). The argument was based on shorter electron transfer distances between a substrate and the porphyrin in CpdI than from a substrate and iron ion in CpdII. . A computational study of HRP CpdII performed by Derat and Shaik revealed that energetically singletic $Fe^{III} = OH$ and a cation radical configuration of porphyrine are

more favorable, producing the overall triplet (Derat and Shaik, 2006). The general opinion favors the two-step sequential electron and proton transfer reduction of CpdI *via* CpdII to the ferric enzyme mechanism. However, there are no data or publications which definitely describe, which of the sequential electron and proton transfer steps comes first and estimates the proton transfer step rate constant. The same general opinion favors electron transfer as the limiting step both in the CpdI and CpdII reduction(Folkes and Candeias, 1997). Therefore, there were many attempts to describe the electron transfer using Marcus electron transfer theory. The theory was applied for the oxidation of structurally similar quinones (Folkes and Candeias, 1997), anilines, phenols and indolacetic acids(Candeias et al., 1996; Candeias et al., 1997; Sakurada et al., 1990), phenylendiamines and phenoxazines/phenothiazines(Kulys et al., 2000; Krikstopaitis et al., 1998) etc., catalyzed by peroxidases. However, all these investigation are based on "homologous" series of substrates and the investigation of rate constants at the same temperature. These limitations are highly artificial and were justified in the following way. The Marcus electron transfer theory provides a general rate constant form:

$$k = \frac{\pi}{\hbar} V_{if}^2 \frac{e^{-\frac{(\Delta G+\lambda)^2}{4\lambda k_b T}}}{\sqrt{\lambda \pi k_b T}} \tag{5.20}$$

Therefore, if some homologous series of substrates (i.e. having same main skeleton of molecule decorated with different substituents) is used for the investigation of the enzymatic electron transfer, it can be hypothesized that the electronic coupling factor V_{if} and the reorganization energy λ are very similar for these homologous compounds. In this case one can probe the rate constant's dependence on ΔG (as calculated from reduction potentials of a relevant enzymatic form and a substrate) and, if the electron transfer is governed by the Marcus theory, one should find the parabolic dependence of rate constants' logarithm on the driving force of the reaction. Indeed, such relation were found for previously mentioned compounds to some extent. However, such approach limits the range of driving forces attainable by series of substrates and is based on hypothetical speculation of similarities of V_{if} and λ between homologous compounds. In the following section, a conceptually novel investigation of CiP CpdII catalyzed oxidation of structurally non-similar substrates is described, which was not attempted before, or at least not

published in the literature. This investigation attempts to expand the application of Marcus theory for various substrates, regardless their structural resemblance.

5.2 Results and discussion

Surprisingly, there were no free energy of activation dependence on reaction driving force investigations undertaken (to the best of our knowledge, there are no such publications concerning peroxidases or other oxidoreductases). Such approach eliminates a variation of reaction rate constants from the Marcus equation (eq. 5.20) due to coupling V_{if} of initial and final states, and allows a direct comparison of the enzymatic electron transfer with Marcus predictions (as summarized in fig. 5.4). The dependence of the activation free energy on solvent and inner reorganization energies can be estimated from quantum mechanical calculations of substrates by using a Marcus definition(Lin et al., 2003). And, finally, molecular docking studies can provide solvent accessible surfaces of substrates in enzyme-substrate complexes, which directly scales the reorganization energy of an enzymatic reaction in comparison with quantum mechanical estimates in a solvent. It was done in this research.

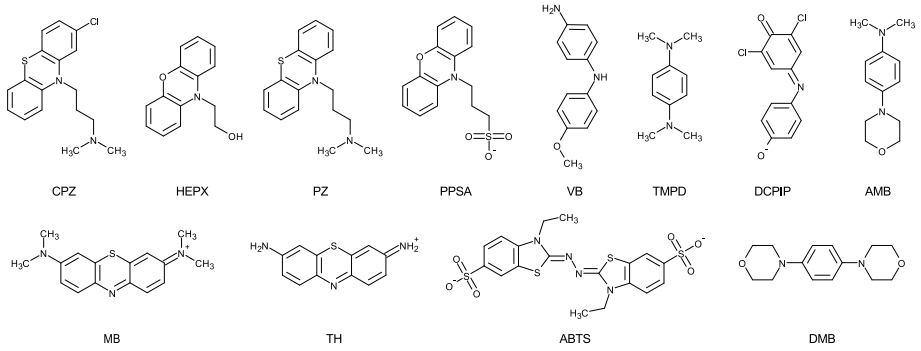

Figure 5.8: Structures of compounds used for CiP CpdII reduction.

Here we investigate an oxidation of 12 different substrates (fig. 5.8) and 13 different oxidation reactions, catalyzed by CiP CpdII, its rate constants and a dependence of the activation free energy on substrates' redox potentials, quantum mechanically calculated reorganization energies and solvent accessible areas of substrates in docked enzyme-substrates complexes. Investigated compounds cover a range of redox potentials,

structural variability and a different number of electrons subtracted in an oxidation process. The relations found fits well in a consecutive electron and proton transfer model, based on the Marcus theory. Relations found imply that both electron and proton transfer reactions are controlled by reaction driving forces, electronic coupling and solvent reorganization factors.

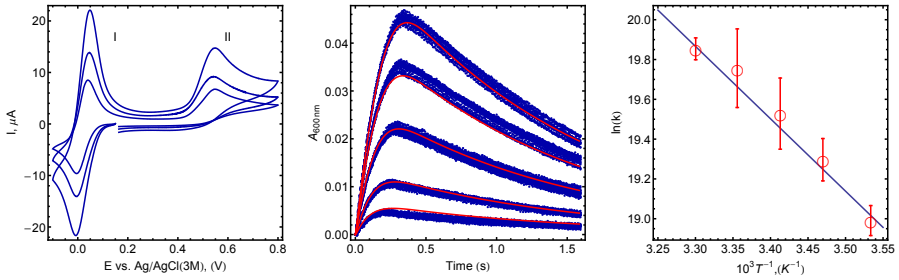

Figure 5.9: From left to right: Cyclic voltammetry of DCPIP ($1\ \mathrm{mM}$) on glassy carbon electrode in 50 mM phosphate buffer, pH 7.00, at $\mathrm{T} = 25^{\circ}\ \mathrm{C}$. DCPIP oxidation kinetics in 50 mM phosphate buffer, pH 7.00, at $\mathrm{T} = 25^{\circ}\ \mathrm{C}$. Blue points – measurements, red curve – fit (a reaction schema is provided in 5.19). Arrhenius plot of DCPIP oxidation rate constants' dependence on temperature.

Standard reduction potentials and energies of reorganization. Standard reduction potentials of compounds investigated were used in calculation of the Gibbs free energy of the oxidation reaction (a standard reduction potential of peroxidase CpdII of $0.982\ \mathrm{V}$ was used in calculations(Farhangrazi et al., 1994b)). Therefore, for each compound its standard reduction potential was measured using cyclic voltammetry in $50\ \mathrm{mM}$ phosphate buffer solution at $\mathrm{pH}\ 7$, as described in Methods and materials section. An example cyclic voltammgram of DCPIP is illustrated in fig. 5.9. The reversible couple around $0\ \mathrm{V}$ vs. $\mathrm{Ag|AgCl(3M)}$ (I) is a two-electron redox process, which standard reduction potential is estimated as the average of cathodic and anodic peaks. The irreversible couple (II) at around $0.6\ \mathrm{V}$ vs. $\mathrm{Ag|AgCl(3M)}$ is an irreversible one-electron oxidation of DCPIP , which standard reduction potential is estimated by subtracting from the anodic peak potential $30\ \mathrm{mV}$. The same approach was use in the calculation of CPZ standard redox potential. However, four of these compounds (TH, MB, VB and the first oxidation of DCPIP) undergo two-electron quasi-reversible redox pro-

cesses. To estimate standard one-electron reduction potentials for these couples, theoretical calculations were used.

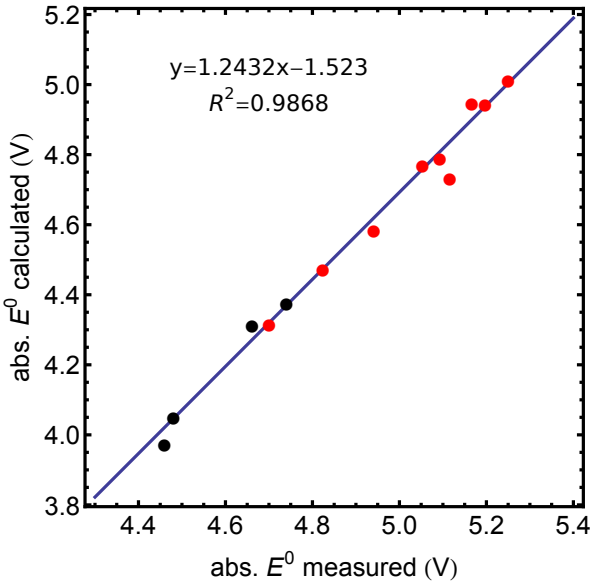

Figure 5.10: Absolute standard redox potentials, calculated by using DFT with hybrid B3LYP functional and 6-31+G(d,p) basis set, *vs.* absolute standard redox potentials, measured experimentally. Red – one-electron redox couples, black – two-electron redox couples.

The calculated potentials using DFT B3LYP functional with 6-31+G(d,p) basis set compare well with the measured potentials for one- and two-electron redox couples (fig. 5.10, red and black dots correspondingly). Zero-point energies, energies and coordinates of optimized structures are available for an example compound in the Appendix. The two-electron standard reduction potentials of TH, MB, VB and DCPIP were calculated from two separate one electron reduction steps . The one electron reduction potentials for two electron reduction couples (TH, MB, VB and first oxidation of DCPIP) were estimated from quantum chemical calculations using a linear regression of calculated and measured redox potentials (fig. 5.10). The calculated one-electron standard reduction potentials of TH (0.25 V) and MB (0.162 V) compare well with *ad hoc* estimation from pulse radiolysis experiments (values compiled by Wardman(Wardman, 1989)) at pH 1.7 and assumption of pK_a 6.7). The measured and calculated standard reduction potential

values are listed in table 5.1. These values span a range from 0.162 V to 0.79 V, which is hardly attainable by any series of homologous compounds. The optimized structures were used to calculate solvent and inner reorganization energies of substrates, as described in Methods and Materials (results are listed in table 5.1). Calculated reorganization energies represent a range from $3\,\mathrm{kcal/mol}$ (0.13 V) to $12\,\mathrm{kcal/mol}$ (0.52 eV) and correlate with compounds' structure. These values reflect reorganization energies in the solvent (water), not mixed environment such as one in substrate-enzyme complex, where a part of substrate is exposed to solvent and another part to enzyme environment. These effects will be addressed further.

Table 5.1: Kinetic and thermodynamic parameters for substrates' oxidation catalyzed by CiP.

Substrate	$E^0_{\text{vs NHE}}$ (V)	$E^0_{1,\text{vs NHE}}$ (V)	λ^*_{sol} (kcal/mol)
ABTS	0.686 ± 0.006	0.686 ± 0.006	3.42
AMB	0.394 ± 0.005	0.394 ± 0.005	11.17
CPZ	0.79 ± 0.01	0.79 ± 0.01	12.04
DCPIP(I)	0.231 ± 0.009	0.568*	12.47
DCPIP(II)	0.736 ± 0.01	0.736 ± 0.01	3.77
DMB	0.511 ± 0.004	0.511 ± 0.004	11.04
HEPX	0.663 ± 0.003	0.663 ± 0.003	3.10
MB	0.030 ± 0.006	0.162*	9.12
PPSA	0.623 ± 0.003	0.623 ± 0.003	2.65
PZ	0.767 ± 0.006	0.767 ± 0.006	11.82
TH	0.060 ± 0.001	0.250*	8.85
TMPD	0.270 ± 0.006	0.270 ± 0.006	11.68
VB	0.310 ± 0.006	0.369*	8.15

* estimated from Quantum chemical calculations.

The oxidation kinetics and rate constants. The investigated substrates are different in terms of structure, reduction potentials and oxidation mechanisms. Some of them form radical cations (HEPX, ABTS, AMB, DMB, TMPD, PPSA, CPZ, PZ and second oxidation of DCPIP) upon the oxidation, others produce stable products *via* two-electron oxidation (TH, MB, VB and first oxidation step of DCPIP). In two-electron oxidation cases, it is assumed that oxidation with enzyme forms a radical cation, which subsequently disproportionates into reduced and oxidized species.

The disproportionation reactions are assumed to be much faster than enzymatic ones (for MB and TH rates are nearly diffusion limited (Solar et al., 1982)).

Peroxidases have a complex reaction pathway scheme (Berglund et al., 2002), which is complicated by various side reactions such as disproportionations of oxidized substrates (AMB, DMB, TMPD), hydrolysis (PZ and CPZ), or even further oxidation (second one-electron oxidation of DCPIP – DCPIP(II)) catalyzed by peroxidase. However, the core of the catalytic cycle is simple and is represented in this research as:

$$\begin{aligned}
(I) \qquad & E_{red} + H_2O_2 \overset{k_p}{\rightarrow} CpdI \\
(II) \qquad & CpdI + S \underset{k_{-1}}{\overset{k_1}{\rightleftharpoons}} CpdIS \\
& CpdIS \overset{k_{1,cat}}{\rightarrow} CpdII + S^{\bullet +} \\
(III) \qquad & CpdII + S \underset{k_{-2}}{\overset{k_2}{\rightleftharpoons}} CpdIIS \\
& CpdIIS \overset{k_{2,cat}}{\rightarrow} E_{red} + S^{\bullet +} \\
(IV) \qquad & S^{\bullet +} + S^{\bullet +} \overset{k_3}{\rightarrow} S + S_{ox}
\end{aligned} \tag{5.21}$$

Here the scheme 5.21 is composed from four major reactions. (I) represents a CpdI formation from reduced enzyme and hydrogen peroxide. (II) is a CpdI reduction to CpdII and is generally faster(Candeias et al., 1997; Candeias et al., 1996; Folkes and Candeias, 1997; Krikstopaitis et al., 1998) than the consecutive reaction (III), which is a CpdII reduction to reduced enzyme. Therefore, it is assumed that reaction III is a limiting-step and measured rate constants represent CpdII reduction to reduced enzyme. All the measurements of reaction kinetics were fitted to the reaction schemes using rModeler software form "Ubique calculus" Ltd., (Vilnius, Lithuania; implementation of algorithm from(Laurynenas and Kulys, 2015)). Detailed schemes used for fitting and examples of substrate kinetics are available in in Appendix B (1.2).

Caution was taken to eliminate possible rate-limiting step in the oxidation of peroxidase with hydrogen peroxide through selection of proper initial concentrations of H_2O_2 and analysis of CpdI formation. Direct kinetics (examples of experiments data and fits in Appendix, 1.1) of CiP reduced with H_2O_2 was investigated and apparent bimolecular rate constant $(8.7 \pm 0.1) \times 10^6 \mathrm{M}^{-1}\mathrm{s}^{-1}$ of CiP CpdI formation at $\mathrm{T} = 25^\circ$ C) was found, which is well comparable to the rate constant measured by

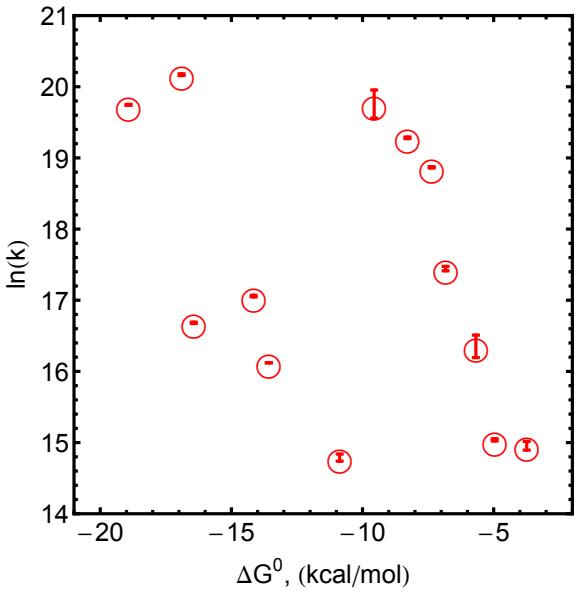

Figure 5.11: Apparent bimolecular CpdII reduction rate constant's dependence on driving force (Gibbs free energy of the reaction) at $\mathrm{T} = 25\ \mathrm{C}^{\circ}$.

Abelskov(Abelskov et al., 1997). From constants' dependence on temperature, free energy of activation of $3.6 \pm 1.0\ \mathrm{kcal/mol}$ was calculated by using Arrhenius equation. This value is smaller than the activation free energy measured for HRP ($5.4 \pm 0.8\ \mathrm{kcal/mol}$ (Baek and Van Wart, 1992)).

The kinetic curves of substrate oxidation with CiP were fitted to the reaction schemas using CpdI formation rate constants measured at different temperatures (data in Appendix). With excess of H_2O_2, this approach eliminates impact of CpdI formation kinetics on rate constants of substrates' oxidation. Exemplary kinetics of DCPIP oxidation at $\mathrm{T} = 25^{\circ}\ \mathrm{C}$ is demonstrated in figure 5.9 including the relevant fit. The rate constants for all the substrates investigated are listed in table 5.2. As one should expect, no obvious relation (fig. 5.11) was found between the rate constants of substrates' oxidation, catalyzed by CpdII, and the reaction driving force, calculated from standard reduction potentials (second one-electron standard reduction potentials were used for two-electron redox couples). A diversity of structures causes a large variability of reorganization energies (calculated quantum-chemically; in table 5.1) and electronic coupling between initial and final states (V_{if} in eq. 5.20).

The unknown electronic coupling factor V_{if} can be eliminated by measuring rate constant's dependence on temperature, because eq. 5.20 is very similar to Arrhenius equation, and therefore can be linearized and separated into preexponential factor and activation free energy term:

$$\ln k(T) = \ln\left(\frac{\pi V_{if}^2}{\hbar\sqrt{\pi\lambda k_b}}\right) - \frac{(\Delta G^\circ + \lambda)^2}{4\lambda k_b T} - \frac{\ln T}{2}$$

$$\ln k(T) = \ln A - \frac{E_a}{k_B T} \tag{5.22}$$

Essentially, this approach brings back to the original Marcus prediction – the free energy of the activation relation to the reaction driving force. Therefore, for each substrate reaction rate constant (more specifically – apparent bimolecular rate constant k_{cat}/K_M), temperature dependence was measured (as an example, Arrhenius plot for DCPIP(I) in fig. 5.9). Preexponential factors and free energies of activation (in table 5.2 and fig. 5.12) were estimated using linearized form of Arrhenius equation (eq. 5.22) and linear regression of rate constants temperature dependence.

Table 5.2: Kinetic and thermodynamic parameters of substrates' oxidation catalyzed by CiP.

Substrate	$k_{cat}/K_M(\mathrm{M^{-1}s^{-1}})$ at 25°C *	$\ln A$	$\Delta G^\ddagger$ (kcal/mol)
ABTS	$3.8 \pm 0.1 \times 10^7$	$26.8 \pm 2.$	5.5 ± 1.1
AMB	$1.003 \pm 0.003 \times 10^7$	31.5 ± 1.9	9.1 ± 1.1
CPZ	$3.1 \pm 0.2 \times 10^6$	14.6 ± 1.7	$0 \pm 1.$
DCPIP(I)	$3.8 \pm 0.8 \times 10^8$	32.2 ± 2.1	7.4 ± 1.2
DCPIP(II)	$1.3 \pm 0.2 \times 10^7$	21.9 ± 0.6	3.3 ± 0.3
DMB	$2.3 \pm 0.1 \times 10^6$	28.7 ± 2.0	8.0 ± 1.2
HEPX	$1.56 \pm 0.01 \times 10^8$	$29.3 \pm 2.$	6.2 ± 1.2
MB	$2.66 \pm 0.03 \times 10^8$	33.5 ± 0.7	8.4 ± 0.4
PPSA	$2.37 \pm 0.03 \times 10^8$	28.3 ± 1.3	5.3 ± 0.8
PZ	$3.40 \pm 0.05 \times 10^6$	18.7 ± 1.3	2.2 ± 0.8
TH	$4.80 \pm 0.07 \times 10^8$	30.0 ± 0.9	5.9 ± 0.8
TMPD	$1.76 \pm 0.01 \times 10^7$	36.3 ± 3.4	$11.6 \pm 2.$
VB	$2.56 \pm 0.03 \times 10^7$	29.3 ± 2.7	7.2 ± 1.6

*The values of rate constants at other temperatures are available in Appendix.

Here some clarification is needed – the Marcus equation 5.20 rep-

resents a first order rate constant (dimensions -s^{-1}), not a bimolecular one ($s^{-1}M^{-1}$). The bimolecular rate constant (as well as first order rate constant) has additional multipliers – equilibrium constants, representing formation of reactant pair at some distance, frequency factors and reactant separation distances (Sutin, 1982; Marcus, 1956b). In the context of this research, all these factors are merged into an electronic coupling factor V_{if}, which now has an energy dimension multiplied by $\sqrt{M^{-1}}$. Therefore, the coupling factor V_{if} is an *apparent coupling factor* in the following text.

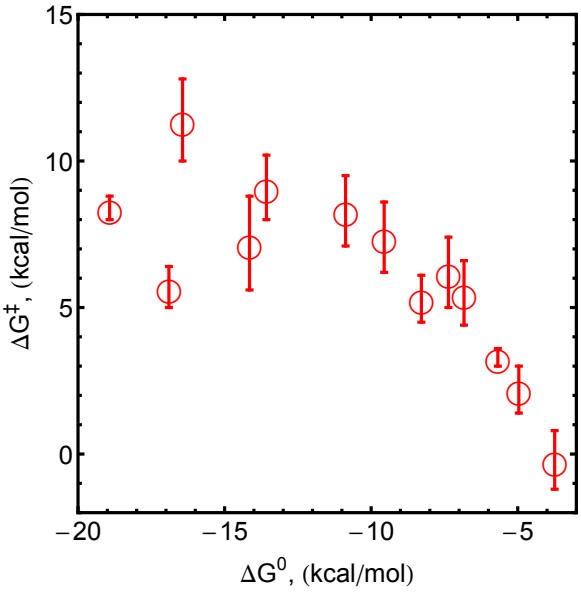

Figure 5.12: Dependence of free energy of activation on Gibbs free energy of reaction.

As seen in the table, apparent bimolecular rate constants (k_{cat}/K_M) span range from $\sim 2 \times 10^6 M^{-1}s^{-1}$ to $\sim 5 \times 10^8 M^{-1}s^{-1}$. The oxidation of reduced forms of HEPX, DCPIP, PPSA, MB and TH are fast processes and relatively close to diffusion-limited reactions. Estimated rate constants of diffusion-controlled reaction are around $10^8 \div 10^9$ $M^{-1}s^{-1}$ and free energy of activation is 4.6 kcal/mol (from Smoluchowski limit (Smoluchowski, 1917), Einsten-Stokes equation (Einstein, 1905) and viscosity of water (Al-Shemmeri, 2012)). Therefore, it is relatively safe to assume that these reactions are not limited by diffusion. However, for the sake of completeness, we measured dependence of reaction rate constant on

viscosity for TH and found only inhibition with PEG 4000 and none of diffusion-limited kinetics.

The estimated free energies of activation span a range from practically barrierless 0 ± 1 kcal/mol for PZ to 11.6 ± 2 kcal/mol for TMPD. From fig. 5.12 it is seen that some trend exists – the oxidation of substrates with high standard reduction potential proceeds with smaller free energies of activation than in case of the oxidation ones with low standard reduction potential. However, it doesn't come even close to the famous parabola.

The electron and proton transfer model. There are four reaction schemes, describing how electron and proton can be transferred in the reaction, namely the proton coupled electron transfer (PCET), the consecutive electron and proton transfer with limiting proton transfer (PT) or electron transfer (ET) step, and the consecutive electron and proton transfer with variable limiting step with reaction driving force (summarized in fig. 5.13). The proton-coupled electron transfer can be ruled out due to small kinetic isotope effect (KIE), which was measured for indolacetic acids and was found to be $k_H/k_D \approx 1.3$ (Candeias et al., 1997). The typical predicted KIE are much larger in proton coupled electron transfer reactions(Edwards et al., 2009).

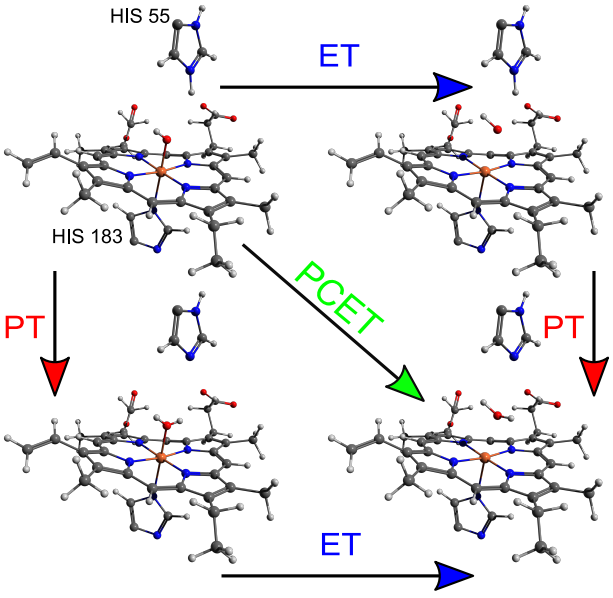

Figure 5.13: Scheme of proton and electron transfer steps in CiP CpdII reduction (active center adapted from PDBID:1h3j).

Assuming electron transfer as limiting step, one can try to explain observed trend of activation free energies in terms of different reorganization energies, which can be calculated straightforward from Marcus relation$\Delta G^{\ddagger} = \frac{(\Delta G^{\circ}+\lambda)^2}{4\lambda}$.It will result in very small energies – around 0.1 eV. Very similar reorganization energies were reported earlier in the study of oxidation of indoleacetic acids catalyzed by HRP. Apparently, the case is very similar, as indoleacetic acids produce radical cations upon oxidation (Candeias et al., 1997). The ET as limiting case can be dismissed by comparing these reorganization energy values with values acquired from DFT calculations, which are not correlated to reorganization energies calculated from Marcus relation discussed above (fig. 5.14, left). Such discrepancy is not in favor of electron transfer as a limiting step.

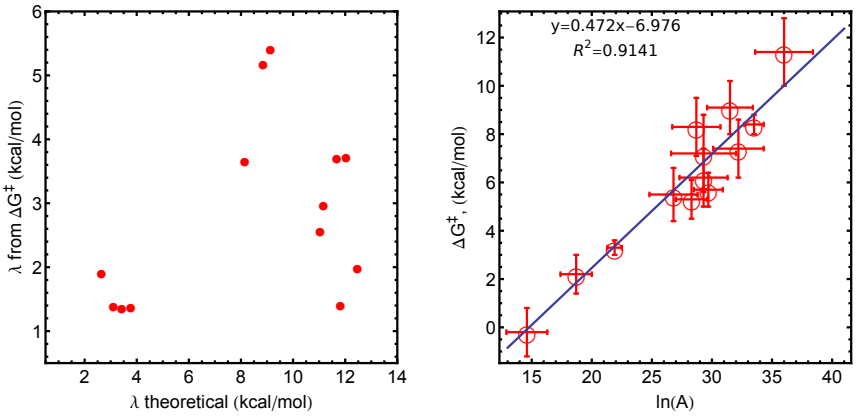

Figure 5.14: Left – λ calculated from $\Delta G^{\ddagger}$ *vs.* theoretical λ; right – dependence of free energy of activation on preexponential factor of a reaction.

Another possibility – the limiting step in proton transfer – would result in similar rate constants, regardless the substrate structure and driving force (because 9 substrates do not donate protons for the reaction and therefore, the PT could be only internal PT from catalytic histidine to heme). None of these two possible schemes predict a linear correlation between preexponential factor and free energy of activation, which is found in this investigation (fig. 5.14, right). This relation can be found in the consecutive electron and proton transfer with a varying limiting step. However, the measured apparent bimolecular oxidation rate constants cannot be directly compared to the proton transfer rate constants, which

are first order rate ones. Therefore, an apparent bimolecular electron transfer scheme should be assumed:

$$E + S \overset{k_e}{\rightarrow} ES, \quad ES \overset{k_p}{\rightarrow} E + P \tag{5.23}$$

This scheme is indistinguishable from the scheme, where the transfer of proton proceeds first:

$$E \overset{k_p}{\rightarrow} E', \quad E' + S \overset{k_e}{\rightarrow} E + P \tag{5.24}$$

and result in the same rate equation under quasi-steady state assumptions:

$$v = \frac{[S][E_0]k_p k_e}{[S]k_e + k_p} \tag{5.25}$$

Therefore, the apparent bimolecular rate constant of the total process should be dependent on the concentration of substrate:

$$k_{ep,app} = \frac{k_p k_e}{[S]k_e + k_p} \tag{5.26}$$

where rate constants k_e are expressed in the framework of Marcus theory for electron transfer (in the analysis of $k_{ep,app}$ the average of initial substrate concentrations $[S]$ were used; listed in Appendix). The question about which process occurs first will be addressed further. Of course, Marcus equation itself does not provide a good description of proton transfer, which is much more complicated due to closely-spaced vibrational levels. Therefore, it can serve as a handy approximation for relatively small region of driving forces. However, even much simpler approximation by Arrhenius equation, as suggested by Hammes-Schiffer et al.(Hammes-Schiffer and Stuchebrukhov, 2010), works well in this investigation. The modified Arrhenius equation, used to describe proton transfer kinetics, is derived in the following way, starting with proton transfer rate constant approximation:

$$k_p = \frac{\pi}{\hbar} V_{if}^2 \frac{e^{-\frac{(\Delta G^\circ + \lambda_p)^2}{4\lambda_p k_b T}}}{\sqrt{\pi \lambda_p k_b T \pi}} \tag{5.27}$$

Assume that activation free energy of proton transfer is independent on the reaction driving force ΔG^0 (preliminary fitting results suggest

negligible dependence of $k_p$on ΔG^0). The equation simplifies to:

$$k_p = \frac{\pi}{\hbar} V'^2 \frac{e^{-\frac{E_a}{kT}}}{\sqrt{\pi k_b T \pi}},\ where\ V'^2 = V_{if}^2 / \sqrt{\lambda_p} \tag{5.28}$$

The parameters V' and E_a should be considered as apparent parameters, accounting for much more complex process of proton transfer. Then the apparent bimolecular rate constant for consecutive electron and proton transfer here is defined as:

$$k(T) = \frac{\frac{\pi}{\hbar} V_{if}^2 \frac{e^{-\frac{(\Delta G^\circ + \lambda)^2}{4\lambda k_b T}}}{\sqrt{\pi \lambda k_b T}} \times \frac{\pi}{\hbar} V'^2 \frac{e^{-\frac{E_a}{kT}}}{\sqrt{\pi k_b T}}}{\frac{\pi}{\hbar} V_{if}^2 \frac{e^{-\frac{(\Delta G^\circ + \lambda)^2}{4\lambda k_b T}}}{\sqrt{\pi \lambda k_b T}} [S] + \frac{\pi}{\hbar} V'^2 \frac{e^{-\frac{E_a}{kT}}}{\sqrt{\pi k_b T}}} \tag{5.29}$$

Where $\lambda = (\lambda_{substrate} + \lambda_{heme})/2$ (Marcus, 1968). However, the quantum chemically-calculated reorganization energies reflect electron transfer properties in solvent. To account reorganization energy in enzyme-substrate complex, the additional factor θ is used:

$$\lambda = (\lambda_{substrate}\theta_{substrate} + \lambda_{heme})/2 \tag{5.30}$$

Here θ is calculated as a solvent accessible surface part of substrate in docked enzyme-substrate complexes (an example of docked structure and solvent accessible surface as depicted in fig. 5.15). This relation is justified on difference of static and optical dielectric constants in water and protein. Therefore, reorganization energies are much larger in water than in protein and are scaled by solvent-accessible area. The necessity of θ was found in preliminary fitting as an additional multiplier with value approx. 0.35, which coincides well with average solvent accessible surface part of substrate in enzyme-substrate complex. The calculated values of θ are listed in SI. However, the docking procedures are not sufficiently advanced to accurately dock structures of substrates in enzymes. Therefore, the parameters θ are estimated, possibly, with substantial uncertainty.

The free energy of activation is defined as:

$$\Delta G^\ddagger = -k_b \frac{\delta \ln(k(T))}{\delta(1/T)} \tag{5.31}$$

It is a second term of corresponding Taylor series:

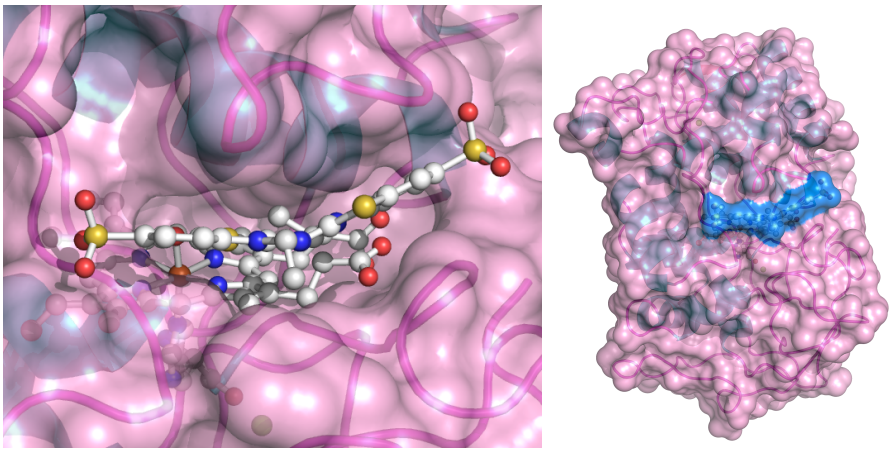

Figure 5.15: Docked structure of ABTS in CiP (PDBID:1h3j)

$$\ln k(T) = \ln k(T_0) + \left.\frac{\delta \ln k(T)}{\delta(\frac{1}{T})}\right|_{T=T_0} (\frac{1}{T} - \frac{1}{T_0}) + ... \tag{5.32}$$

This results to apparent preexponential factor defined as:

$$\ln A = \ln k(T_0) - \left.\frac{\delta \ln k(T)}{\delta(\frac{1}{T})}\right|_{T=T_0} \frac{1}{T_0} \tag{5.33}$$

and apparent free energy of activation defined as:

$$\Delta G^{\ddagger}_{\frac{1}{T_0}} = -k_b \left.\frac{\delta \ln k(T)}{\delta(\frac{1}{T})}\right|_{T=T_0} \tag{5.34}$$

It is clearly seen that consecutive electron and proton transfer described by equation 5.29 will result the dependence of apparent preexponential factor (eq. 5.33) on reaction driving force. Therefore a linear relation between logarithm of apparent preexponential factor and apparent free energy of the activation is possible, as seen in fig. 5.14.

The data (apparent preexponential factors and free energies of activation, listed in table 5.2) were fitted to a model (eq. 5.33 and 5.34) using a simultaneous least squares, weighted by errors in table 5.2 with Nelder-Mead(Nelder and Mead, 1965) optimization algorithm. The quantum mechanically-calculated reorganization energies λ (table 5.1) and solvent accessible surface parts θ (in Appendix D, 1.4), calculated from docking

studies, were used in the fitting procedure. The fitted parameters with calculated activation free energies of electron transfer $\Delta G^{\ddagger}_{Marcus\ ET}$ are listed in table 5.3. The fitted apparent preexponential factors and free energies of the activation are plotted in fig. 5.16. As seen from from figure 5.16, the consecutive electron and proton transfer model corresponds to measured parameters very well.

Table 5.3: Fitted parameters of consecutive electron and proton transfer model (eq 5.29).

Parameter	Value	$\Delta G^{\ddagger}_{Marcus\ ET}$ (kcal/mol)
V_{if}^{ABTS}	$0.76 \pm 0.08\,\mathrm{cal\,M^{-\frac{1}{2}}\,mol^{-1}}$	0.4 ± 0.01
V_{if}^{AMB}	$3.5 \pm 0.4\,\mathrm{cal\,M^{-\frac{1}{2}}\,mol^{-1}}$	1.5 ± 0.1
V_{if}^{CPZ}	$0.12 \pm 0.02\,\mathrm{cal\,M^{-\frac{1}{2}}\,mol^{-1}}$	0.5 ± 0.03
$V_{if}^{DCPIP(I)}$	$4.0 \pm 0.5\,\mathrm{cal\,M^{-\frac{1}{2}}\,mol^{-1}}$	0.16 ± 0.02
$V_{if}^{DCPIP(II)}$	$1.4 \pm 0.2\,\mathrm{cal\,M^{-\frac{1}{2}}\,mol^{-1}}$	0.001 ± 0.002
V_{if}^{DMB}	$2.0 \pm 0.2\,\mathrm{cal\,M^{-\frac{1}{2}}\,mol^{-1}}$	0.5 ± 0.05
V_{if}^{HEPX}	$0.83 \pm 0.09\,\mathrm{cal\,M^{-\frac{1}{2}}\,mol^{-1}}$	0.13 ± 0.02
V_{if}^{MB}	$260 \pm 30\,\mathrm{cal\,M^{-\frac{1}{2}}\,mol^{-1}}$	5.1 ± 0.2
V_{if}^{PPSA}	$1.7 \pm 0.1\,\mathrm{cal\,M^{-\frac{1}{2}}\,mol^{-1}}$	0.3 ± 0.04
V_{if}^{PZ}	$0.44 \pm 0.05\,\mathrm{cal\,M^{-\frac{1}{2}}\,mol^{-1}}$	0.2 ± 0.02
V_{if}^{TH}	$76 \pm 8\,\mathrm{cal\,M^{-\frac{1}{2}}\,mol^{-1}}$	3.9 ± 0.2
V_{if}^{TMPD}	undefined	3.0 ± 0.2
V_{if}^{VB}	$4.7 \pm 0.5\,\mathrm{cal\,M^{-\frac{1}{2}}\,mol^{-1}}$	2.1 ± 0.1
V'	$4.3 \pm 0.5\,\mathrm{cal\,mol^{-1}}$	
E_a	11.7 ± 0.2 kcal/mol	
λ_{heme}	10.2 ± 0.3 kcal/mol	

The values of apparent electronic coupling V_{if} (table 5.3) are hardly comparable for reactions between transitional metal complexes(Sutin, 1982) due to implicit equilibrium constant and frequencies of reactant pair formation in the V_{if}. However, these values provide another point of view in oxidoreductase-catalyzed oxidation reactions. For example, the largest apparent electronic coupling factor found is for MB, which rate constant is smaller than the rate constant of TH oxidation. This difference comes entirely from a few kilocalories change of the driving force. A closer inspection of V_{if} values in the table 5.3 reveals that the assumption about V_{if} similarities between similar compounds is not quite true. The V_{if} can vary between compound as much as 5 times (for example, the same TH and MB). The model allows deconvolution

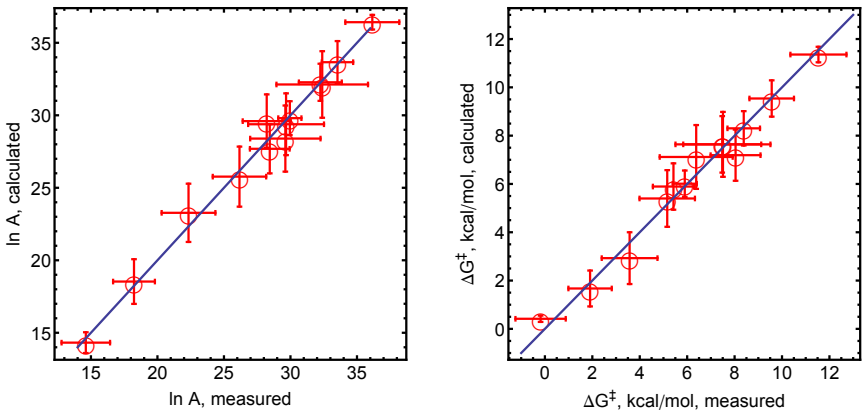

Figure 5.16: Measured *vs.* predicted preexponential factors and free energies of activation, including measurement and prediction confidence intervals. Blue thick lines represent the perfect agreement.

of consecutive electron and proton transfer in separate steps, and the Marcus activation free energy of electron transfer for each compound can be estimated. All the Marcus activation free energies of electron transfer are very small and fall in the rage from 0 kcal/mol to 5 kcal/mol, which indicates that the proton transfer step is the main factor controlling the activation free energy of the reaction. The calculated rate constants of electron transfer step are generally larger than observed apparent rate constants (table 5.4). The fitted proton transfer rate constant at 298 K is 520 ± 40 s^{-1}. The reorganization energy of heme (table 5.3) of 0.44 eV is very close to the reorganization energy of electron transfer of 0.5 eV found in cytochrome *c* by Bortolotti et al.(Bortolotti et al., 2011) and in HRP by Andreu et al.(Andreu et al., 2007) .

Very large activation free energy and apparent coupling between states V' (table 5.3) indicates a much more complex proton transfer (with multiple contributions from vibronic levels; as described by Borgis et al.(Borgis and Hynes, 1996)) than assumed in this research. However, the more complex treatment is also possible. There are two possible reaction schemes – the proton transfer precedes electron transfer with transfer distance of 1.7 Å and the electron transfer precedes proton transfer with proton transfer distance of 1 Å. The rate constants for these PT steps can be calculated by using a model, which describes the proton transfer due to solvent reorganization as described by Cukier and Morillo(Cukier and Morillo, 1989; Morillo and Cukier, 1990). Assume that

Table 5.4: Calculated constants of electron transfer rate, apparent bimolecular ET-PT rate in water and in deuterium oxide, and predicted kinetic isotope effects at 25°C .

Substrate	$k_{cat}/K_M(\mathrm{M^{-1}s^{-1}})^a$	$k_e(\mathrm{M^{-1}s^{-1}})^b$	$k_{app}^{H_2O}(\mathrm{M^{-1}s^{-1}})^b$	$k_{app}^{D_2O}(\mathrm{M^{-1}s^{-1}})^b$	KIE[b]
ABTS	$3.8 \pm 0.1 \times 10^7$	$3.2 \pm 0.6 \times 10^7$	$1.7 \pm 0.3 \times 10^7$	$1.4 \pm 0.3 \times 10^7$	1.3
AMB	$1.003 \pm 0.003 \times 10^7$	$4 \pm 1 \times 10^7$	$1 \pm 1 \times 10^7$	$7 \pm 2 \times 10^6$	1.5
CPZ	$3.1 \pm 0.2 \times 10^6$	$9 \pm 4 \times 10^5$	$9 \pm 10 \times 10^5$	$9 \pm 4 \times 10^5$	1.0
DCPIP(I)	$3.8 \pm 0.8 \times 10^8$	$6 \pm 1 \times 10^8$	$2 \pm 2 \times 10^8$	$1.6 \pm 4 \times 10^8$	1.4
DCPIP(II)	$1.3 \pm 0.2 \times 10^7$	$1.2 \pm 0.3 \times 10^8$	$9 \pm 8 \times 10^7$	$8 \pm 2 \times 10^7$	1.2
DMB	$2.3 \pm 0.1 \times 10^6$	$9 \pm 2 \times 10^7$	$4 \pm 3 \times 10^7$	$3 \pm 0.5 \times 10^7$	1.3
HEPX	$1.56 \pm 0.01 \times 10^8$	$3.2 \pm 0.6 \times 10^7$	$1 \pm 8 \times 10^7$	$1 \pm 0.2 \times 10^7$	1.4
MB	$2.66 \pm 0.03 \times 10^8$	$3 \pm 6 \times 10^8$	$3 \pm 3 \times 10^8$	$3 \pm 5 \times 10^8$	1.3
PPSA	$2.37 \pm 0.03 \times 10^8$	$1.0 \pm 0.1 \times 10^8$	$5 \pm 4 \times 10^7$	$4 \pm 0.7 \times 10^7$	1.3
PZ	$3.40 \pm 0.05 \times 10^6$	$8 \pm 2 \times 10^6$	$7 \pm 6 \times 10^6$	$6 \pm 1 \times 10^6$	1.1
TH	$4.80 \pm 0.07 \times 10^8$	$5 \pm 1 \times 10^8$	$3 \pm 3 \times 10^8$	$3 \pm 0.6 \times 10^8$	1.2
TMPD	$1.76 \pm 0.01 \times 10^7$	$4 \pm 3 \times 10^8$	$3 \pm 10 \times 10^7$	$2 \pm 2 \times 10^7$	1.5
VB	$2.56 \pm 0.03 \times 10^7$	$3.3 \pm 0.7 \times 10^7$	$2 \pm 1 \times 10^7$	$1 \pm 0.2 \times 10^7$	1.3

[a] measured
[b] calculated

proton transfer coordinate corresponds to collective solvent movement (reorganization) coordinate. Using Marcus definition the reorganization energy in such picture would be $\lambda = k\delta x^2/2$, where δx is proton transfer distance and k is a force constant of harmonic oscillator used to model solvent reorganization. The multistate nonadiabatic rate constant of proton transfer(Borgis and Hynes, 1996) is used to model proton transfer:

$$k_p = \sum_n \sum_m P_n \frac{V_{nm}^2}{\hbar} \sqrt{\frac{\pi}{\lambda_p k_B T}} \exp\left(-\frac{\Delta G_{nm}^{\ddagger}}{k_B T}\right) \tag{5.35}$$

$$\Delta G_{nm}^{\ddagger} = \frac{(\Delta G_p + E_m - E_n + \lambda_p)}{4\lambda_p} \tag{5.36}$$

Here P_n is probability (from Boltzmann distribution) of transition from n-th reactant state, V_{nm} vibrational coupling between reactant and product wave functions (calculated as described in (Farazdel et al., 1990)), λ_p reorganization energy of proton transfer; E_n and E_m energies of reactants and products respectively in states n and m. The energies and overlap integrals can be calculated using harmonic oscillator potential

approximation with resulting wave functions(Piela, 2013):

$$\psi_n(x) = \frac{e^{-\frac{1}{2}x^2\sqrt{\frac{k\,m_p}{\hbar^2}}}\sqrt{\frac{2^{-n}\sqrt[4]{\frac{k\,m_p}{\hbar^2}}}{n!}}H_n\left(x\sqrt[4]{\frac{k\,m_p}{\hbar^2}}\right)}{\sqrt[4]{\pi}} \tag{5.37}$$

where k is a force constant, associated with reorganization energy ($k = 2\lambda/\delta x^2$), and m_p is a mass of proton. The rate constant and activation free energy of proton transfer over distance of 1.7 Å can be reproduced with 3.72 eV reorganization energy and reaction Gibbs free energy of -48.3 kcal/mol. The proton transfer rate constants and activation free energy over distance of 1 Å is reproduced with reorganization energy of 2.01 eVand the Gibbs free energy of -3.54 kcal/mol. The later values are much more consistent with published reorganization energy values of proton transfer, which are around 2 eV (Takada et al., 2005; Smedarchina and Enchev, 1994), and much more consistent with assumed $\mathrm{pK_a}$ values (in PT-ET case, the $\mathrm{pK_a}$ of water, bound to reduced heme, should be around 24). This approach can be used to calculate kinetic isotope effect as well. Assuming reduced mass of deuteron is 1.8 times larger than proton mass, same Gibbs free energy -3.56 kcal/mol and transfer distance of 1 Å, a deuteron transfer rate constant can be calculated. This results a deuteron transfer rate constant of 295 ± 30 s^{-1} and kinetic isotope effect of 1.8 for proton transfer step. The kinetic isotope effect on full ET-PT process varies from substrate to substrate (table 5.4). The lowest value (KIE ≈ 1) predicted is for CPZ, a substrate with low electronic coupling and smallest driving force of the reaction. The largest value of KIE ≈ 1.5 is found for phenilendiamines - TMPD and AMB. The average of KIE over investigated set is ≈ 1.3 which coincides to value found for indolacetic acids by Candeias et al (Candeias et al., 1997). However, for the sake of completeness, we measured KIE for three CpdII-catalyzed oxidation reactions with substrates TMPD, CPZ and ABTS for CIP. The resultant values were 1.6±0.2, 1.0±0.1 and 1.3±0.1, respectively . These values agree well with calculated ones (table 5.4) and further support the ET followed by PT mechanism for the oxidation of substrates catalyzed by CpdII.

Final remarks. The devised model reveals a new picture of reduction of CiP CpdII by structurally diverse substrates. However, in order to use this model for making sensible predictions, a single rate constant

for each of the substrate is not enough. The original Marcus electron transfer theory was formulated around free energy of activation conception, which was later simplified to the prediction of rate constants behavior with assumption about very similar electronic coupling factors. The measurements of activation free energy made this assumption unnecessary and revealed new perspective of CiP CpdII reduction with structurally diverse compounds.

Quantum chemical DFT calculations allowed to calculate standard reduction potentials of separate steps for two-electron couples and use them to calculate reaction driving forces and relate the electrochemically measured standard reduction potential to the theoretical estimates. Calculated solvent and inner reorganization energies of substrates allowed accounting influence of this parameter upon the reaction rate constant and the free energy of activation. However, during preliminary fitting it was found that reorganization energies are greatly overestimated. This discrepancy was explained by the change of solvent reorganization energies upon the binding to the enzyme, as the process reduces the solvent accessible surface of substrate and therefore scales associated solvent reorganization energies. For the first time the proton transfer rate constant for CiP CpdII reduction was estimated. The rate constant was found to be well explained in the terms of molecular geometry and solvent reorganization energies of proton transfer using a harmonic oscillator approximation and nonadiabatic proton transfer theory. The catalytic efficiency of CiP CpdII is strictly related to physicochemical properties of substrates. Therefore, a structural diversity of substrates oxidized is possible. These findings are consistent with findings published by other authors. Further research directions concerning catalysis of substrates oxidation by CiP CpdIIcan be focused on the theoretical modeling of enzyme substrate structures and quantum-chemical computation of electronic coupling factor.

5.3 Résumé

The kinetics of oxidation of 12 diverse substrates catalyzed by CiP were investigated. The rate constants and free energies of activation were measured for peroxidase CpdII reduction step. The standard one-electron reduction potentials for two-electron reduction couples were calculated using DFT B3LYP methodology with solvent density model.

Using the same methodology the reorganization energies of each substrate were calculated. The structures of substrates docked in to the enzyme were used to estimate solvent-accessible surface. The calculated parameters were used to explain measured rate constants, free energies of activation in the terms of Marcus electron transfer and consecutive nonadiabatic proton transfer theory. It was found that the electron and proton transfer in the reactions with CiP CpdII are controlled by electronic coupling, reaction driving force (Gibbs free energy of the reaction) and solvent reorganization energies, and is very well described by consecutive electron and proton transfer model. The assumed model of nonadiabatic internal proton transfer in CpdII reduction from protonated histidine to heme bound hydroxide ion predicts the rate constant of proton transfer and kinetic isotope effect very well. The model and parameters found can be used to predict the reaction rate constants of other substrates oxidation by CiP.

CONCLUSIONS OF THE THESIS

1. A method was developed for modeling of complex homogeneous (bio)chemical kinetics and estimation of relevant rate parameters from limited amount of experimental data.

2. Oxygen electroreduction catalyzed by the immobilized on the electrode laccase from *Didymocrea* sp. J6 proceeds *via* direct electron transfer from electrode to T2/T3 active center of laccase.

3. It was found that inhibition of laccase from *Didymocrea* sp. J6 with fluoride ions in homogeneous media is based on the potential shift of T2/T3 center to lower values and disruption of electron transfer between T1 and T2/T3 centers.

4. It was found that the observed activation free energies in oxidation of substrates catalyzed by peroxidase compound II from *Coprinopsis cinerea* are explained in terms of separate electron and proton transfer steps.

5. It was found that the rates of peroxidase compound II from *Coprinopsis cinerea* catalyzed oxidations are described by Marcus electron transfer and nonadiabatic proton transfer theories.

Abelskov, A. K., Smith, A. T., Rasmussen, C. B., Dunford, H. B., and Welinder, K. G. (1997). ph dependence and structural interpretation of the reactions of coprinus cinereus peroxidase with hydrogen peroxide, ferulic acid, and 2, 2'-azinobis (3-ethylbenzthiazoline-6-sulfonic acid). *Biochemistry*, 36(31):9453–9463.

Al-Shemmeri, T. (2012). *Engineering Fluid Mechanics*. Bookboon.

Andréasson, L.-E., Brändén, R., and Reinhammar, B. (1976). Kinetic studies of rhus vernicifera laccase: Evidence for multi-electron transfer and an oxygen intermediate in the reoxidation reaction. *Biochimica et Biophysica Acta (BBA)-Enzymology*, 438(2):370–379.

Andreu, R., Ferapontova, E. E., Gorton, L., and Calvente, J. J. (2007). Direct electron transfer kinetics in horseradish peroxidase electrocatalysis. *The Journal of Physical Chemistry B*, 111(2):469–477.

Arakane, Y., Muthukrishnan, S., Beeman, R. W., Kanost, M. R., and Kramer, K. J. (2005). Laccase 2 is the phenoloxidase gene required for beetle cuticle tanning. *Proceedings of the National Academy of Sciences of the United States of America*, 102(32):11337–11342.

Armarego, W. L. and Chai, C. L. L. (2013). *Purification of laboratory chemicals*. Butterworth-Heinemann.

Armstrong, F. A., Heering, H. A., and Hirst, J. (1997). Reaction of complex metalloproteins studied by protein-film voltammetry. *Chemical Society Reviews*, 26(3):169–179.

Armstrong, J. M. (1964). The molar extinction coefficient of 2, 6-dichlorophenol indophenol. *Biochimica et Biophysica Acta (BBA)-General Subjects*, 86(1):194–197.

Avriel, M. (2003). *Nonlinear programming: analysis and methods*. Courier Corporation.

Awasthi, M., Jaiswal, N., Singh, S., Pandey, V. P., and Dwivedi, U. N. (2015). Molecular docking and dynamics simulation analyses unraveling the differential enzymatic catalysis by plant and fungal

laccases with respect to lignin biosynthesis and degradation. *Journal of Biomolecular Structure and Dynamics*, 33(9):1835–1849.

Bader, J. S., Cortis, C. M., and Berne, B. (1997). Solvation and reorganization energies in polarizable molecular and continuum solvents. *The Journal of chemical physics*, 106(6):2372–2387.

Baek, H. K. and Van Wart, H. E. (1992). Elementary steps in the reaction of horseradish peroxidase with several peroxides: kinetics and thermodynamics of formation of compound 0 and compound i. *Journal of the American Chemical Society*, 114(2):718–725.

Bagley, R. (1999). Shang archaeology. *The Cambridge history of ancient China*, pages 124–231.

Ballardini, R., Varani, G., Indelli, M., Scandola, F., and Balzani, V. (1978). Free energy correlation of rate constants for electron transfer quenching of excited transition metal complexes. *Journal of the American Chemical Society*, 100(23):7219–7223.

Bard, A. and Faulkner, L. (2000). *Electrochemical Methods: Fundamentals and Applications*. Wiley.

Barshop, B. A., Wrenn, R. F., and Frieden, C. (1983). Analysis of numerical methods for computer simulation of kinetic processes: development of kinsim—a flexible, portable system.

Basto, C., Tzanov, T., and Cavaco-Paulo, A. (2007). Combined ultrasound-laccase assisted bleaching of cotton. *Ultrasonics sonochemistry*, 14(3):350–354.

Bates, D. M. and Watts, D. G. (1988). *Nonlinear regression: iterative estimation and linear approximations*. Wiley Online Library.

Bauer, R. and Rupe, C. O. (1971). Use of syringaldazine in a photometric method for estimating" free" chlorine in water. *Analytical Chemistry*, 43(3):421–425.

Berglund, G. I., Carlsson, G. H., Smith, A. T., Szöke, H., Henriksen, A., and Hajdu, J. (2002). The catalytic pathway of horseradish peroxidase at high resolution. *nature*, 417(6887):463–468.

Blankert, B., Hayen, H., van Leeuwen, S., Karst, U., Bodoki, E., Lotrean, S., Sandulescu, R., Diez, N. M., Dominguez, O., Arcos, J., et al. (2005). Electrochemical, chemical and enzymatic oxidations of phenothiazines. *Electroanalysis*, 17(17):1501–1510.

Bligny, R. and Douce, R. (1983). Excretion of laccase by sycamore (acer pseudoplatanus l.) cells. purification and properties of the enzyme. *Biochemical Journal*, 209(2):489–496.

Borgis, D. and Hynes, J. T. (1996). Curve crossing formulation for proton transfer reactions in solution. *The Journal of Physical Chemistry*, 100(4):1118–1128.

Bortolotti, C. A., Siwko, M. E., Castellini, E., Ranieri, A., Sola, M., and Corni, S. (2011). The reorganization energy in cytochrome c is controlled by the accessibility of the heme to the solvent. *The Journal of Physical Chemistry Letters*, 2(14):1761–1765.

Bowers, G. N. and McComb, R. B. (1966). A continuous spectrophotometric method for measuring the activity of serum alkaline phosphatase. *Clinical Chemistry*, 12(2):70–89.

Bowers, G. N., McComb, R. B., Christensen, R., and Schaffer, R. (1980). High-purity 4-nitrophenol: purification, characterization, and specifications for use as a spectrophotometric reference material. *Clinical chemistry*, 26(6):724–729.

Brändén, R., Malmström, B. G., and Vänngård, T. (1973). The effect of fluoride on the spectral and catalytic properties of three copper-containing oxidases. *The FEBS Journal*, 36(1):195–200.

Briggs, G. E. and Haldane, J. B. S. (1925). A note on the kinetics of enzyme action. *Biochemical journal*, 19(2):338.

Buch-Rasmussen, T., Olsen, B., Kulys, J., Bechgaard, K., Christensen, J., and Wang, J. (1992). M.(s.) ozsoz, f. colin and o. garcia. *International Patent Application, WO*, 92:07263.

Bukh, C., Lund, M., and Bjerrum, M. J. (2006). Kinetic studies on the reaction between trametes villosa laccase and dioxygen. *Journal of inorganic biochemistry*, 100(9):1547–1557.

Butler, J. A. V. (1924). Studies in heterogeneous equilibria. part ii.-the kinetic interpretation of the nernst theory of electromotive force. *Trans. Faraday Soc.*, 19:729–733.

Camarero, S., Garcıa, O., Vidal, T., Colom, J., del Rıo, J. C., Gutiérrez, A., Gras, J. M., Monje, R., Martınez, M. J., and Martınez, Á. T. (2004). Efficient bleaching of non-wood high-quality paper pulp using laccase-mediator system. *Enzyme and Microbial Technology*, 35(2):113–120.

Candeias, L. P., Folkes, L. K., Porssa, M., Parrick, J., and Wardman, P. (1996). Rates of reaction of indoleacetic acids with horseradish peroxidase compound i and their dependence on the redox potentials. *Biochemistry*, 35(1):102–108.

Candeias, L. P., Folkes, L. K., and Wardman, P. (1997). Factors controlling the substrate specificity of peroxidases: kinetics and thermodynamics of the reaction of horseradish peroxidase compound i with phenols and indole-3-acetic acids. *Biochemistry*, 36(23):7081–7085.

Casadei, C. M., Gumiero, A., Metcalfe, C. L., Murphy, E. J., Basran, J., Teixeira, S. C., Schrader, T. E., Fielding, A. J., Ostermann, A., Blakeley, M. P., et al. (2014). Neutron cryo-crystallography captures the protonation state of ferryl heme in a peroxidase. *Science*, 345(6193):193–197.

Chang-Guo Zhan*, [U+FFFD] , and David A. Dixon*, [U+FFFD]2003). The nature and absolute hydration free energy of the solvated electron in water. *The Journal of Physical Chemistry B*, 107(18):4403–4417.

Chen, C., Xie, Q., Yang, D., Xiao, H., Fu, Y., Tan, Y., and Yao, S. (2013). Recent advances in electrochemical glucose biosensors: a review. *Rsc Advances*, 3(14):4473–4491.

CHIDSEY, C. E. D. (1991). Free energy and temperature dependence of electron transfer at the metal-electrolyte interface. *Science*, 251(4996):919–922.

Childs, R. E. and Bardsley, W. G. (1975). The steady-state kinetics of peroxidase with 2,2'-azino-di-(3-ethyl-benzthiazoline-6-sulphonic acid) as chromogen. *Biochemical Journal*, 145(1):93–103.

Chou, M., Creutz, C., and Sutin, N. (1977). Rate constants and activation parameters for outer-sphere electron-transfer reactions and comparisons with the predictions of marcus theory. *Journal of the American Chemical Society*, 99(17):5615–5623.

Christenson, A., Shleev, S., Mano, N., Heller, A., and Gorton, L. (2006). Redox potentials of the blue copper sites of bilirubin oxidases. *Biochimica et Biophysica Acta (BBA)-Bioenergetics*, 1757(12):1634–1641.

Cole, J. L., Ballou, D. P., and Solomon, E. I. (1991). Spectroscopic characterization of the peroxide intermediate in the reduction of dioxygen catalyzed by the multicopper oxidases. *Journal of the American Chemical Society*, 113(22):8544–8546.

Crank, J. and Nicolson, P. (1947). A practical method for numerical evaluation of solutions of partial differential equations of the heat-conduction type. In *Mathematical Proceedings of the Cambridge Philosophical Society*, volume 43, pages 50–67. Cambridge Univ Press.

Cukier, R. and Morillo, M. (1989). Solvent effects on proton-transfer reactions. *The Journal of chemical physics*, 91(2):857–863.

Cyboron, G. W. and Wuthier, R. E. (1981). Purification and initial characterization of intrinsic membrane-bound alkaline phosphatase from chicken epiphyseal cartilage. *Journal of Biological Chemistry*, 256(14):7262–7268.

Dagys, M., Laurynėnas, A., Ratautas, D., Kulys, J., Vidžiūnaitė, R., Talaikis, M., Niaura, G., Marcinkevičienė, L., Meškys, R., and Shleev, S. (2017). Oxygen electroreduction catalysed by laccase wired to gold nanoparticles via the trinuclear copper cluster. *Energy & Environmental Science*, 10(2):498–502.

Derat, E. and Shaik, S. (2006). Two-state reactivity, electromerism, tautomerism, and "surprise" isomers in the formation of compound ii of the enzyme horseradish peroxidase from the principal species, compound i. *Journal of the American Chemical Society*, 128(25):8185–8198.

Desai, S. and Nityanand, C. (2011). Microbial laccases and their applications: a review. *Asian J Biotechnol*, 3(2):98–124.

Dunford, H. B. (1991). Spectral and kinetic properties of oxidized intermediates of coprinus cinereus peroxidase. *Acta Chemica Scandinavia*, 45:1080–1086.

Eberson, L. (1982). Electron transfer reactions in organic chemistry. ii. an analysis of alkyl halide reduction by electron transfer reagents on the basis of the marcus theory. *Acta Chemica Scandinavica. B*, 36:533–543.

Edwards, S. J., Soudackov, A. V., and Hammes-Schiffer, S. (2009). Analysis of kinetic isotope effects for proton-coupled electron transfer reactions†. *The Journal of Physical Chemistry A*, 113(10):2117–2126.

Einstein, A. (1905). Über die von der molekularkinetischen theorie der wärme geforderte bewegung von in ruhenden flüssigkeiten suspendierten teilchen. *Annalen der physik*, 322(8):549–560.

Farazdel, A., Dupuis, M., Clementi, E., and Aviram, A. (1990). Electric field induced intramolecular electron transfer in spiro π-electron systems and their suitability as molecular electronic devices. a theoretical study. *Journal of the American Chemical Society*, 112(11):4206–4214.

Farhangrazi, Z. S., Copeland, B. R., Nakayama, T., Amachi, T., Yamazaki, I., and Powers, L. S. (1994a). Oxidation-reduction properties of compounds i and ii of arthromyces ramosus peroxidase. *Biochemistry*, 33(18):5647–5652. PMID: 8180190.

Farhangrazi, Z. S., Copeland, B. R., Nakayama, T., Amachi, T., Yamazaki, I., and Powers, L. S. (1994b). Oxidation-reduction properties of compounds i and ii of arthromyces ramosus peroxidase. *Biochemistry*, 33(18):5647–5652.

Farver, O., Hosseinzadeh, P., Marshall, N. M., Wherland, S., Lu, Y., and Pecht, I. (2014). Long-range electron transfer in engineered azurins exhibits marcus inverted region behavior. *The journal of physical chemistry letters*, 6(1):100–105.

Farver, O., Wherland, S., Koroleva, O., Loginov, D. S., and Pecht, I. (2011). Intramolecular electron transfer in laccases. *The FEBS journal*, 278(18):3463–3471.

Fischer, L. M., Tenje, M., Heiskanen, A. R., Masuda, N., Castillo, J., Bentien, A., Émneus, J., Jakobsen, M. H., and Boisen, A. (2009). Gold cleaning methods for electrochemical detection applications. *Microelectronic engineering*, 86(4):1282–1285.

Folkes, L. K. and Candeias, L. P. (1997). Interpretation of the reactivity of peroxidase compounds i and ii with phenols by the marcus equation. *FEBS letters*, 412(2):305–308.

Fu, Y., Liu, L., Yu, H.-Z., Wang, Y.-M., and Guo, Q.-X. (2005). Quantum-chemical predictions of absolute standard redox potentials of diverse organic molecules and free radicals in acetonitrile. *Journal of the American Chemical Society*, 127(19):7227–7234.

Goličnik, M. (2012). On the lambert w function and its utility in biochemical kinetics. *Biochemical engineering journal*, 63:116–123.

Goudar, C. T., Harris, S. K., McInerney, M. J., and Suflita, J. M. (2004). Progress curve analysis for enzyme and microbial kinetic reactions using explicit solutions based on the lambert w function. *Journal of microbiological methods*, 59(3):317–326.

Hammel, K. E. and Cullen, D. (2008). Role of fungal peroxidases in biological ligninolysis. *Current opinion in plant biology*, 11(3):349–355.

Hammes-Schiffer, S. and Stuchebrukhov, A. A. (2010). Theory of coupled electron and proton transfer reactions. *Chemical reviews*, 110(12):6939–6960.

Hayashi, Y. and Yamazaki, I. (1979). The oxidation-reduction potentials of compound i/compound ii and compound ii/ferric couples of horseradish peroxidases a2 and c. *Journal of biological chemistry*, 254(18):9101–9106.

Hildebrandt, A. G. and Roots, I. (1975). Reduced nicotinamide adenine dinucleotide phosphate (nadph)-dependent formation and breakdown of hydrogen peroxide during mixed function oxidation reactions in liver microsomes. *Archives of biochemistry and biophysics*, 171(2):385–397.

Hofrichter, M., Ullrich, R., Pecyna, M. J., Liers, C., and Lundell, T. (2010). New and classic families of secreted fungal heme peroxidases. *Applied Microbiology and Biotechnology*, 87(3):871–897.

Jin, S., Kurtz, D. M., Liu, Z.-J., Rose, J., and Wang, B.-C. (2002). X-ray crystal structures of reduced rubrerythrin and its azide adduct: a structure-based mechanism for a non-heme diiron peroxidase. *Journal of the American Chemical Society*, 124(33):9845–9855.

Johnson, K. A. (2013). A century of enzyme kinetic analysis, 1913 to 2013. *FEBS letters*, 587(17):2753–2766.

Johnson, K. A. and Goody, R. S. (2011). The original michaelis constant: translation of the 1913 michaelis–menten paper. *Biochemistry*, 50(39):8264–8269.

Jones, S. M. and Solomon, E. I. (2015). Electron transfer and reaction mechanism of laccases. *Cellular and molecular life sciences*, 72(5):869–883.

Karlin, K. D. (2010). Bioinorganic chemistry: Model offers intermediate insight. *Nature*, 463(7278):168–169.

Kawaoka, A., Kawamoto, T., Ohta, H., Sekine, M., Takano, M., and Shinmyo, A. (1994). Wound-induced expression of horseradish peroxidase. *Plant cell reports*, 13(3-4):149–154.

Kepp, K. P. (2014). Halide binding and inhibition of laccase copper clusters: the role of reorganization energy. *Inorganic chemistry*, 54(2):476–483.

King, E. L. and Altman, C. (1956). A schematic method of deriving the rate laws for enzyme-catalyzed reactions. *The Journal of physical chemistry*, 60(10):1375–1378.

Krikstopaitis, K., Kulys, J., Pedersen, A. H., and Schneider, P. (1998). N-substituted p-phenylenediamines as peroxidase and laccase substrates. *Acta Chemica Scandinavica*, 52(4):469–474.

Kulys, J., Buch-Rasmussen, T., Bechgaard, K., Razumas, V., Kazlauskaite, J., Marcinkeviciene, J., Christensen, J. B., and Hansen, H. (1994).

Study of the new electron transfer mediators in glucose oxidase catalysis. *Journal of molecular catalysis*, 91(3):407–420.

Kulys, J. and Dapkūnas, Ž. (2007). The effectiveness of synergistic enzymatic reaction with limited mediator stability. *Nonlinear Anal. Model. Control*, 12:495–501.

Kulys, J., Krikstopaitis, K., and Ziemys, A. (2000). Kinetics and thermodynamics of peroxidase-and laccase-catalyzed oxidation of n-substituted phenothiazines and phenoxazines. *Journal of Biological Inorganic Chemistry*, 5(3):333–340.

Kulys, J., Tetianec, L., and Bratkovskaja, I. (2010). Pyrroloquinoline quinone-dependent carbohydrate dehydrogenase: Activity enhancement and the role of artificial electron acceptors. *Biotechnology Journal*, 5(8):822–828.

Kuzmič, P. (1996). Program dynafit for the analysis of enzyme kinetic data: application to hiv proteinase. *Analytical biochemistry*, 237(2):260–273.

Kuzmič, P. (2009). Dynafit–a software package for enzymology. *Methods in enzymology*, 467:247–280.

Kwon, H., Basran, J., Casadei, C. M., Fielding, A. J., Schrader, T. E., Ostermann, A., Devos, J. M., Aller, P., Blakeley, M. P., Moody, P. C., et al. (2016). Direct visualization of a fe (iv)–oh intermediate in a heme enzyme. *Nature communications*, 7:13445.

Laurynenas, A. and Kulys, J. (2015). An exhaustive search approach for chemical kinetics experimental data fitting, rate constants optimization and confidence interval estimation. *Nonlinear Analysis: Modelling and Control*, 20(1):145–157.

Le Goff, A., Holzinger, M., and Cosnier, S. (2015). Recent progress in oxygen-reducing laccase biocathodes for enzymatic biofuel cells. *Cellular and molecular life sciences*, 72(5):941–952.

Lee, C.-W., Gray, H. B., Anson, F. C., and Malmström, B. G. (1984). Catalysis of the reduction of dioxygen at graphite electrodes coated with fungal laccase a. *Journal of electroanalytical chemistry and interfacial electrochemistry*, 172(1):289–300.

Li, D., Luo, L., Pang, Z., Ding, L., Wang, Q., Ke, H., Huang, F., and Wei, Q. (2014). Novel phenolic biosensor based on a magnetic polydopamine-laccase-nickel nanoparticle loaded carbon nanofiber composite. *ACS applied materials & interfaces*, 6(7):5144–5151.

Li, H. and Jensen, J. H. (2004). Improving the efficiency and convergence of geometry optimization with the polarizable continuum model: new energy gradients and molecular surface tessellation. *Journal of computational chemistry*, 25(12):1449–1462.

Li, Y., Hodak, M., and Bernholc, J. (2015). Enzymatic mechanism of copper-containing nitrite reductase. *Biochemistry*, 54(5):1233–1242.

Libby, W. (1952). Theory of electron exchange reactions in aqueous solution. *The Journal of Physical Chemistry*, 56(7):863–868.

Lin, B. C., Cheng, C. P., and Lao, Z. P. M. (2003). Reorganization energies in the transports of holes and electrons in organic amines in organic electroluminescence studied by density functional theory. *The Journal of Physical Chemistry A*, 107(26):5241–5251.

Loew, G. and Dupuis, M. (1997). Characterization of a resting state model of peroxidases by ab initio methods: Optimized geometries, electronic structures, and relative energies of the sextet, quartet, and doublet spin states. *Journal of the American Chemical Society*, 119(41):9848–9851.

Lowry, O. H., Rosebrough, N. J., Farr, A. L., Randall, R. J., et al. (1951). Protein measurement with the folin phenol reagent. *J biol Chem*, 193(1):265–275.

Marcus, R. (1959). On the theory of electrochemical and chemical electron transfer processes. *Canadian Journal of Chemistry*, 37(1):155–163.

Marcus, R. (1960). Exchange reactions and electron transfer reactions including isotopic exchange. theory of oxidation-reduction reactions involving electron transfer. part 4.—a statistical-mechanical basis for treating contributions from solvent, ligands, and inert salt. *Discussions of the Faraday Society*, 29:21–31.

Marcus, R. (1999). Electron transfer past and future. *Advances in Chemical Physics: Electron Transfer-from Isolated Molecules to Biomolecules. Part 1, Volume 106*, pages 1–6.

Marcus, R. A. (1956a). Electrostatic free energy and other properties of states having nonequilibrium polarization. i. *The Journal of Chemical Physics*, 24(5):979–989.

Marcus, R. A. (1956b). On the theory of oxidation-reduction reactions involving electron transfer. i. *The Journal of Chemical Physics*, 24(5):966–978.

Marcus, R. A. (1968). Theoretical relations among rate constants, barriers, and brønsted slopes of chemical reactions. *The Journal of Physical Chemistry*, 72(3):891–899.

Martinello, F. and da Silva, E. L. (2006). Mechanism of ascorbic acid interference in biochemical tests that use peroxide and peroxidase to generate chromophore. *Clinica chimica acta*, 373(1):108–116.

Mayer, A. M. and Staples, R. C. (2002). Laccase: new functions for an old enzyme. *Phytochemistry*, 60(6):551–565.

Mendes, P. (1997). Biochemistry by numbers: simulation of biochemical pathways with gepasi 3. *Trends in biochemical sciences*, 22(9):361–363.

Menten, L. and Michaelis, M. (1913). Die kinetik der invertinwirkung. *Biochem Z*, 49(333-369):5.

Messerschmidt, A., Ladenstein, R., Huber, R., Bolognesi, M., Avigliano, L., Petruzzelli, R., Rossi, A., and Finazzi-Agró, A. (1992). Refined crystal structure of ascorbate oxidase at 1.9 å resolution. *Journal of molecular biology*, 224(1):179–205.

Mikolasch, A., Niedermeyer, T. H. J., Lalk, M., Witt, S., Seefeldt, S., Hammer, E., Schauer, F., Gesell, M., Hessel, S., Jülich, W.-D., et al. (2006). Novel penicillins synthesized by biotransformation using laccase from trametes spec. *Chemical and pharmaceutical bulletin*, 54(5):632–638.

Miller, J., Calcaterra, L., and Closs, G. (1984). Intramolecular long-distance electron transfer in radical anions. the effects of free energy

and solvent on the reaction rates. *Journal of the American Chemical Society*, 106(10):3047–3049.

Minussi, R. C., Pastore, G. M., and Durán, N. (2002). Potential applications of laccase in the food industry. *Trends in Food Science & Technology*, 13(6):205–216.

Morillo, M. and Cukier, R. (1990). On the effects of solvent and intermolecular fluctuations in proton transfer reactions. *The Journal of chemical physics*, 92(8):4833–4838.

Nelder, J. A. and Mead, R. (1965). A simplex method for function minimization. *The computer journal*, 7(4):308–313.

Nickel, U., Borchardt, M., Bapat, M. R., and Jaenicke, W. (1979). 1-and 2-electron steps in the oxidation of substituted p-phenylenediamines with different oxidants in aqueous solution i. the reaction with iodine. *Berichte der Bunsengesellschaft für physikalische Chemie*, 83(9):877–884.

Paczkowski, J., Pietrzak, M., and Kucybala, Z. (1996). Generalization of the kinetic scheme for photoinduced polymerization via an intermolecular electron transfer process. 2. application of the marcus theory. *Macromolecules*, 29(15):5057–5064.

Papoulis, A. and Pillai, S. U. (2002). *Probability, random variables, and stochastic processes*. Tata McGraw-Hill Education.

Passardi, F., Cosio, C., Penel, C., and Dunand, C. (2005). Peroxidases have more functions than a swiss army knife. *Plant cell reports*, 24(5):255–265.

Peisach, J. and Levine, W. G. (1963). On the mechanism of ceruloplasmin-catalyzed oxidations. *Biochimica et Biophysica Acta*, 77:615–628.

Petzold, L. (1983). Automatic Selection of Methods for Solving Stiff and Nonstiff Systems of Ordinary Differential Equations. *SIAM Journal on Scientific and Statistical Computing*, 4(1):136–148.

Pezzella, C., Guarino, L., and Piscitelli, A. (2015). How to enjoy laccases. *Cellular and molecular life sciences*, 72(5):923–940.

Piela, L. (2013). *Ideas of quantum chemistry*. Elsevier.

Portaccio, M., Di Tuoro, D., Arduini, F., Moscone, D., Cammarota, M., Mita, D., and Lepore, M. (2013). Laccase biosensor based on screen-printed electrode modified with thionine–carbon black nanocomposite, for bisphenol a detection. *Electrochimica Acta*, 109:340–347.

Powell, M. J. (1964). An efficient method for finding the minimum of a function of several variables without calculating derivatives. *The computer journal*, 7(2):155–162.

Reiss, H. and Heller, A. (1985). The absolute potential of the standard hydrogen electrode: a new estimate. *The Journal of Physical Chemistry*, 89(20):4207–4213.

Rivera-Hoyos, C. M., Morales-Álvarez, E. D., Poutou-Piñales, R. A., Pedroza-Rodríguez, A. M., RodrÍguez-Vázquez, R., and Delgado-Boada, J. M. (2013). Fungal laccases. *Fungal Biology Reviews*, 27(3):67–82.

Rovati, G. E., Shrager, R., Nicosia, S., and Munson, P. J. (1996). Kinfit ii: a nonlinear least-squares program for analysis of kinetic binding data. *Molecular pharmacology*, 50(1):86–95.

Sagui, F., Chirivì, C., Fontana, G., Nicotra, S., Passarella, D., Riva, S., and Danieli, B. (2009). Laccase-catalyzed coupling of catharanthine and vindoline: an efficient approach to the bisindole alkaloid anhydrovinblastine. *Tetrahedron*, 65(1):312–317.

Sakurada, J., Sekiguchi, R., Sato, K., and Hosoya, T. (1990). Kinetic and molecular orbital studies on the rate of oxidation of monosubstituted phenols and anilines by horseradish peroxidase compound ii. *Biochemistry*, 29(17):4093–4098.

Sakurai, T. and Kataoka, K. (2007). Structure and function of type i copper in multicopper oxidases. *Cellular and molecular life sciences*, 64(19):2642–2656.

Salaj-Kosla, U., Pöller, S., Beyl, Y., Scanlon, M. D., Beloshapkin, S., Shleev, S., Schuhmann, W., and Magner, E. (2012). Direct electron transfer of bilirubin oxidase (myrothecium verrucaria) at an unmodi-

fied nanoporous gold biocathode. *Electrochemistry Communications*, 16(1):92–95.

Schiele, B. C. (1962). Newer drugh for mental illness: A review. *JAMA*, 181(2):126–133.

Schiesser, W. E. (2012). *The numerical method of lines: integration of partial differential equations*. Elsevier.

Schlesener, C., Amatore, C., and Kochi, J. (1986). Marcus theory in organic chemistry. mechanisms of electron and proton transfers from aromatics and their cation radicals. *The Journal of Physical Chemistry*, 90(16):3747–3756.

Schmidt, M. W., Baldridge, K. K., Boatz, J. A., Elbert, S. T., Gordon, M. S., Jensen, J. H., Koseki, S., Matsunaga, N., Nguyen, K. A., and Su, S. (1993). General atomic and molecular electronic structure system. *Journal of computational chemistry*, 14(11):1347–1363.

Schulz, C., Rutter, R., Sage, J., Debrunner, P., and Hager, L. (1984). Mössbauer and electron paramagnetic resonance studies of horseradish peroxidase and its catalytic intermediates. *Biochemistry*, 23(20):4743–4754.

Selinheimo, E., Kruus, K., Buchert, J., Hopia, A., and Autio, K. (2006). Effects of laccase, xylanase and their combination on the rheological properties of wheat doughs. *Journal of Cereal Science*, 43(2):152–159.

Shiro, Y., Kurono, M., and Morishima, I. (1986). Presence of endogenous calcium ion and its functional and structural regulation in horseradish peroxidase. *Journal of Biological Chemistry*, 261(20):9382–9390.

Shleev, S., Christenson, A., Serezhenkov, V., Burbaev, D., Yaropolov, A., Gorton, L., and Ruzgas, T. (2005a). Electrochemical redox transformations of t1 and t2 copper sites in native trametes hirsuta laccase at gold electrode. *Biochemical Journal*, 385(3):745–754.

Shleev, S., El Kasmi, A., Ruzgas, T., and Gorton, L. (2004). Direct heterogeneous electron transfer reactions of bilirubin oxidase at a spectrographic graphite electrode. *Electrochemistry Communications*, 6(9):934–939.

Shleev, S., Jarosz-Wilkolazka, A., Khalunina, A., Morozova, O., Yaropolov, A., Ruzgas, T., and Gorton, L. (2005b). Direct electron transfer reactions of laccases from different origins on carbon electrodes. *Bioelectrochemistry*, 67(1):115–124.

Shleev, S., Pita, M., Yaropolov, A. I., Ruzgas, T., and Gorton, L. (2006). Direct heterogeneous electron transfer reactions of trametes hirsuta laccase at bare and thiol-modified gold electrodes. *Electroanalysis*, 18(19-20):1901–1908.

Shleev, S., Shumakovich, G., Morozova, O., and Yaropolov, A. (2010). Stable 'floating'air diffusion biocathode based on direct electron transfer reactions between carbon particles and high redox potential laccase. *Fuel Cells*, 10(4):726–733.

Shleev, S., Tkac, J., Christenson, A., Ruzgas, T., Yaropolov, A. I., Whittaker, J. W., and Gorton, L. (2005c). Direct electron transfer between copper-containing proteins and electrodes. *Biosensors and Bioelectronics*, 20(12):2517–2554.

Silverman, D. N. (2000). Marcus rate theory applied to enzymatic proton transfer. *Biochimica et Biophysica Acta (BBA)-Bioenergetics*, 1458(1):88–103.

Silverman, D. N., Tu, C., Chen, X., Tanhauser, S. M., Kresge, A. J., and Laipis, P. J. (1993). Rate-equilibria relationships in intramolecular proton transfer in human carbonic anhydrase iii. *Biochemistry*, 32(40):10757–10762.

Smedarchina, Z. and Enchev, V. (1994). Comparative theoretical study of intramolecular proton transfer in the photochemical cycles of 2-(2′-hydroxyphenyl) benzoxazole and 5, 8-dimethyl-1-tetralone. *Journal of Photochemistry and Photobiology A: Chemistry*, 80(1-3):135–144.

Smoluchowski, M. v. (1917). Grundriß der koagulationskinetik kolloider lösungen. *Colloid & Polymer Science*, 21(3):98–104.

Solar, S., Solar, W., and Getoff, N. (1982). Pulse radiolysis of thionine and methylene blue in acid aqueous solutions. *Radiation Physics and Chemistry (1977)*, 20(2):165–174.

Solomon, E. I. (2006). Spectroscopic methods in bioinorganic chemistry: blue to green to red copper sites. *Inorganic chemistry*, 45(20):8012–8025.

Solomon, E. I., Sundaram, U. M., and Machonkin, T. E. (1996). Multicopper oxidases and oxygenases. *Chemical reviews*, 96(7):2563–2606.

Strong, P. and Claus, H. (2011). Laccase: a review of its past and its future in bioremediation. *Critical Reviews in Environmental Science and Technology*, 41(4):373–434.

Sutin, N. (1982). Nuclear, electronic, and frequency factors in electron transfer reactions. *Accounts of Chemical Research*, 15(9):275–282.

Svir, I., Klymenko, O., and Platz, M. (2002). kinfitsim software to fit kinetic data to a user selected mechanism. *Computers & chemistry*, 26(4):379–386.

Takada, T., Kawai, K., Fujitsuka, M., and Majima, T. (2005). Contributions of the distance-dependent reorganization energy and proton-transfer to the hole-transfer process in dna. *Chemistry–A European Journal*, 11(13):3835–3842.

Tanaka, F., Chosrowjan, H., Taniguchi, S., Mataga, N., Sato, K., Nishina, Y., and Shiga, K. (2007). Donor-acceptor distance-dependence of photoinduced electron-transfer rate in flavoproteins. *The Journal of Physical Chemistry B*, 111(20):5694–5699.

Tarasevich, M., Yaropolov, A., Bogdanovskaya, V., and Varfolomeev, S. (1979). 293-electrocatalysis of a cathodic oxygen reduction by laccase. *Bioelectrochemistry and Bioenergetics*, 6(3):393–403.

Tetianec, L., Chaleckaja, A., Vidziunaite, R., Kulys, J., Bachmatova, I., Marcinkeviciene, L., and Meskys, R. (2014). Development of a laccase/syringaldazine system for nad (p) h oxidation. *Journal of Molecular Catalysis B: Enzymatic*, 101:28–34.

Tominaga, M., Sasaki, A., Tsushida, M., and Togami, M. (2017). Biosurfactant functionalized single-walled carbon nanotubes to promote laccase bioelectrocatalysis. *New Journal of Chemistry*, 41(1):231–236.

Trott, O. and Olson, A. J. (2010). Autodock vina: improving the speed and accuracy of docking with a new scoring function, efficient optimization, and multithreading. *Journal of computational chemistry*, 31(2):455–461.

Van Belle, H. (1976). Kinetics and inhibition of rat and avian alkaline phosphatases. *General Pharmacology: The Vascular System*, 7(1):53–58.

Vaz-Dominguez, C., Campuzano, S., Rüdiger, O., Pita, M., Gorbacheva, M., Shleev, S., Fernandez, V. M., and De Lacey, A. L. (2008). Laccase electrode for direct electrocatalytic reduction of o 2 to h 2 o with high-operational stability and resistance to chloride inhibition. *Biosensors and Bioelectronics*, 24(4):531–537.

Veitch, N. C. (2004). Horseradish peroxidase: a modern view of a classic enzyme. *Phytochemistry*, 65(3):249–259.

Veitch, N. C. and Smith, A. T. (2000). Horseradish peroxidase. *Advances in inorganic chemistry*, 51:107–162.

Wang, J., Wolf, R. M., Caldwell, J. W., Kollman, P. A., and Case, D. A. (2004). Development and testing of a general amber force field. *Journal of computational chemistry*, 25(9):1157–1174.

Wardman, P. (1989). Reduction potentials of one-electron couples involving free radicals in aqueous solution. *Journal of Physical and Chemical Reference Data*, 18(4):1637–1755.

Weiss, J. N. (1997). The hill equation revisited: uses and misuses. *The FASEB Journal*, 11(11):835–841.

Weiss, R. (1970). The solubility of nitrogen, oxygen and argon in water and seawater. In *Deep Sea Research and Oceanographic Abstracts*, volume 17, pages 721–735. Elsevier.

Wherland, S. and Pecht, I. (1978). Protein-protein electron transfer. a marcus theory analysis of reactions between c type cytochromes and blue copper proteins. *Biochemistry*, 17(13):2585–2591.

Wolfram Research, I. (2001-2008). Inverse of the regularized incomplete beta function.

Xu, D. and Schulten, K. (1994). Coupling of protein motion to electron transfer in a photosynthetic reaction center: investigating the low temperature behavior in the framework of the spin—boson model. *Chemical physics*, 182(2):91–117.

Xu, F. (1996). Oxidation of phenols, anilines, and benzenethiols by fungal laccases: correlation between activity and redox potentials as well as halide inhibition. *Biochemistry*, 35(23):7608–7614.

Yaropolov, A., Skorobogat KO, O., Vartanov, S., and Varfolomeyev, S. (1994). Laccase. *Applied Biochemistry and Biotechnology*, 49(3):257–280.

APPENDIX

1.1 A.

Table 1.5: Final solutions of three biased curves fitting with estimated errors (with 95% confidence level).

Case	Data points	Critical fitting score contour value	Estimated mean and confidence interval (in logarithmic form)
#1	859	$1.0888 * 10^{-11}$	lg(k_1)= 6.303 [-0.010, +0.006] lg(k_2)= 7.303 [-0.006, +0.016] lg(k_3)= 5.2 [-1.4,+ 2.8] lg(k_{-3})= 4.2 [-1.5,+ 2.8] lg(K)=lg(k_3/k_{-3})= 1.02 [-0.02, +0.05]
#2	1057	$1.3518 * 10^{-11}$	lg(k_1)= 5.300 [-0.013,+ 0.003] lg(k_2)= 7.305 [-0.004,+ 0.023] lg(k_3)= 5.3 [-1.6,+ 2.7] lg(k_{-3})= 4.3 [-1.7,+ 2.7] lg(K)=lg(k_3/k_{-3})= 1.01 [-0.02, +0.08]
#3	8573	$1.1509 * 10^{-11}$	lg(k_1)= 5.304 [-0.002, +0.002] lg(k_2)= 6.302 [-0.001, +0.002] lg(k_3)= 5.3 [-1.6, +2.7] lg(k_{-3})= 4.3 [-1.6, +2.7] lg(K)=lg(k_3/k_{-3})= 0.98 [-0.01, +0.01]
#4	10514	$1.2144 * 10^{-11}$	lg(k_1)= 5.297 [-0.003, +0.002] lg(k_2)= 6.302 [-0.002, +0.004] lg(k_3)= 4.7 [-1.5, +3.3] lg(k_{-3})= 4.7 [-1.5, +3.3] lg(K)=lg(k_3/k_{-3})=-0.003 [-0.003, +0.003]
#5	8576	$1.1818 * 10^{-11}$	lg(k_1)= 5.297 [-0.003, +0.001] lg(k_2)= 6.301 [-0.002, +0.004] lg(k_3)= 5.3 [-2.0, +2.7] lg(k_{-3})= 4.3 [-2.0, +2.7] lg(K)=lg(k_3/k_{-3})= 1.011 [-0.005,+ 0.011]
#6	765	$1.1997 * 10^{-11}$	lg(k_1)= 5.000 [-0.001, +0.001] lg(k_2)= 8.000 [0, 0] lg(k_3)= 5.5 [-1.1, +2.5] lg(k_{-3})= 5.5 [-1.1, +2.5] lg(K)=lg(k_3/k_{-3})= 0.006 [-0.006, +0.012]

1.2 B. Examples of kinetics, thermodynamics and electrochemistry

Rate constant of diffusion controlled reaction

Rate constant of diffusion controlled reaction is defined as Smoluchowski limit(Smoluchowski, 1917):

$$k_{diff} = \alpha 4\pi(R_s + R_e)(D_s + D_e)N_A \tag{1.38}$$

Where dimension of k_{diff} is $\mathrm{M^{-1}s^{-1}}$, R_s and R_e are radiuses of substrate and enzyme (in spherical approximation), respectively,D_s and D_e are diffusion coefficients of substrate and enzyme, respectively; N_A - Avogadro number and α – ratio of active and total enzyme surface. Diffusion coefficients can be calculated from Stokes-Einstein equation(Einstein, 1905):

$$D = \frac{k_B T}{6\pi R \mu(T)} \tag{1.39}$$

Where $\mu(T)$ is a function which describes viscosity dependence on temperature. Here $\mu(T) = 2.414 \times 10^{-5} \times 10^{\frac{247.8}{T-140}}$ $(\mathrm{kg\,m^{-1}s^{-1}})$(Al-Shemmeri, 2012) describes viscosity of water at different temperatures. By assuming radius of enzyme $\backsim 30$ Å (from pdb:1h3j structure), radius of substrate (from molecular structures) $\backsim 5$ Å and $\alpha = 0.01 \div 0.1$, rate constants values $\backsim 10^8 \div 10^9\ \mathrm{M^{-1}s^{-1}}$ are calculated. The free energy of activation is such cases is $4.6\ \mathrm{kcal/mol}$.

The apparent bimolecular rate constants (k_{cat}/K_M) span range from $\sim 2 \times 10^6$ to $\sim 5 \times 10^8$. The oxidation of reduced forms of HEPX, DCPIP, PPSA, MB and TH are fast processes and relatively close to diffusion limited reactions. Estimated rate constants of diffusion controlled reaction are around $10^8 \div 10^9\ \mathrm{M^{-1}s^{-1}}$ and free energy of activation is $4.6\ \mathrm{kcal/mol}$ (from Smoluchowski limit (Smoluchowski, 1917), Einsten-Stokes equation (Einstein, 1905) and viscosity of water (Al-Shemmeri, 2012)). Therefore it is relatively safe to assume that these reactions are not diffusion-limited.

Activation energy of Compound I formation

The following scheme is postulated for CpdI formation from reduced CiP form:

$$E_{red} + H_2O_2 \overset{k_{H_2O_2}}{\rightarrow} Cpd\ I \tag{1.40}$$

Measurements was carried out at $\lambda = 405$ nm and experiments were repeated for at least 10 times. Mean absorbance change time course was fitted directly into reaction scheme 1.40, using extinction coefficients $109\ \mathrm{mM^{-1}cm^{-1}}$, $109\ \mathrm{mM^{-1}cm^{-1}}$ and $66\ \mathrm{mM^{-1}cm^{-1}}$ for reduced and oxidized enzyme forms, respectively. Initial concentrations of enzyme were calculated from first curve point (~0.850 μM), hydrogen peroxide concentration was 4.09 μM .

Table 1.6: Rate constants of CiP CpdI formation at various temperatures

Temperature (Celsius)	Apparent bimolecular rate constant
15	$7.12 \pm 0.09 \times 10^6\ \mathrm{M^{-1}s^{-1}}$
17.5	$7.32 \pm 0.06 \times 10^6\ \mathrm{M^{-1}s^{-1}}$
20	$7.9 \pm 0.2 \times 10^6\ \mathrm{M^{-1}s^{-1}}$
22.5	$8.05 \pm 0.07 \times 10^6\ \mathrm{M^{-1}s^{-1}}$
25	$8.8 \pm 0.1 \times 10^6\ \mathrm{M^{-1}s^{-1}}$
27.5	$9.3 \pm 0.2 \times 10^6\ \mathrm{M^{-1}s^{-1}}$

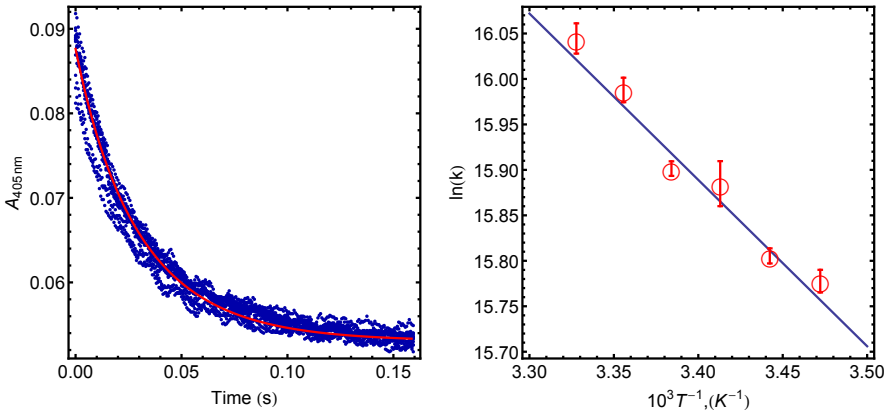

Figure 1.17: CiP CpdI formation kinetics at $T = 25°\mathrm{C}$ and dependence of apparent rate constant on temperature.

Estimated free activation energy is 3.6 ± 1.0 kcal/mol, calculated pre-

exponential factor is $4 \pm 18 \times 10^9$ $\mathrm{M^{-1}s^{-1}}$.

For further calculations, apparent CpdI formation rate constant will be estimated from:

$$k_{H_2O_2} = e^{22.1087 - \frac{1829.34}{T}} \tag{1.41}$$

HEPX oxidation activation energy and standard redox potential

HEPX oxidation scheme was postulated as:

$$\begin{gathered} E_{red} + H_2O_2 \overset{k_{H_2O_2}}{\rightarrow} CompI \\ CompI + S \underset{k_{-1}}{\overset{k_1}{\rightleftharpoons}} CompI \bullet S \\ CompI \bullet S \overset{k_{cat,1}}{\rightarrow} CompII + S^{\bullet +} \\ CompII + S \underset{k_{-2}}{\overset{k_2}{\rightleftharpoons}} CompII \bullet S \\ CompII \bullet S \overset{k_{cat,2}}{\rightarrow} E_{red} + S^{\bullet +} \end{gathered} \tag{1.42}$$

where $k_{H_2O_2}$ during fitting process was fixed to apparent CpdI formation rate constant at relevant temperature. Limiting apparent bimolecular rate constant calculated from:

$$k_{lim} = \frac{k_{cat}}{K_M},\ where\, k_{cat} = \frac{k_{cat,1}k_{cat,2}}{k_{cat,1} + k_{cat,2}} and\, K_M = \frac{k_{cat,1}K_{M,2} + K_{M,1}k_{cat,2}}{k_{cat,1} + k_{cat,2}} \tag{1.43}$$

$$K_{M,n} \rightarrow \frac{k_{cat,n} + k_{-n}}{k_n}.$$

where k_{lim} was calculated from fitted k_{cat} and K_M (). The initial concentrations of HEPX were varied from 6.3 μM to 48 μM. Initial concentration of CiP was 4.84 nM.

Estimated free activation energy is 6.2 ± 1.2 kcal/mol, calculated pre-exponential factor is $6 \pm 42 \times 10^{12}$ $\mathrm{M^{-1}s^{-1}}$.

Due to limited HEPX solubility in water, 10 μL 6.38 mM solution in acetonitrile was mixed with 10 μL deionized water and evaporated on clean glassy carbon electrode. Measurements were was performed in pH 7, 50 mM phosphate buffer solution. Estimated standard reduction potential was 0.453 ± 0.003 V vs Ag/AgCl (3M), difference between oxidation and reduction peaks is 78 ± 8 mV

Table 1.7: HEPX apparent bimolecular oxidation rate constants at various temperatures

Temperature (Celsius)	Apparent bimolecular rate constant
11	$9.3 \pm 0.2 \times 10^7$ $M^{-1}s^{-1}$
15	$9.9 \pm 0.6 \times 10^7$ $M^{-1}s^{-1}$
20	$1.24 \pm 0.01 \times 10^8$ $M^{-1}s^{-1}$
25	$1.56 \pm 0.01 \times 10^8$ $M^{-1}s^{-1}$
30	$1.82 \pm 0.02 \times 10^8$ $M^{-1}s^{-1}$

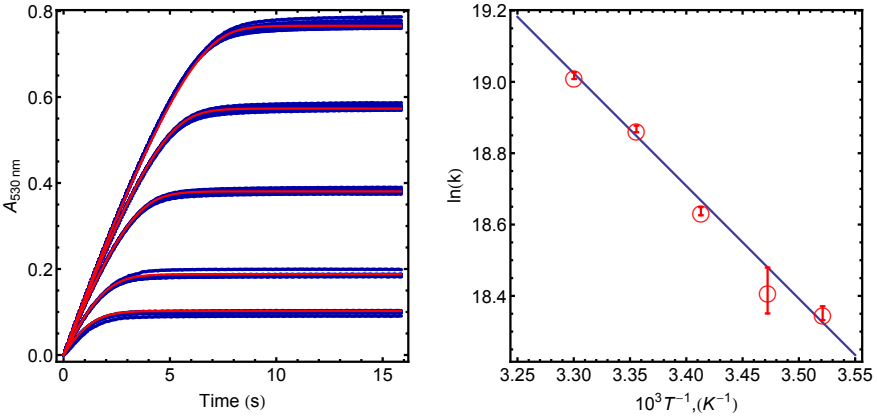

Figure 1.18: HEPX kinetics in pH 7.00, 50 mM phosphate buffer solution at $T = 25°C$ and apparent rate constant dependence on temperature.

PZ oxidation activation energy and standard redox potential

PZ oxidation scheme was postulated as:

$$
\begin{aligned}
E_{red} + H_2O_2 &\overset{k_p}{\rightarrow} CompI \\
CompI + S &\underset{k_{-1}}{\overset{k_1}{\rightleftharpoons}} CompI \bullet S \\
CompI \bullet S &\overset{k^1_{cat}}{\rightarrow} CompII + S^{\bullet +} \\
CompII + S &\underset{k_{-2}}{\overset{k_2}{\rightleftharpoons}} CompII \bullet S \\
CompII \bullet S &\overset{k^2_{cat}}{\rightarrow} E_{red} + S^{\bullet +} \\
S^{\bullet +} + S^{\bullet +} &\overset{k_3}{\rightarrow} S + S_{ox} \\
S_{ox} &\overset{k_4}{\rightarrow} S_{hydrolized}
\end{aligned}
\tag{1.44}
$$

The rate constants were calculated as in case of HEPX. The initial concentrations of PZ were varied from 2.52 μM to 23 μM. Initial concen-

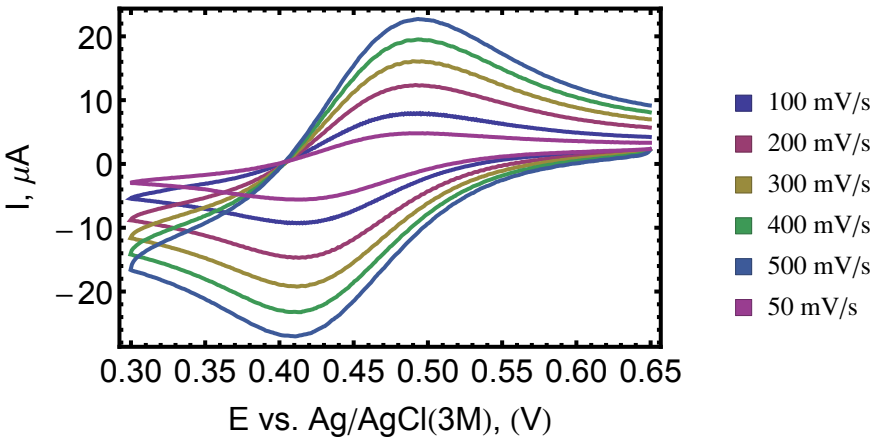

Figure 1.19: Cyclic voltammetry of HEPX adsorbed on glassy carbon electrode measured in 50 mM phosphate buffer solution at pH 7.00, $T = 25°\mathrm{C}$, and apparent rate constant dependence on temperature.

tration of CiP was $25\ \mathrm{nM}$.

Estimated free activation energy is $2.2 \pm 0.8\ \mathrm{kcal/mol}$, calculated pre-exponential factor is $1.3 \pm 4.7 \times 10^8\ \mathrm{M^{-1}s^{-1}}$.

Table 1.8: Apparent PZ bimolecular oxidation rate constants at various temperatures.

Temperature (Celsius)	Apparent bimolecular rate constant
10	$2.75 \pm 0.03 \times 10^6\ \mathrm{M^{-1}s^{-1}}$
15	$3.07 \pm 0.07 \times 10^6\ \mathrm{M^{-1}s^{-1}}$
20	$3.12 \pm 0.06 \times 10^6\ \mathrm{M^{-1}s^{-1}}$
25	$3.40 \pm 0.05 \times 10^6\ \mathrm{M^{-1}s^{-1}}$
30	$3.5 \pm 0.1 \times 10^6\ \mathrm{M^{-1}s^{-1}}$

PZ ($1\ \mathrm{mM}$) cyclic voltammetry experiments were carried out on clean glassy carbon electrode, in 50 mM phosphate buffer solution, pH 7.00. Estimated first electron standard reduction potential was $0.557 \pm 0.006\ \mathrm{V}$ vs $\mathrm{Ag/AgCl\ (3M)}$, difference between oxidation and reduction peaks is $73 \pm 7\ \mathrm{mV}$

DCPIP oxidation kinetics

DCPIP oxidation scheme was postulated as:

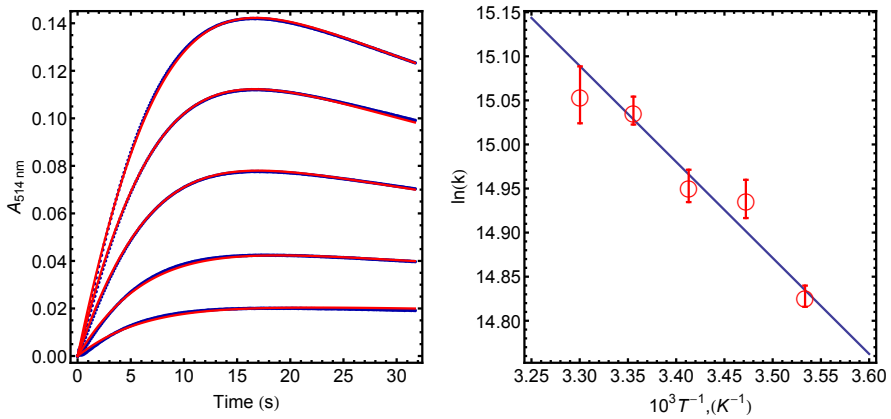

Figure 1.20: PZ kinetics in 50 mM phosphate buffer solution at pH 7.00, $T = 25°\mathrm{C}$, and apparent rate constant dependence on temperature.

$$
\begin{aligned}
E_{red} + H_2O_2 &\overset{k_{H_2O_2}}{\rightarrow} CompI \\
CompI + S &\overset{k_1}{\rightarrow} CompII + S^{\bullet+} \\
CompII + S &\overset{k_2}{\rightarrow} E_{red} + S^{\bullet+} \\
S^{\bullet+} + S^{\bullet+} &\overset{k_{dis}}{\rightarrow} S_{ox} + S \\
CompI + S_{ox} &\overset{k_3}{\rightarrow} CompII + S_{ox}^{\bullet+} \\
CompII + S_{ox} &\overset{k_4}{\rightarrow} E_{red} + S_{ox}^{\bullet+}
\end{aligned}
\tag{1.45}
$$

The limiting rate constants were calculated as $k_{lim,1} = \frac{k_1 k_2}{k_1 + k_2}$ and $k_{lim,2} = \frac{k_3 k_4}{k_3 + k_4}$. The initial concentrations of DCPIP were varied from 0.037 μM to 3 μM. Initial concentration of CiP was 29 nM.

Estimated free activation energy is 7.4 ± 1.2 kcal/mol, calculated pre-exponential factor is $7 \pm 53 \times 10^{13}$ $\mathrm{M^{-1}s^{-1}}$.

Estimated free activation energy is 3.3 ± 0.3 kcal/mol, calculated pre-exponential factor is $3 \pm 6 \times 10^{9}$ $\mathrm{M^{-1}s^{-1}}$.

DCPIP (1 mM) cyclic voltammetry experiments carried out on clean glassy carbon electrode in 50 mM phosphate buffer solution at pH 7.00. Estimated first electron standard reduction potential was 0.021 ± 0.003 V vs Ag/AgCl (3M), difference between oxidation and reduction peaks is 60 ± 7 mV.

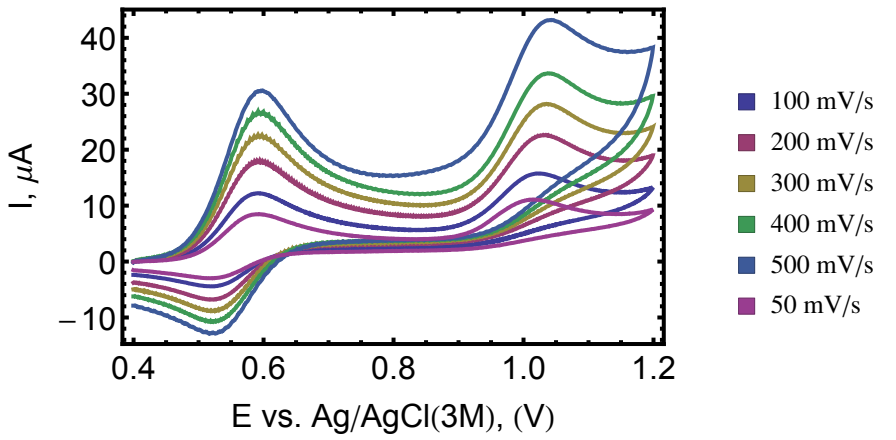

Figure 1.21: Cyclic voltammetry of PZ (1 mM) measured on glassy carbon electrode in 50 mM phosphate buffer solution at pH 7.00, $T = 25°C$.

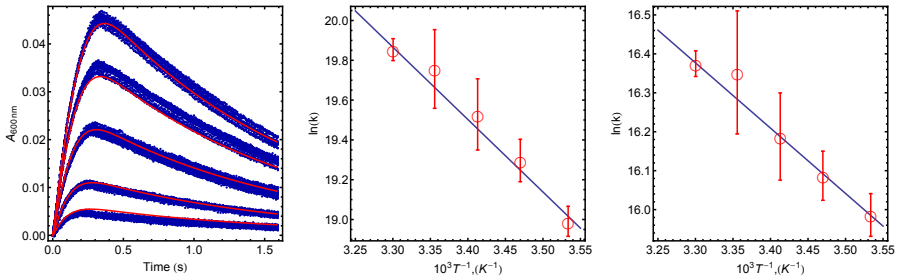

Figure 1.22: DCPIP kinetics in 50 mM phosphate buffer solution at pH 7.00, $T = 25°C$, and apparent rate constant dependence on temperature.

1.3 C. Examples of Quantum computations

HEPX

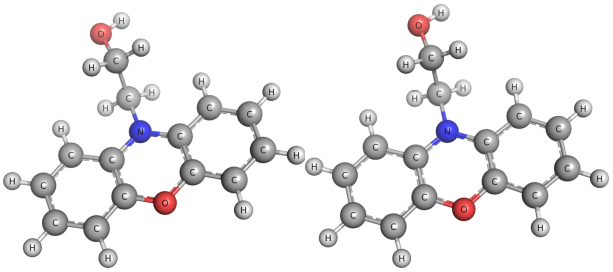

Figure 1.24: Structures of HEPX and HEPX radical cation.

Table 1.9: Apparent DCPIP bimolecular oxidation rate constants at various temperatures.

Temperature (Celsius)	k_1	k_2
10	$1.7 \pm 0.1 \times 10^8$ $M^{-1}s^{-1}$	$8.8 \pm 0.5 \times 10^6$ $M^{-1}s^{-1}$
15.2	$2.4 \pm 0.3 \times 10^8$ $M^{-1}s^{-1}$	$9.7 \pm 0.6 \times 10^6$ $M^{-1}s^{-1}$
20	$3.0 \pm 0.6 \times 10^8$ $M^{-1}s^{-1}$	$1.1 \pm 0.1 \times 10^7$ $M^{-1}s^{-1}$
25	$3.8 \pm 0.8 \times 10^7$ $M^{-1}s^{-1}$	$1.3 \pm 0.2 \times 10^7$ $M^{-1}s^{-1}$
30	$4.2 \pm 0.2 \times 10^7$ $M^{-1}s^{-1}$	$1.30 \pm 0.04 \times 10^7$ $M^{-1}s^{-1}$

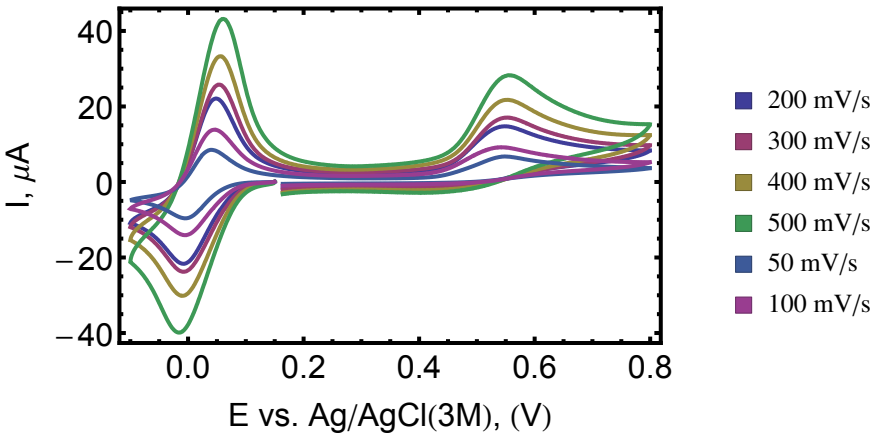

Figure 1.23: Cyclic voltammetry of DCPIP (1 mM) on glassy carbon electrode in 50 mM phosphate buffer solution at pH 7.00, $T = 25°C$.

Table 1.10: Energies of HEPX and HEPX radical cation (DFT/B3LYP/6-31+G(d,p)) in Ha and zero point energies (HF/6-31+G(d,p)) in kcal/mol.

$HEPX$	$HEPX^{\bullet+}$
Energy: -746.1122451 Ha	Energy: -745.9379546 Ha
Zero point energy: 163.440989 kcal/mol	Zero point energy: 164.585432 kcal/mol

Configuration	E(Ha)	λ	
$E(A\ at\ A^+\ geometry)$	-746.1080792847	0.113 eV	3.104 kcal/mol
$E(A\ at\ A\ geometry)$	-746.1122450819		
$E(A^+\ at\ A\ geometry)$	-745.9322279615	0.156 eV	
$E(A^+\ at\ A^+\ geometry)$	-745.9379546038		

Table 1.11: DFT/B3LYP/6-31+G(d,p) optimized coordinates of HEPX reduced and oxidised forms in angstroms (XYZ format).

Reduced				**Oxidised**			
N	-0.02001	0.45745	-0.31922	N	-0.01283	0.45222	-0.27309
C	-1.23966	-0.21103	-0.10033	C	-1.23014	-0.20542	-0.11784
C	-2.47390	0.44431	0.03460	C	-2.47783	0.45769	-0.12716
C	-3.65919	-0.28247	0.21447	C	-3.65192	-0.26568	0.00477
C	-3.63325	-1.67440	0.28888	C	-3.62692	-1.66782	0.14682
C	-2.40737	-2.34348	0.17021	C	-2.41520	-2.34210	0.17410
C	-1.24136	-1.61852	-0.03005	C	-1.23267	-1.61314	0.05333
O	-0.06645	-2.34358	-0.21641	O	-0.06617	-2.31468	0.11657
C	1.13529	-1.65838	-0.04621	C	1.12503	-1.65321	0.07915
C	2.27941	-2.42156	0.13712	C	2.27708	-2.42516	0.22366
C	3.52701	-1.79296	0.25236	C	3.51515	-1.80120	0.17847
C	3.59586	-0.40199	0.19121	C	3.59712	-0.40789	-0.01413
C	2.43357	0.36232	0.02031	C	2.45321	0.35965	-0.16500
C	1.17856	-0.25186	-0.11169	C	1.17954	-0.25010	-0.12395
C	-0.00113	1.88455	-0.62964	C	0.00721	1.89484	-0.58439
C	0.02861	2.81368	0.59708	C	0.03124	2.78562	0.67709
O	-0.09977	4.18802	0.20081	O	-0.13071	4.15323	0.30783
H	-2.52567	1.52607	-0.00688	H	-2.52650	1.53354	-0.22311
H	-4.59885	0.25506	0.30515	H	-4.60092	0.26072	0.00105
H	-4.54835	-2.24049	0.43516	H	-4.55472	-2.22254	0.24376
H	-2.34563	-3.42688	0.21369	H	-2.35561	-3.41839	0.29203
H	2.18641	-3.50307	0.17396	H	2.17621	-3.49535	0.36975
H	4.42360	-2.39060	0.38711	H	4.41774	-2.39211	0.29560
H	4.55196	0.10574	0.28142	H	4.56796	0.07645	-0.03840
H	2.51977	1.44217	-0.00854	H	2.55497	1.42856	-0.29688
H	0.86432	2.08289	-1.27186	H	0.87035	2.09431	-1.22112
H	-0.88297	2.11597	-1.23426	H	-0.86996	2.12305	-1.18886
H	-0.82151	2.61143	1.25467	H	-0.80996	2.53687	1.33005
H	0.94081	2.66816	1.18776	H	0.95299	2.63555	1.25007
H	0.72501	4.48931	-0.21174	H	0.71411	4.52851	0.01424

1.4 D. Docking studies and calculations of solvent accessible surface areas

Best docked structures of substrates in CiP.

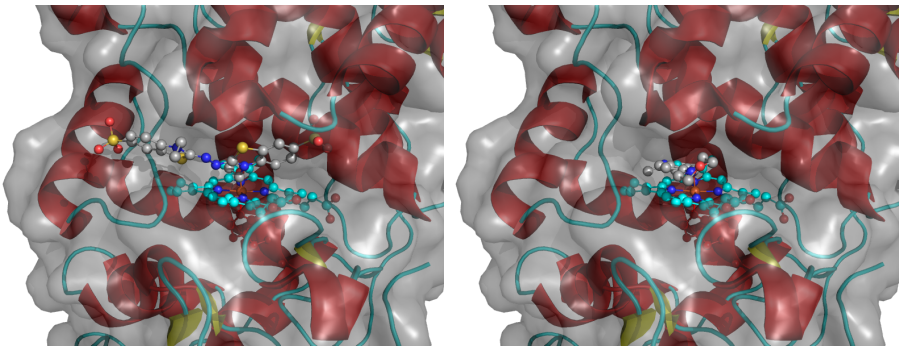

Figure 1.25: Best structures of ABTS and AMB docked in CiP.

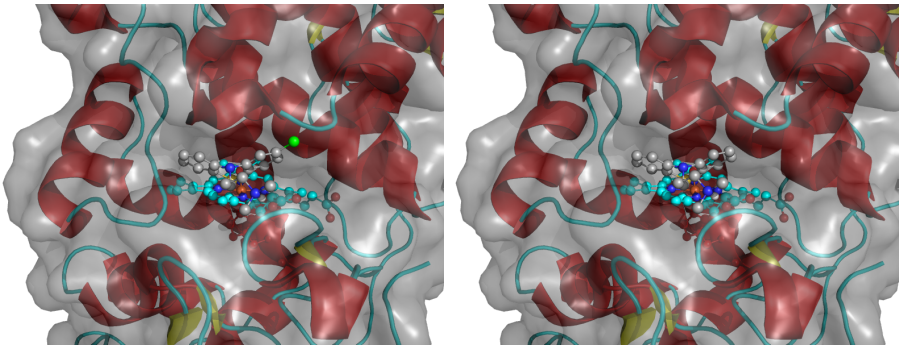

Figure 1.26: Best structures of CPZ and PZ docked in CiP.

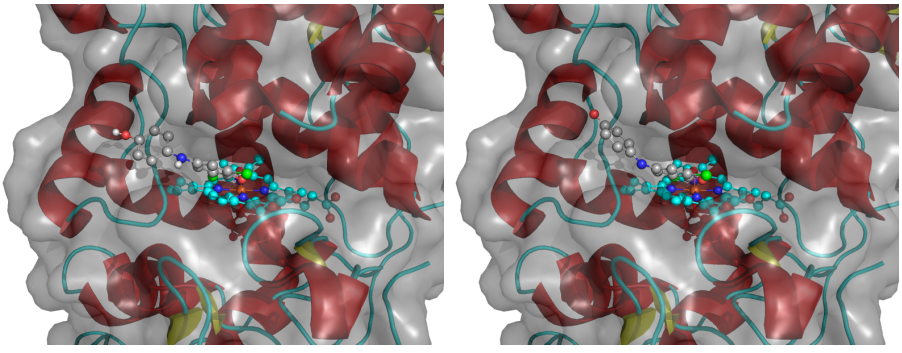

Figure 1.27: Best structures of reduced DCPIP and oxidized DCPIP docked in CiP.

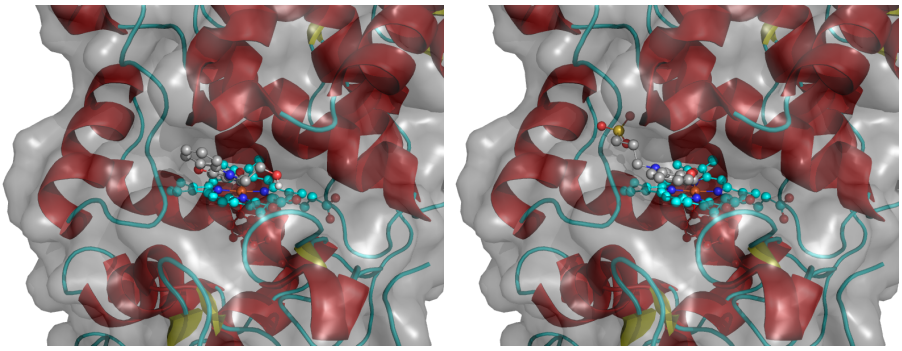

Figure 1.28: Best structures of HEPX and PPSA docked in CiP.

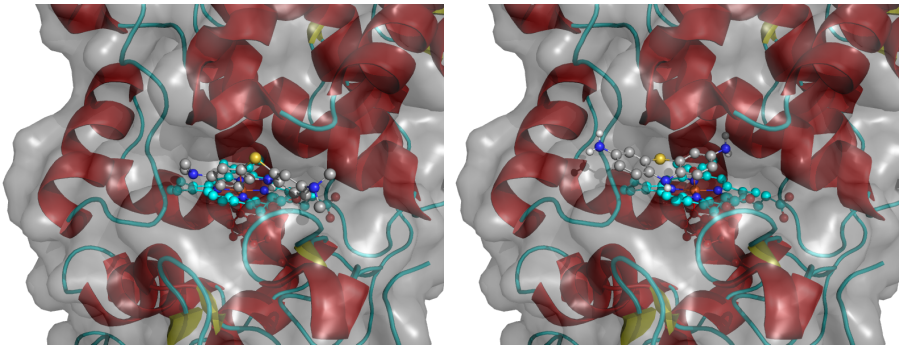

Figure 1.29: Best structures of reduced MB and reduced TH docked in CiP.

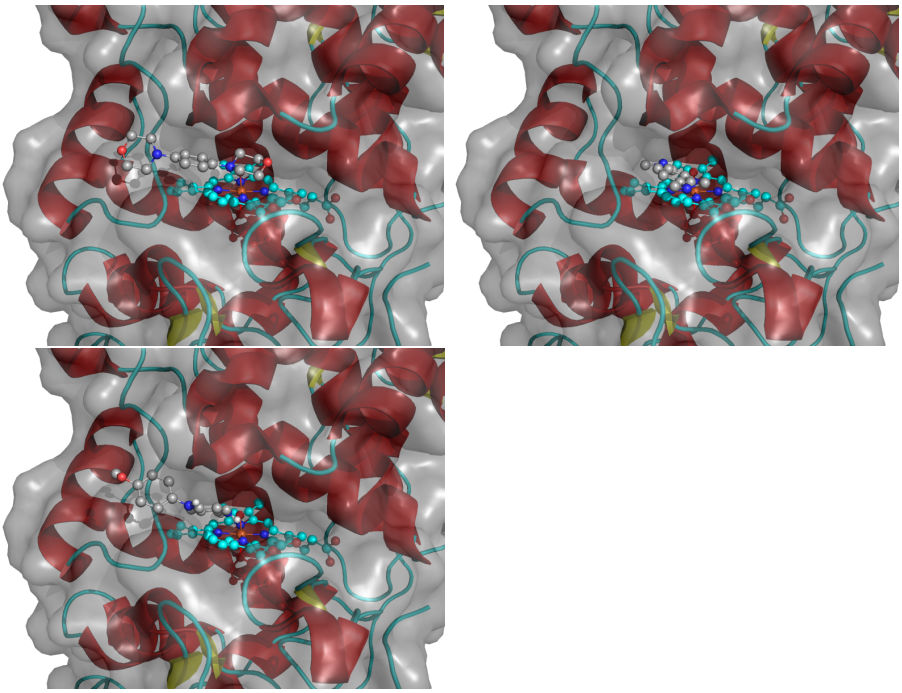

Figure 1.30: Best structures of DMB, TMPD and VB docked in CiP.

Docking scores and solvent-accessible surface areas.

Table 1.12: Docking scores of best structures of docked structures and part of solvent-accessible surface area (θ) of substrate bound to CiP.

Substrate	Docking score/affinity (kcal/mol)	θ
ABTS	-7.6	0.43
AMB	-5.2	0.36
CPZ	-5.8	0.41
DCPIP(I)	-6.2	0.36
DCPIP(II)	-6.7	0.39
DMB	-5.6	0.37
HEPX	-6.6	0.35
MB	-6.4	0.41
PPSA	-6.9	0.37
PZ	-5.8	0.39
TH	-6.1	0.36
TMPD	-4.8	0.36
VB	-5.6	0.38

Sudėtingų biokatalizinių bei bioelektrokatalizinių procesų tyrimas ir modeliavimas

SANTRAUKA

1.1 Įvadas

Dauguma cheminių reakcijų gyvojoje gamtoje yra oksidacijos-redukcijos procesai. Šios reakcijos yra katalizuojamos fermentų, kurie yra vadinami oksidoreduktazėmis. Jų esminė funkcija yra pagreitinti elektronų pernašą nuo vienų molekulių kitoms. Dažniausiai, oksidoreduktazės turi pagalbinių molekulių – kofaktorių (pvz., NAD, FAD, PQQ, hemas, geležies-sieros klasteriai, vario jonai). Išvardinti kofaktoriai yra būtina fermentų aktyvių centrų sudėtinė dalis. Pavyzdžiui, nitrogenazės katalizuoja azoto redukciją iki amoniako, kaip elektronų šaltinį naudodamos redukuotą feredoksiną. Nitrogenazės kofaktorius yra geležies, molibdeno ir sieros klasteris. Gliukozės oksidazė yra pavyzdys fermento, kurio aktyviajame centre yra FAD. Šis fermentas yra gaminamas įvairių grybų ir jo funkcija yra oksiduoti gliukozę iki gliukonolaktono ir redukuoti deguonį iki vandenilio peroksido, kuris toliau kaip antimikrobinė medžiaga žudo bakterijas ar stabdo jų dauginimąsį. Dar kitoks fermentas yra lakazė, kuris turi keturis vario jonus ir to užtenka katalizuoti įvairias oksidacijos reakcijas kaip elektronų akceptorių naudojant deguonį. Šis fermentas yra aptinkamas augaluose, kur jo funkcija yra padėti polimerizuoti monolignolius, ir grybuose, kur jo funkcija yra atvirkščia – padėti skaidyti lingniną į paprastesnes molekules.

Oksidoreduktazių katalizinių mechanizmų įvairovė skatina jų teorinius ir praktinius tyrimus. Žinomos oksidoreduktazių struktūros atskleidžia, kaip yra vienoks ar kitoks katalizės mechanizmas įgyvendinamas gamtoje, kaip fermentus būtų galima racionaliai keisti, gauti kitokius savo savybėmis katalizatorius. Oksidoreduktazės yra plačiai naudojamos organinių ir neorganinių medžiagų transformacijai, įvairiuose biojutikliuose, biocheminės diagnostikos sistemose, yra biokuro elementų

pavyzdžių ar galimybių pritaikyti šiuos fermentus teršalų ir atliekų biodegradacijoje.

Bio(elektro)kataliziniai procesai dažnai būna sudėtingi ir gali būti sumodeliuoti tik ypač sudėtingais modeliais. Todėl dažnai tyrinėjami bio(elektro)kataliziniai procesai yra analizuojami kokybiniais, o ne kiekybiniais modeliais. Išvados daromos apibendrinant labai paprastus atvejus, kurie turi mažai bendra su tyrinėjama sistema. Remiantis kokybiniais modeliais yra prarandamas tyrinėjamo proceso kiekybinis tikslumas ir galimybė kiekybiškai patikrinti iškeltas hipotezes.

Sudėtingi modeliai dažnai yra sunkiai pritaikomi aprašant stebimus procesus. Pavyzdžiui, bio(elektro)kataliziniai modeliai dažnai yra daugiaparametriniai. Todėl sudėtinga iš anksto numatyti, kokie yra reikalingi eksperimentai norint juos charakterizuoti. Naudojami matematiniai algoritmai modeliams simuliuoti ar optimizuoti dažnai remiasi prielaidomis, kurios ne visada yra teisingos nagrinėjamam fiziniam procesui. Dažnai tenka žinomus konkrečių problemų sprendimo būdus pritaikyti naujoms problemos spręsti. Vien optimizacijos ir integravimo algoritmų įvairovė, matyt, gerai iliustruoja pačių jais sprendžiamų problemų įvairovę.

Biochemikams aktualios tyrimų sritys, kuriose, norint interpretuoti ir suprasti eksperimentinius rezultatus, yra būtinas kiekybinis modelis yra labai įvairios –pradedant homogenine ir heterogenine katalize, baigiant elektronų ir protonų pernaša biomolekulėse. Bendras homogeninės kinetikos modeliavimo ir analizės algoritmas leistų greitai ir efektyviai atskirti skirtingas katalizės mechanizmų hipotezes ir apskaičiuoti greičio parametrus remiantis eksperimentiniais duomenimis. Pastarieji yra būtini bet kokiame kontekste susijusiame su katalizės efektyvumu ir mechanizmo supratimu.

Pirmoji disertacijos dalis yra skirta sudėtingų biokatalizinių reakcijų greičio parametrų skaičiavimo algoritmo sukūrimui. Antrojoje disertacijos dalyje šis algoritmas yra naudojamas tirti lakazės katalizuojamų reakcijų kinetiką homogeninėje terpėje ir susieti jos greičio parametrus su gautaisiais imobilizavus lakazę ant elektrodo paviršiaus. Trečiojoje disertacijos dalyje algoritmas yra naudojamas analizuojant peroksidazės katalizuojamų reakcijų kinetiką ir nustatant peroksidazės formos II (ang. „compound II“) elektronų ir protonų pernašos ypatumus ir susiejant juos su kvantinės chemijos ir molekulinės mechanikos metodais apskaičiuo-

tomis substratų savybėmis.

1.1.1 Disertacijos tikslai ir keliami uždaviniai

Šio darbo tikslas yra sudėtingų daugiastadijinių biokatalizinių reakcijų kinetinių parametrų apskaičiavimo metodo sukūrimas bei jo pritaikymas tiriant fermentų katalizuojamas oksidacijos/redukcijos reakcijas homogeninėje terpėje bei fazių riboje.

Šiam tikslui pasiekti buvo suformuluoti šie uždaviniai:

1. Sukurti efektyvius biocheminės kinetikos modeliavimo ir eksperimentinių duomenų analizės metodus tinkančius tirti įvairius sudėtingus homogeninės kinetikos procesus.

2. Pritaikyti sukurtus metodus tiriant sudėtingas daugiastadijines biokatalizines reakcijas homogeninėje terpėje ir fazių riboje vykstančius, oksidoreduktazių katalizuojamus, procesus.

3. Pritaikyti sukurtus metodus tiriant elektrono ir protono pernašą oksidoreduktazių katalizuojamuose procesuose.

1.1.2 Ginamieji teiginiai

1. Daugybinių lokaliųjų greičio parametrų minimumų paieškos ir statistinės analizės metodas yra pritaikomas cheminės ir biocheminės kinetikos uždavinių sprendimui.

2. Sukurtas kinetinių parametrų paieškos metodas leidžia apskaičiuoti iš eksperimentinių duomenų biokatalizines konstantas su didesniu tikslumu ir modeliuoti sudėtingus homogeninius ir heterogeninius biokatalizinius procesus.

3. Eletronų pernaša ant elektrodo imobilizuotai lakazei iš *Didymocrea* sp. J6 vyksta tiesiogiai iš elektrodo į lakazės T2/T3 aktyvųjį centrą.

4. *Coprinus cinereus* peroksidazės II formos redukcijos greitį lemia elektrono ir protono pernašų greičiai.

5. Elektrono ir protono pernašos procesai peroksidazinėse reakcijose yra aprašomi Marcus elektrono pernašos bei neadiabatine vidumolekuline protonų pernašos teorijomis.

1.1.3 Mokslinis naujumas

1. Sukurtas algoritmas ir programinė įranga skirta modeliuoti bendriems homogeninės biocheminės ir cheminės kinetikos uždaviniams bei analizuoti eksperimentinius duomenis su didesniu tikslumu.

2. Nustatytas neįprastas imobilizuotos ant elektrodo lakazės iš *Didymocrea* sp. J6 tiesioginės elektronų pernašos kelias į T2/T3 aktyvųjį centrą aplenkiant T1 centrą. Šis kelias yra silpnai inhibuojamas fluorido jonais ir leidžia pasiekti aukštesnį lakazinio elektrodo veikimo potencialą.

3. Nustatyta, kad *Coprinus cinereus* peroksidazės II formos redukcija yra sudaryta iš atskirų ir eksperimentiškai stebimų elementarių žingsnių, kurių pirmas yra elektrono pernaša, o antras – vidumolekulinė protono pernaša.

4. Parodyta, kad *Coprinus cinereus* peroksidazės II formos redukcijos greitį gali riboti tiek elektrono, tiek protono pernaša. Šių procesų greičiai yra aprašomi Marcus ir vidumolekulinės protono pernašos teorijomis.

1.1.4 Autoriaus indėlis

Visi homogeninės kinetikos, klampos ir elektrocheminiai substratų redukcijos potencialų matavimai buvo atlikti autoriaus. Lakazės biokatodas buvo pagamintas ir matavimai buvo atlikti dr. Daliaus Ratauto. Spektroelektrocheminiai lakazės matavimai buvo atlikti dr. Mariaus Dagio ir prof. Sergey Shleev. Sistemų modeliavimai, duomenų analizė, kvantinės chemijos skaičiavimai, lygčių išvedimai, reakcijų greičio parametrų apskaičiavimo metodo sukūrimas buvo atlikti autoriaus su disertacijos vadovo prof. Juozo Kulio pagalba ir patarimais. Greičio parametrų skaičiavimo metodas buvo implementuotas į "rModeler" programinę įrangą bendru autoriaus ir Justino V. Daugmaudžio darbu. Visos publikacijos paruoštos bendru visų autorių darbu.

1.2 Disertacijos rezultatai

1.2.1 Homogeninės kinetikos modeliavimas ir greičio parametrų skaičiavimas iš eksperimentinių duomenų

Kiekybiniai modeliai yra būtini norint prognozuoti procesus ar apskaičiuoti jiems būdingus greičio parametrus. Jau 1913 metais Leonor Michaelis ir Maud Menten publikavo pirmąjį kiekybinį fermentinės kinetikos modelį(Menten and Michaelis, 1913) žinomą Michaelis-Menten lygties vardu:

$$\frac{d[S]}{dt} = -\frac{v_{max}[S]}{K_M + [S]} \tag{1.46}$$

kur substrato $[S]$ suvartojimo greitis aprašomas su dviem konkrečiam fermentui būdingais greičio parametrais v_{max} ir K_M. Ši lygtis yra išvedama darant prielaidą, kad fermentinė katalizė yra aprašoma tokia reakcijos schema:

$$S + E \underset{k_{-1}}{\overset{k_1}{\rightleftharpoons}} ES \overset{k_2}{\rightarrow} E + P, \tag{1.47}$$

ir tariant, kad fermento formų E ir ES koncentracijos beveik nekinta laike (kvazistacionarumo prielaida fermento formoms,(Briggs and Haldane, 1925)).Remiantis kvazistacionarumo prielaida ir turint reakcijos schemą , galima išvesti praktiškai bet kokios reakcijos greičio lygtį. Sudėtingų schemų atvejų greičio lygties išvedimo procesą stipriai supaprastina King-Altman diagramų metodas(King and Altman, 1956).

Gautosios greičio lygtys toliau gali būti naudojamos iš eksperimentinių duomenų nustatant fermentų greičio parametrus. Dažnai praktikoje yra taikomas pradinio greičio metodas, kuris, išmatavus pradinį reakcijos greitį leidžia apskaičiuoti reakcijos greičio parametrus tiriamajai fermentinei reakcijai. Norint nustatyti fermentinės reakcijos greičio parametrus, reikia atlikti daug pradinio greičio matavimo eksperimentų, kurie kartais gali būti itin brangūs ar dėl fizikocheminių priežasčių neįmanomi. Antra, eksperimentas turi būti suplanuotas tokiu būdu, kad kvazistacionarumo prielaida būtų validi. Šie dalykai kartais yra neįmanomi. Pavyzdžiui, fermentas yra aktyvuojamas ar inaktyvuojamas reakcijos metu. Arba, įmanoma stebėti tik trumpai gyvuojantį reaktantą.

Šioms problemoms spręsti egzistuoja alternatyvūs metodai. Jų visų pagrindas yra greičio lygčių integravimas. Greičio lygtys yra diferencia-

linės lygtys, kurios gaunamos panaudojant reakcijos greičio apibrėžimą ir masių tvermės dėsnį. Kai kuriais atvejais diferencialines lygtis galima suintegruoti analitiškai ir gautą sprendinį panaudoti skaičiuojant greičio parametrus iš eksperimentų duomenų. Tokiu būdu gali būti panaudojama visa reakcijos kinetinė kreivė, o ne tik pradinės jos reikšmės, kaip kad pradinio greičio skaičiavime. Vienoje eksperimento kinetinėje kreivės dažnai egzistuoja informacija apie keletą greičio parametrų. Tad pilnų kinetinių kreivių analizė yra gerokai efektyvesnis duomenų analizės metodas. Deja, analitiniai sprendiniai retai egzistuoja sudėtingoms netiesinėms diferencialinėms lygtims.

Pirmoji programinė įranga, kuri naudojo homogeninių kinetinių procesų aprašymui diferencialinių lygčių skaitinį integravimą buvo KINSIM(Barshop et al., 1983). Ši programinė įranga tegalėjo su vartotojo parinktais greičio parametrais ir pradinėmis reagentų koncentracijomis pagal reakcijos schemą sugeneruoti diferencialines lygtis ir jas skaitiškai suintegruoti. Šio programos versija dar neleido iš kinetinių duomenų apskaičiuoti greičio parametrų ir vartotojas tegalėjo lyginti sumodeliuotas ir pamatuotas kreives ir pamėginti atspėti greičio parametrus, kurie duoda geriausią sutapimą. Vėliau buvo sukurti kiti programinės įrangos paketai, kaip FITSIM ir DYNAFIT (Svir et al., 2002; Kuzmič, 1996; Kuzmič, 2009), kurie jau turėjo optimizacijos algoritmus. Šie jau leido skaičiuoti greičio parametrus iš eksperimentinių duomenų. Šie greičio parametrų skaičiavimo algoritmai turi keletą ydų. Norit gauti prasmingus greičio parametrus, vartotojas turi atspėti (tikrąja ta žodžio prasme) tinkamą pradinių greičio parametrų rinkinį, nuo kurio optimizavimo algoritmas gali konverguoti į prasmingus greičio parametrus. Tai yra beveik neįmanoma sudėtingoms reakcijų schemoms. Antra, visi anksčiau paminėti metodai remiasi hipoteze, kad optimalūs greičio parametrai, kaip apibrėžti reakcijos schemoje, suformuoja unikalų ir globalų minimumą. Mūsų tyrimai parodė, kad taip nėra.

Pirmo laipsnio reakcijos greičio parametrų tikslo funkcijos analizė Pirmąją problemą – gero pradinio greičių parametrų rinkinio spėjimo uždavinį galime iliustruoti pirmojo laipsnio reakcija:

$$A \xrightarrow{k} B \tag{1.48}$$

Ši reakcija yra užrašoma šiomis diferencialinėmis lygtimis:

$$\frac{dA}{dt} = -kA, \;\; \frac{dB}{dt} = kB \tag{1.49}$$

Jas galima išspręsti analitiškai su, tarkime, pradinėmis sąlygomis $A(0) = A_0$ ir $B(0) = 0$. Sprendinys yra $A(t) = A_0 e^{-kt}$. Greičio parametras k iš eksperimentinių duomenų čia gali būti suskaičiuojamas įvairiai. Greičio parametro k radimo problema yra formuluojama kaip optimizacijos uždavinys mažiausių kvadratų metodu (MKM). Tarkime, kad k yra tikroji greičio konstanta, o r yra parametras, kuris turėtų būti optimizuotas iki k. Tuomet MKM remiantis, mūsų tikslo funkcija yra:

$$S(r) = \int_0^T (e^{-kt} - e^{-rt})^2 dt \tag{1.50}$$

Kurią suintegravus gaunama:

$$S(r) = \frac{1}{2}\left(\frac{4(e^{T(-k-r)} - 1)}{k+r} + \frac{1 - e^{-2kT}}{k} + \frac{1 - e^{-2rT}}{r}\right) \tag{1.51}$$

kur T yra matavimo trukmė. Funkcijos ir jos išvestinės elgesys priklausomai nuo optimizuojamo parametro r iliustruotas pav. 1.31. Iš paveikslo akivaizdu, kad kai eksperimento trukmė yra ribota, bet koks pradinio optimizuojamo greičio parametro spėjimas, kuris yra nutolęs nuo optimalios greičio parametro k reikšmės per daugiau nei dvi eiles, veikiausiai nekonverguos iki norimo sprendinio ir konstantos k surasti nepavyks.

Natūralu, kad ši problema ieškant iš eksperimentinių duomenų daugiau greičio parametrų sudėtingesnei reakcijos schemai dar labiau komplikuosis (augs eksponentiškai priklausomai nuo greičio parametrų skaičiaus). Taigi, tokiais atvejais būtų geriau:

- Perrinkti greičio parametrus tam tikru žingsniu (gerai žinomas globalios optimizacijos metodas).
- Pasirinkti aibę greičio parametrų rinkinių, kur tikslo funkcija yra mažiausia.
- Optimizuoti pasirinktos aibės parametrų rinkinius.
- Analizuoti gautus optimalius greičio parametrų rinkinius.

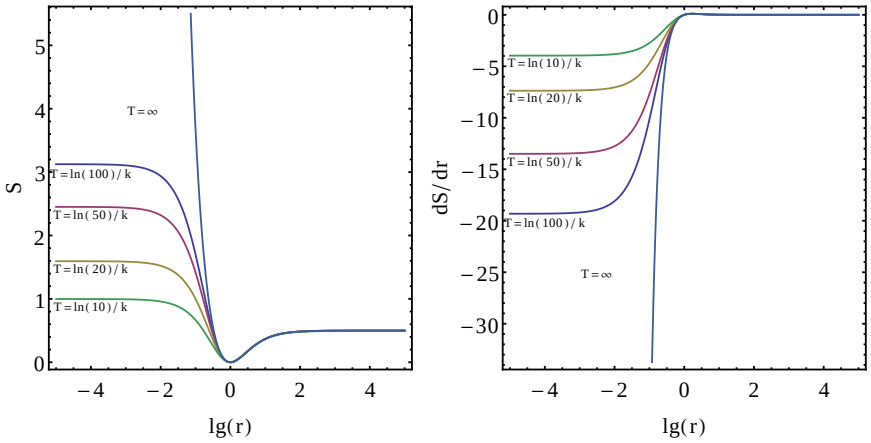

1.31 pav.: Kairėje – S (lygtis 1.51) priklausomybė nuo r; dešinėje – S išvestinės priklausomybė nuo r su $k = 1$.

Sudėtingos reakcijos greičio parametrų tikslo funkcijos analizė Aukščiau aprašytas algoritmas buvo išmėgintas su sudėtingesne reakcijos schema, kuri aprašoma keturiais greičio parametrais:

$$\begin{aligned} E_{ox} + S &\overset{k_1}{\rightarrow} E_{red} + P \\ E_{red} + M_{ox} &\overset{k_2}{\rightarrow} E_{ox} + M_{red} \\ F_{ox} + M_{red} &\underset{k_{-3}}{\overset{k_3}{\rightleftarrows}} F_{red} + M_{ox} \end{aligned} \tag{1.52}$$

Schemoje E_{ox}ir E_{red} yra oksiduota ir redukuota fermento formos, Substratas yra pažymėtas S, reakcijos mediatoriaus oksiduotos ir redukuotos formos kaip M,substratas mediatoriui regeneruoti kaip F(supaprastintas mechanizmas iš (Kulys et al., 2010)). Ši schema yra reprezentuojama diferencialinėmis lygtimis:

$$\begin{gathered}
\frac{d[E_{ox}]}{dt} = -k_1[E_{ox}][S] + k_2[E_{red}][M_{ox}] \\
\frac{d[E_{red}]}{dt} = k_1[E_{ox}][S] - k_2[E_{red}[M_{ox}] \\
\frac{d[F_{ox}]}{dt} = k_{-3}[F_{red}][M_{ox}] - k_3[F_{ox}][M_{red}] \\
\frac{d[F_{red}]}{dt} = -k_{-3}[F_{red}][M_{ox}] + k_3[F_{ox}][M_{red}] \\
\frac{d[M_{ox}]}{dt} = -k_2[E_{red}][M_{ox}] + k_3[F_{ox}][M_{red}] - k_{-3}[F_{red}][M_{ox}] \\
\frac{d[M_{red}]}{dt} = k_2[E_{red}][M_{ox}] - k_3[F_{ox}][M_{red}] + k_{-3}[F_{red}][M_{ox}] \\
\frac{d[P]}{dt} = k_1[E_{ox}][S] \\
\frac{d[S]}{dt} = -k_1[E_{ox}][S]
\end{gathered} \quad , \tag{1.53}$$

Su pradinėmis sąlygomis $S(0),\ P(0),\ E(0),\ E_{red}(0)\ ,F(0),\ F_{red}(0),$ $M_{ox}(0)$ ir $M_{red}(0)$. Kadangi lygtys yra netiesinės, analitinio sprendinio gauti neįmanoma ir jos yra integruojamos skaitiškai. Pasirinkus pradines koncentracijas $E_{ox} = 10^{-9}$ M, $M_{ox} = 10^{-6}$ M, $F_{ox} = 10^{-4}$ M, $S = 10^{-3}$ M, greičio konstantas $k_1 = 10^5$ $\mathrm{M^{-1}s^{-1}}$, $k_2 = 10^8$ $\mathrm{M^{-1}s^{-1}}$, $k_{-3} = 10^5$ $\mathrm{M^{-1}s^{-1}}$, $k_3 = 10^6$ $\mathrm{M^{-1}s^{-1}}$(pagal analogiją su (Kulys et al., 2010; Kulys and Dapkūnas, 2007)) ir tariant kad stebima F_{ox} koncentracijos kitimas laike, galima iliustruoti, kaip priklauso tikslo funkcija nuo visų keturių greičio konstantų (pav. 1.32).

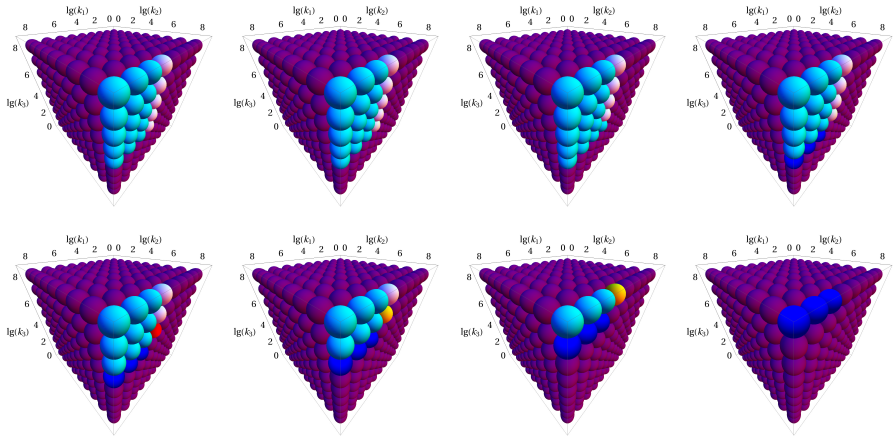

1.32 pav.: Tikslo funkcijos priklausomybė nuo greičio konstantų reikšmių, nuo kairės viršaus iki dešinės apačios $k_{-3} = \{10^0,\ 10^2,\ 10^3\ ,10^4,\ 10^5,\ 10^6,\ 10^7,\ 10^8\}$. Violetinė – labai blogas tikslo funkcijos įvertis, raudona – puikus tikslo funkcijos įvertis.

Pav. 1.32 yra iliustruotas tikslo funkcijos elgesys. Kaip matoma iš

iliustracijos, tikslo funkcija nutolus nuo tikrųjų greičio konstantų pasidaro plokščia ir todėl ne bet koks pradinių konstantų rinkinys gali būti optimizuotas iki ieškomųjų. Tai yra paradoksalus rezultatas, nes tyrėjas turi žinoti savo tyrinėjamos sistemos greičio parametrus eilės tikslumu, kad galėtų juos apskaičiuoti iš eksperimentinių duomenų. Taigi, vienintelis būdas rasti pradinius greičio parametrus, kurie gali būti optimizuoti iki tikrųjų yra pakankamai tankus greičio parametrų tinklelio perrinkimas.

Nagrinėjant greičio parametrų radimo iš vienos kinetinės kreivės uždavinį, buvo nustatyta, kad vienos kinetinės kreivės neužtenka rasti visus schemoje esančius greičio parametrus ir minimaliai tam reikia bent trijų skirtingų eksperimentų su skirtingomis pradinėmis M_{ox} koncentracijomis ($10^{-4},\ 10^{-5},\ 10^{-6}$). Lentelėje 1.13 yra pateikti optimizavimo rezultatai nagrinėjant 81 pradinių parametrų rinkinį rastą po paieškos greičio parametrų tinklelyje.

1.13 lentelė: Greičio parametrų skaičiavimas iš trijų kinetinių kreivių. $E_{ox} = 10^{-9},\ M_{ox} = 10^{-(4\div 6)},\ F_{ox} = 10^{-4},\ S = 10^{-3}$.

	Simuliacijos konstantos $\lg(k_1)\ \lg(k_2)$ $\lg(k_3)\ \lg(k_{-3})$	Blogiausias rinkinys	Geriausias rinkinys
#1	6.3 7.3 6.3 5.3	$S = 2.86 * 10^{-10}$ 6.75 8.00 5.54 6.30	$S = 1.10 * 10^{-15}$ 6.30 7.30 6.43 5.43
#2	5.3 7.3 6.3 5.3	$S = 3.23 * 10^{-10}$ 5.60 8.00 7.17 8.00	$S = 1.48 * 10^{-19}$ 5.30 7.30 6.30 5.30
#3	5.3 6.3 6.3 5.3	$S = 4.19 * 10^{-10}$ 5.64 8.00 6.12 8.00	$S = 2.11 * 10^{-19}$ 5.30 6.30 6.24 5.24
#4	5.3 6.3 5.3 5.3	$S = 1.72 * 10^{-10}$ 4.69 6.09 6.86 0.00	$S = 4.14 * 10^{-20}$ 5.30 6.30 5.35 5.35
#5	5.3 6.3 5.3 4.3	$S = 2.71 * 10^{-11}$ 5.63 8.00 1.42 2.74	$S = 2.87 * 10^{-20}$ 5.30 6.30 5.24 4.24
#6	5.0 8.0 7.0 7.0	$S = 4.08 * 10^{-10}$ 4.78 8.00 8.00 2.24	$S = 5.29 * 10^{-20}$ 5.00 8.00 7.00 7.00

Iš lentelės matyti, kad geriausias rinkinys yra visais atvejais labai arti simuliacijos greičio konstantų, tačiau geriausio greičio konstantų

rinkinio tikslo įvertis iš tiesų labai menkai skiriasi nuo blogiausio greičio parametrų rinkinio. Tai reiškia, kad net nedidelis eksperimentinių duomenų išsibarstymas, kuris yra neišvengiamas bet kokiuose eksperimentiniuose matavimuose, gali paversti greičio parametrų rinkinius neatskiriamais. Tariant, kad $(x_{i,exp} - x_{i,calc})$, kur $x_{i,exp}$ yra matavimo rezultatas, yra pasiskirstę pagal normalinį dėsnį su nuliniu vidurkiu, ir, naudojant vidurinės tikėtinos reikšmės apibrėžimą:

$$E[g(x)] \stackrel{\text{def}}{=} \int_{-\infty}^{\infty} g(x)f(x)dx \tag{1.54}$$

kur $g(x)$ yra funkcija, o $f(x)$ yra tikimybės pasiskirstymo funkcija (čia – $g(x) = x^2$ ir $f(x) = \frac{e^{-\frac{x^2}{2\sigma^2}}}{\sigma\sqrt{2\pi}}$), tuomet tikslo įverčio reikšmė yra :

$$\sum_{i=1}^{n}(x_{i,exp} - x_{i,calc})^2 \approx \int_{-\infty}^{\infty} \frac{e^{-\frac{x^2}{2\sigma^2}}}{\sigma\sqrt{2\pi}} x^2 dx = \sigma^2 \tag{1.55}$$

Šis rezultatas rodo, kad triukšmas tiesiog turėtų padidinti tikslo įverčio funkciją σ^2. Bet taip nėra – iš trijų kreivių su pridėtu triukšmu ($\sigma^2 = 2{*}10^{-6}$) įmanoma apskaičiuoti tik pirmąsias dvi greičio konstantas (lentelė 1.14).

1.14 lentelė: Greičio parametrų skaičiavimas iš trijų kreivių su pridėtu triukšmu ($\sigma^2 = 2 * 10^{-6}$). Pradinės sąlygos: $E_{ox} = 10^{-9}$, $M_{ox} = 10^{-(4\div6)}$, $F_{ox} = 10^{-4}$, $S = 10^{-3}$.

	Simuliacijos konstantos $\lg(k_1)$ $\lg(k_2)$ $\lg(k_3)$ $\lg(k_{-3})$	blogiausias rinkinys	Geriausias rinkinys
#1	6.3 7.3 6.3 5.3	$S = 2.95 * 10^{-10}$	$S = 1.06 * 10^{-11}$
		6.75 8.00 5.55 6.31	6.30 7.31 4.05 3.01
#2	5.3 7.3 6.3 5.3	$S = 3.35 * 10^{-10}$	$S = 1.33 * 10^{-11}$
		5.60 8.00 7.17 8.00	5.30 7.31 4.45 3.44
#3	5.3 6.3 6.3 5.3	$S = 4.19 * 10^{-10}$	$S = 1.15 * 10^{-11}$
		8.00 6.20 8.00 0.11	5.30 6.30 8.00 7.02
#4	5.3 6.3 5.3 5.3	$S = 2.04 * 10^{-10}$	$S = 1.21 * 10^{-11}$
		4.69 6.09 6.48 0.11	5.30 6.30 7.56 7.56
#5	5.3 6.3 5.3 4.3	$S = 4.32 * 10^{-10}$	$S = 1.18 * 10^{-11}$
		5.63 8.00 6.12 8.00	5.30 6.30 3.75 2.74
#6	5.0 8.0 7.0 7.0	$S = 4.17 * 10^{-10}$	$S = 1.18 * 10^{-11}$
		4.78 8.00 8.00 2.09	5.00 8.00 7.00 7.00

Šio rezultato paaiškinimas tiesiogiai kyla iš reakcijos mechanizmo. Nepaisant to, kad nebuvo rastos greičio konstantų teisingos absoliučios reikšmės, jų santykis (k_3/k_{-3}) yra išlaikytas teisingas. Šis santykis yra paaiškinamas diferencialine lygtimi iš reakcijos mechanizmo:

$$\frac{d[F_{ox}]}{dt} = k_{-3}[F_{red}][M_{ox}] - k_3[F_{ox}][M_{red}] \tag{1.56}$$

Esant tam tikroms sąlygoms, pvz., kai $[F_{ox}] \gg [M_{ox}]$, F_{ox} koncentracija kinta labai lėtai. Vadinasi, galima padaryti kvazistacionarumo prielaidą, kad :

$$0 = k_{-3}[F_{red}][M_{ox}] - k_3[F_{ox}][M_{red}]$$

iš kurios gaunama:

$$\frac{k_3}{k_{-3}} = \frac{[F_{red}][M_{ox}]}{[F_{ox}][M_{red}]} = K_{eq} \tag{1.57}$$

kas reiškia, kad greičio konstantų k_3 ir k_{-3} absoliučios reikšmės yra nenustatomos šiuose eksperimentuose ir įmanoma rasti tik pusiausvyros konstantą K_{eq} kaip greičio parametrą. Tai yra bendra visoms nagrinėjamos reakcijoms, kuriose yra kvazistacionarumo kokio nors reagento atžvilgiu apraiškų. Kartu šis rezultatas rodo, kad kai kurių greičio parametrų neįmanoma apskaičiuoti iš kinetinių kreivių vienareikšmiškai ir duomenų analizės metodai, kurie remiasi prielaida, kad egzistuoja kažkoks unikalus greičio parametrų rinkinys, kuris minimizuoja tikslo funkciją, randa greičio konstantas, kurios iš esmės yra neteisingos ir neprasmingos. Šito įmanoma išvengti tik analizuojant visus rastus statistiškai reikšmingus lokalius minimumus – galimus greičio parametrų rinkinius (statistiniai kriterijai išdėstyti pilnoje disertacijos versijoje). Tokia analizė leidžia nustatyti, kurios konstantos dėl eksperimentinių sąlygų ypatumų yra tarpusavyje susijusios ir turėtų būti pakeistos greičio parametrais, kurie gali būti tiksliai nustatomi iš eksperimento duomenų.

Metodo pritaikymas reakcijų, katalizuojamų šarminės fosfatazės ir peroksidazės, analizei. Šioje dalyje yra pademonstruota, kaip aprašytas reakcijos greičio parametrų apskaičiavimo metodas yra pritaikomas eksperimentinės biocheminės kinetikos duomenų analizei. Tam buvo pa-

sirinktos dvi biokatalizinės reakcijos, kurios turi įvairių komplikacijų, tad jų kontekste gali būti atskleisti metodo privalumai ir trūkumai.Pirmoji reakcija yra šarminės fosfatazės katalizuojama paranitrofenolfosfato hidrolizė. Dažniausiai biocheminės kinetikos tyrimai prasideda nuo prielaidos, kad stebimi eksperimentai gali būti aprašomi pačiu paprasčiausiu Michaelis-Menten mechanizmu:

$$\begin{array}{rcl} E + S & \underset{k_{-1}}{\overset{k_1}{\rightleftharpoons}} & ES, \\ ES & \overset{k_{cat}}{\rightarrow} & E + P. \end{array} \tag{1.58}$$

Kur E yra fermentas, S– substratas, P – produktas, o ES fermento ir substrato kompleksas. Kvazistacionariomis sąlygomis, sistema gali būti aprašyta lygtimis:

$$\frac{d[S_0]}{dt} = -\frac{v_{max}[S_0]}{K_M + [S_0]},\ kur\ K_M = \frac{k_{-1} + k_{cat}}{k_1}\ ir\ v_{max} = k_{cat}[E_0]. \tag{1.59}$$

Šios shemos ir lygčių pagrindinė problema yra, kad praktiškai labai didelė dalis net labai komplikuotų mechanizmų gali būti aprašomi šia paprasta schema jeigu yra matuojamas tik pradinis greitis. Tai gerai iliustruoja šarminės fosfatazės reakcijos duomenys su apskaičiuotais iš pradinio greičio parametrais$K_m = 92 \pm 15\ \mu$M ir $v_{max} = 0.13 \pm 0.1\ \mu\mathrm{Ms}^{-1}\mathrm{mg}^{-1}$ (pav. 1.34, d). Tačiau, iš tiesų šarminė fosfatazė yra inhibuojama reakcijos produktų (Bowers and McComb, 1966) ir pradinio greičio analizė šito negali aptikti, nebent eksperimentų metu būtų pridedama reakcijos produktų ir tiriama jų įtaka pradiniam reakcijos greičiui. Tuo tarpu, skaitinis modeliavimas remiantis paprasta schema (1.58) iš karto parodo, kad ji nėra tinkama duomenims aprašyti (pav. 1.33, kairė).

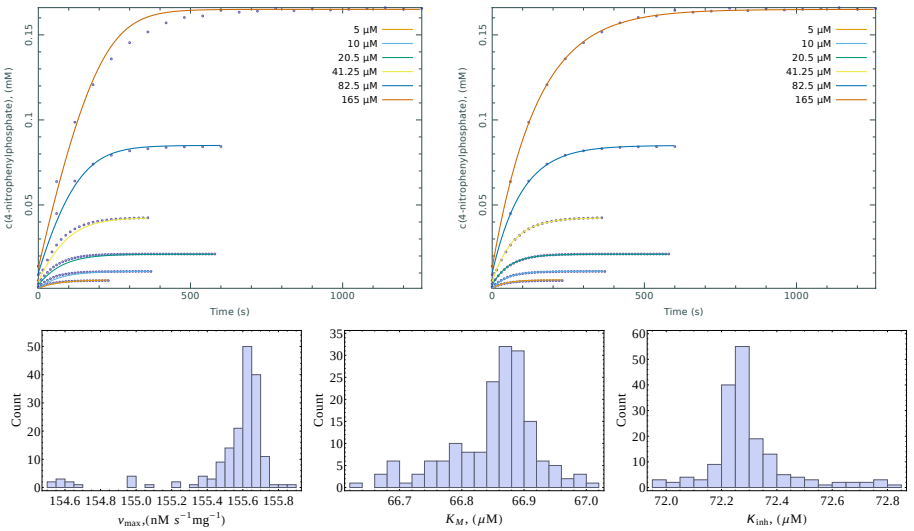

1.33 pav.: Paranitrofenolfosfato hidrolizės duomenys analizuoti remiantis schema (1.58) (kairėje – Michaelis-Menten kinetika) ir schema (1.60) (dešinėje – Michaelis-Menten kinetika su inhibicija). Duomenys (apskritimai) iš eksperimentų su skirtingomis paranitrofenolfosfato koncentracijomis, kreivės reprezentuoja modelius su geriausiai tinkančiais greičio parametrais. Histogramos žemiau – apskaičiuotų parametrųk_{cat}, K_M ir K_{inh} pasiskirstymai.

Šiems duomenims aprašyti yra reikalinga papildoma reakcija schemoje:

$$\begin{aligned} E + S &\underset{k_{-1}}{\overset{k_1}{\rightleftharpoons}} ES, \\ ES &\overset{k_{cat}}{\rightarrow} EP, \\ E + P &\underset{k_{-2}}{\overset{k_2}{\rightleftharpoons}} E_{inh}. \end{aligned} \tag{1.60}$$

Kuri esmingai keičia analizės rezultatus ir rodo, kad papildyta schema puikiai aprašo eksperimentų duomenis (pav. 1.33, dešinė). Analizuojant daugybinius gerai duomenis aprašančių konstantų rinkinius ir jų tarpusavio ryšius (1.34, a, b, c) galima nustatyti visus reikalingus kinetinius parametrus, kurių neįmanoma rasti iš pradinio greičio ir apskaičiuoti juos gerokai tiksliau. Šiuo atveju yra gaunama $K_M = \frac{k_{-1}+k_{cat}}{k_1} = 66.9 \pm 0.5\ \mu$M, $v_{max} = [E_0]k_{cat} = 156 \pm 1$ nMs^{-1}mg^{-1}, $K_{inh} = \frac{k_2}{k_{-2}} = 72.3 \pm 0.1\ \mu$M.

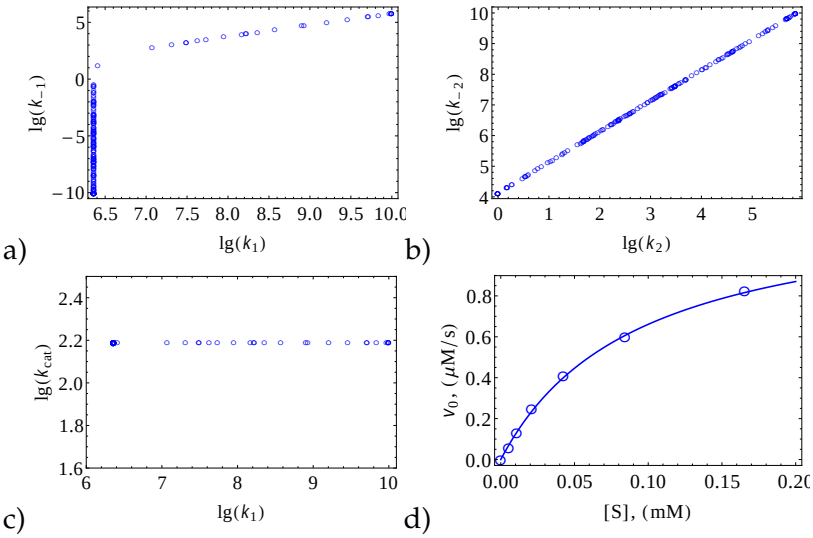

1.34 pav.: Aptikti ryšiai tarp greičio konstantų (a, b, c) ir pradinio greičio priklausomybė nuo pradinės koncentracijos (d).

Šie parametrai yra palyginami su publikuotais literatūroje (Cyboron and Wuthier, 1981; Van Belle, 1976) ir yra rasti gerokai didesniu tikslumu nei įmanoma iš pradinio greičio analizės. Kartu tai iliustruoja, kad iš daugybinių greičio konstantų rinkinių, taip pat gerai aprašančių reakcijos schemą, galima nustatyti ar jai tinka kvazistacionarumo prielaida ir išgauti papildomą tikslumą skaičiuojant greičio parametrus, kurie iš tiesų aprašo eksperimentinius duomenis.

Kita sudėtinga reakcijos schema yra aptinkama peroksidazės katalizuojamoje promazino oksidacijoje – susidaręs promazino oksidacijos produktas, radikal-katijonas toliau greitai disproporcionuoja ir dvielektroninės oksidacijos produktas yra hidrolizuojamas vandeniu iki promazino sulfoksido. Tokiu atveju, pradinio greičio metodu yra neįmanoma tiksliai nustatyti teisingų kinetinių greičio parametrų. Šis atvejis yra sudėtingas ir kitu požiūriu – peroksidazės katalizuojamų reakcijos schemos yra gerokai sudėtingesnės ir aprašomos su daugiau greičio konstantų (Berglund et al., 2002; Blankert et al., 2005; Kulys et al., 2000). Promazino oksidacijos atveju reakcijos schema atrodo šitaip:

$$
\begin{aligned}
E_{red} + H_2O_2 &\overset{k_p}{\rightarrow} Comp_I, \\
Comp_I + S &\underset{k_{-1}}{\overset{k_1}{\rightleftharpoons}} Comp_IS, \\
Comp_IS &\overset{k_{cat,1}}{\rightarrow} Comp_{II} + S^{\bullet +}, \\
Comp_{II} + S &\underset{k_{-2}}{\overset{k_2}{\rightleftharpoons}} Comp_{II}S, \\
Comp_{II}S &\overset{k_{cat,2}}{\rightarrow} E_{red} + S^{\bullet +}, \\
S^{\bullet +} + S^{\bullet +} &\underset{k_{-3}}{\overset{k_3}{\rightleftharpoons}} S + S_{ox}, \\
S_{ox} + H_2O &\overset{k_{hyd}}{\rightarrow} S_{sulfoxide} + 2H^+,
\end{aligned}
\tag{1.61}
$$

Čia $S^{\bullet +}$ yra promazino radikal-katijonas ir eksperimento eiga yra stebima pagal jį prie 514 nm bangos ilgio ($\epsilon_{514} = 8.9\ \mathrm{mM^{-1}cm^{-1}}$ (Kulys et al., 2000)). Schema yra apibrėžta dideliu rinkiniu greičio konstantų ir tikėtina, kad ne visas jas įmanoma vienareikšmiškai apskaičiuoti iš eksperimentinių duomenų pavaizduotų pav. 1.35. Nagrinėjant tik fermentinės katalizės dalį, galima išvesti greičio lygtį:

$$
[S^{\bullet +}]'[t] = \frac{2[E_0]k_{cat,1}k_{cat,2}k_p[H_2O_2][S]}{k_{cat,2}(k_{cat,1}[S] + k_p[H_2O_2](K_{M,1} + [S])) + k_{cat,1}k_p[H_2O_2](K_{M,2} + [S])},
\tag{1.62}
$$

kur $K_{M,n} \rightarrow \frac{k_{cat,n}+k_{-n}}{k_n}$. Tariant, kad reakcija su vandenilio peroksidu yra daug greitesnė nei likusios reakcijos, lygtis supaprastėja iki:

$$
[S^{\bullet +}]'[t] = \frac{2[E_0]k_{cat,1}k_{cat,2}[S]}{k_{cat,2}(K_{M,1} + [S]) + k_{cat,1}(K_{M,2} + [S])}.
\tag{1.63}
$$

Kuri gali būti perrašyta į Michaelis-Menten formą:

$$
\begin{gathered}
[S^{\bullet +}]'[t] = v = \frac{2[E_0]k_{cat}[S]}{K_M + [S]},\ where\ k_{cat} = \frac{k_{cat,1}k_{cat,2}}{k_{cat,1}+k_{cat,2}} \\
and\ K_M = \frac{k_{cat,1}K_{M,2}+K_{M,1}k_{cat,2}}{k_{cat,1}+k_{cat,2}}
\end{gathered}
\tag{1.64}
$$

Visiškai natūralus klausimas yra kodėl pradinės greičio konstantos sutraukiamos šiuo atveju iki dviejų greičio parametrų. Taip yra dėl to, kad reakcija yra stebima pagal promazino radikal-katijono susidarymą ir šiame eksperimente yra neaišku, kuri iš stadijų yra greitį ribojanti ir kokią jos įtaka. Jei reakcijoje būtų stebimos skirtingos peroksidazės formos, tuomet būtų įmanoma iš eksperimentinių duomenų apskaičiuoti visas

atskiras greičio konstantas. Bet kokiu atveju, analizuojant visus rastus geriausius greičio konstantų rinkinius pagal aukščiau surašytą schemą, galima tiksliai apskaičiuoti tariamuosius reakcijos greičio parametrus bei greičio konstantas cheminėms reakcijoms iš duomenų pavaizduotų pav. 1.35.

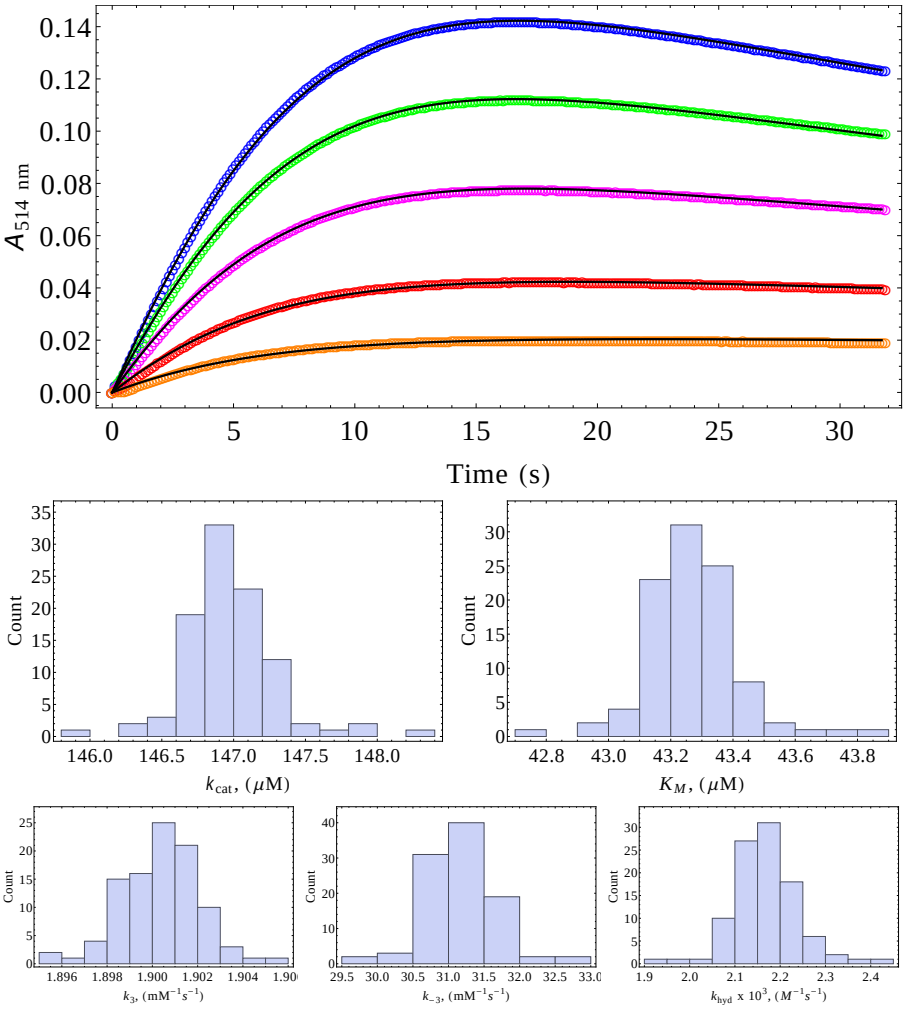

1.35 pav.: Promazino oksidacijos peroksidaze duomenys (apskritimai) ir geriausiai tinkantys modeliai (juodos kreivės). Histogramos žemiau – kinetinių parametrų skirstiniai.

Tai ir buvo padaryta ir buvo nustatyta, kad $k_{cat} = \frac{k_{cat,1}k_{cat,2}}{k_{cat,1}+k_{cat,2}} = 147 \pm 1\ \mathrm{s}^{-1}$, $K_M = \frac{k_{cat,1}K_{M,2}+K_{M,1}k_{cat,2}}{k_{cat,1}+k_{cat,2}} = 43.2 \pm 0.3\ \mu\mathrm{M}$, $k_{ox} = \frac{k_{cat}}{K_M} = (3.40 \pm 0.05) \times 10^6\ \mathrm{M}^{-1}\mathrm{s}^{-1}$, $k_3 = 1900 \pm 4\ \mathrm{M}^{-1}\mathrm{s}^{-1}$, $k_{-3} = (3.12 \pm 0.07) \times 10^4\ \mathrm{M}^{-1}\mathrm{s}^{-1}$, $k_{hyd} = (2.2 \pm 0.1) \times 10^{-3}\ \mathrm{M}^{-1}\mathrm{s}^{-1}$. Geriausiai

tinkantys modeliai pavaizduoti 1.35. Šiuos skaičius galima palyginti su parametrais, kuriuos įmanoma rasti tik iš reakcijos pradinio greičio $k_{cat} = (1.6 \pm 0.3) \times 10^2\ \mathrm{s}^{-1}$, $K_M = 60 \pm 20\ \mu\mathrm{M}$. Akivaizdu, kad pasiūlytu metodu atlikta analizė gerokai išsamesnė ir greičio parametrai nustatomi gerokai tiksliau.

1.2.2 Lakazės homogeninės kinetikos ir elektrokatalizės tyrimai ir modeliavimas

Lakazės yra oksidoreduktazių poklasis katalizuojantis įvairių substratų oksidaciją ir deguonies redukciją. Jos turi du aktyviuosius centrus, kurių pirmajame yra vienas vario jonas (T1), o antrame – trijų vario jonų klasteris (T2/T3 centras). T1 centras oksiduoja substratus ir perduoda elektronus T2/T3 centrui, kuriame jais yra redukuojamas deguonis (Jones and Solomon, 2015; Solomon et al., 1996).

Dėl savo katalizinio mechanizmo ypatybių ir gebėjimo oksiduoti įvairius junginius, lakazės yra radusios įvairių pritaikymų. Jos gali būti panaudojamos tekstilės ar popieriaus balinimui, džinsinio audinio dažymui „žaliuoju procesu“(Basto et al., 2007; Camarero et al., 2004). Tačiau šiuo metu populiariausia lakazių tyrimo sritis yra jų pritaikymas biosensoriams ir biokuro elementams(Chen et al., 2013; Li et al., 2014; Portaccio et al., 2013). Pastarieji yra reikšminga mokslinių tyrimų dalis, kurios tikslas yra sukonstruoti ekologiškus ir miniatiūrinius elektros srovės šaltinius. Lakazės čia yra panaudojamos kuriant biokatodus. Pagrindinė siekiamybė yra užtikrinti tiesioginę elektronų pernašą nuo elektrodo fermentui, nes tai padeda išvengti energijos nuostolių ir didina elektrodo veikimo potencialą. Tiesioginė elektronų pernaša lakazėms buvo pademonstruota praėjusio amžiaus aštuntajame dešimtmetyje ir nuo to laiko tapo populiariu tyrimų objektu (Tarasevich et al., 1979; Tominaga et al., 2017; Shleev et al., 2010; Shleev et al., 2004; Shleev et al., 2006; Shleev et al., 2005a). Šioje dalyje yra aptariami *Didymocrea* sp. J6 lakazės homogeninės ir heterogeninės kinetikos (lakazinio biokatodo sukonstruoto ant aukso nanodalelėmis modifikuoto elektrodo) eksperimentinių tyrimų ir modeliavimo rezultatai.

Lakazės katalizuojama ferocianido ir ABTS oksidacija Siekiant palyginti lakazės iš *Didymocrea* sp. J6 savybes homogeninėje terpėje su savybėmis imobilizavus ant elektrodo, buvo atlikti homogeninės kinetikos

tyrimai. Lakazės pasižymi didele galimų substratų įvairove, tad tyrimui buvo pasirinkti du substratai – ABTS ir ferocianidas. Matavimai buvo atlikti fosfato citratiniuose buferiniuose tirpaluose su pH reikšmėmis 4.0, 5.5 ir 7.4, matavimų metu buvo palaikoma $25°\mathrm{C}$ temperatūra. Lakazės inhibicija fluoridu buvo tiriama naudojant abu substratus. Pavyzdiniai eksperimentų duomenys pavaizduoti pav. 1.36 kartu su modeliais.

Tyrimų metu buvo pastebėta, kad ferocianidas yra oksiduojamas lakazės su aiškiai išreikšta *lag* faze, kuri nebuvo aptikta ABTS oksidacijos atveju. Lag fazės dažniausiai aptinkamos konsekutyvinėse reakcijose, medijuojamuose procesuose ar reakcijose, kur fermentas yra inaktyvuojamas arba reaktyvuojamas(Martinello and da Silva, 2006; Tetianec et al., 2014). Tokiais atvejais, pradinis greitis pagal apibrėžimą yra lygus nuliui, tad standartiniai duomenų analizės metodai negali būti taikomi. Todėl duomenys buvo analizuojami naudojant sukurtą greičio parametrų apskaičiavimo metodą. Šiems duomenims analizuoti buvo sudaryta reakcijos schema remiantis Solomon et al. (Solomon et al., 1996)ir ji yra vienoda tiek ferocianido, tiek ABTS oksidacijai:

$$\begin{aligned}
Lac_{resting} + S_{red} &\overset{k_{act}}{\rightarrow} Lac_2 + S_{ox},\\
Lac_1 + S_{red} &\overset{k_1}{\rightarrow} Lac_2 + S_{ox},\\
Lac_2 + S_{red} &\overset{k_2}{\rightarrow} Lac_3 + S_{ox},\\
Lac_3 + S_{red} &\overset{k_3}{\rightarrow} Lac_4 + S_{ox},\\
Lac_4 + S_{red} &\overset{k_4}{\rightarrow} Lac_{red} + S_{ox},\\
Lac_{red} + O_2 &\overset{k_{ox}}{\rightarrow} Lac_1 + 2H_2O,\\
Lac_1 &\overset{k_{inact}}{\rightarrow} Lac_{resting}.
\end{aligned} \tag{1.65}$$

Kur S_{red} ir S_{ox} yra oksiduotos ir redukuotos substratų formos, o Lac_* reprezentuoja skirtingai oksiduotas/redukuotas lakazės formas. Lag fazė šioje schemoje atsiranda dėl reakcijų su k_{act} ir k_{inact} greičio konstantomis, kurių pirma aktyvuoja fermentą, o antra inaktyvuoja. Sąlyga apibrėžianti, kada lakazės kinetikoje stebima lag fazė yra $min\{k_1,\ k_2,\ k_3,\ k_4\} \gg k_{act}$. Kvazistacionarios sąlygos neleidžia nustatyti, kuri iš k_1,k_2, $k_3$ar k_4 yra greitį ribojanti greičio konstanta, tačiau galima apibrėžti sintetinę k_{red} greičio konstantą:

$$\frac{1}{k_{red}} = \frac{1}{k_1} + \frac{1}{k_2} + \frac{1}{k_3} + \frac{1}{k_4}. \tag{1.66}$$

Lakazės inhibicija fluoridu yra modeliuojama papildoma reakcija

(Yaropolov et al., 1994):

$$Lac_{red} + F^- \underset{k_d}{\overset{k_a}{\rightleftharpoons}} Lac_{red}F, \tag{1.67}$$

kur $Lac_{red}F$ yra inhibuota lakazės forma, o inhibicijos konstanta apibrėžiama kaip $K_{inh} = k_d/k_a$. Eksperimentų duomenys buvo išanalizuoti prie visų nagrinėtų pH, nustatyto greičio konstantos yra lentelėje 1.15

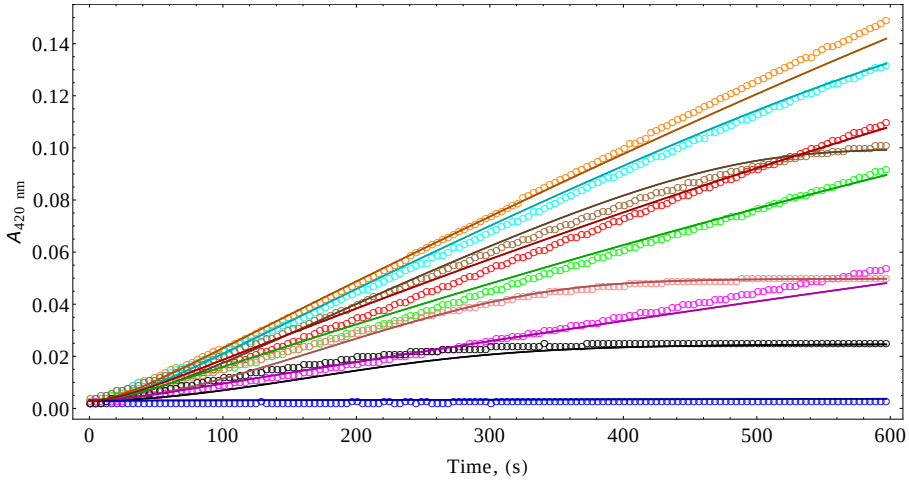

1.36 pav.: Kalio ferocianido oksidacija deguonimi katalizuojama lakazės ir jos inhibicija fluorido jonais pH 4.0 fosfato citratiniame buferiniame tirpale (duomenys – apskritimai, modeliai – kreivės).

1.15 lentelė: Nustatyti greičio parametrai *Didymocrea* sp. J6 lakazės katalizuojamai ABTS ir ferocianido oksidacijai (100 mM fosfatcitratinis buferinis tirpalas su 50 mM kalio sulfato), temperatūra -- 25°C.

pH	$k_{act\ ABTS}(\mathrm{M^{-1}s^{-1}})$	$k_{act\ Ferro}(\mathrm{M^{-1}s^{-1}})$	$k_{inact}(\mathrm{s^{-1}})$	$k_{ox}\ (\mathrm{M^{-1}s^{-1}})$
4.0	$> 6.3 \times 10^6$	$(2.7 \pm 0.1) \times 10^2$	0.71 ± 0.05	$(4.17 \pm 0.06) \times 10^4$
5.5	$(1.3 \pm 0.4) \times 10^4$	$> 3.2 \times 10^6$	0.037 ± 0.003	$(2.31 \pm 0.02) \times 10^4$
7.4	$(9.4 \pm 0.2) \times 10^2$	$(1.06 \pm 0.06) \times 10^3$	0.12 ± 0.03	$(7.14 \pm 0.07) \times 10^3$

pH	$k_{red\ ABTS}$	$k_{red\ Ferro}$	K_{inh}
4.0	$(1.548 \pm 0.007) \times 10^5\ \mathrm{M^{-1}s^{-1}}$	$(8.2 \pm 0.3) \times 10^5\ \mathrm{M^{-1}s^{-1}}$	$22.9 \pm 0.2\ \mu\mathrm{M}$
5.5	$(5.18 \pm 0.02) \times 10^4\ \mathrm{M^{-1}s^{-1}}$	$(4.66 \pm 0.08) \times 10^5\ \mathrm{M^{-1}s^{-1}}$	$187 \pm 3\ \mu\mathrm{M}$
7.4	$(1.2 \pm 0.1) \times 10^4\ \mathrm{M^{-1}s^{-1}}$	$(2.8 \pm 0.9) \times 10^5\ \mathrm{M^{-1}s^{-1}}$	$290 \pm 20\ \mu\mathrm{M}$

Iš lentelės matyti, kad rūgštiniame pH lakazės reakcijos su deguonimi greičio konstanta yra $(4.17 \pm 0.06) \times 10^4\ \mathrm{M^{-1}s^{-1}}$ ir toliau mažėja kylant

tirpalo pH. Tai yra gan netikėta, nes paprastai lakazių greičio konstantos su deguonimi yra $> 10^6$ $M^{-1}s^{-1}$(Cole et al., 1991; Andréasson et al., 1976; Bukh et al., 2006). Nustatyta inhibicijos fluoridu konstanta K_{inh} yra labai maža (22.9 ± 0.2 μM, pH 4.0) ir didėja su kylančiu tirpalo pH. Netikėta yra, kad imobilizuotos lakazės ant aukso elektrodo dengto aukso nanodalelėmis inhibicijos fluoridu konstanta yra daugiau nei 100 kartų didesnė tokiuose pačiuose buferiniuose tirpaluose.

Lakazės elektrochemija Elektrocheminiai lakazės iš *Didymocrea* sp. J6 adsorbuotos ant aukso nanodalelėmis modifikuoto elektrodo buvo atlikti dr. Daliaus Ratauto Vilniaus universitete. Tyrimų metu buvo tirta elektrocheminės elektrodų savybės nuo buferinio tirpalo pH ir lakazės inhibitoriaus fluorido jonų koncentracijos (pav. 1.37). Šie matavimo rezultatai netikėtai skyrėsi nuo anksčiau aptartų rezultatų homogeninėje terpėje. Pirmiausia, imobilizuota ant elektrodo lakazė pasižymi didele inhibicijos fluoridu konstanta. Antra, priklausomai nuo fluorido jonų koncentracijos lakazinio elektrodo pusbangis slenkasi į mažesnių potencialų pusę.

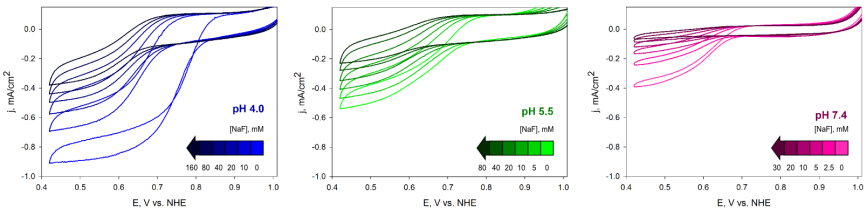

1.37 pav.: Volamperometrinės lakazės iš *Didymocrea* sp. J6 adsorbuotos ant aukso nanodalelėmis modifikuoto elektrodo priklausomybės nuo fluorido jonų koncentracijos ir buferinio tirpalo pH (naudotas sukamojo disko elektrodas su 1000 rpm sukimo greičiu).

Šiems duomenims suprasti ir paaiškinti buvo sudaryti kiekybiniai lakazės imobilizuotos ant elektrodo elektrokatalizinės deguonies redukcijos modeliai. Šiems modeliams reikėjo papildomų eksperimentinių duomenų – lakazės T1 centro redukcijos potencialo, kuris buvo pamatuotas spektroelektrocheminio titravimo metodu dr. Mariaus Dagio ir prof. Sergey Shleev Malmö universitete, Švedijoje (pav. 1.38). Iš sugerties priklausomybių nuo elektrodo potencialo buvo apskaičiuoti lakazės T1 centro redukcijos potencialai. Jie yra 683, 716, ir 720 mV buferiniuose tirpaluose su pH 4.0, pH 4.0 su 20 mM NaF, bei pH 7.4 be NaF.

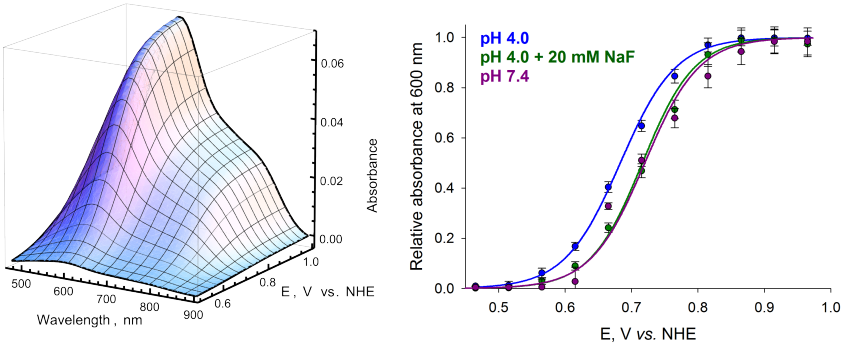

1.38 pav.: Spektroelektrocheminiai lakazės matavimai. Kairėje – absorbcijos spektro priklausomybė nuo elektrodo potencialo $\mathrm{pH}\ 4.0$ buferiniame tirpale. Dešinėje – santykinės absorbcijos prie $600\ \mathrm{nm}$ priklausomybė nuo darbinio elektrodo potencialo.

Priimta, kad deguonies redukcijas mechanizmas lakazėmis homogeninėje terpėje vyksta pirmiausiai elektronams nuo elektronų donorų patenkant į T1 centrą ir tada iš jo pernešant į T2/T3 centrą, kur ir vyksta galutinė deguonies redukcijos į vandenį stadija(Solomon et al., 1996; Sakurai and Kataoka, 2007). Bendra opinija yra, kad lakazės imobilizuotos ant elektrodo paviršiaus mechanizmas yra toks pats, kaip ir homogeninėje terpėje. Todėl, siekiant pagaminti efektyvius fermentinius elektrodus lakazių pagrindu, yra bandoma kuo efektyviau užtikrinti elektronų pernašą iš elektrodo į T1 centrą. Tačiau literatūroje esama ir publikacijų, kai elektrochemiškai stebimas T2/T3 centras, tačiau elektrodas nekatalizavo deguonies elektroredukcijos (Shleev et al., 2005a). Skirtingos galimos lakazės orientacijos schemos pavaizduotos pav. 1.39.

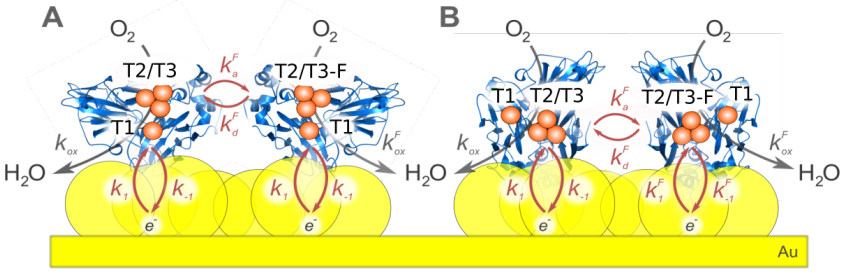

1.39 pav.: Schemos su galimomis lakazės orientacijomis ant elektrodo paviršiaus su elektronų pernaša per T1 centrą (A) ir per T2/T3 centrą (B).

Pirmiausia, lakazės elektrocheminis veikimas buvo modeliuojamas remiantis priimta schema, pavaizduota pav. 1.39 A dalyje (modelis

ir jo pilna analizė pateikiama angliškoje disertacijos versijoje). Tačiau gautasis modelis nepaaiškino stebimų eksperimentų teisingai. Todėl buvo sumodeliuota alternatyvi lakazės orientacija ant elektrodo pagal schemą pav. 1.39 B. Jos prielaidos yra tokios:

1. Matavimai atlikti esant tokioms deguonies koncentracijoms, kurios yra mažesnės nei lakazės Michaelis konstanta deguoniui.
2. T1 centras nedalyvauja elektrokatalizėje.
3. Fluorido jonai jungiasi T2/T3 centre ir keičia heterogeninę elektronų pernašos konstantą bei bimolekulinę deguonies redukcijos konstantą.
4. Srovės tankis yra ribojamas katalizinės deguonies redukcijos.
5. Fermento-fluorido asociacija yra labai greita.

Remiantis šiomis prielaidomis, galime užrašyti diferencialinių lygčių sistemą aprašančią procesus vykstančius elektrodo paviršiuje:

$$\begin{aligned}
\frac{d\Gamma^O}{dt} &= k_2\Gamma^R - k_1\Gamma^O + k_{ox}\Gamma^R[O_2]) + k_d^f\Gamma^{FO} - k_a^f\Gamma^O[F^-] \\
\frac{d\Gamma^R}{dt} &= k_1\Gamma^O - k_2\Gamma^R - k_{ox}\Gamma^R[O_2] + k_d^f\Gamma^{FR} - k_a^f\Gamma^R[F^-] \\
\frac{d\Gamma^{FO}}{dt} &= k_2^f\Gamma^{FR} - k_1^f\Gamma^{FO} + k_{ox}^f\Gamma^{FR}[O_2] + k_a^f\Gamma^O[F^-] - k_d^f\Gamma^{FO} \\
\frac{d\Gamma^{FR}}{dt} &= -k_2^f\Gamma^{FR} + k_1^f\Gamma^{FO} - k_{ox}^f\Gamma^{FR}[O_2] - k_d^f\Gamma^{FR} + k_a^f\Gamma^R[F^-]
\end{aligned} \tag{1.68}$$

Kur Γ $(\mathrm{mol/cm^2})$ yra atitinkamų fermento formų (O – oksiduota, R – redukuota, F – prisijungusi fluorido joną) paviršinės koncentracijos, $[F]$ ir $[O_2]$ yra fluorido jonų ir deguonies koncentracijos tirpale. Tariant, kad yra nusistovėjusios kvazistacionarios koncentracijos ir pridedant masių balanso fermentui lygtį bei srovės tankio lygtį:

$$\Gamma^O + \Gamma^R + \Gamma^{FO} + \Gamma^{FR} = \Gamma^{Tot} \tag{1.69}$$

$$i/A = -nF(k_{ox}^f\Gamma^{FR}[O_2] + k_{ox}\Gamma^R[O_2]) \tag{1.70}$$

$$\frac{k_d^f}{k_a^f} = K_{inh} \tag{1.71}$$

įmanoma apskaičiuoti visas kvazistacionarias fermento formų paviršines koncentracijas ir įstačius jas į srovės tankio lygtį bei suprastinus gauti:

$$i = \frac{-nF\Gamma^{Tot}[O_2]([F]k_1^f + k_1K_{inh})([F]k_{ox}^f + K_{inh}k_{ox})}{([F] + K_{inh})([F](k_1^f + k_2^f + k_{ox}^f[O_2]) + K_{inh}(k_1 + k_2 + k_{ox}[O_2]))} \tag{1.72}$$

Kur heterogeninės greičio konstantos aprašytos Butler-Volmer lygtimis:

$$k_1 = k_0 e^{-\alpha(E-E_{T2}^0)\frac{F}{RT}} \tag{1.73}$$

$$k_2 = k_0 e^{(1-\alpha)(E-E_{T2}^0)\frac{F}{RT}} \tag{1.74}$$

$$k_1^f = k_0^f e^{-\alpha(E-E_{T2}^{F0})\frac{F}{RT}} \tag{1.75}$$

$$k_2^f = k_0^f e^{(1-\alpha)(E-E_{T2}^{F0})\frac{F}{RT}} \tag{1.76}$$

Lygtis 1.72 puikiai aprašo eksperimentinius duomenis, kaip pavaizduota pav. 1.40, ko negali padaryti modelis paremtas elektronų pernaša per T1 centrą. Todėl modeliavimas leidžia daryti išvadą, kad šiomis sąlygomis lakazės veikimo mechanizmas yra paremtas tiesiogine elektronų pernaša iš elektrodo į T2/T3 centrą.

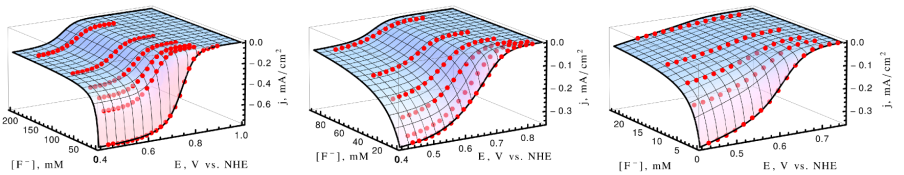

1.40 pav.: Modelis su tiesiogine elektronų pernaša į T2/T3 centrą (lyg. 1.72) pritaikytas duomenims iš pav. 1.37.

Naudojant modelį buvo paskaičiuoti visi kinetiniai parametrai, kurie surašyti lent. 1.16. Iš jos matyti, kad deguonies redukcijos greičio konstanta ir puikiai palyginama su reikšmėmis gautomis homogeninėje terpėje. Netikėta yra, kad fluorido prisijungimas lakazės T2/T3 centre

neinhibuoja deguonies redukcijos, o tiktai mažina jos greičio konstantą. Modelis leidžia apskaičiuoti T2/T3 redukcijos potencialus. Šie atskleidžia termodinamines lakazės katalizuojamos deguonies redukcijos ypatybes. pH 4.0 buferiniuose tirpaluose $E^0_{T2/T3}$ (752 ± 1 mV) yra didesnis nei E^0_{T1} (683 mV) ir mažesnis nei deguonies redukcijos potencialas (989 mV pH 4.0). Tai užtikrina elektronų srauto kryptį homogeninėmis sąlygomis. Tačiau, šarmingesniuose tirpaluose $E^0_{T2/T3}$ tampa mažesnis nei, kas trikdo elektronų pernašą tarp aktyviųjų centrų ir mažina katalizės efektyvumą, kaip ir stebima homogeninėje lakazės kinetikoje.

1.16 lentelė: Apskaičiuoti greičio parametrai (lyg. 1.72) duomenis iš pav. 1.40

	pH 4.0	pH 5.5	pH 7.4
k_0, s^{-1}	30 ± 1	3.4 ± 0.2	6.0 ± 0.4
k_{ox}, $\mathrm{M}^{-1}\mathrm{s}^{-1}$	$(3.72 \pm 0.01) \times 10^4$	$(1.71 \pm 0.01) \times 10^4$	$(2.3 \pm 0.2) \times 10^4$
$E^0_{T2/T3}$, mV	752 ± 1	674 ± 1	599 ± 3
α	0.31 ± 0.01	0.36 ± 0.01	0.13 ± 0.03
k^f_0, s^{-1}	7.0 ± 0.3	2.3 ± 1.5	0.36 ± 0.21
$E^{F0}_{T2/T3}$, mV	600 ± 1	570 ± 1	500 ± 90
k^f_{ox}, $\mathrm{M}^{-1}\mathrm{s}^{-1}$	$(1.01 \pm 0.01) \times 10^4$	$(0.17 \pm 0.03) \times 10^4$	$(2 \pm 170) \times 10^4$
α^f	0.34 ± 0.03	0.21 ± 0.07	0.16 ± 0.02
K_{inh}, mM	5.63 ± 0.06	19.6 ± 0.7	6.9 ± 1.4

Lakazės homogeninės ir heterogeninės kinetikų palyginimas Paradoksalu, kad k_{ox} reikšmės homogeninėje terpėje ir ant elektrodo sutampa, tačiau inhibicijos fluorido jonais konstanta K_{inh} skiriasi beveik 200 kartų ($K_{inh} = 22.9 \pm 0.2$ μM ir $K_{inh} = 5.63 \pm 0.06$ mM, pH $= 4.0$). Šis skirtumas yra esminis ir reikalauja paaiškinimo, kodėl taip nutinka. Trivialus ir dažniausiai naudojamas argumentas tokiems skirtumams paaiškinti yra, imobilizuotas baltymas ant paviršiaus keičia struktūrą ir dėl to keičiasi jo parametrai. Tačiau, egzistuoja geresnis kiekybinis paaiškinimas.

Pirmiausia, K_{inh} reikšmės yra apskaičiuotos naudojant skirtingas reakcijos schemas homogeninėse ir heterogeninėse sąlygose. Šie skirtumai yra dėl to, kad skirtingose sistemose įmanoma pamatuoti skirtingas savybes ir racionalus modelis turi turėti kiek įmanoma mažiau parametrų, kurių reikia paaiškinti sistemos elgesį. Todėl homogeninės kinetika buvo aproksimuota tokia reakcijos schema:

$$
\begin{aligned}
Lac_1 + S_{red} &\overset{k_1}{\rightarrow} Lac_2 + S_{ox},\\
Lac_2 + S_{red} &\overset{k_2}{\rightarrow} Lac_3 + S_{ox},\\
Lac_3 + S_{red} &\overset{k_3}{\rightarrow} Lac_4 + S_{ox},\\
Lac_4 + S_{red} &\overset{k_4}{\rightarrow} Lac_{red} + S_{ox},\\
Lac_{red} + O_2 &\overset{k_{ox}}{\rightarrow} Lac_1 + 2H_2O,\\
Lac_{red} + F^- &\underset{k_d}{\overset{k_a}{\rightleftharpoons}} Lac_{red}F.
\end{aligned}
\tag{1.77}
$$

Šiai schemai pritaikius kvazistacionarumo prielaidą fermento formų atžvilgiu, galime apskaičiuoti deguonies suvartojimo greičio lygtį:

$$
\frac{d[O_2]}{dt} = -\frac{[S_{red}][O_2][E_0]k_{red}k_{ox}K_{inh}}{4[O_2]k_2K_{inh} + [S_{red}]k_{red}([F^-] + K_{inh})} \tag{1.78}
$$

kur k_{red} kaip ir anksčiau yra apibrėžtas:

$$
\frac{1}{k_{red}} = \frac{1}{k_1} + \frac{1}{k_2} + \frac{1}{k_3} + \frac{1}{k_4}. \tag{1.79}
$$

Šis schema neaprašo T1 ir T2/T3 redoks centrų dalyvavimo reakcijoje. Jų tikrieji kinetiniai parametrai yra sutraukti į tariamuosius kinetinius parametrus kaip k_{red}, k_{ox} ir K_{inh}. Tačiau ši schema gali būti palyginta su išsamesne schema kuri buvo naudojama analizuojant imobilizuotos ant elektrodo lakazės kinetiką:

$$
\begin{aligned}
Lac_1 + S_{red} &\overset{k_1}{\rightarrow} Lac_2 + S_{ox},\\
Lac_2 + S_{red} &\overset{k_2}{\rightarrow} Lac_3 + S_{ox},\\
Lac_3 + S_{red} &\overset{k_3}{\rightarrow} Lac_4 + S_{ox},\\
Lac_4 + S_{red} &\overset{k_4}{\rightarrow} Lac^{ox}_{red} + S_{ox},\\
Lac^{ox}_{red} &\underset{k_b}{\overset{k_f}{\rightleftharpoons}} Lac^{red}_{ox}\\
Lac^{red}_{ox} + O_2 &\overset{k_{ox}}{\rightarrow} Lac_1 + 2H_2O,\\
Lac^{ox}_{red} + F^- &\underset{k_d}{\overset{k_a}{\rightleftharpoons}} Lac^{ox}_{red}F.
\end{aligned}
\qquad
\begin{aligned}
Lac_1F + S_{red} &\overset{k_1}{\rightarrow} Lac_2F + S_{ox},\\
Lac_2F + S_{red} &\overset{k_2}{\rightarrow} Lac_3F + S_{ox},\\
Lac_3F + S_{red} &\overset{k_3}{\rightarrow} Lac_4F + S_{ox},\\
Lac_4F + S_{red} &\overset{k_4}{\rightarrow} Lac^{ox}_{red}F + S_{ox},\\
Lac^{ox}_{red}F &\underset{k_b^F}{\overset{k_f^F}{\rightleftharpoons}} Lac^{red}_{ox}F\\
Lac^{red}_{ox}F + O_2 &\overset{k_{ox}^F}{\rightarrow} Lac_1F + 2H_2O,
\end{aligned}
\tag{1.80}
$$

Iš šios schemos su kvazistacionarumo prielaida gali išvesti tokią deguonies suvartojimo greičio lygtį:

$$\begin{aligned}\frac{d[O_2]}{dt} = \quad & -[S_{red}][O_2][E_0]k_{red}([F^-]k_{ox}^F + k_{ox}K_{inh})/ \\ & (4[O_2]([F^-]k_{ox}^F + k_{ox}K_{inh})+ \\ & [S_{red}]k_{red}([F^-](1+\beta[O_2] + (K_{eq}^F)^{-1}) \\ & +K_{inh}(1+\alpha[O_2] + (K_{eq})^{-1})))\end{aligned} \tag{1.81}$$

kur, $(K_{eq})^{-1} = \frac{k_b}{k_f}$, $(K_{eq}^F)^{-1} = \frac{k_b^F}{k_f^F}$, $\alpha = \frac{k_f}{k_{ox}}$ ir $\beta = \frac{k_f^F}{k_{ox}^F}$. Konstantos k_f ir k_b yra ribojančios elektronų pernašos greitį iš T1 į T2/T3 ir atgal (mes tariame, kad egzistuoja šiame keturių elektronų pernašos procese lėčiausias žingsnis). ši lygtis labai skiriasi nuo paprastesnės lygties 1.78 aptartos aukščiau. Tačiau tariant, kad fluorido jonų koncentracija yra maža ir atmetant narius, kurie nepriklauso nuo fluorido jonų koncentracijos, galime rasti, kaip siejasi K_{inh}^{hom}, pamatuota homogeninėje terpėje ir K_{inh}^{het} ir heterogeninės katalizės eksperimentų:

$$K_{inh}^{hom} = \frac{K_{inh}^{het}}{1+\beta[O_2] + (K_{eq}^F)^{-1}} \tag{1.82}$$

Ši lygtis, tariant, kad $1+\beta[O_2] \ll (K_{eq}^F)^{-1}$, susipaprastina iki:

$$K_{inh}^{hom} = K_{inh}^{het}K_{eq}^F \tag{1.83}$$

Taigi, pusiausvyros konstantos K_{eq}^F gali būti tiesiogiai susietos su T1 ir T2/T3 centrų redukcijos potencialais, kurie yra eksperimentiškai nustatyti anksčiau. K_{eq}^F gali būti išreikšta naudojant Nernst lygtį per atitinkamus redukcijos potencialus:

$$K_{eq}^F = \exp(\frac{(E_{T2/T3}^F - E_{T1})nF}{RT}) \tag{1.84}$$

Taigi, santykis $K_{inh}^{het}/K_{inh}^{hom}$ buvo panaudotas apskaičiuoti redukcijos potencialų skirtumą tarp T1 ir T2/T3 centrų su prisijungusiu fluorido jonu ir buvo gauta, kad potencialų skirtumai yra -120 mV, -130 mV ir -120 mV skirtinguose pH 4.0, 5.5 ir 7.4. Šie potencialų skirtumai yra puikiai sutampantys su tai, kurie buvo gauti elektrocheminių eksperimentų metu (atitinkamai -140 mV, -120 mV ir -80 mV). Iš to darytina išvada, kad inhibicinių konstantų skirtumai iš homogeninių ir heterogeninių eksperimentų yra paaiškinami pasiūlytų modelių. Įdomu yra tai, kad inhibicinė konstanta nustatyta homogeninių eksperimentų metu iš tiesų

reprezentuoja ne klasikinę inhibiciją, bet kompleksinį procesą, kai inhibitorius modifikuoja aktyvaus centro potencialą ir jo modifikacija sutrikdo elektronų pernašos greitį ir termodinaminę kryptį.

1.2.3 Elektrono ir protono pernaša peroksidazių katalizuojamoje substratų oksidacijoje

Protono ir elektrono pernašos peroksidazių katalizėje Hemą turinčios peroksidazės yra svarbūs fermentai, atrasti antrojoje 19 amžiaus pusėje ir per pusantro šimto metų istoriją radę pritaikymų organinėje sintezėje, biotransformacijose, liuminescensinėje ir imunocheminėje analizėje (Veitch, 2004). Tai yra įmanoma dėl didelio peroksidazių specifiškumo vienam iš substratų – vandenilio peroksidui ir menko substratinio specifiškumo oksiduojamiems substratams. Dėl pastarosios savybės hemą turinčios peroksidazės yra dar ir vertingas tyrimų objektas. Peroksidazės, oksiduotos vandenilio peroksidu iki pirmos oksiduotos formos (CpdI, „compound I“) tolesnė redukcija per antrą oksiduotą (CpdII) iki redukuotos peroksidazės formos yra procesas susidedantis iš dviejų elektrono pernašų ir dviejų protono pernašų. Bendrai literatūroje yra sutariama, kad greitį ribojantis katalizės žingsniai yra elektrono pernaša tiek CpdI tiek CpdII redukcijoje(Folkes and Candeias, 1997). Todėl peroksidazių katalizinėms savybėms paaiškinti buvo naudojama Marcus elektronų pernašos teorija. Ji buvo pritaikyta homologiškų chinonų (Folkes and Candeias, 1997), anilinų, fenolių ir indolacetinių rūgščių (Candeias et al., 1996; Candeias et al., 1997; Sakurada et al., 1990), fenilendiaminų ir fenoksazinų, fenotiazinų(Kulys et al., 2000; Krikstopaitis et al., 1998) oksidacijai peroksidazėmis. Visi šie tyrimai yra paremti homologinėmis – struktūriškai panašių – substratų aibėmis. Šis substratų pasirinkimų apribojimas kyla iš Marcus elektronų pernašos teorijos, kuri elektronų pernašos greičio konstantą aprašo šia lygtimi:

$$k = \frac{\pi}{\hbar} V_{if}^2 \frac{e^{-\frac{(\Delta G+\lambda)^2}{4\lambda k_b T}}}{\sqrt{\lambda \pi k_b T}} \tag{1.85}$$

Kur ΔG yra reakcijos Gibbs laisvoji energija, λ – reakcijos reorganizacijos energija, V_{if} – elektroninis susietumas tarp reakcijos reaktantų ir produktų (angl. – „electronic coupling“). Taigi, jei tyrinėjami substratai priklauso homologinei aibei, tai jų reakcijų λ ir V_{if} turėtų būti tarpusa-

vyje panašūs ir reakcijos greičio konstanta turėtų priklausyti tik nuo ΔG. Tokiu atveju greičio konstantos logaritmas turėtų paraboliškai priklausyti nuo reakcijos laisvosios energijos. Ši priklausomybė buvo apytiksliai stebėta daugeliu atvejų. Deja, lygtis 1.85 yra pritaikoma tik homologinių substratų eilei ir yra paremta hipoteze, kad V_{if} ir λ yra panašūs homologiniams substratams, o tyrinėjamos reakcijos greitis yra ribojamas elektrono pernašos žingsnio. Šioje disertacijos dalyje buvo tiriama, ar galima Marcus elektronų pernašos teorija pritaikyti ir nehomologinėms – struktūriškai nepanašioms – substratų aibėms.

Lygties 1.85 pritaikymą nehomologinėms substratų serijoms riboja du nežinomi kiekvienam substratui parametrai – V_{if} ir λ. V_{if} parametras elektronų pernašos ribojamoms reakcijoms gali būti nustatytas matuojant reakcijos greičio priklausomybę nuo temperatūros. Iš priklausomybės įmanoma atskirti preeksponentinį daugiklį nuo reakcijos aktyvacijos energijos. λ yra nustatomas gerokai sunkiau, bet jį įmanoma apskaičiuoti kvantinės chemijos metodais. Dėl šios priežasties buvo panaudoti kvantinės chemijos metodai apskaičiuoti substratų struktūras, jų redukcijos potencialus bei reorganizacijos energijas. Molekulinės mechanikos metodais buvo naudojami sumodeliuoti fermento ir substrato kompleksus ir nustatyti komplekso įtaką bendrai reakcijos reorganizacijos energijai.Tokie tyrimai, mūsų žiniomis, dar nebuvo atliekami fermentinėms elektronų pernašos reakcijoms su nehomologinių substratų serija. Siekiant ištirti kaip Marcus elektronų pernašos teorija gali būti pritaikyti nehomologiniams substratams bei nustatyti jiems V_{if} ir λ reikšmes buvo pasirinkta 12 substratų, kurių struktūros ir santrumpos yra pavaizduotos pav. 1.41. Šie substratai dalyvauja 13 oksidacijos reakcijų katalizuojamų *Coprinopsis cinerea* peroksidazės (Cip) CpdII.

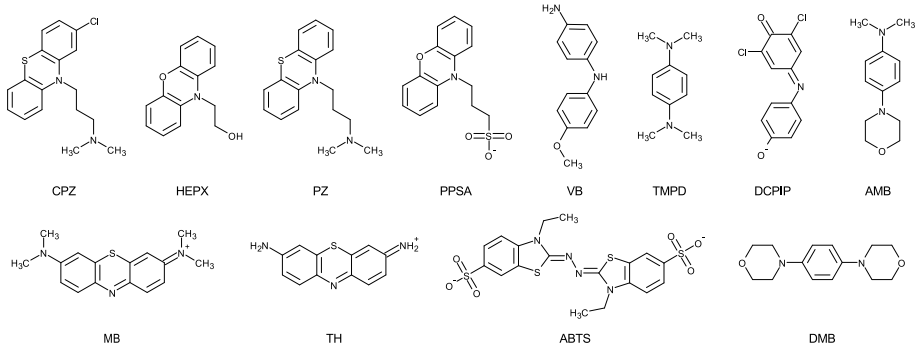

1.41 pav.: Substratai naudoti CiP CpdII redukcijos kinetikos tyrimams.

Šiems substratams buvo nustatyti redukcijos potencialai, pamatuotos reakcijos su CpdII greičio konstantos, kvantinės chemijos metodais apskaičiuotos λ ir molekulinės mechanikos metodais sumodeliuoti fermento ir substrato kompleksai. Tyrimai leido nustatyti, kad net ir homologiniams substratams V_{if} skiriasi kartais, o CpdII redukcijos greičio konstanta nėra ribojama tik elektrono pernašos kaip postuluojama literatūroje, o yra sintetinė greičio konstanta iš protono ir elektrono pernašos greičių.

Redukcijos potencialų ir reorganizacijos energijų nustatymas Tyrime naudotų substratų redukcijos potencialai ($50\ \mathrm{mM}$ fosfato buferinis tirpalas su $\mathrm{pH} = 7.0$), kurie yra reikalingi apskaičiuojant oksidacijos reakcijos Gibbs laisvąją energiją, buvo nustatyti naudojant ciklinės voltamperometrijos metodą. Peroksidazės antros formos (angl., „compound II“) redukcijos potencialas buvo rastas literatūroje (0.982 V,(Farhangrazi et al., 1994b)). Pavyzdinė eksperimento kreivė substratui DCPIP yra pavaizduota pav. 1.42. Šiuo konkrečiu atveju yra stebimi du redukcijos procesai, kurių pirmas (I) yra dvielektroninis, o antras (II) yra vienelektroninis. Šiems procesams yra atitinkamai iš eksperimentinių duomenų priskirti redukcijos potencialai. Keturių substratų (TH, MB, VB ir pirma DCPIP oksidacija) yra dvielektroniniai procesai, kuriems vienelektroniniai redukcijos potencialai buvo apskaičiuoti teoriškai.

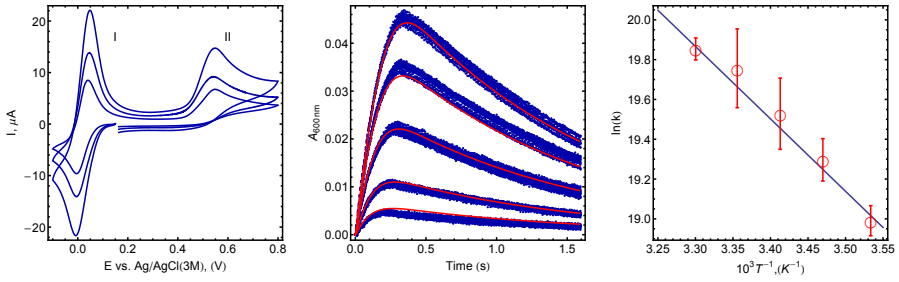

1.42 pav.: Iš kairės į dešinę: Ciklinė voltamperometrija DCPIP ($1\ \mathrm{mM}$) ant stiklo anglies elektrodo 50 mM fosfato buferiniame tirpale, pH 7.00, $T = 25\ \mathrm{C}^\circ$. DCPIP oksidacijos kinetika 50 mM fosfato buferiniame tirpale, pH 7.00, $T = 25\ \mathrm{C}^\circ$. Mėlyni taškai matavimai, raudonos kreivės – modelis (reakcijos schema 1.86). Arrhenius grafikas DCPIP oksidacijos greičio konstantos priklausomybei nuo temperatūros.

Apskaičiuoti teoriniai redukcijos potencialai su DFT su hibridiniu B3LYP funkcionalu ir 6-31+G(d,p) bazinių funkcijų rinkiniu yra gerai

palyginami su eksperimentiškai nustatytaisiais (pav. 1.43). Dvielektroniniu būdu besioksiduojančių substratų vienelektroniai potencialai buvo apskaičiuoti iš atitinkamų tarpinių vienelektroninių oksidacijų energijų naudojant pav. 1.43 pateiktą tiesinės regresijos lygtį. Apskaičiuoti vienelektroniniai redukcijos potencialai TH (0.25 V) ir MB (0.162 V) yra gerai palyginami su žinomai duomenimis iš pulsinės radiolizės eksperimentų (sukompiliuoti Wardman (Wardman, 1989)).

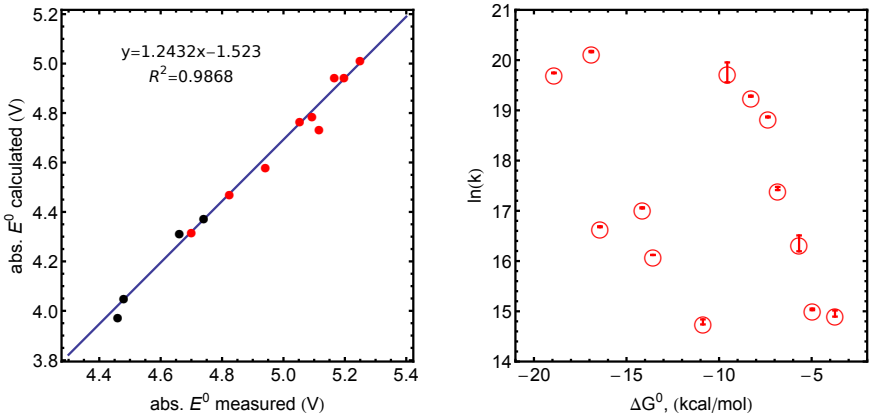

1.43 pav.: Kairėje – Absoliutūs redukcijos potencialai, apskaičiuoti naudojant DFT su hibridiniu B3LYP funkcionalu ir 6-31+G(d,p) bazinių funkcijų rinkiniu *vs.* eksperimentiškai nustatyti redukcijos potencialai. Raudoni – vienelektroniškai besioksiduojančių junginių potencialai, juodi – dvielektroniškai besioksiduojančių junginių potencialai. Dešinėje – Bimolekulinės CpdII redukcijos greičio konstantos priklausomybė nuo reakcijos Gibbs laisvosios energijos $T = 25$ C°.

Apskaičiuoti ir pamatuoti redukcijos potencialai yra surašyti lentelėje 1.17. Redukcijos potencialai dengia platų laisvųjų energijų ruožą nuo 0.162 V iki 0.79 V, kas yra beveik nepasiekiama naudojant homologines junginių serijas. Iš teorinių skaičiavimų gautos optimizuotos struktūros buvo panaudotas apskaičiuojant savireorganizacijos (tirpiklio ir vidines) energijas. Apskaičiuotos reorganizacijos energijos kinta nuo 3 kcal/mol (0.13 V) iki 12 kcal/mol (0.52 eV).

Oksidacijos kinetika ir greičio konstantos Tyrinėti substratai skiriasi struktūromis, reorganizacijos energijomis, redukcijos potencialais ir oksidacijos mechanizmais. Dalis jų yra oksiduojami vienelektroniškai iki radikal-katijonų (HEPX, ABTS, AMB, DMB, TMPD, PPSA, CPZ, PZ

1.17 lentelė: Termodinaminiai substratų parametrai.

Substratas	$E^0_{\text{vs NHE}}$ (V)	$E^0_{1,\text{vs NHE}}$ (V)	λ^*_{sol} (kcal/mol)
ABTS	0.686 ± 0.006	0.686 ± 0.006	3.42
AMB	0.394 ± 0.005	0.394 ± 0.005	11.17
CPZ	0.79 ± 0.01	0.79 ± 0.01	12.04
DCPIP(I)	0.231 ± 0.009	0.568*	12.47
DCPIP(II)	0.736 ± 0.01	0.736 ± 0.01	3.77
DMB	0.511 ± 0.004	0.511 ± 0.004	11.04
HEPX	0.663 ± 0.003	0.663 ± 0.003	3.10
MB	0.030 ± 0.006	0.162*	9.12
PPSA	0.623 ± 0.003	0.623 ± 0.003	2.65
PZ	0.767 ± 0.006	0.767 ± 0.006	11.82
TH	0.060 ± 0.001	0.250*	8.85
TMPD	0.270 ± 0.006	0.270 ± 0.006	11.68
VB	0.310 ± 0.006	0.369*	8.15

* apskaičiuota teoriškai.

ir antra DCPIP oksidacija). Kiti yra oksiduojami dvielektroniškai iki stabilių produktų (TH, MB, VB ir pirma DCPIP oksidacija). Dvielektroninės oksidacijos atveju yra daroma prielaida, kad fermentas vienelektroniškai oksiduoja substratą iki radikal-katijono ir pastarasis greitai disproporcionuoja. Disproporcionacijos reakcija, manoma, yra greita ir yra limituojama tik difuzijos (Solar et al., 1982).

Bendruoju atveju, peroksidazės katalizuojamos reakcijos schema (Berglund et al., 2002) yra sudėtinga ir dažnai yra komplikuojama disproporcionacijos, hidrolizės ar tolesnės oksidacijos. Tačiau bendruoju atveju katalizinis ciklas yra gan paprastas ir čia naudojamas tokiu pavidalu :

$$\begin{aligned}
(I) \quad & E_{red} + H_2O_2 \overset{k_p}{\rightarrow} CpdI \\
(II) \quad & CpdI + S \underset{k_{-1}}{\overset{k_1}{\rightleftharpoons}} CpdIS \\
& CpdIS \overset{k_{1,cat}}{\rightarrow} CpdII + S^{\bullet +} \\
(III) \quad & CpdII + S \underset{k_{-2}}{\overset{k_2}{\rightleftharpoons}} CpdIIS \\
& CpdIIS \overset{k_{2,cat}}{\rightarrow} E_{red} + S^{\bullet +} \\
(IV) \quad & S^{\bullet +} + S^{\bullet +} \overset{k_3}{\rightarrow} S + S_{ox}
\end{aligned} \tag{1.86}$$

Ši schema yra sudaryta iš keturių pagrindinių reakcijų. (I) yra CpdI (peroksidazės pirmos oksiduotos formos) susidarymas iš redukuotos fermento formos reakcijoje su vandenilio peroksidu. (II) yra CpdI redukcija iki CpdII (antra oksiduota forma). Pastaroji reakcija yra daug greitesnės nei reakcija (III), kur CpdII suredukuojamas iki redukuotos fermento formos (Candeias et al., 1997; Candeias et al., 1996; Folkes and Candeias, 1997; Krikstopaitis et al., 1998). Todėl šiame tyrime mes tariame, kad pamatuotos greičio konstantos reprezentuoja (III) reakcijos greitį. Visi kinetiniai eksperimentų duomenys buvo analizuojami pirmoje disertacijos dalyje aprašytu metodu. Pavyzdinė DCPIP oksidacijos kreivė pavaizduota pav. 1.42.

1.18 lentelė: Kinetiniai ir termodinaminiai CiP redukcijos įvairiais substratais parametrai.

Substratai	$k_{cat}/K_M(M^{-1}s^{-1})$ $at\ 25\ \mathrm{C}^\circ$	$\ln A$	$\Delta G^\ddagger$ $(kcal/mol)$
ABTS	$3.8 \pm 0.1 \times 10^7$	$26.8 \pm 2.$	5.5 ± 1.1
AMB	$1.003 \pm 0.003 \times 10^7$	31.5 ± 1.9	9.1 ± 1.1
CPZ	$3.1 \pm 0.2 \times 10^6$	14.6 ± 1.7	$0 \pm 1.$
DCPIP(I)	$3.8 \pm 0.8 \times 10^8$	32.2 ± 2.1	7.4 ± 1.2
DCPIP(II)	$1.3 \pm 0.2 \times 10^7$	21.9 ± 0.6	3.3 ± 0.3
DMB	$2.3 \pm 0.1 \times 10^6$	28.7 ± 2.0	8.0 ± 1.2
HEPX	$1.56 \pm 0.01 \times 10^8$	$29.3 \pm 2.$	6.2 ± 1.2
MB	$2.66 \pm 0.03 \times 10^8$	33.5 ± 0.7	8.4 ± 0.4
PPSA	$2.37 \pm 0.03 \times 10^8$	28.3 ± 1.3	5.3 ± 0.8
PZ	$3.40 \pm 0.05 \times 10^6$	18.7 ± 1.3	2.2 ± 0.8
TH	$4.80 \pm 0.07 \times 10^8$	30.0 ± 0.9	5.9 ± 0.8
TMPD	$1.76 \pm 0.01 \times 10^7$	36.3 ± 3.4	$11.6 \pm 2.$
VB	$2.56 \pm 0.03 \times 10^7$	29.3 ± 2.7	7.2 ± 1.6

Siekiant parinkti tinkamas eksperimentines sąlygas ir užtikrinti, kad CpdI formavimasis nėra reakcijos greitį ribojantis žingsnis, buvo atlinkti tiesioginiai peroksidazės oksidacijos vandenilio peroksidu iki CpdI kinetiniai tyrimai. Jų metu nustatyta, kad CiP reakcijos su H_2O_2 tariamoji bimolekulinė greičio konstanta $T = 25\ \mathrm{C}^\circ$ yra $(8.7 \pm 0.1) \times 10^6 \mathrm{M}^{-1}\mathrm{s}^{-1}$. Ši konstanta gerai sutampa su literatūroje publikuota reikšme (Abelskov et al., 1997). Iš greičio konstantos priklausomybės nuo temperatūros buvo nustatyta, kad CiP oksidacijos iki CpdI aktyvacijos energija yra $3.6 \pm 1.0\ \mathrm{kcal/mol}$ ir ji yra mažesnė nei aktyvacijos energija pamatuota krienų peroksidazei ($5.4 \pm 0.8\ \mathrm{kcal/mol}$ (Baek and Van Wart, 1992)).

Visų CpdII redukcijos eksperimentų kinetinės kreivės buvo panaudotos apskaičiuoti substratų oksidacijos greičio konstantas pirmoje disertacijos dalyje pateiktu metodu. Pavyzdinės kinetinės kreivės iliustruotos pav. 1.42 kartu su geriausiu modeliu. Apskaičiuotos greičio konstantos yra pateiktos lentelėje 1.18. Kaip ir tikėtasi, šios greičio konstantos niekaip tiesiogiai nesisieja su reakcijos laisvąja energija (pav. 1.43). Tai yra visiškai natūralu, nes substratų struktūrų įvairovė lemia greičio konstantą sudarančių parametrų – reorganizacijos energijos ir elektroninės sąveikos („electronic coupling“) – įvairovę.

Tačiau gautuosius duomenis galima panaudoti apskaičiuoti aktyvacijos energijas taip eliminuojant V_{if} įtaką ir palyginti aktyvacijos energijas su nustatytomis reakcijos laisvosiomis energijomis bei teoriškai apskaičiuotomis reorganizacijos energijomis. Kadangi lygtis 1.85 yra labai panaši į Arrhenius lygtį, jas logaritmavus ir išskleidus akivaizdu, kaip siejasi reakcijos aktyvacijos energijos su ΔG ir λ bei kaip atsiskiria V_{if} daugiklis:

$$\ln k(T) = \ln\left(\frac{\pi V_{if}^2}{\hbar\sqrt{\lambda k_b}}\right) - \frac{(\Delta G^\circ + \lambda)^2}{4\lambda k_b T} - \frac{\ln T}{2} \tag{1.87}$$

$$\ln k(T) = \ln A - \frac{E_a}{k_B T} \tag{1.88}$$

Panaudojant logaritmuotą Arrhenius lygties formą iš tariamųjų bimolekulinių reakcijos greičio konstantų (k_{cat}/K_M) priklausomybės nuo temperatūros (pavyzdys pav. 1.42) kiekvienam substratui buvo apskaičiuotos aktyvacijos energijos ir preeksponentiniai faktoriai (lentelė 1.18). Pastebėtina, kad Marcus lygtis 1.85 aprašo pirmo laipsnio greičio konstantą. Antro laipsnio greičio konstantai aprašyti yra reikalingi papildomi daugikliai kaip pvz. pereinamojo komplekso pusiausvyros konstanta ir t.t.(Sutin, 1982; Marcus, 1956b). Šio tyrimo kontekste šie nežinomieji yra sutraukti į vieną sintetinį parametrą V_{if}. Todėl toliau tekste yra turima omenyje ne tikrasis V_{if}, bet tariamasis V_{if}.

Pamatuotos greičio konstantos k_{cat}/K_M (lentelė 1.18) kinta ribose nuo $\sim 2 \times 10^6 \mathrm{M}^{-1}\mathrm{s}^{-1}$ iki $\sim 5 \times 10^8 \mathrm{M}^{-1}\mathrm{s}^{-1}$. Nustatytos aktyvacijos energijos yra nuo 0 ± 1 kcal/mol su iki 11.6 ± 2 kcal/mol su TMPD. Iš paveikslo 1.44 matyti, kad egzistuoja apytikslė tendencija mažėjant ΔG° didėti $\Delta G^\ddagger$.

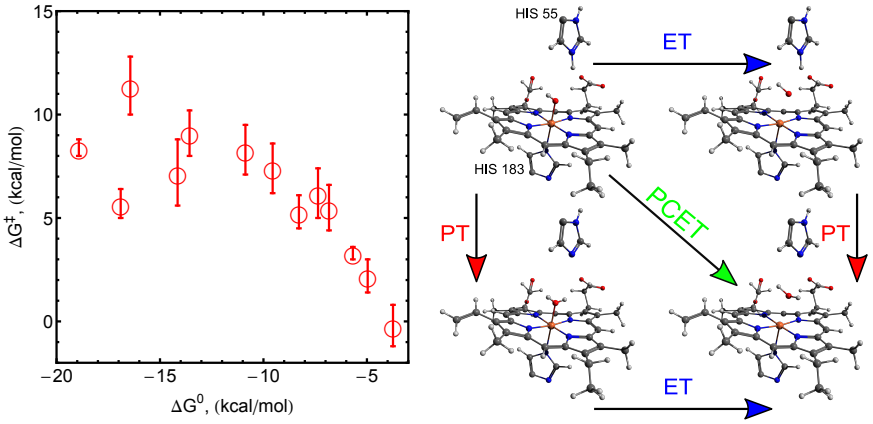

1.44 pav.: Kairėje $-\Delta G^{\ddagger}$ priklausomybė nuo ΔG°. Dešinėje – CiP CpdII redukcijos galimi keliai (aktyvusis centras iš PDBID:1h3j).

Elektrono ir protono pernašos modelis Iš viso egzistuoja keturi galimi mechanizmai, kaip gali vykti CiP CpdII redukcija. Jie yra: su protonu susieta elektrono pernaša (angl., proton coupled electron transfer - PCET), konsekutyvinė ribojanti greitį elektrono pernaša (ET) arba ribojanti greitį protono pernaša (PT) ir konsekutyvinė ET ir PT su ribojančia greitį stadija priklausančia nuo reakcijos laisvosios energijos. PCET mechanizmas gali būti atmestas dėl literatūroje publikuotų mažų kinetinio izotopinio efekto reikšmių $k_H/k_D \approx 1.3$(Candeias et al., 1997). Tipinės tokio mechanizmo k_H/k_D PCET mechanizmuose būna gerokai didesnės (Edwards et al., 2009).

Jeigu elektrono pernaša būtų reakcijos greitį ribojantis žingsnis, Tiesiogiai iš aktyvacijos energijos lygties $\Delta G^{\ddagger} = \frac{(\Delta G^{\circ}+\lambda)^2}{4\lambda}$ galima apskaičiuoti eksperimentines reorganizacijos energijas. Kadangi pastarosios visiškai nekoreliuoja su apskaičiuotomis kvantinės chemijos metodais, elektrono pernašos greitis nėra reakciją ribojantis žingsnis (pav. 1.45). Jeigu reakcijos greitį ribotų protono pernaša, tokiu atveju visiems substratams reakcijos greitis turėtų būti vienodas, turint omeny, kad 9 substratai nedonuoja reakcijai protono ir vienintelė protono pernaša, kuri gali vykti reakcijoje yra vidumolekulinė –nuo katalizinio histidino hemui. Galų gale, nei vienas aptartų variantų teoriškai neprognozuoja tiesinės priklausomybės tarp ln(A) ir $\Delta G^{\ddagger}$ matomos paveiksle 1.45.

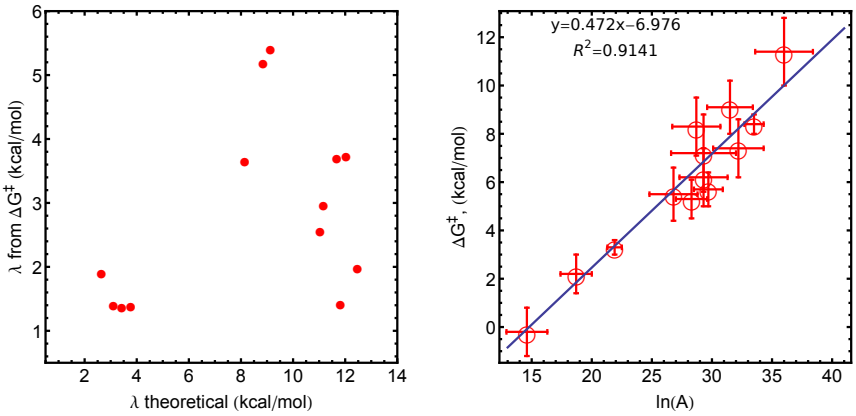

1.45 pav.: Kairėje – λ apskaičiuotas iš $\Delta G^{\ddagger}$ *vs.*teorinis λ; dešinėje – $\Delta G^{\ddagger}$ priklausomybė nuo ln(A)

Vienintelė likusi schema galinti paaiškinti gautuosius rezultatus yra konsekutyvinė elektrono ir protono pernaša su aiškiai neapibrėžta ribojančia stadija, priklausančia nuo reakcijos laisvosios energijos. Tokiu atveju CpdII redukcija gali būti aprašyta tokiomis reakcijomis:

$$E + S \overset{k_e}{\rightarrow} ES, \quad ES \overset{k_p}{\rightarrow} E + P \tag{1.89}$$

Kurios kvazistacionariomis sąlygomis neatskiriamos nuo:

$$E \overset{k_p}{\rightarrow} E', \quad E' + S \overset{k_e}{\rightarrow} E + P \tag{1.90}$$

Abiem atvejais tariamoji bimolekulinė reakcijos greičio konstanta įgyja tokį pavidalą:

$$k_{ep,app} = \frac{k_p k_e}{[S]k_e + k_p} \tag{1.91}$$

Kur k_e yra išreikšta per Marcus elektrono pernašos greičio lygtį. Marcus teorija nėra tinkama aprašyti protono pernašos greičiui, nes pastarasis yra sudėtingesnis dėl vibracinių lygmenų įtakos. Tačiau, kadangi protono pernaša yra vidumolekulinis procesas, kuriame dalyvauja hemas ir katalizinis histidinas ir reakcijos laisvoji energija tokiu atveju nekinta, protono pernašos greitį galima aproksimuoti pavidalu:

$$k_p = \frac{\pi}{\hbar} V'^2 \frac{e^{-\frac{E_a}{kT}}}{\sqrt{\pi k_b T \pi}}, \; kur \; V'^2 = V_{if}^2 / \sqrt{\lambda_p} \tag{1.92}$$

Kur E_a yra tariamoji protono pernašos aktyvacijos energija. Sustačius išraiškas yra gaunama galutinė tariamosios bimolekulinės greičio konstantos lygtis:

$$k(T) = \frac{\frac{\pi}{\hbar} V_{if}^2 \frac{e^{-\frac{(\Delta G^\circ + \lambda)^2}{4\lambda k_b T}}}{\sqrt{\pi \lambda k_b T}} \times \frac{\pi}{\hbar} V'^2 \frac{e^{-\frac{E_a}{kT}}}{\sqrt{\pi k_b T}}}{\frac{\pi}{\hbar} V_{if}^2 \frac{e^{-\frac{(\Delta G^\circ + \lambda)^2}{4\lambda k_b T}}}{\sqrt{\pi \lambda k_b T}} [S] + \frac{\pi}{\hbar} V'^2 \frac{e^{-\frac{E_a}{kT}}}{\sqrt{\pi k_b T}}} \tag{1.93}$$

Čia $\lambda = (\lambda_{substrate} + \lambda_{heme})/2$ (Marcus, 1968). Kadangi apskaičiuotosios anksčiau reorganizacijos energijos reprezentuoja reakciją vandenyje, o ne fermente, yra naudojamas papildomas θ daugiklis reprezentuoti substrato reorganizacijos energiją fermente:

$$\lambda = (\lambda_{substrate}\theta_{substrate} + \lambda_{heme})/2 \tag{1.94}$$

Čia θ yra tirpikliui pasiekiama substrato paviršiaus dalis fermentiniame-substratiniame komplekse. θ buvo apskaičiuota iš molekulinės mechanikos metodais apskaičiuotų fermento ir substrato kompleksų kiekvienam substratui. Panaudojant lygtį 1.93 ir eksperimentų duomenis, buvo apskaičiuotos visų parametrų reikšmės (lentelė 1.19). Paveiksle 1.46 pavaizduota kaip gerai modelis prognozuoja preeksponentinius faktorius ir reakcijos aktyvacijos energijas.

Iš lentelės matyti, kad V_{if} parametrai net struktūriškai panašiems substratams, kaip kad MB ir TH, skiriasi kartais ir iliustruoja, kad prielaida apie struktūriškai panašių substratų V_{if} panašumą yra neteisinga. Modelis leidžia apskaičiuoti protono pernašos greičio konstantą, kuri yra nepriklausoma nuo substrato ir yra lygi $520 \pm 40\ \mathrm{s}^{-1}$ $298\ \mathrm{K}$ temperatūroje. Iš eksperimentinių duomenų apskaičiuota hemo reorganizacijos energija yra $0.44\ \mathrm{eV}$ ir yra labai artima literatūroje publikuotoms reikšmėms (Bortolotti et al., 2011)(Andreu et al., 2007). Taigi, darytina išvada, kad kitaip nei teigiama literatūroje, CpdII redukcija nėra ribojama tik elektrono pernašos greičio.

1.19 lentelė: Apskaičiuoti parametrai lygčiai 1.93.

	Reikšmė	$\Delta G^{\ddagger}_{Marcus\ ET}$ (kcal/mol)
V_{if}^{ABTS}	$0.76 \pm 0.08\,\mathrm{cal\,M^{-\frac{1}{2}}\,mol^{-1}}$	0.4 ± 0.01
V_{if}^{AMB}	$3.5 \pm 0.4\,\mathrm{cal\,M^{-\frac{1}{2}}\,mol^{-1}}$	1.5 ± 0.1
V_{if}^{CPZ}	$0.12 \pm 0.02\,\mathrm{cal\,M^{-\frac{1}{2}}\,mol^{-1}}$	0.5 ± 0.03
$V_{if}^{DCPIP(I)}$	$4.0 \pm 0.5\,\mathrm{cal\,M^{-\frac{1}{2}}\,mol^{-1}}$	0.16 ± 0.02
$V_{if}^{DCPIP(II)}$	$1.4 \pm 0.2\,\mathrm{cal\,M^{-\frac{1}{2}}\,mol^{-1}}$	0.001 ± 0.002
V_{if}^{DMB}	$2.0 \pm 0.2\,\mathrm{cal\,M^{-\frac{1}{2}}\,mol^{-1}}$	0.5 ± 0.05
V_{if}^{HEPX}	$0.83 \pm 0.09\,\mathrm{cal\,M^{-\frac{1}{2}}\,mol^{-1}}$	0.13 ± 0.02
V_{if}^{MB}	$260 \pm 30\,\mathrm{cal\,M^{-\frac{1}{2}}\,mol^{-1}}$	5.1 ± 0.2
V_{if}^{PPSA}	$1.7 \pm 0.1\,\mathrm{cal\,M^{-\frac{1}{2}}\,mol^{-1}}$	0.3 ± 0.04
V_{if}^{PZ}	$0.44 \pm 0.05\,\mathrm{cal\,M^{-\frac{1}{2}}\,mol^{-1}}$	0.2 ± 0.02
V_{if}^{TH}	$76 \pm 8\,\mathrm{cal\,M^{-\frac{1}{2}}\,mol^{-1}}$	3.9 ± 0.2
V_{if}^{TMPD}	neapibrėžta	3.0 ± 0.2
V_{if}^{VB}	$4.7 \pm 0.5\,\mathrm{cal\,M^{-\frac{1}{2}}\,mol^{-1}}$	2.1 ± 0.1
V'	$4.3 \pm 0.5\,\mathrm{cal\,mol^{-1}}$	
E_a	11.7 ± 0.2 kcal/mol	
λ_{heme}	10.2 ± 0.3 kcal/mol	

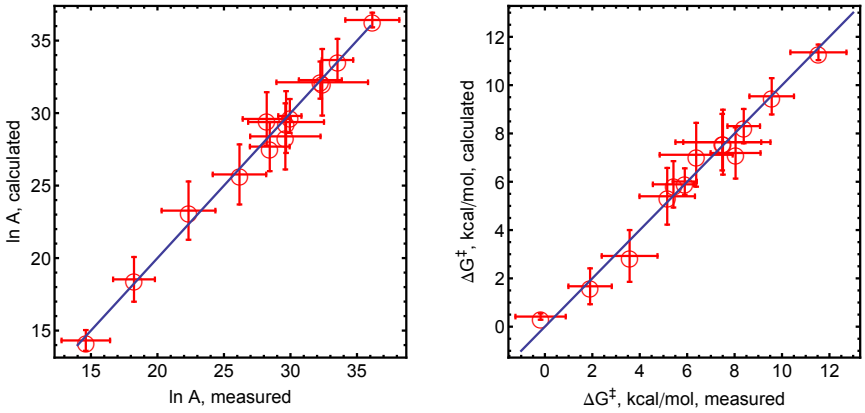

1.46 pav.: Pamatuoti vs apskaičiuoti preeksponentiniai faktoriai ir reakcijos aktyvacijos energijos pagal lygtį 1.93 ir nustatytus parametrus iš lentelės 1.19.

Skaitiškai didelės V' ir E_a reikšmės apskaičiuotos protono pernašos stadijai rodo kad protono pernaša yra sudėtingesnis procesas nei reprezentuoja aukščiau naudota protono pernašos greičio lygtis. Šios konkrečios peroksidazės atveju egzistuoja du skirtingos tvarkos mechanizmai – vienu atveju redukuojant CpdII pirmiau įvyksta protono pernaša, kitu

atveju – elektrono. Jei protono pernaša vyksta pirmiau, jos atstumas yra 1.7 Å, jei pirma vyksta elektrono pernaša, protono pernašos atstumas yra 1 Å. Protono pernašos greičio konstantos šiems žingsniams gali būti apskaičiuotos naudojant modelį, kuris aprašo aplinkos reorganizacijos įtaką protono pernašos greičiui (Cukier and Morillo, 1989; Morillo and Cukier, 1990). Atsižvelgiant į vibracinius efektus, greičio konstantos lygtis yra lygtis yra (Borgis and Hynes, 1996):

$$k_p = \sum_n \sum_m P_n \frac{V_{nm}^2}{\hbar} \sqrt{\frac{\pi}{\lambda_p k_B T}} \exp\left(-\frac{\Delta G_{nm}^{\ddagger}}{k_B T}\right) \tag{1.95}$$

$$\Delta G_{nm}^{\ddagger} = \frac{(\Delta G_p + E_m - E_n + \lambda_p)}{4\lambda_p} \tag{1.96}$$

Kur P_n yra pernašos tikimybė iš n-tojo vibracinio lygmens, V_{nm} – vibracinio susietumo konstanta ir λ_p protono pernašos aplinkos reorganizacijos energija. E_n ir E_m atitinkamai yra n-tojo reaktanto ir m-tojo produkto vibracinio lygmens energijos. Energijos ir vibracinio susietumo parametrai apskaičiuojami naudojant harmoninio potencialo banginę funkciją(Piela, 2013):

$$\psi_n(x) = \frac{e^{-\frac{1}{2}x^2\sqrt{\frac{k\,m_p}{\hbar^2}}} \sqrt{\frac{2^{-n}\sqrt[4]{\frac{k\,m_p}{\hbar^2}}}{n!}} H_n\left(x\sqrt[4]{\frac{k\,m_p}{\hbar^2}}\right)}{\sqrt[4]{\pi}} \tag{1.97}$$

kur k yra jėgos konstanta susijusi su reorganizacijos energija ($k = 2\lambda/\delta x^2$, δx – protono pernašos atstumas), o m_p protono masė. Protono pernašos greičio konstanta ir aktyvacijos energija atstumui 1.7 Å gali būti reprodukuota su reorganizacijos energija 3.72 eV ir reakcijos laisvąja energija -48.3 kcal/mol. Atitinkamai atstumui 1 Å reikalinga reorganizacijos energija 2.01 eV ir reakcijos laisvoji energija -3.54 kcal/mol. Pastarosios reikšmės yra gerokai prasmingesnės publikuotų λ_p (2 eV, (Takada et al., 2005; Smedarchina and Enchev, 1994)) ir $\mathrm{pK_a}$ skirtumų tarp histidino ir hemo surištos vandens molekulės kontekste (PT-ET atveju $\mathrm{pK_a}$ skirtumas turėtų būti ~ 24, kas yra neįmanoma). Naudojant apskaičiuotus parametrus ir tariant, kad redukuota deuterono masė yra 1.8 protono masės galima apskaičiuoti deuterono pernašos greičio konstantą, kuri yra $295 \pm 30\ \mathrm{s}^{-1}$ ir PT žingsnio kinetinis izotopinis efektas atitinkamai yra 1.8. Remiantis šiais rezultatais buvo apskaičiuoti teoriniai kineti-

niai izotopiniai efektai visiems substratams. Jie buvo eksperimentiškai pamatuoti substratams TMPD, CPZ ir ABTS. Gautosios reikšmės yra 1.6±0.2, 1.0±0.1 ir 1.3±0.1. Tad, modelis teisingai prognozuoja kinetinius izotopinius efektus, gerai aprašo greičio konstantas visiems tirtiems substratams ir leidžia nustatyti, kad CpdII redukcijos mechanizmas yra ET-PT, kur priklausomai nuo substrato reakcijos greitis yra sintetinė greičio konstanta sudaryta iš ET ir PT greičių.

1.3 Disertacijos išvados

1. Sukurtas homogeninės cheminės ir biocheminės kinetikos modeliavimo ir analizės metodas leidžiantis iš riboto duomenų kiekio nustatyti tiriamų procesų kinetinius parametrus.

2. Lakazės iš Didymocrea sp. J6 katalizuojamos deguonies elektroredukcijos ant elektrodo metu vyksta tiesioginė elektronų pernaša iš elektrodo į T2/T3 aktyvųjį centrą.

3. Lakazės iš *Didymocrea* sp. J6 inhibicijos fluorido jonais homogeninėje terpėje mechanizmas yra paremtas T2/T3 aktyviojo centro redukcijos potencialo sumažėjimu ir dėl to sutrikdoma elektronų pernaša iš T1 centro į T2/T3 centrą

4. *Coprinopsis cinerea* peroksidazės katalizuojamų reakcijų aktyvacijų energijos yra paaiškinamos atskirais elektrono ir protono pernašos žingsniais.

5. *Coprinopsis cinerea* peroksidazės katalizuojamų reakcijų greičiai yra paaiškinami Marcus elektronų ir neadiabatine protonų pernašos teorijomis.

Padėka

Ši disertacija būtų neįmanoma be daugelio žmonių indėlio savo žinomis, patarimais ir palaikymu. Be jokios abejonės neįmanoma išvardyti jų visų, tad ypatingas ačiū šiems:

Akad. prof. habil. dr. Juozas Kulys, dr. Marius Dagys, dr. Dalius Ratautas, prof. dr. Rolandas Meškys, prof. dr. Sergey Shleev, dr. Lidija Tetianec, Irina Bratkovskaja, dr. Žilvinas Anusevičius, dr. Regina Vidžiūnaitė, Marius Butkevičius, dr. Liucija Marcinkevičienė.

Ir visiems nuolat uždavinėjusiems klausimą „Tai kada ginsiesi?“

PUBLICATIONS

1.1 Publications of the author directly related to the dissertation

1. Laurynėnas, A., and Kulys J. (2015). An exhaustive search approach for chemical kinetics experimental data fitting, rate constants optimization and confidence interval estimation. Nonlinear Anal., Model. Control 20.1: 145-157.

2. Dagys, M., Laurynėnas, A., Ratautas, D., Kulys, J., Vidžiūnaitė, R., Talaikis, M., Niaura G., Marcinkevičienė L., Meškys R. & Shleev, S. (2017). Oxygen electroreduction catalysed by laccase wired to gold nanoparticles via the trinuclear copper cluster. Energy & Environmental Science, 10(2), 498-502.

3. Laurynėnas, A., Butkevičius, M., Dagys, M., Shleev, S., & Kulys, J. (2019). Consecutive Marcus electron and proton transfer in Heme peroxidase compound II-catalysed oxidation Revealed by Arrhenius plots. Scientific reports, 9(1), 1-11.

1.2 Other publications of the author

1. Ratautas, D., Laurynėnas, A., Dagys, M., Marcinkevičienė, L., Meškys, R., & Kulys, J. (2016). High current, low redox potential mediatorless bioanode based on gold nanoparticles and glucose dehydrogenase from Ewingella americana. Electrochimica Acta, 199, 254-260.

2. Šarlauskas, J., Misevičienė, L., Marozienė, A., Karvelis, L., Stankevičiūtė, J., Krikštopaitis, K., Čėnas, N., Yantsevich, A., Laurynėnas, A., Anusevičius, Ž. (2014). The study of NADPH-dependent flavoenzyme-catalyzed reduction of benzo [1, 2-c] 1, 2, 5-oxadiazole N-oxides (Benzofuroxans). International journal of molecular sciences, 15(12), 23307-23331.

3. Kosychova, L., Karalius, A., Staniulytė, Z., Sirutkaitis, R., Palaima, A., Laurynėnas, A., & Anusevičius, Ž. (2015). New 1-(3-Nitrophenyl)-5, 6-dihydro-4H-[1, 2, 4] triazolo [4, 3-a][1, 5] benzodiazepines: Synthesis and Computational Study. Molecules, 20(4), 5392-5408.

4. Gružauskaitė, J., Jasinskaitė, J., Meškys, R., Gaidamavičienė, G., Žalga, A., Laurynėnas, A., Tetianec, L. & Dagys, M. (2019). Gold-coated magnetic nanocatalyst containing wired oxidoreductases for mediatorless catalysis of carbohydrate oxidation by oxygen. Catalysis Communications, 105848.

5. Stanislauskienė, R., Laurynėnas, A., Rutkienė, R., Aučynaitė, A., Tauraitė, D., Meškienė, R., Urbelienė, N., Kaupinis, A., Valius, M., Kaliniene, L. & Meškys, R. (2020). YqfB protein from Escherichia coli: an atypical amidohydrolase active towards N4-acylcytosine derivatives. Scientific reports, 10(1), 1-12.

1.3 Conferences

1. Laurynėnas A., Kulys J. Modeling and thermodynamic study of syringaldazine and 10-(2-hydroxyethyl-)phenoxazine oxidation catalyzed by *Coprinus cinerea* peroxidase. Biotrans 2015 (2015), Vienna, Austria

2. Laurynėnas A., Kulys J. Probing temperature dependence of peroxidase catalyzed substrates oxidation. Life Sciences Baltics 2016 conference (2016), Vilnius, Lithuania

3. Dagys M., Laurynėnas A., Ratautas D., Kulys J., Niaura G., Meškys R., Shleev S. Oxygen Electroreduction Catalysed by Laccase Wired to Gold Nanoparticles via the Trinuclear Copper Cluster, 28th Anniversary World Congress on Biosensors (2018), Miami, USA

4. Dagys M., Laurynėnas A., Ratautas D., Kulys J., Vidžiūnaitė R., Talaikis M., Niaura G., Marcinkevičienė L., Meškys R., Shleev S. Deguonies elektroredukcija, katalizuojama lakazės sąveikaujančios su aukso nanodalelėmis per T2/T3 aktyvųjį centrą, 7th Young Scientists' Conference „Interdisciplinary Research in Physical and Technological Sciences" (2017), Lithuanian Academy of Sciences, Vilnius, Lithuania

5. Dagys M., Laurynėnas A., Ratautas D., Kulys J., Vidžiūnaitė R., Talaikis M., Niaura G., Marcinkevičienė L., Meškys R., Shleev S. Oxygen Electroreduction Catalysed by Laccase Wired to Gold Nanoparticles via the Trinuclear Copper Cluster, 23rd Topical Meeting

of the International Society of Electrochemistry (2018), Vilnius, Lithuania

6. Dagys M., Laurynėnas A., Ratautas D., Kulys J., Vidžiūnaitė R., Talaikis M., Niaura G., Marcinkevičienė L., Meškys R., Shleev S. Oxygen Electroreduction Catalysed by Laccase Wired to Gold Nanoparticles via the Trinuclear Copper Cluster. Open Readings (2017), Vilnius, Lithuania

Trumpos žinios apie disertantą

Disertantas 2009 metais baigė biochemijos bakalauro studijas Vilniaus universitete (suteiktas biochemijos bakalauro laipsnis); 2011 metais baigė biochemijos magistro studijas Vilniaus universitete (suteiktas biochemijos magistro laipsnis).

2010-2011 metais disertantas dirbo jaunesniuoju mokslo darbuotoju ThermoFisher Scientific padalinyje Vilniuje, Lietuvoje. Nuo 2015 iki dabar disertantas yra Vilniaus universiteto, Gyvybės mokslų centro jaunesnysis mokslo darbuotojas. 2015-2020 metais disertantas lektoriaus pareigose dėstė modelių biologijoje, biologinių sistemų modeliavimo, bioinformatikos ir bioinformatikos įvado kursus Vilniaus Gedimino technikos universitete.

Disertantas yra paskelbęs aštuonias publikacijos recenzuojamuose leidiniuose bei yra pateikęs savo darbus šešiose konferencijose. Disertanto moksliniai interesai ir veiklos sritys yra biochemija, fizikinė chemija ir elektrochemija. Baltymų modeliavimas bei kvantinė chemija, procesų modeliavimas diferencialinėmis lygtimis.

Kontaktai: tel. +370 69 269 623 ; el. paštas audrius.laurynenas@bchi.vu.lt
.